Université de Montréal

Préparation et réactivité de nouveaux complexes indényles de palladium et de platine

Par
Christine Sui-Seng

Département de Chimie
Faculté des Arts et des Sciences

Thèse présentée à la Faculté des études supérieures
en vue de l'obtention du grade de Philosophiæ Doctor (Ph.D.) en chimie

Mars 2006

Université de Montréal

Faculté des études supérieures

Cette thèse intitulée :

Préparation et réactivité de nouveaux complexes

indényles de palladium et de platine

présentée par

Christine SUI-SENG

a été évaluée par un jury composé des personnes suivantes :

Dr. André L. Beauchamp.....Président rapporteur

Dr. Davit Zargarian.....Directeur de recherche

Dr Frank Schaper.....Membre du jury

Dr. Michel Étienne.....Examinateur externe

Dr. André L. Beauchamp.....Représentant du doyen de la FES

Résumé

Une vaste gamme de nouveaux complexes indényles de palladium et de platine comportant des ligands phosphines, halogénures, alkyles, triflates ou encore isocyanures et amines a été préparée.

La première méthode mise au point pour leur obtention repose sur l'addition métathétique du (1-R-Ind)Li et de PPh_3 sur $(PhCN)_2PdCl_2$ et a permis la préparation des composés (1-R-Ind)Pd(PPh_3)Cl (R = H, Me, Me_3Si). Une autre voie de synthèse, hautement plus efficace, basée sur l'addition oxydante du 1-$SiMe_3$-IndH sur Na_2PdCl_4, a mené à la formation du dimère $[(\eta^3\text{-Ind})Pd(\mu\text{-Cl})]_2$. Ce dernier constitue un précurseur idéal pour l'obtention d'autres composés Ind-Pd et par simple addition de 2 équivalents de ligand L, des dérivés η^1- ou $(\eta^3 \leftrightarrow \eta^5)$-Ind de Pd tels que $[(\eta^1\text{-Ind})_2(t\text{-BuNC})_2Pd_2(\mu\text{-Cl})_2]$, $L_2Pd(\eta^1\text{-Ind})Cl$ (L = $BnNH_2$, py), $(\eta^{3\text{-}5}\text{-Ind})Pd(L)Cl$ (L = PR'_3, NEt_3), ont pu être préparés. L'addition simultanée de PR'_3 (R' = Ph, Cy) et de $BnNH_2$ sur le dimère $[(\eta^3\text{-Ind})Pd(\mu\text{-Cl})]_2$, a ensuite permis d'isoler les espèces η^1-Ind mixtes de formule $(PR'_3)(BnNH_2)Pd(\eta^1\text{-Ind})Cl$. En solution, il a été démontré que ces complexes subissaient alors une transformation graduelle pour générer des composés dinucléaires de Pd(I), $(\mu,\eta^3\text{-Ind})(\mu\text{-Cl})Pd_2(PR'_3)_2$ qui résultent en fait d'une réaction de comproportionnation entre les complexes Ind-Pd(II) et des espèces de $Pd(0)(PR_3)_n$ générées in situ.

Dans le cas du platine, la voie de synthèse établie repose sur la réaction métathétique de IndLi sur les précurseurs (COD)PtClX (X = Cl, Me). Il en résulte ainsi des complexes η^1-Ind de Pt(II), $(COD)Pt(\eta^1\text{-Ind})X$ (X = Cl, Me, η^1-Ind), qui après addition d'$AgBF_4$ ou de HBF_4, ont permis d'isoler le complexe cationique $[(\eta\text{-Ind})Pt(COD)]^+$.

Les composés obtenus ont été caractérisés par spectroscopie RMN (^1H, $^{13}C\{^1H\}$, $^{31}P\{^1H\}$) et par analyse élémentaire. L'analyse par diffraction des rayons X a été utilisée pour résoudre la structure à l'état solide de la plupart de ces composés,

tandis que les études électrochimiques ont permis de déterminer la richesse électronique des centres métalliques.

L'étude de leur réactivité a démontré que certains complexes Ind de Pd(II), notamment les composés $[(\eta^3\text{-Ind})Pd(\mu\text{-Cl})]_2$ et $(\eta\text{-Ind})Pd(PPh_3)Cl$, activés par le méthylaluminoxane, constituaient des précatalyseurs efficaces pour la polymérisation de l'éthylène. Les complexes triflates $(\eta\text{-1-R-Ind})Pd(PPh_3)OTf$ se sont avérés être d'excellents catalyseurs pour l'hydrosilylation du styrène et du phénylacétylène en présence de trichlorosilane, ainsi que pour l'isomérisation du 1-hexène, la dimérisation de l'éthylène, l'oligo- et la polymérisation de certains dérivés du *p*-X-styrène (X = H, NH_2, Me, OMe).

Quelques réactions de couplage de Heck et d'arylamination, catalysées par le composé $(\eta\text{-1-SiMe}_3\text{-Ind})Pd(PPh_3)Cl$, y sont également présentées.

Enfin, les études préliminaires des réactivités des composés Ind de Pt(II) obtenus ont montré qu'ils pouvaient promouvoir la redistribution du $PhSiH_3$ et son addition sur le styrène.

Mots clés: palladium, platine, indényle, phosphine, amine, polymérisation, hydrosilylation, oléfine, silane, diffraction des rayons X, RMN, voltammétrie cyclique.

Abstract

A large variety of new indenyl palladium and platinum complexes with phosphine, halide, alkyl, triflate, isocyanide and amine ligands have been prepared.

The first route developed for their preparation involved the metathetic addition of (1-R-Ind)Li and PPh_3 on $(PhCN)_2PdCl_2$ and has allowed the isolation of the compounds (1-R-Ind)Pd(PPh_3)Cl (R = H, Me, Me_3Si). Another synthetic method, highly effective, consisted in adding 1-$SiMe_3$-IndH on Na_2PdCl_4 and has led to the formation of the dimeric compound $[(\eta^3\text{-Ind})Pd(\mu\text{-Cl})]_2$. The latter constitutes a versatile precursor to other Ind-Pd complexes, and by adding 2 equivalents of L ligand, the η^1- or ($\eta^3 \leftrightarrow \eta^5$)-Ind palladium derivatives, such as $[(\eta^1\text{-Ind})_2(t\text{-BuNC})_2Pd_2(\mu\text{-Cl})_2]$, $L_2Pd(\eta^1\text{-Ind})Cl$ (L = $BnNH_2$, py) and (η-Ind)Pd(L)Cl (L = PR'$_3$, NEt_3) have been obtained. The one-pot reaction of $[(\eta^3\text{-Ind})Pd(\mu\text{-Cl})]_2$ with a mixture of $BnNH_2$ and the phosphines ligands PR'$_3$ (R' = Ph, Cy) gives the mixed-ligand, amino and phosphine species (PR'$_3$)($BnNH_2$)Pd(η^1-Ind)Cl. In solution, these complexes undergo a gradual decomposition to generate the dinuclear Pd(I) compounds, $(\mu,\eta^3\text{-Ind})(\mu\text{-Cl})Pd_2(PR'_3)_2$, which in fact proceed by a comproportionation reaction between in-situ generated Pd(II) and Pd(0) intermediates.

The route developed for the preparation of Ind-Pt compound is based on the addition of IndLi on the precursors (COD)PtClX (X = Cl, Me). The compounds (COD)Pt(η^1-Ind)X (X = Cl, Me, η^1-Ind) have thus been obtained and after addition of $AgBF_4$ or HBF_4, the cationic complex $[(\eta\text{-Ind})Pt(COD)]^+$ has been isolated.

The synthesized complexes have been characterized mainly by solution nuclear magnetic resonance spectroscopy (NMR ^1H, $^{13}C\{^1H\}$, and $^{31}P\{^1H\}$), elemental analyses and, in some cases, the solid state structural analysis has been carried out crystallographically by X-ray diffraction, whereas the electrochemical measurements (cyclic voltammetry) allowed the determination of the electronic density on the metal centers.

Reactivity studies of some of the Ind-Pd compounds obtained, in particular $[(\eta^3\text{-Ind})Pd(\mu\text{-Cl})]_2$ and $(\eta\text{-Ind})Pd(PPh_3)Cl$, have shown that they can be activated by methylaluminoxane to polymerize ethylene. Reactions of the triflate compounds $(\eta\text{-1-R-Ind})Pd(PPh_3)(OTf)$ with various olefins result in isomerization (1-hexene), dimerization and (or) trimerization (ethylene, styrene, and *p*-fluoro-styrene), oligomerization (*p*-amino- and *p*-methyl-styrene), or polymerization (*p*-methoxy-styrene). They can also promote the addition of $HSiCl_3$ to styrene and phenylacetylene.

Heck coupling and arylamination reactions, catalyzed by the complex $(\eta\text{-1-SiMe}_3\text{-Ind})Pd(PPh_3)Cl$, are also reported.

Finally, preliminary reactivity studies of the Ind-Pt compounds have shown that they can promote $PhSiH_3$ redistribution and its addition to styrene.

Key words: palladium, platinum, indenyl, phosphine, amine, polymerization, hydrosilylation, olefin, silane, X-Ray diffraction, NMR, cyclic voltammetry.

Table des matières

Liste des tableaux

Liste des figures

Liste des abréviations

Å	Angstrom
Δ	chaleur
δ	déplacement chimique
AE	analyse élémentaire
B	base
bipy	2,2'-bipyridine
BINAP	2,2'-bis(diphénylphosphino)-1,1'binaphtyl
Bn	benzyle
$BnNH_2$	benzylamine
br	*broad*
Bu	butyle
cif	*crystallographic information file*
CO	monoxyde de carbone
COD	1,5-cyclooctadiène
COSY	*correlation spectroscopy*
Cp	cyclopentadiényle
Cp*	1,2,3,4,5-pentaméthylcyclopentadiényle
CpH	cyclopentadiène
CV	*cyclic voltammetry*
Cy	cyclohexyle
d	doublet
D	deutérium
Dba	dibenzylidèneacétone
DCM	dichlorométhane
DEPT	*distortionless enhancement by polarization transfer*
deg	degrés
$\Delta G^{\neq}$	enthalpie libre d'activation

DMF	*N*,*N*-Diméthylformamide
DMSO	Diméthylsulfoxyde
DPPF	1,1'-bis(diphénylphosphino)-ferrocène
DQPH	*double quantum filtered phase sensitive*
equiv	équivalents
Et	éthyl
Et_2O	diéthyléther
F	facteur de structure
FA	*fold angle*
FID	*Flame ionisation detector*
GC	*gaz chromatography*
GPC	*gel permeation chromatography*
h	heure
HA	*hinge angle*
HMQC	*heteronuclear multiple-quantum correlation*
HOMO	*highest occupied molecular orbital*
i	ipso
Ind	indényle
Ind_2	1,1'-biindène
IndH	indène
I_p	indice de polydispersité (M_w/M_n)
IR	infrarouge
J	constante de couplage
L	ligand neutre
m	méta
M	métal
m	multiplet
m/z	masse/charge
MAO	méthylaluminoxane
min	minute
Me	méthyle

Mes	mésityle = 2,4,6-triméthylphényl
M_n	masse moléculaire moyenne en nombre
M_w	masse moléculaire moyenne en poids
NMR	*nuclear magnetic resonance*
*n*Bu	*n*-butyle
NEt_3	triéthylamine
o	ortho
OAc	acétate
ORTEP	*Oak Ridge thermal ellipsoid program*
OTf	= OSO_2CF_3, triflate
p	para
PE	polyéthylène
Ph	phényle
ppm	parties par million
py	pyridine
q	quadruplet
quin	quintuplet
R	facteur d'accord ($\sum ||F_o| - |F_c|| / \sum |F_o|$)
R	groupement alkyle
RMN	résonance magnétique nucléaire
s	singulet
sec	secondaire
sept	septuplet
sext	sextuplet
SHOP	*Shell higher olefin process*
MS	*mass spectrometry*
t	triplet
r.t.	*room temperature*
*t*Bu	*tert*-butyle
T.A.	température ambiante
Tc	température de coalescence

tert	tertiaire
THF	tétrahydrofurane
tol	toluène
VT	*variable temperature*
X	ligand anionique

Remerciements

Mes premiers remerciements vont à mon directeur de recherche, le professeur Davit Zargarian. Je voudrais lui exprimer ma profonde reconnaissance pour m'avoir accueillie dans son groupe de recherche et pour son soutien constant tout au long de cette thèse. Son expérience et ses conseils toujours judicieux ont été particulièrement précieux et ont apporté beaucoup au développement de ce travail.

Je tiens également à exprimer toute ma gratitude au professeur André L. Beauchamp dont j'ai sollicité l'aide depuis Toulouse et remercier aussi le comité des études supérieures de l'Université de Montréal, pour l'octroi d'une bourse d'excellence qui m'a permis de poursuivre ma formation libre de tout souci financier.

J'adresse mes sincères remerciements au professeur André L. Beauchamp et au professeur Franck Schaper pour avoir accepté de juger ce travail en tant que président rapporteur et membre du jury, ainsi qu'au professeur Michel Étienne pour avoir participé au jury malgré la distance qui sépare Toulouse de Montréal.

Mes remerciements s'adressent également à Madame Francine Bélanger-Gariépy et au Dr. Michel Simard du Laboratoire de diffraction des rayons X, grâce à vous j'ai pu être initiée à la cristallographie. Je vous suis gré de m'avoir permis d'apprendre cette technique et surtout d'avoir été aussi patients et disponibles à mon égard. J'associe à ces remerciements le Dr. Laurent F. Groux, le Dr. Christian Tessier et Awaleh Mohamed Osman. De plus, je remercie Huguette Dinel du service d'Analyse élémentaire, Sylvie Bilodeau et le Dr. Tan Phan Viet pour leur aide dans les analyses RMN, Julie Boivin pour la GC, ainsi que le groupe du professeur Hélène Lebel qui a eu la courtoisie de me permettre d'utiliser leur appareil de GC/MS.

J'ai eu le plaisir de travailler dans une atmosphère agréable durant quatre années auprès des différents membres, actuels et anciens, de l'aile A-6. Qu'ils trouvent ici l'expression de ma sympathie pour la bonne ambiance qu'ils ont su maintenir. À Annie et Yi Jing, j'espère qu'il y aura un "après la thèse" car j'attends votre visite à Toronto avec impatience!

Un GROS MERCI également à Annie Castonguay qui a eu le courage de lire et corriger cette thèse et qui m'a évité bien des démarches pour le dépôt. J'ai fortement apprécié ta complicité et travailler en ta compagnie fut un pur plaisir !

Finalement, je ne pourrais passer sous silence les encouragements de ma famille, en particulier de mes chers parents; sans eux, rien n'aurait été possible. Je les remercie pour leur soutien et leur confiance.

Entamer la rédaction d'une thèse, c'est un peu comme se préparer pour un voyage: malgré la meilleure des planifications, nul ne peut prédire comment sera la route ni quelle sera la destination finale. Un point commun néanmoins, au terme du projet: le souvenir de moments heureux, parfois plus difficiles, mais surtout la satisfaction d'avoir surmonté plusieurs défis…

À mes parents

À Rachid

Chapitre 1: Introduction

Les complexes organométalliques des métaux de transition occupent une place prépondérante dans l'industrie chimique, de par leurs applications en synthèse organique mais aussi en catalyse homogène, qui compte désormais pour près de 15% de l'ensemble des procédés catalytiques industriels[1]. La recherche de nouveaux catalyseurs a suscité un grand intérêt au niveau académique et industriel, et a permis entre autres de mieux comprendre leurs réactivités, d'améliorer leur design, de diminuer les coûts de production des systèmes et d'augmenter considérablement l'éventail de produits finaux disponibles. Parmi les nombreux systèmes catalytiques existants, ceux contenant un métal du groupe 10 (Ni, Pd et Pt), fortement étudiés ces dernières années, se sont avérés être très efficaces dans plusieurs réactions catalytiques. Parallèlement, depuis 1995, le groupe du Professeur Zargarian a ouvert la voie à une étude complète de la chimie des complexes indényles de nickel et l'étude de leur réactivité a démontré qu'ils pouvaient agir en tant que précatalyseurs dans de multiples réactions, telles que l'oligo- et la polymérisation des alcènes,[2] des alcynes,[3] et du phénylsilane,[4] ainsi que l'hydrosilylation des oléfines et des cétones.[5] Contrairement au nickel, la chimie des composés indényles de palladium et de platine en est à un stade beaucoup moins avancé. Ce sont donc sur ces derniers que nos efforts se sont concentrés. L'objectif de ce projet de recherche consiste à explorer la chimie de ces espèces, de mettre au point des voies de synthèse fiables et d'étudier leurs réactivités. L'intérêt des complexes indényles de palladium et de platine ne réside pas seulement dans la suggestion de nouveaux catalyseurs mais surtout dans l'étude de l'évolution de leurs propriétés structurales et catalytiques avec leurs analogues de nickel, afin de mieux cerner l'influence du centre métallique sur la chimie des composés indényles.

Ce premier chapitre d'introduction constitue une présentation bibliographique destinée à situer ce travail par rapport aux connaissances actuelles. Après une présentation générale du ligand indényle et de ses principales caractéristiques (§1.1), la

chimie des complexes métalliques du groupe 10, en particulier celle des composés indényles parus à ce jour, sera décrite (§1.2) et finalement, suivront les objectifs de recherche (§1.3) et la description des travaux (§1.4).

1.1 Ligand Indényle

Les ligands cyclopentadiényle (Cp) et indényle (Ind), dont les propriétés stériques et électroniques sont facilement ajustables par substitution des cycles, ont joué un rôle important dans le développement de la chimie organométallique. En comparaison à leurs analogues Cp, les composés Ind ont démontré fréquemment une activité accrue dans de multiples réactions stœchiométriques et catalytiques. Ces dernières années, les complexes Ind ont donc fait l'objet de nombreuses études et s'avèrent être une alternative au composé à ligand Cp. La raison principale de cet intérêt s'explique par l'existence d'un effet indényle[6] qui se manifeste par une augmentation de la réactivité,[7] en particulier dans les réactions de substitution de ligands et les réactions d'insertion. Cet effet est le résultat de l'hapticité flexible de l'indényle, qui peut adopter les modes de coordination η^5, η^3 et aussi η^1,[8] selon un processus réversible (Figure 1.1).

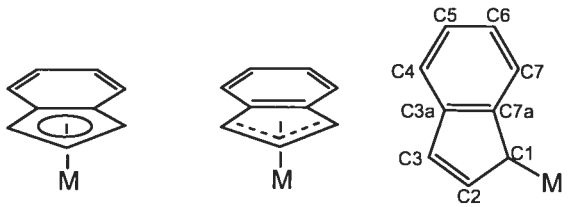

Figure 1.1: Modes de coordination du ligand indényle

Le nombre d'exemples reflétant cet effet indényle est considérable, surtout avec les composés des groupes 6, 8 et 9. Le premier exemple à être rapporté dans la littérature fut décrit par Hart-Davis et Mawby en 1969.[9] Il consiste en la substitution d'un groupement carbonyle par une phosphine, suivie de l'insertion du CO dans la liaison métal-alkyle (Figure 1.2). Il a été démontré qu'en présence du ligand indényle, la réaction était deux fois plus rapide comparativement au composé à ligand

cyclopentadiényle. Cette hausse de réactivité est due au glissement de l'indène, qui adopte alors une coordination η^3 stabilisée par la réaromatisation du cycle benzénique de l'indène, libérant ainsi un site de coordination et facilitant l'attaque nucléophile du nouveau ligand. Une fois le ligand CO substitué, l'indène adapte à nouveau sa contribution électronique et retrouve un mode de coordination η^5. Ce mécanisme de stabilisation, via une réhybridation du système π du ligand indényle implique pour le ligand cyclopentadiényle une rupture d'aromaticité du cycle à 5 en localisant sa densité électronique sur le fragment allylique, ce qui est donc défavorisé, et entraîne par conséquent des substitutions de ligands généralement plus lentes pour les complexes cyclopentadiényles.

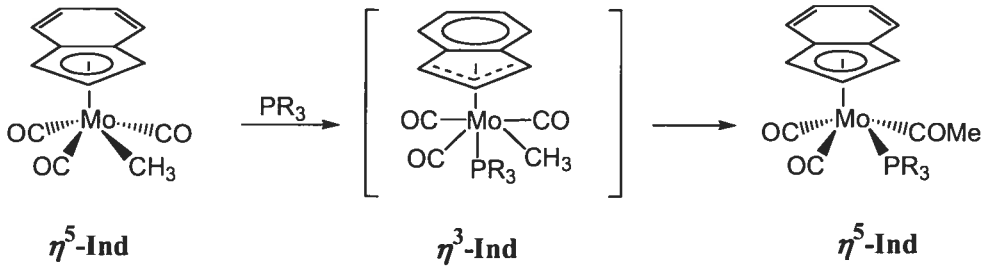

Figure 1.2: Réaction de substitution associative facilitée par l'effet indényle

Diverses études ont également démontré l'impact que pouvait avoir l'effet indényle avec d'autres métaux, et il a été évalué que la substitution pouvait procéder parfois jusqu'à 10^8 fois plus rapidement pour un complexe indényle que pour un complexe Cp analogue dans les mêmes conditions expérimentales (Figure 1.3) .[6a]

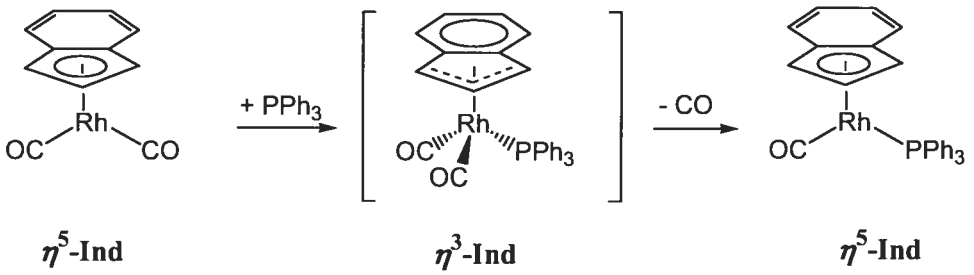

Figure 1.3: Réaction de substitution associative facilitée par l'effet indényle

Dans un même ordre d'idée, il a été démontré qu'un changement d'hapticité inverse facilitait la dissociation d'un ligand pour donner un intermédiaire réactionnel (η^3-Ind)Fe, probablement stabilisé par la présence du système π électronique du cycle benzénique, et favorisait de ce fait significativement la réaction de substitution dissociative, qui dans ce cas est 600 fois plus rapide en présence du ligand Ind comparativement au complexe analogue à ligand Cp (Figure 1.4).[10]

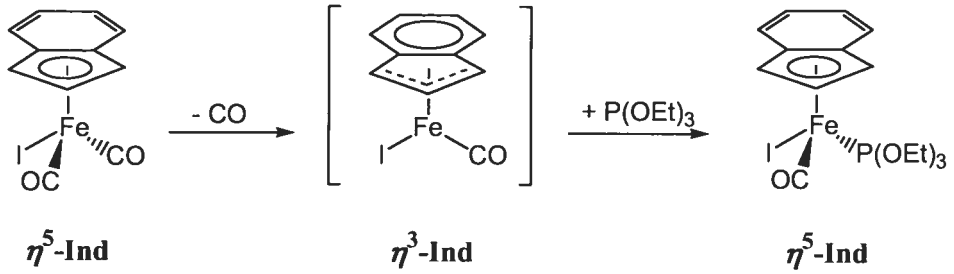

Figure 1.4: Réaction de substitution dissociative facilitée par l'effet indényle

Par ailleurs, il est intéressant de souligner que dans certains cas, l'utilisation de l'indényle peut ralentir les réactions pour des raisons stériques ou électroniques; il s'agit alors de l'effet indényle inverse.[11]

Étant donné l'influence que peut avoir l'hapticité de l'indényle sur les réactivités des complexes Ind, plusieurs paramètres quantitatifs ont été définis par Baker et Marder, afin d'évaluer le degré de coordination de l'indényle et l'importance de son glissement par rapport à une pentahapticité idéale. Le paramètre structural ΔM-C représente le degré de glissement du métal par rapport au centre du cycle à 5 de l'Ind et se calcule à partir des distances métal-carbone: $\Delta(M\text{-}C) = 0.5\ \{(M\text{-}C3a + M\text{-}C7a)\} - 0.5\{(M\text{-}C1 + M\text{-}C3)$.[12] D'autres paramètres structuraux comme le HA (*hinge angle*) et le FA (*fold angle*), viennent compléter le premier pour caractériser le mode de coordination du ligand Ind à l'état solide. Le HA constitue l'angle de pliage du cycle à 5, c'est-à-dire l'angle dièdre entre le plan des atomes C1, C2 et C3, et celui des atomes C1, C3, C3a et C7a, tandis que FA représente l'angle dièdre entre le plan des atomes C1, C2 et C3, et celui du cycle benzénique (atomes C3a, C4, C5, C6, C7 et C7a).

Selon ces définitions, un complexe η^5 aura donc des valeurs proches de zéro alors que les valeurs d'un complexe η^3 auront tendance à s'en éloigner. À titre d'exemple, le complexe $(\eta^5\text{-Ind})_2\text{Fe}$ possède un Δ(M-C) de 0.043 Å et des angles HA et FA d'environ 1 à 2 degrés,[12b] alors que les valeurs des Δ(M-C) et FA du composé $[(\eta^3\text{-Ind})\text{Fe(CO)}_3]^-$ s'élèvent respectivement à 0.689 Å et 22°.[13]

En solution, le type de coordination de l'indényle peut également être déterminé par spectroscopie RMN ^{13}C. Une fois coordonné au métal, les signaux correspondant aux atomes C3a et C7a de la jonction de cycle du ligand Ind se déplacent à plus haut champ et leurs déplacements chimiques peuvent alors être comparés à ceux de l'indène (moyenne de 144,0 ppm dans $CDCl_3$)[14] ou à ceux de l'IndNa (130,7 ppm dans le THF-d^8)[11] et ainsi fournir une mesure de l'hapticité du ligand en solution: $\Delta\delta^{13}C = \delta$(C3a/C7a du IndM) – δ(C3a/C7a du IndNa) ppm. Un Δδ négatif correspondrait ainsi à une hapticité η^5 (-43.7 ppm pour $(\eta^5\text{-Ind})_2\text{Fe}$)[11b] alors qu'il serait proche de 20-30 ppm pour une hapticité η^3 (+27 ppm pour $[(\eta^3\text{-Ind})\text{Fe(CO)}_3]^-$).[12]

1.2 Généralités sur les Complexes Métalliques du Groupe 10

La chimie de coordination des métaux du groupe 10 (Ni, Pd et Pt) a connu un important développement ces dernières années, notamment à cause de la grande variété de complexes que ces métaux peuvent former, mais également à cause des nombreuses réactions auxquelles ils peuvent participer. La polyvalence de la chimie de ces métaux est étroitement liée au fait que leurs composés sont connus dans de nombreux degrés d'oxydation, tels que 0, +I, +II, +III, +IV, et aussi dans des états d'oxydation plus élevés, à savoir très rarement +V et +VI pour certains composés fluorés de platine.[15] Les degrés d'oxydation les plus courants pour les composés du Ni sont 0 et +II puisque les complexes peu stables de Ni(I) ont tendance à se disproportionner facilement en Ni(0) et Ni(II), alors que les espèces de Ni(III) ne se limitent qu'à certains complexes chélates amines et les espèces de Ni(IV) aux complexes inorganiques comportant des ligands fortement donneurs, tels que les fluorures. En ce qui concerne les composés de

Pd et Pt, les principaux états d'oxydation rencontrés sont 0, +II et +IV, bien que les composés à degré d'oxydation +I et +III, où des liaisons métal-métal sont généralement impliquées, soient également assez répandus.

Généralement, les changements de degré d'oxydation du centre métallique qui peuvent survenir, impliquent une modification de son nombre de coordination via des réactions d'addition oxydante ou d'élimination réductrice. Les complexes inorganiques adoptent ainsi des nombres de coordination très divers pouvant varier de 2 à 6 suivant leur état d'oxydation. Cependant, la coordination 4 pseudo plan carré pour les métaux d^8 est également très souvent favorisée, tel est le cas du Ni(II), du Pd(II) et du Pt(II). Toutefois, certains composés du Ni(II) peuvent parfois adopter une géométrie tétraédrique lorsque leurs ligands sont stériquement encombrants. Les systèmes catalytiques basés sur les métaux du groupe 10, dont quelques exemples seront présentés dans le prochain paragraphe, sont très nombreux et mettent en jeu, la plupart du temps, des espèces aux états d'oxydation 0 et +II.

1.2.1 Potentiel catalytique

Le Ni possède une chimie riche avec de nombreuses applications en synthèse organique, principalement dans les réactions de couplage, ainsi que dans la chimie macromoléculaire, comme catalyseur pour l'oligo- et la polymérisation des oléfines.[16] Les catalyseurs découverts par Keim pour le procédé SHOP,[17] ceux de Brookhart[18] et de Grubbs[19], tous à base de Ni(II), figurent parmi les plus connus (Figure 1.5).

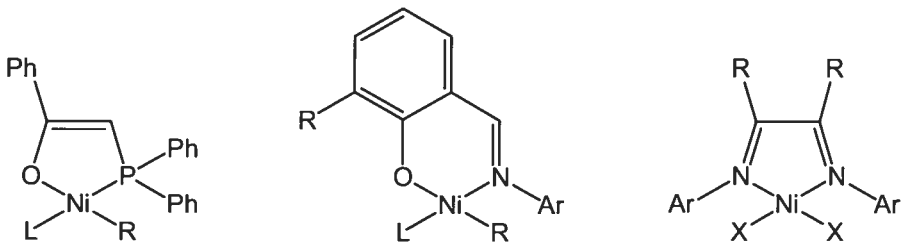

Keim **Grubbs** **Brookhart**

Figure 1.5: Catalyseurs de Ni(II) pour l'oligo- et la polymérisation des oléfines

De l'ensemble des éléments de transition, le palladium constitue probablement l'un des métaux les plus utilisés, de par l'étendue de ses applications au niveau industriel mais aussi à l'échelle du laboratoire.[15b,20] Parmi les plus connues, le procédé de copolymérisation alternée du monoxyde de carbone avec les oléfines, catalysée par des complexes de Pd(II),[21] permet la formation de polycétones et est employé par Shell et BP depuis 1995. Le procédé industriel Wacker, quant à lui, découvert dès les années 1950 par Smidt et ses collaborateurs,[22] fut longtemps un des seuls exemples de chimie du palladium en synthèse organique. Il permet, grâce au système redox formé in situ par le couple $PdCl_2$-$CuCl_2$, la production d'acétaldéhyde par oxydation de l'éthylène et reste aussi adaptable à tout autre type d'oléfines. Depuis, la chimie du palladium a connu un développement considérable, en particulier dans la formation des liens C-X (X = C, N, O, S). Cette méthodologie catalytique de couplage a connu une rapide expansion et se trouve désormais largement utilisée pour la synthèse de produits pharmaceutiques et naturels.[23] Par exemple, la réaction de Heck,[24] qui est parmi l'une des réactions de couplage palladocatalysées les plus répandues, permet la formation de liaisons C-C, en présence de Pd(0), par couplage entre un dérivé oléfinique et un halogénure ou triflate d'aryle. Cette réaction tolère les différentes fonctionnalités sur les substrats oléfiniques, ce qui ajoute à la diversité de ces composés. De nombreuses autres réactions de couplage, telles que les réactions de Suzuki (R = aryl, M = BR_2),[25] Stille (R = aryl, M = SnR_3)[26] et Hartwig-Buchwald (R = NR_2, M = H),[27] basées sur le même modèle, ont par la suite été établies et permettent ainsi l'accès à une large gamme de composés (Figure 1.6).

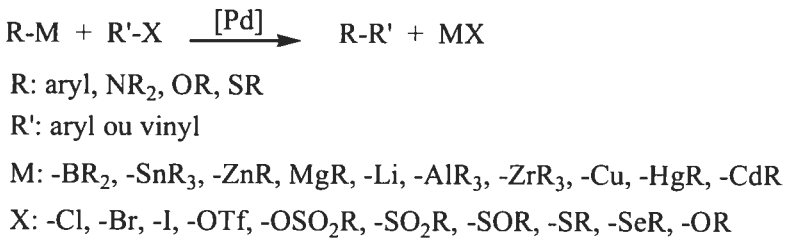

Figure 1.6: Réactions de couplage palladocatalysées

Ces transformations sont catalysées par un grand nombre de complexes de palladium, ou simplement par un mélange de $Pd(OAc)_2$ ou $Pd_2(dba)_3$ et de dérivés

phosphoniques mono- ou bidentates PX (X = P, N, O). Comme l'illustre la figure 1.7, elles impliquent généralement la réduction initiale du Pd(II) en Pd(0), suivie de l'addition oxydante de R'X pour générer un intermédiaire LPd(II)(R')(X). Le ligand anionique X est ensuite substitué par le groupement nucléophile R (aryl, NR_2) du co-substrat et l'étape finale d'élimination réductrice donne alors le produit de couplage.

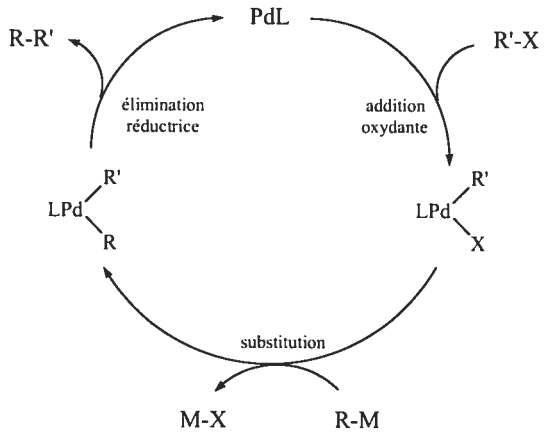

Figure 1.7: Cycle catalytique simplifié des réactions de Suzuki (R = aryl, M = BR_2), Stille (R = aryl, M= SnR_3) et Hartwig-Buchwald (R = NR_2, X = H)

Pour la réaction de Heck, l'espèce intermédiaire LPd(II)(R')(X) subit quant à elle une réaction d'insertion du co-substrat oléfinique, suivie d'une β-élimination qui mène au produit de couplage. Dans ce cas-ci, la présence d'une base, par exemple le NaOAc, est nécessaire et permet de régénérer le palladium par élimination du HX ainsi formé (Figure 1.8).

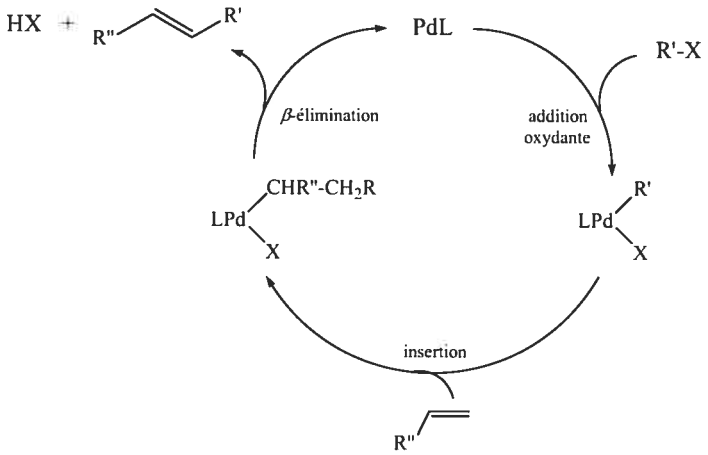

Figure 1.8: Cycle catalytique simplifié de la réaction de Heck

Les catalyseurs développés pour ce type de réaction comportent des ligands très diversifiés, comme par exemple des phosphine-imines[28] pour la réaction de Heck (Figure 1.9, **a**), des carbènes N-hétérocycliques pour la réaction de Suzuki (Figure 1.9, **b**),[29] le DPPF (Figure 1.9, **c**)[30] et le BINAP (Figure 1.9, **d**)[31] pour les réactions d'arylamination.

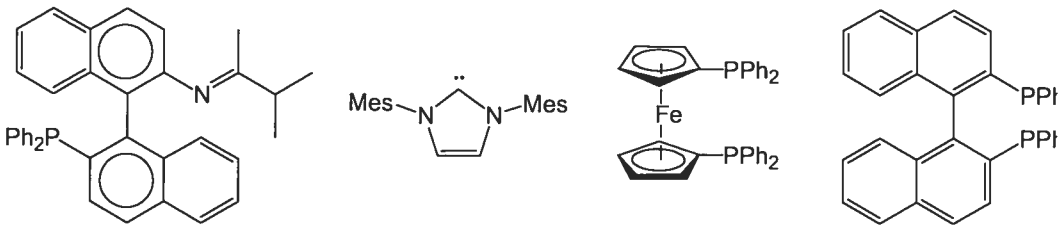

a **b** **c** **d**

Figure 1.9: Exemples de ligands utilisés avec le Pd pour les réactions de couplage

De nombreuses autres transformations organiques peuvent être catalysées par les complexes de palladium, parmi celles-ci, la substitution allylique de Tsuji-Trost,[32] les réactions de carbonylation,[33] l'hydroamination[34] et l'hydrosilylation.[35] Notons par contre qu'outre les composés de palladium, les deux composés les plus efficaces pour l'hydrosilylation des oléfines sont le catalyseur de Speier, qui consiste en l'acide platinique H_2PtCl_6, et le catalyseur de Karstedt, $Pt(Me_2CCHSiOSiCHCMe_2)_3$. Ces derniers démontrent une très grande activité et ce, même à des concentrations très faibles (10^{-8} mole de catalyseur par mole de réactif).[36]

Le point clé de la plupart de ces réactions de catalyse réside donc dans la nature du centre métallique et celle du ligand lui-même, dont la fonction peut également, dans certains cas, consister à rendre les réactions énantiosélectives. Étant donné l'étendue du potentiel catalytique des métaux du groupe 10 et l'influence que le ligand indényle peut avoir sur la vitesse des réactions, l'étude des composés indényles du Ni, Pd et Pt constitue donc un champ de recherche à l'avenir prometteur, bien qu'il ait été jusqu'à lors relativement peu exploré.

1.2.2 Composés nickel-indényle

Seuls trois exemples de composés nickel-indényle, le $Ni(Ind)_2$,[12b] le $(Ind)Ni(PBu_3)I$[37] et le $(Ind)Ni(P(C_{10}H_{21})_3)Br)$,[37] ont été rapportés dans la littérature antérieurement à l'année 1995 où le groupe du Pr. Zargarian a ouvert la voie à une étude complète de ce type de complexes. Les résultats de ces travaux, compilés dans une revue récente,[38] ont permis la préparation et la caractérisation des composés de type $(Ind)Ni(PR_3)X$ (Ind = ligand indényle et ses analogues substitués en position 1, 2 et 3; R = Ph, Cy, Me, Bu ; X = halogénures,[2b,39] alkyles,[39b,39e,39f,21] alcényles,[3a] imides,[40] thiols,[41] triflate[3b] et thiophène[3c]), ainsi que celles de dérivés comportant différents bras amines[2c,2e,2f,42] et oléfines[21,43] sur le ligand indényle (Figure 1.10).

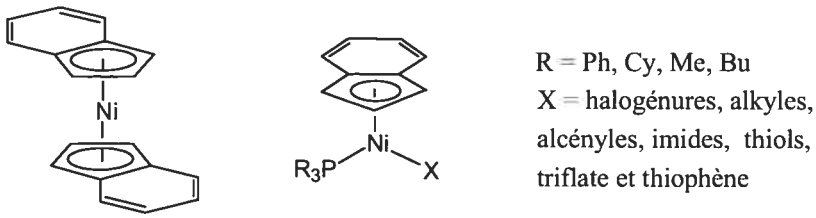

Figure 1.10: $Ni(Ind)_2$ et composés typiques nickel-indényle

L'étude de la réactivité de ces composés a démontré qu'ils pouvaient agir en tant que précatalyseurs dans de multiples réactions, telles que l'oligo- et la polymérisation des alcènes,[2] des alcynes,[3] et du phénylsilane,[4] ainsi que l'hydrosilylation des oléfines et des cétones[5] (Figure 1.11).

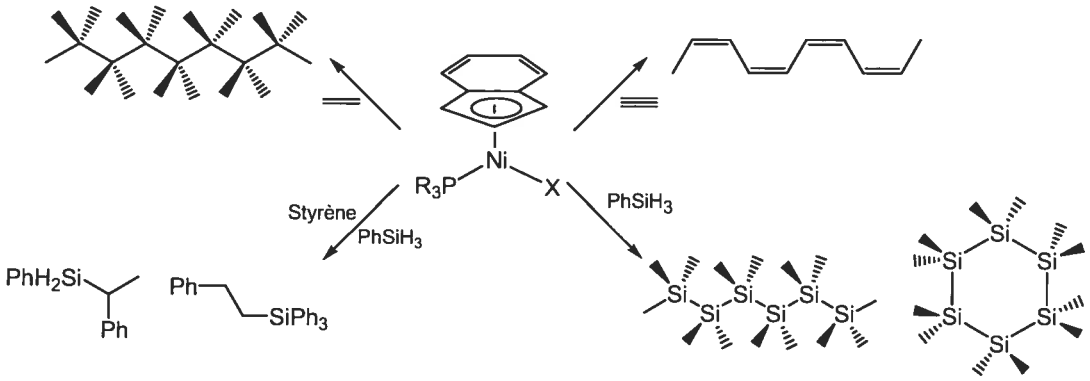

Figure 1.11: Réactivité catalytique des complexes nickel-indényle

1.2.3 Composés palladium-indényle

Contrairement aux composés nickel-indényle, la liste des complexes indényles de palladium existants est beaucoup moins exhaustive. Seuls six exemples de ces complexes ont été décrits dans la littérature. Le premier complexe indényle de palladium(II) fut synthétisé en 1975 par Battiste *et al.* grâce à une réaction de cyclisation intramoléculaire d'un complexe π-allylique intermédiaire, qui est issu de la réaction entre des cyclopropènes tétra-substitués et le dichlorobis(benzonitrile)palladium(II) (Figure 1.12).[44]

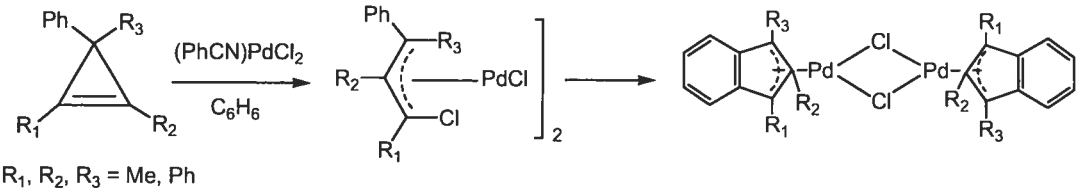

Figure 1.12: Synthèse du premier complexe indényle de Palladium(II)

Quelques années plus tard, Murata *et al.* isolèrent également un complexe indényle de Pd, sous forme dimérique: le bis(μ-chloro)-bis[(η^3-indényl)-palladium(II)] (Figure 1.13).[45]

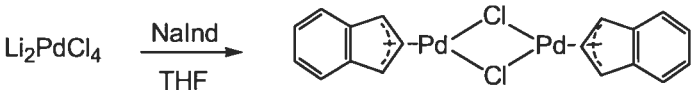

Figure 1.13: Synthèse du complexe bis(μ-chloro)-bis-[(η^3-indényl)-palladium(II)]

Ce complexe fut déjà synthétisé en 1969 par Samuel et Bigorgne par réaction entre $PdCl_2$ et NaInd, mais ne fut pas entièrement caractérisé.[46]

L'utilisation d'un autre anion organique tel que l'indényllithium a ensuite permis l'obtention d'un complexe de palladium(I) comportant des ligands η^3-indényles pontants (Figure 1.14).[47] Il s'agit là du premier complexe indényle d'un métal du groupe 10 au degré d'oxydation +I.

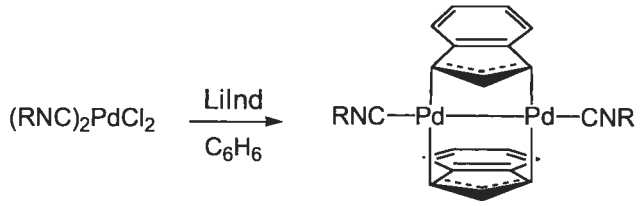

R = *t*-Bu, 2,6-$(CH_3)_2C_6H_3$; 2,4,6-$(CH_3)_3C_6H_2$; 2,4,6-$(t\text{-Bu})_3C_6H_2$

Figure 1.14: Synthèse du premier complexe indényle de Pd(I)

La réaction métathétique de l'indényllithium sur un complexe monohalogénure de type L_nPdRX (R = alkyl, X = Cl, L_n = phosphine) conduit également à un complexe η^3-indényle de palladium(II) (Figure 1.15).[48]

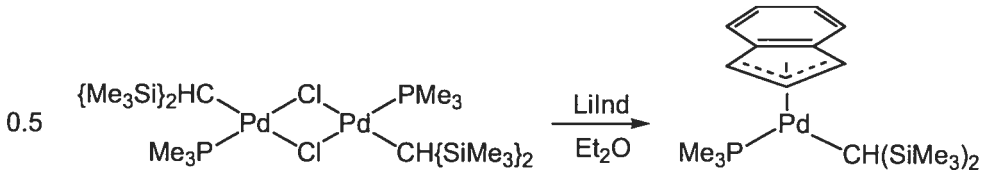

Figure 1.15: Synthèse du (η^3-Ind)Pd(PMe_3)($CH(SiMe_3)_2$)

Une autre voie de synthèse impliquant non plus un anion organique de type IndM (M = Na, Li), mais le 1-triméthylsilylindène, en présence de Na_2PdCl_4, permet, grâce à une réaction d'addition oxydante suivie de l'élimination réductrice de chlorotriméthylsilane, d'obtenir un composé η^3-indényle de palladium(II) de type polymérique (Figure 1.16).[49]

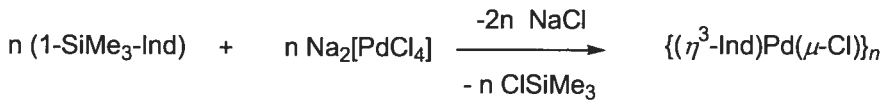

Figure 1.16: Synthèse du $[(\eta^3\text{-Ind})Pd(\mu\text{-Cl})]_n$

D'après la mesure osmométrique de la masse moléculaire moyenne en poids de ce polymère, les auteurs suggèrent que ce composé consiste en fait en un mélange de trimère et tétramère.

Récemment, une nouvelle procédure impliquant de multiples réactions d'insertion au sein de liaisons Pd-C et Pd-H a été rapportée dans la littérature.[50] Cette dernière approche offre la possibilité de synthétiser des complexes de palladium(II) comportant des ligands indényles hautement substitués (Figure 1.17).

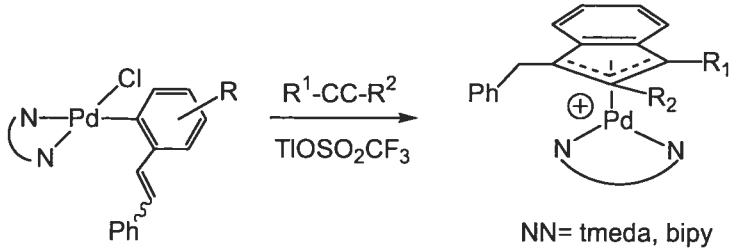

Figure 1.17: Synthèse de complexes indényles hautement substitués de Pd(II)

Concernant la réactivité des complexes indényles de palladium, son étude est à ce jour très limitée et se cantonne aux réactions suivantes:

- En présence d'un excès d'isocyanure, le composé Ind de Pd(II) précédemment décrit, (η^3-Ind)Pd(PMe_3)($CH(SiMe_3)_2$), subit une réaction d'insertion de l'isocyanide dans la liaison Pd-indényl du complexe intermédiaire (η^1-Ind)Pd(II) formé, dont la présence fut détectée par RMN à basse température, pour mener à la formation d'un fulvène d'indène (Figure1.18). [48a]

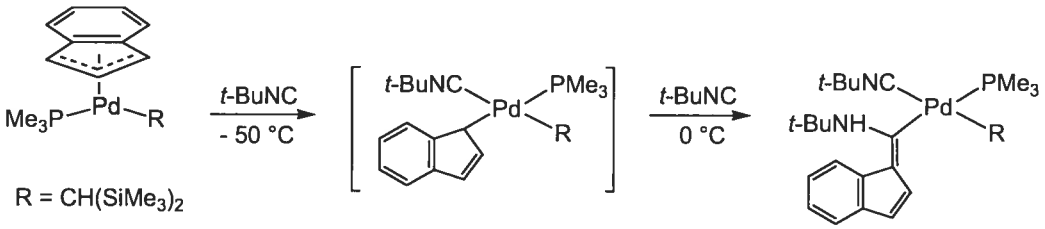

Figure 1.18: Formation du complexe fulvénique de Pd(II)

- L'ajout d'acide acétique sur le complexe indényle de Pd(I) [(μ,η^3-Ind)Pd(CNR)]$_2$ (R = *t*-Bu, 2,6-$(CH_3)_2C_6H_3$; 2,4,6-$(CH_3)_3C_6H_2$; 2,4,6-(*t*-Bu)$_3C_6H_2$) conduit à la protonation du ligand (μ,η^3-Ind) pour donner un cluster tétranucléaire de Pd(I), $Pd_4(\mu,\eta^2\text{-OAc})_4(\mu,\eta^1\text{-RNC})_4$.[47b]

1.2.4 Composés platine-indényle

C'est par réaction métathétique de l'IndNa sur le dichloro(1,5-cyclooctadiène) platine(II) que les premiers complexes indényles de platine ont été obtenus, sous forme de dérivés η^1-indényle, le (COD)Pt(η^1-Ind)Cl ou le (COD)Pt(η^1-Ind)$_2$, selon le rapport Pt:Ind qui a été utilisé (Figure 1.19).[51]

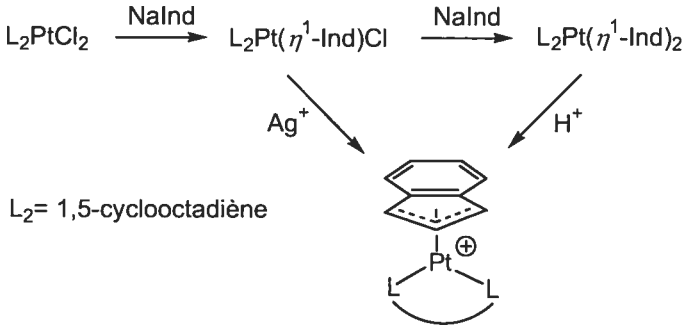

Figure 1.19: Synthèse des premiers complexes indényles de Pt(II)

La préférence inattendue d'une hapticité η^1 comparativement à un mode de coordination $\eta^3 \leftrightarrow \eta^5$ peut s'expliquer par la présence du ligand 1,5-cyclooctadiène bidentate qui empêche la libération d'un site de coordination autour du métal, et de ce fait l'isomérisation vers un complexe Ind d'hapticité $\eta^3 \leftrightarrow \eta^5$. Seule l'addition d'$AgBF_4$ et de HBF_4, sur les complexes (COD)Pt(η^1-Ind)Cl et (COD)Pt(η^1-Ind)$_2$, respectivement, ont ensuite permis la préparation du cation [(η-Ind)Pt(COD)]$^+$.

Plus récemment, un autre exemple de complexe η^1-1*H*-inden-2-yl de Pt(II), le sel triflate du *trans*-[(PPh$_3$)$_2$Pt(η^1-1*H*-inden-2-yl)(CNC(CH$_3$)$_3$)]$^+$, obtenu par réarrangement du complexe *trans*-[(PPh$_3$)$_2$Pt(η^1-CH$_2$C≡CPh)(CNC(CH$_3$)$_3$)]$^+$ en solution a été rapporté dans la littérature (Figure 1.20).[52]

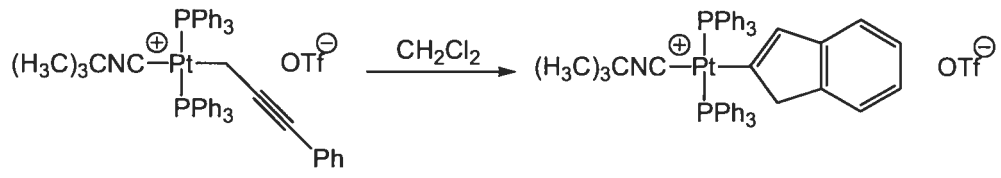

Figure 1.20: Synthèse du *trans*-[(PPh$_3$)$_2$Pt(η^1-1*H*-inden-2-yl)(CNC(CH$_3$)$_3$)]OTf

1.3 Objectifs de Recherche

Comme mentionné ci-dessus, la chimie des complexes indényles de Pd et Pt en est pour l'instant à une phase préliminaire de son développement et ne compte que quelques exemples, dont les réactivités catalytiques n'ont jamais été explorées. L'objectif de ce projet de recherche consistera donc à mettre au point des voies de synthèse efficaces pour l'obtention d'une série de composés Ind de Pd et de Pt présentant divers ligands tels que des phosphines, des halogénures, des isocyanures, des groupements alkyles et des amines, dans le but d'étudier leur activité de manière plus systématique principalement dans les réactions de polymérisation des oléfines, du phénylsilane, et l'hydrosilylation du styrène ainsi que dans certaines réactions de couplage, tels que les réactions de Heck et d'arylamination. Les composés synthétisés seront caractérisés par spectroscopie RMN en solution et, dans certains cas, par diffraction des rayons X à l'état solide. La collection de nombreux complexes Ind du Pd et Pt préparés permettra ainsi d'évaluer et de comparer l'influence attribuable à la nature du centre métallique sur les structures et les réactivités.

1.4 Description des Travaux

Le chapitre 1 de cette thèse consiste en une introduction bibliographique sur l'utilisation du ligand indényle dans la chimie des métaux du groupe 10, tout en soulignant l'importance de chacun en catalyse, et comporte une description des objectifs ainsi qu'une vue d'ensemble des travaux accomplis.

Le chapitre 2 est plus particulièrement consacré à la préparation et la réactivité de nouveaux complexes η^1- et ($\eta^3 \leftrightarrow \eta^5$)-indényles de Pd(II). Ce travail a permis d'établir deux voies de synthèse fiables pour leur obtention. La première implique la réaction métathétique de l'IndLi avec le complexe précurseur $(PhCN)_2PdCl_2$ et conduit, après addition de phosphines, à la formation de complexes du type (η-Ind)Pd(PR_3)Cl. La seconde méthode procède par addition oxydante du 1-Me_3Si-IndH sur le Na_2PdCl_4 et conduit à la formation du dimère $\{(\eta^3$-Ind)Pd(μ-Cl)$\}_2$, qui constitue

un excellent précurseur pour la formation d'autres complexes Ind de Pd(II), tels que $\{(\eta^1\text{-Ind})(t\text{-BuNC})\text{Pd}(\mu\text{-Cl})\}_2$ et $(\eta\text{-Ind})\text{Pd}(\text{PR}_3)\text{Cl}$, par simple addition respective de 2 équivalents de *t*-BuNC et PR_3 (Figure 1.21). Les composés ont été isolés et entièrement caractérisés par spectroscopie RMN, voltammétrie cyclique, diffraction des rayons X, et analyse élémentaire. Les études structurales effectuées ont démontré des différences significatives entre ces complexes et leurs analogues Ind-Ni, révélant une interaction métal-indényle davantage dissymétrique dans le cas des composés Ind-Pd. Les études préliminaires de leur réactivité ont également démontré qu'ils présentaient une activité catalytique supérieure à celle obtenue pour les complexes analogues Ind-Ni, notamment dans la polymérisation de l'éthylène et du phénylsilane.

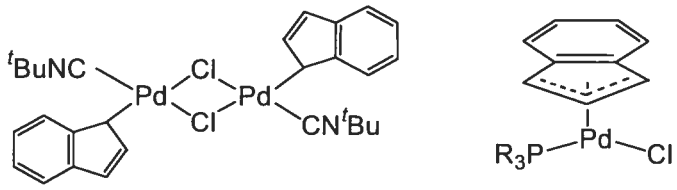

Figure 1.21: Composés Ind de Pd(II) présentés dans le chapitre 2

Le chapitre 3 de cette thèse présente la suite de nos résultats concernant l'étude des complexes Ind de Pd(II). Les composés indényles de palladium halogénés (Pd-Cl) décrits dans le chapitre précédent, ont servi de précurseurs pour l'obtention d'une autre variété de complexes indényl-palladium, Pd-X (X = méthyl, triphénylphosphine ou triflate), et ont permis d'étudier l'influence du ligand anionique X sur la structure et la réactivité de ces composés. Ils constituent d'excellents catalyseurs pour l'hydrosilylation du styrène et du phénylacétylène en présence de trichlorosilane. Les composés indényles triflate de palladium se sont aussi avérés être très efficaces pour catalyser l'isomérisation du 1-hexène, la dimérisation de l'éthylène et du styrène, l'oligomérisation et la polymérisation du p-X-styrène (X = NH_2, Me, OMe). Cette étude a ainsi permis de développer de nouveaux systèmes catalytiques grâce aux complexes indényl-palladium (Figure 1.22). Ces derniers diffèrent de leurs analogues de nickel, de par leurs caractéristiques structurales, mais aussi de par leur réactivité.

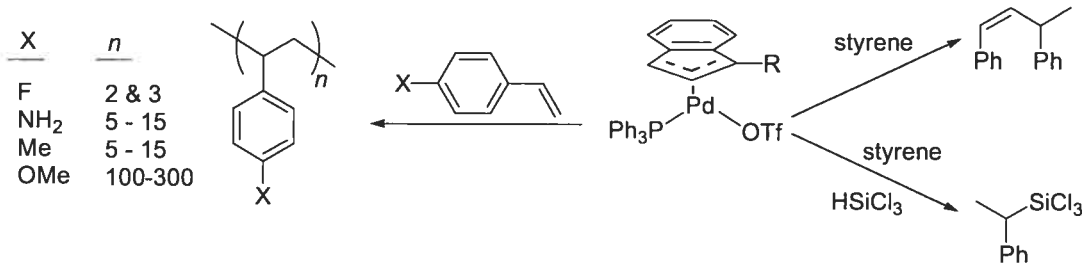

Figure 1.22: Réactivité catalytique du complexe triflate de Pd(II)

Le chapitre 4 est axé sur la préparation d'une série de nouveaux composés Ind de Pd comportant des ligands neutres L autres que des phosphines et des isocyanures, afin de permettre d'établir l'importance de ces ligands sur les caractéristiques structurales et les réactivités de ce type de composés. La réaction du dimère précédemment obtenu, $\{(\eta^3\text{-Ind})Pd(\mu\text{-Cl})\}_2$, avec des amines y est pour la première fois décrite. Ainsi, en présence de NEt_3, la réaction mène à la formation de $(\eta^3\text{-Ind})Pd(NEt_3)Cl$, tandis qu'avec $BnNH_2$ et py, des complexes comportant un ligand $(\eta^1\text{-Ind})$, *trans*-$L_2Pd(\eta^1\text{-Ind})Cl$ (L = $BnNH_2$, py), sont formés, ce qui démontre l'influence de la nature du ligand L sur l'hapticité de l'indényle. D'autre part, l'addition simultanée de $BnNH_2$ et de PR_3 sur le dimère $\{(\eta^3\text{-Ind})Pd(\mu\text{-Cl})\}_2$ conduit quant à elle à la formation des espèces mixtes: $(PR_3)(BnNH_2)Pd(\eta^1\text{-Ind})Cl$. En solution, il a été démontré que ces complexes subissaient une transformation graduelle pour générer des composés dinucléaires de Pd(I), contenant un ligand indényle pontant sur les deux centres métalliques, ce qui est peu commun. Les études préliminaires de réactivité de ces composés sont également décrites dans ce chapitre et semblent démontrer que ces espèces dinucléaires de Pd(I) sont le résultat d'une réaction de comproportionnation entre les complexes Ind-Pd(II) et des espèces de $Pd(0)(PR_3)_n$ générées in situ (Figure 1.23).

Le chapitre 5 rapporte brièvement les résultats non publiés sur les réactivités catalytiques du nouveau complexe Ind de Pd(II) obtenu, le $(1\text{-SiMe}_3\text{-Ind})Pd(PPh_3)Cl$, notamment dans les réactions de couplage de Heck et d'arylamination.

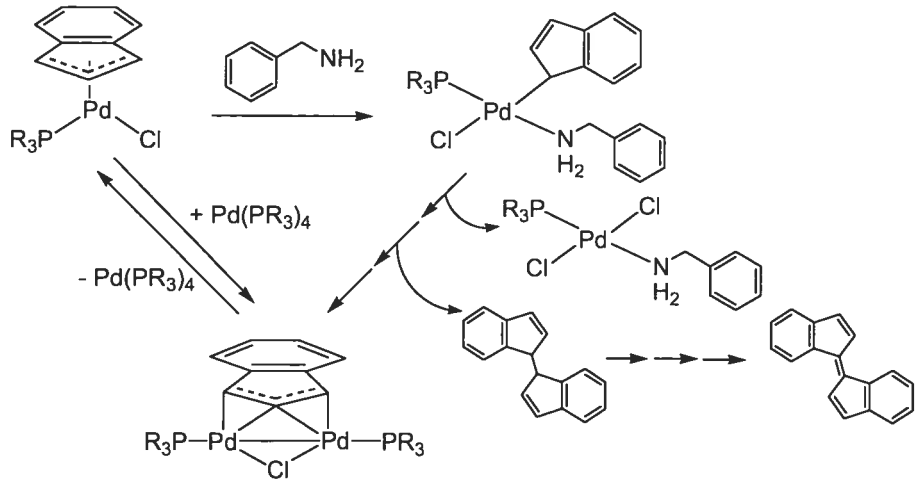

Figure 1.23: Synthèse de complexes amino η^1-Ind-Pd(II) et (μ,η^3)-Ind-Pd_2(I)

Le chapitre 6 décrit les débuts d'un projet montrant de belles perspectives: la chimie des composés indényles de platine. Les stratégies de synthèse employées jusque là dans l'obtention des composés Ind de Pd et de Ni se sont avérées infructueuses dans le cas du Pt, et la seule voie établie au cours de cette étude pour l'obtention de composés Ind-Pt repose sur la réaction métathétique de l'IndLi sur des précurseurs de type (COD)PtClX (X = Cl, Me). Il en résulte ainsi des complexes (η^1-Ind) de Pt(II), qui après addition d'$AgBF_4$ ou de HBF_4 ont permis pour la première fois, l'isolation et la caractérisation complète de complexes ($\eta^3 \leftrightarrow \eta^5$)-indényle de Pt(II). Les premiers résultats obtenus concernant leurs réactivités envers les silanes seront également présentés dans ce chapitre.

Enfin, une revue des résultats, une discussion sur l'ensemble du projet et quelques perspectives constitueront le dernier chapitre de conclusion (**chapitre 7**).

1.5 Références

[1] Schriver, D. F.; Atkins, P. W. *Inorganic Chemistry* 3rd edition; W. H. Freeman and Company: New-York, USA, **1999**, pp 583-600.

[2] (a) Vollmerhaus, R.; Bélanger-Gariépy, F.; Zargarian, D. *Organometallics* **1997**, *16*, 4762. (b) Dubois, M.-A.; Wang, R.; Zargarian, D.; Tian, J.; Vollmerhaus, R.; Li, Z.; Collins, S. *Organometallics* **2001**, *20*, 663. (c) Groux, L. F.; Zargarian, D. *Organometallics* **2001**, *20*, 3811. (d) Groux, L. F.; Zargarian, D.; Simon, L. C.; Soares, J. B. P. *J. Mol. Catal. A* **2003**, *193(1-2)*, 51. (e) Groux, L. F.; Zargarian D. *Organometallics* **2003**, *22*, 3124. (f) Groux, L. F.; Zargarian D. *Organometallics* **2003**, *22*, 4759. (h) Sun, H.; Li, W.; Han, X.; Shen, Q.; Zhang, Y. *J. Organomet. Chem.* **2003**, *688*, 132. (i) Li, W.-F.; Sun, H.-M.; Shen, Q.; Zhang, Y.; Yu, K.-B. *Polyhedron* **2004,** *23*, 1473. (j) Jimenez-Tenorio, M.; Puerta, M. C.; Salcedo, I.; Valerga, P.; Costa, S. I.; Silva, L. C.; Gomes, P. T. *Organometallics* **2004**, *23*, 3139. (k) Sun, H. M.; Shao, Q.; Hu, D. M.; Li, W. F.; Shen, Q.; Zhang, Y. *Organometallics* **2005**, *24*, 331. (l) Gareau, D.; Sui-Seng, C.; Groux, L. F.; Brisse, F.; Zargarian, D. *Organometallics* **2005**, *24*, 4003.

[3] (a) Wang, R.; Bélanger-Gariépy, F.; Zargarian, D. *Organometallics* **1999**, *18*, 5548. (b) Wang, R.; Groux, L. F.; Zargarian D. *Organometallics* **2002**, *21*, 5531. (c) Wang, R.; Groux, L. F.; Zargarian, D. *J. Organomet. Chem* **2002**, *660*, 98. (d) Rivera, E.; Wang, R; Zhu, X. X.; Zargarian, D.; Giasson, R. *J. Molec. Catal. A* **2003**, *204-205*, 325.

[4] (a) Fontaine, F. -G.; Kadkhodazadeh, T.; Zargarian, D. *J. Chem. Soc., Chem. Commun.* **1998**, 1253. (b) Fontaine, F.-G.; Zargarian, D. *Organometallics* **2002**, *21*, 401.

[5] (a) Fontaine, F.-G.; Nguyen, R.-V.; Zargarian, D. *Can. J. Chem.* **2003**, *81*, 1299. (b) Chen, Y, F.; Sui-Seng, C.; Boucher, S.; Zargarian, D. *Organometallics* **2005**, *24*, 149.

[6] (a) Rerek, M. E.; Ji, L.-N.; Basolo, F. *J. Chem. Soc., Chem. Commun.* **1983**, 1208. (b) Ji, L.-N.; Rerek, M. E.; Basolo, F. *Organometallics* **1984**, *3*, 740. (c) Casey, C. P.;

O'Connor, J. M. *Organometallics* **1985**, *4*, 384. (d) O'Connor, J. M.; Casey, C. P. *Chem. Rev.* **1987**, *87*, 307.

[7] (a) Frankom, T. M.; Green, J. C.; Nagy, A.; Kakkar, A. K.; Marder, T.B. *Organometallics* **1993**, *12*, 3688. (b) Gamasa, M. P.; Gimeno, J.; Gonzalez-Bernado, C.; Martin-Vaca B., M.; Monti, D.; Basseti, M. *Organometallics* **1995**, *15*, 302.

[8] Revue portant sur les complexes η^1-Ind des métaux de transition: Stradiotto, M.; McGlinchey, M. J. *Coord. Chem. Rev.* **2001**, *219-221*, 311.

[9] Hart-Davis, A. J.; Mawby, R. J. *J. Chem. Soc. (A)* **1969**, 2403.

[10] Jones, D. J.; Mawby, R. J. *Inorg. Chem. Acta* **1972**, *6*, 157

[11] Pevear, K. A.; Banaszak, Holl, M. M.; Capenter, A. L.; Rieger, P. H.; Sweigart, D. A. *Organometallics* **1995**, *14*, 212.

[12] (a) Baker, T.; Tulip, T. H. *Organometallics* **1986**, *5*, 839. (b) Wetscott, S. A.; Kakkar, A. K.; Stringer, G.; Taylor, N. J.; Marder, T. B. *J. Organomet. Chem.* **1990**, *394*, 777.

[13] Forschner, T. C.; Cutler, A. R.; Kullnig, R. K. *Organometallics* **1987**, *6*, 889.

[14] Köhler, F. H. *Chem. Ber.* **1974**, *107*, 570.

[15] (a) Cotton, F. A.; Wilkinson, G.; Murillo, C. A.; Bochmann, M. *Advanced Inorganic Chemistry* 6th edition, Wiley-Interscience, New-York, USA, **1999**, pp. 1005-1006, 1063-1084. (b) Collman, J. P.; Hegedus, L. S.; Norton, J. R.; Finke, R. G. *Principles and Application of Organotransition Metal Chemistry;* University Science Books: Sausalito, California, USA, **1987,** pp. 58-59, 66-72, 80-100.

[16] Gibson, V. C.; Spitzmesser, S. K. *Chem. Rev.* **2003**, *103*, 283.

[17] (a) Keim, W.; Kowaldt, F. H.; Goddard, R.; Krüger, C. *Angew. Chem. Int. Ed.* **1978**, *17*, 466. (b) Klabunde, U.; Mulhaupt, R.; Herskovitz, T.; Janowicz, A. H.; Calabrese, J.; Ittel, S. D. *J. Polym. Sci. A* **1987**, *25*, 1989.

[18] (a) Johnson, L. K.; Killan, C. M.; Brookhart, M. *J. Am. Chem. Soc.* **1995**, *117*, 6414. (b) Svejda, S. A.; Johnson, L. K.; Brookhart, M. *J. Am. Chem. Soc.* **1999**, *121*, 10 634.

[19] Younkin, T. R.; Connor, E. F.; Henderson, J. I.; Friedrich, S. K.; Grubbs, R. H.; Bansleben, D. A. *Science* **2000**, *287*, 460.

[20] (a) Tsuji, J. *Palladium Reagents and Catalysts*; John Wiley & Sons, Chichester, England, **1995**. (b) Heck, R. F. *Palladium Reagents in Organic Synthesis*; Academic Press, New-York, USA, **1985**. (c) Trost, B. M.; Verhoven, T. R. in *Comprehensive Organometallic Chemistry*; Wilkinson, G; Stone, F. G.; Abel, E. W. Eds.; Pergamon: Oxford **1982**, *8*, 799-938.

[21] (a) Lai, T. W.; Sen, A. *Organomeallics* **1984**, *3*, 866. (b) Sen, A.; Lai, T. W. *J. Am. Chem. Soc* **1982**, *104*, 3520. (c) Drent, E.; Van Broekhoven, J. A. M.; Doyle, M. J. *J. Organomet. Chem.* **1991**, *417*, 235. (d) Drent, E. Budzelaar, P. H. M. *Chem. Rev.* **1996**, *96*, 663.

[22] (a) Smidt J.; Hafner, W.; Jira, R.; Sedlmeier, J.; Sieber, R.; Ruttingen, R.; Kojer, H. *Angew. Chem.* **1959,** *71*, 176. (b) Smidt, J.; Hafner, W.; Jira, R.; Sieber, J.; Sedlmeier, J.; Sabel, A. *Angew. Chem.* **1962,** *74*, 93.

[23] Dounay, A. B.; Overmann, L. E. *Chemical Reviews* **2003**, *103*, 2945.

[24] (a) Heck, R. F.; Nolley, J. P. *J. Org. Chem.* **1972**, *37*, 2320. (b) Dieck, H. A.; Heck, R. F. *J. Am. Chem. Soc.* **1974**, *96*, 1133. (c) Dieck, H. A.; Heck, R. F.; Nolley, J. P. *J. Org. Chem.* **1975**, *40*, 1083.

[25] (a) Suzuki, A. in *Metal-Catalyzed Cross-Coupling Reactions*; Diederich, F.; Stang, P. J.; Eds; Wiley-VCH: Weinheim, Germany, **1998**, 49-97. (b) Suzuki, A. *Pure Appli. Chem.* **1991**, *63*, 419.

[26] (a) Stille, J. K.; Milstein, D. *J. Am. Chem. Soc.* **1978**, *100*, 3636. (b) Stille, J. K. *Angew. Chem.* **1986**, *98*, 504. (c) Scott, W. J.; Stille, J. K. *J. Am. Chem. Soc.* **1986**, *108*, 3033.

[27] (a) Yang, B. H. ; Buchwald, S. L. *J. Organomet. Chem.* **1999**, *576*, 125. (b) Hartwig, J. F. *Acc. Chem. Res.* **1998**, *31*, 852. (c) Hartwig, J. F. *Angew. Chem., Int Ed. Engl.* **1998**, *37*, 2046.

[28] Ogasarawa, M.; Yoshida, K.; Hayashi, T. *Heterocycles* **2000**, *52*, 195.

[29] (a) Zhang, C.; Huang, J.; Trudell, M. L.; Nolan, S. P. *J. Org. Chem* . **1999**, *64*, 3804. (b) Grasa, G. A.; Viciu, M. S.; Huang, J. ; Zhang, C.; Trudell, M. L. ; Nolan, S. P. *Organometallics* **2002**, *21*, 2866.

[30] (a) Alcazar-Roman, L. M.; Hartwig, J. F.; Rheingold, A. L.; liable-Sands, l. M.; Guzer, I. A. *J . Am. Chem. Soc.* **2000**, *122*, 4618. (b) Driver, M. S.; Hartwig, J. F. *J. Am. Chem. Soc.* **1996**, *118*, 7217. (c) Louie, J.; Driver, M. S. ; Hamann, B. C.; Hartwig, J. F.; *J. Org. Chem.* **1997**, *62*, 1268.

[31] (a) Old, D. W.; Wolfe, J. P.; Buchwald, S. L. *J. Am. Chem. Soc.* **1998**, *120*, 9722. (b) Singer, R. A.; Sadighi, J. P.; Buchwald, S. L. *J. Am. Chem. Soc.* **1998**, *120*, 213.

[32] (a) Trost B. M. ; Dietsch, T. J. *J. Am. Chem. Soc.* **1973**, *95*, 8200. (b) Trost B. M. ; Fullerton, T. J. *J. Am. Chem. Soc.* **1973**, *95*, 292. (b) Tsuji, J.; Takahashi, H. ; Morikawa, M. *Tetrahedron Lett.* **1965**, 4387.

[33] Heck, R. F. *Pure Appl. Chem.* **1978**, *50*, 691.

[34] (a) Kawatsura, M.; Hartwig, J. F. *J. Am. Chem. Soc.* **2000**, *122*, 9546. (a) Nettekoven, U.; Hartwig, J. F. *J. Am. Chem. Soc.* **2002**, *124*, 1166.

[35] Lapointe, A. M.; Rix, F. C.; Brookhart, M. *J. Am. Chem. Soc.* **1997**, *119*, 906.

[36] Ojima, I. *The Chemistry of Organic Silicon Compounds,* Chapter 25, Patai and Rappoport; John Wiley & Sons, New-York, USA, **1989**.

[37] Schroll, G. E. US patent-3 054 815, **1962**.

[38] Zargarian, D. *Coord. Chem. Rev.* **2002**, *233-234*, 157.

[39] (a) Huber, T. A.; Bélanger-Gariépy, F.; Zargarian, D. *Organometallics* **1995**, *14*, 4997. (b) Huber, T. A.; Bayrakdarian, M.; Dion, S.; Dubuc, I.; Bélanger-Gariépy, F.; Zargarian, D. *Organometallics* **1997**, *16*, 5811. (c) Fontaine, F. –G.; Dubois, M. –A.; Zargarian, D. *Organometallics* **2001**, *20*, 5156. (d) Dubois M. –A., Mémoire de Maîtrise, Université de Montréal, **2000**. (e) Fontaine F. –G., Thèse de Doctorat, Université de Montréal, **2003**. (f) Boucher S., Mémoire de Maîtrise, Université de Montréal, **2006**.

[40] (a) Dubuc, I.; Dubois, M. –A.; Bélanger-Gariépy, F. ; Zargarian, D. *Organometallics* **2002**, *18*, 30. (b) Isabelle Dubuc, Mémoire de Maîtrise, Université de Montréal, **1998**.

[41] Wang, R., Zargarian, D. Résultats non publiés.

[42] Groux, L. F.; Zargarian, D. *Organometallics* **2000**, *19*, 1507.

[43] Gareau D., Mémoire de Maîtrise, Université de Montréal, **2005**.

[44] (a) Mushak, P.; Battiste, M. A. *J. Organomet. Chem.* **1969**, *17*, P46. (b) Fiato, R. A.; Mushak, P.; Battiste, M. A. *J. Chem. Soc., Chem. Commun.* **1975**, 869.

[45] Nakasuji, K.; Yamaguchi, M.; Murata, I.; Tatsumi, K.; Natamura, A. *Organometallics* **1984**, *3*, 1257.

[46] Samuel, E.; Bigorgne, M. *J. Organomet. Chem.* **1969**, *19*, 9.

[47] (a) Tanase, T.; Nomura, T; Yamamoto, Y.; Kobayashi, K. *J. Organomet. Chem.* **1991**, *410*, C25. (b) Tanase, T.; Nomura, T.; Fukushina, T.; Yamamoto, Y.; Kobayashi, K. *Inorg. Chem.* **1993**, *32*, 4578

[48] (a) Alias, F. M.; Belderrain, T. R.; Paneque, M.; Poveda, M. L.; Carmona, E. *Organometallics* **1998**, *17*, 5620; (b) Alias, F. M.; Belderrain, T. R.; Carmona, E.; Graiff, C.; Paneque, M.; Poveda, M. L. *J. Organomet. Chem.* **1999**, *577*, 316.

[49] Lin, S.; Boudjouk, P. *J. Chin. Chem. Soc.* **1989**, *36*, 35.

[50] (a) Vicente, J.; Abad, J.-A.; Bergs, R.; Jones, P. G.; De Arellano, M. C. R. *Organometallics* **1996**, *15*, 1422. (b) Vicente, J.; Abad, J.-A.; Bergs, R.; De Arellano, M. C. R.; Martinez-Vivente, E.; Jones, P. G. *Organometallics* **2000**, *19*, 5597.

[51] (a) O'Hare, D. *Organometallics* **1987**, *6*, 1766. (b) O'Hare, D. *J. Organomet. Chem.* **1987**, *323*, C13-C17.

[52] Ackermann, M. N.; Ajmera, R. K.; Barnes, H. E.; Gallucci, J. C.; Wojicicki, A. *Organometallics* **1999**, *18*, 787.

Chapitre 2: New Routes to η^1- and $(\eta^3 \leftrightarrow \eta^5)$-Indenylpalladium Complexes: Synthesis, Characterization, and Reactivities

Article 1

Christine Sui-Seng,[a] Gary D. Enright,[b] and Davit Zargarian*[a]

[a] Département de chimie, Université de Montréal, Québec, Canada H3C 3J7

[b] Steacie Institute for Molecular Sciences, National Research Council, Ottawa, Ontario, Canada K1A 0R6

Organometallics **2004**, *23*, 1236-1246

Abstract

The dimer $\{(\eta^3\text{-Ind})\text{Pd}(\mu\text{-Cl})\}_2$ (**6**) reacts with *t*-BuNC to give the dimeric species $\{(\eta^1\text{-Ind})(t\text{-BuNC})\text{Pd}(\mu\text{-Cl})\}_2$ (**10**), whereas reaction with PR_3 gives the complexes $(\eta\text{-Ind})\text{Pd}(PR_3)\text{Cl}$ (R = Ph (**4**), Cy (**7**), Me (**8**), OMe (**9**)). Complexes **4** and (1-Me-Ind)Pd(PPh_3)Cl (**5**) can also be prepared via the reaction of $(PhCN)_2PdCl_2$ with LiInd and PPh_3. The structural characterization of complexes **4**-**7**, **9**, and **10** by ^1H and ^{13}C NMR spectroscopy and single crystal X-ray diffraction studies has allowed an analysis of the indenyl ligand's mode of coordination, both in the solid-state and in solution. Compounds **4**, **6**, and **7** react with $PhSiH_3$ in the absence of cocatalysts, whereas reaction with ethylene requires the presence of excess MAO to give polyethylene.

Introduction

In comparison to their Cp analogues, some indenyl complexes of transition metals possess enhanced reactivities in catalysis and in various stoichiometric reactions, notably ligand substitution. This characteristic has been attributed to the relative ease with which metals can slip reversibly across the indenyl ligand's five-membered ring, thus forming a reactive η^3-indenyl tautomer that has both benzenoid resonance stabilization and an accessible coordination site on the metal. Various manifestations of this so-called "indenyl effect",[1] including superior catalytic activities,[2] have been observed for many indenyl complexes, in particular those of group 6-9 metals.[3] In contrast, the chemistry of group 10 metal indenyl complexes is at an early phase of its development.[4]

Our group has studied the chemistry of the complexes IndNi(L)(X) (Ind = indenyl and its substituted derivates),[5] some of which can act as precatalysts in the oligo- and polymerization of alkenes,[6] alkynes,[7] and $PhSiH_3$,[8] and in the hydrosilylation of alkenes and ketones.[9] Our interest in the structures and catalytic activities of the IndNi complexes prompted us to explore the chemistry of analogous

Pd compounds in order to elucidate the influence of the metal center on the chemistry of these compounds. Relatively little is known about the reactivities of IndPd complexes, but the preparation and characterization of the following compounds have been reported: $\{(\eta^3\text{-Ind})Pd(\mu\text{-Cl})\}_2$,[10] $\{(\mu\text{-}\eta^3\text{-Ind})Pd(CNR)\}_2$ (R = *t*-Bu, 2,6-$(CH_3)_2C_6H_3$; 2,4,6-$(CH_3)_3C_6H_2$; 2,4,6-(*t*-Bu)$_3C_6H_2$),[11] $(\eta^3\text{-Ind})Pd(PMe_3)(CH(SiMe_3)_2)$,[12] and $[(\eta^3\text{-Ind})Pd(LL)]^+$ [13] (LL = bipy, tmeda). In addition, a preliminary communication has appeared on the preparation of a series of Ind derivates from the reaction of cyclopropene and $(PhCN)_2PdCl_2$.[14]

Herein we report two different synthetic routes to the complexes $(\eta\text{-Ind})Pd(PR_3)Cl$ (R= Ph, Cy, Me, OMe) and compare their structures and reactivities to those of their analogous Ni complexes. The preparation of the dimeric complex $\{(\eta^1\text{-Ind})(t\text{-BuNC}))Pd(\mu\text{-Cl})\}_2$ from the precursor $\{(\eta^3\text{-Ind})Pd(\mu\text{-Cl})\}_2$ and the solid-state structures of these dimeric species will also be described.

Results and Discussion

Synthesis. The main synthetic pathway to IndPd compounds involves the metathetic reactions of MInd (M = Li, Na) with various L_nPdCl_m precursors (Scheme 2.1).[10-12]

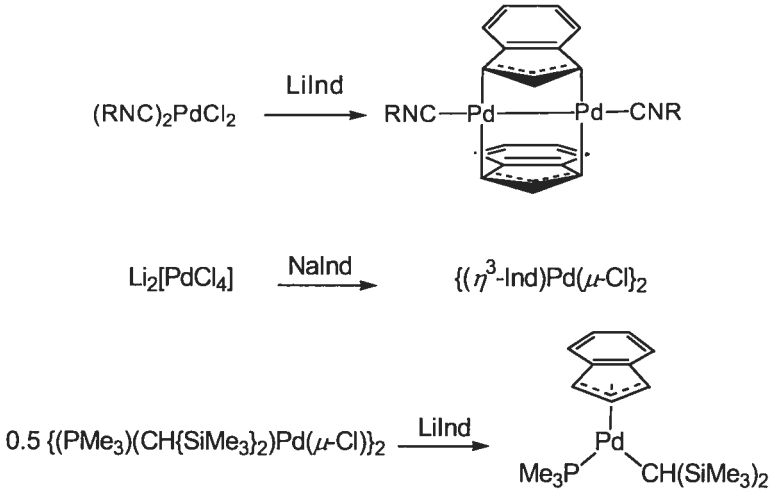

Scheme 2.1

However, when we applied this methodology for the synthesis of the complexes $IndPd(PR_3)Cl$ from the precursors $(PR_3)_2PdCl_2$ (R= Ph, Me), we obtained the homocoupling products 1,1'-biindene and $Pd(PR_3)_n$ (Scheme 2.2). A similar observation has been made during the syntheses of the analogous $IndNi(PR_3)Cl$ complexes.[5a] These side reactions may be attributed to the sequence of steps depicted in Scheme 2.2: reaction of Ind^- with the precursors gives the initial intermediate (η^1-Ind)$M(PR_3)_2Cl$; conversion of the latter to the desired (η-Ind)$M(PR_3)Cl$ is hampered by the slow dissociation of one of the phosphine ligands;[15] this brings about the competitive addition of a second equivalent of Ind^- to give $(\eta^1\text{-Ind})_2M(PR_3)_2$, which produces 1,1'-biindene and $M^{(0)}(PR_3)_n$ presumably by reductive elimination.[16]

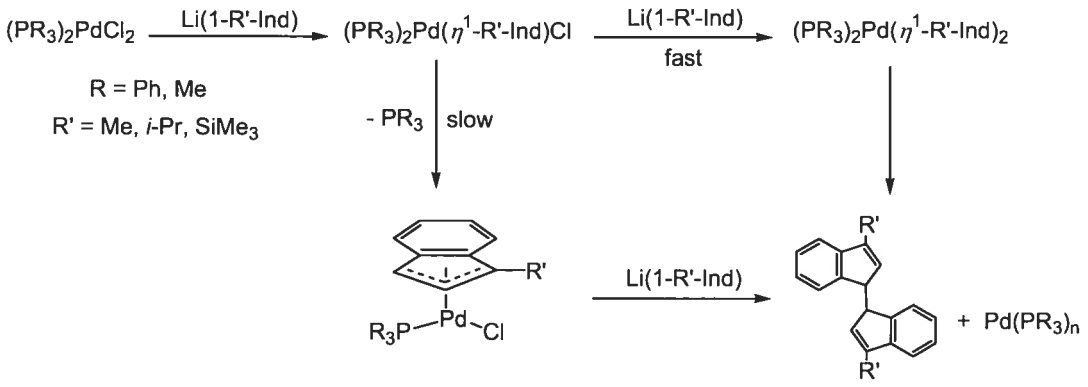

Scheme 2.2

In an attempt to circumvent the above-discussed homocoupling side reaction, we studied the use of alkyl-substituted Ind precursors Li(1-R-Ind), (R= Me, *i*-Pr, $SiMe_3$), a strategy that was successful in suppressing the coupling side reaction in the case of Ni precursors.[5c] Interestingly, however, this approach had no effect on the course of the Pd reactions, implying that the Pd precursors are more effective for the coupling reaction.[17]

We surmised that the use of Pd precursors bearing more labile auxiliary ligands would accelerate ligand dissociation from the putative intermediate (η^1-Ind)PdL_2Cl (Scheme 2.2), thereby favoring the formation of the target complexes. Indeed, reacting $(PhCN)_2PdCl_2$ (**1**) with Li(1-R-Ind) (R= H, Me) appeared to give the target complexes

IndPd(NCPh)Cl, as indicated by a color change from yellow to dark brown; the isolation of the new products was hampered, however, by a gradual decomposition that occurred even at -78 °C to give an insoluble black solid. To circumvent this decomposition, we added ca. 0.6 equiv of PPh_3 to the reaction mixture following the addition of Li(1-R-Ind) in order to convert the presumably thermally unstable IndPd(NCPh)Cl to the phosphine adduct (Scheme 2.3). This approach led to the isolation of (1-R-Ind)Pd(PPh_3)Cl (R = H (4), R = Me (5)) as brown-red powders in moderate yields (36% on the basis of $(PhCN)_2PdCl_2$, 60% on the basis of PPh_3). It is noteworthy that reacting **1** with a mixture of LiInd and PPh_3 at -78 °C, or adding LiInd to a mixture of **1** and PPh_3 at low temperature, produced mainly $(PPh_3)_2PdCl_2$, Pd(0), and 1,1'-biindene, and only a small amount of the target complexes **4** and **5**.

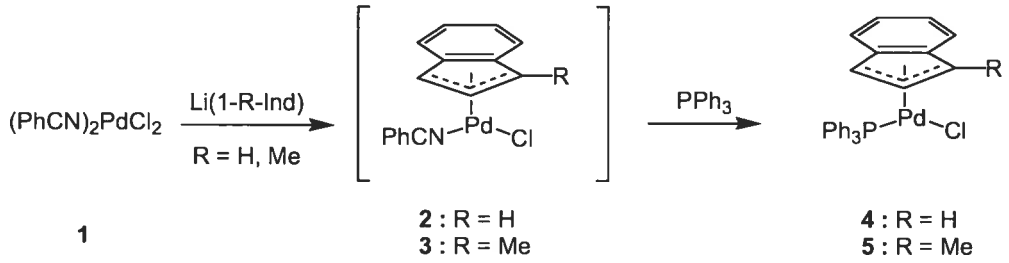

1

2 : R = H
3 : R = Me

4 : R = H
5 : R = Me

Scheme 2.3

The low yields obtained from the metathetic reactions outlined above prompted us to explore alternative routes not involving anionic sources of Ind in order to minimize the homocoupling side reaction. Indeed, Boudjouk and Lin have reported that 1-$SiMe_3$-Ind can be an effective source for the preparation of the polymeric species $\{(\eta^3\text{-Ind})Pd(\mu\text{-Cl})\}_n$ (Scheme 2.4).[18] The latter seemed like a promising precursor to the complexes (η-Ind)Pd(L)Cl. This approach was attempted and proved successful, as described below.

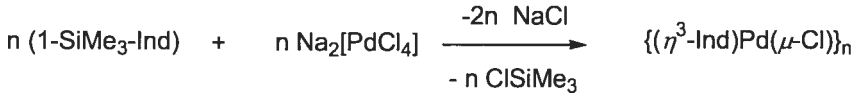

Scheme 2.4

Reacting 8.3 mmol of 1-$SiMe_3$-Ind with 7.2 mmol of $Na_2[PdCl_4]$ in ethanol gave a brown mixture from which a brown solid precipitated gradually. Filtration and successive washing of the collected solid with distilled water, Et_2O, and ethanol gave a material whose physical appearance matched that of the compound $\{(\eta^3\text{-Ind})Pd(\mu\text{-Cl})\}_n$ reported by Boudjouk and Lin.[18] Interestingly, however, the NMR data for this product were different from those reported by Boudjouk and Lin, but exactly similar to the data reported by Murata's group for the dimer $\{(\eta^3\text{-Ind})Pd(\mu\text{-Cl})\}_2$ **6**.[10a] To establish the identity of this compound unequivocally, we undertook an X-ray diffraction study that confirmed the dimeric structure of the product of our synthesis (vide infra). The factors responsible for the preferred formation in our syntheses of the dimer, as opposed to the polymeric species proposed by Boudjouk and Lin, are not known. Nevertheless, in our hands Boudjouk's procedure gives access to 80-90% yields of complex **6**, which has served as a versatile precursor for the preparation of other IndPd complexes, as outlined below.

The monomeric phosphine adducts (η-Ind)Pd(PR_3)Cl (R = Ph (**4**), Cy (**7**), Me (**8**), OMe (**9**)) were obtained by reacting the dimeric product **6** with PR_3 (Scheme 2.5); these complexes have been isolated as orange-red solids in ca. 70-90% yields. On the other hand, a different reactivity was observed when **6** was reacted with CO and *t*-BuNC. Thus, reaction with CO resulted in a color change from brown to red, but this change was maintained only as long as the solution was saturated with CO. The ^1H NMR spectrum of the mixture (with CO present in the head gas) showed that the signals due to **6** had been replaced by a series of broad peaks, while the $^{13}C\{^1H\}$ NMR spectrum displayed no signals at all, implying an exchange process. Curiously, the IR spectrum did not show any absorption in the ν(CO) region. All attempts at isolating the new species were unsuccessful, as evaporation of the solvent or addition of hexane to precipitate the product resulted in the regeneration of the starting material. We conclude, therefore, that the putative CO adduct is in equilibrium with **6**.

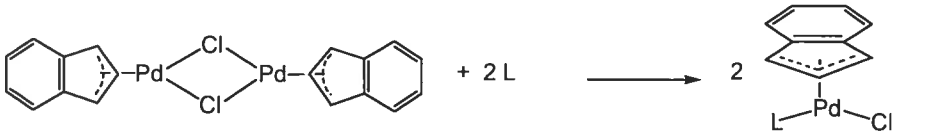

6

4 : L = PPh_3
7 : L = PCy_3
8 : L = PMe_3
9 : L = $P(OMe)_3$

Scheme 2.5

In contrast, *t*-BuNC converted **6** to the dimeric derivative $\{(\eta^1\text{-Ind})(t\text{-BuNC})Pd(\mu\text{-Cl})\}_2$ (**10,** Scheme 2.6), which could be isolated in 57% yield. Complex **10** is the first example of an isolated and fully characterized $Pd^{(II)}$ complex featuring an η^1-Ind moiety, but Poveda and co-workers have reported the in situ generation and spectroscopic characterization of a monomeric $(\eta^1\text{-Ind})Pd^{(II)}$ complex (Scheme 2.7).[12a] The conversion of **6** to the complexes **4** and **7-10** is analogous to a ligand displacement reaction and likely proceeds by the initial coordination of the incoming ligand (associative mechanism); it is interesting to note, however, that phosphine ligands displace the bridging Cl, whereas *t*-BuNC causes a change in the hapticity of Ind.

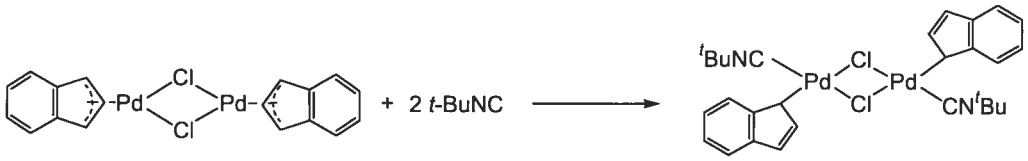

6 **10**

Scheme 2.6

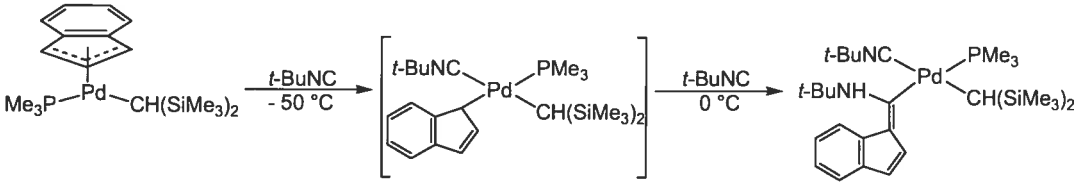

Scheme 2.7

Compounds **4-10** are thermally stable and can be handled in air for a few hours (both in the solid and in solution) without appreciable decomposition. The identities of these complexes were deduced from their NMR spectra and confirmed by the results of elemental analyses and single-crystal X-ray diffraction studies. These studies have provided valuable information on the structural features of this family of complexes, as described in the following section.

Spectroscopic Characterization. A singlet resonance is observed in the $^{31}P\{^{1}H\}$ NMR spectra of the complexes **4**, **5**, and **7-9**, similar to those of the analogous Ni compounds; in the case of **4**, **5**, and **8**, the ^{31}P chemical shifts are close to the corresponding signals of their Ni homologues (Table 2.I).

Table 2.I. Electrochemical and NMR Data for Complexes **4-9** and Analogous Nickel Complexes[a]

Compound	$^{31}P\{^{1}H\}$ (δ, ppm)	H1/H3 (δ, ppm)	C1/C3 (δ, ppm)	$\Delta\delta_{av}$ (ppm)	E_{red1}[c] (V)	E_{red2}[c] (V)
(Ind)Pd(PPh_3)Cl, **4**	27.98	6.51/4.57	97.2/79.9	6.7	-0.94	-1.41
(Ind)Ni(PPh_3)Cl, **11**	28.20	5.91/3.33[b]	90.2/69.71[b]	-2	-0.64	
(1-Me-Ind)Pd(PPh_3)Cl, **5**	30.03	---/4.28	113.3/76.5	8.5	-1.03	-1.48
(1-Me-Ind)Ni(PPh_3)Cl, **12**	31.10	---/3.37	103.4/67.2[c]	-2.0	-0.75	-1.05
(Ind)Pd(PCy_3)Cl, **7**	49.04	6.21/5.11	94.3/ 70.9	8.5	-1.07	-1.64
(1-Me-Ind)Ni(PCy_3)Cl	37.17	---/4.11	97.10/55.42	-1.0		
(Ind)Pd(PMe_3)Cl, **8**	-7.56	6.42/5.26	97.0/ 70.2	6.6	-1.24	
(1-Me-Ind)Ni(PMe_3)Cl	-10.61	---/3.58	101.29/59.53	-2.0		
(Ind)Pd($P(OMe)_3$Cl, **9**	131.21[d]	6.49/5.69[d]	99.4/ 73.2[d]	6.3[d]		

[a]Unless otherwise indicated, all spectroscopic data collected at r.t. in C_6D_6. [b]233 K, Toluene-D_8. [c]Acetone-D_6. [d]$CDCl_3$. [e]CH_3CN

The ^{1}H NMR and $^{13}C\{^{1}H\}$ NMR spectra of these compounds were also quite similar to those of the corresponding Ni compounds. Reliable peak assignments were made by

means of inverse-gated decoupling, COSY, and HMQC experiments; the results of these detailed studies have proven particularly informative for the coordination mode of the Ind ligand in these compounds. For instance, the ^{13}C NMR spectra of Ind complexes can help identify the type of M-Ind interactions present in solution following an empirical protocol described by Baker[19] and Marder.[20] According to this protocol, the magnitude of the parameter $\Delta\delta_{av}(^{13}C) = \delta_{av}$(C3a/ C7a of M-Ind) – δ_{av}(C3a/C7a of $Na^{+}Ind^{-}$) (ca. 130.7 ppm) reflects the solution hapticity of the Ind ligand in a given complex; thus, the solution hapticity is thought to be closer to η^5 when $\Delta\delta_{av}(C) \ll 0$ (e.g., $\Delta\delta_{av}$(C) for Ind_2Fe is ca. – 42 ppm),[20] closer to η^3 when $\Delta\delta_{av}(C) \gg 0$ (e.g., $\Delta\delta_{av}$(C) for $(Ind)Ir(PMe_3)_3$ is ca. +28 ppm),[21] and intermediate when $\Delta\delta_{av}(C) \approx 0$ (e.g., $\Delta\delta_{av}$(C) for $(Ind)_2Ni$ [22] is ca. +5 ppm).[20] The $\Delta\delta_{av}$(C) for our complexes are ca. +6.5 ppm for **4**, **6**, **8** and **9** and ca. +8.5 ppm for **5** and **7** (Table 2.I); in comparison, $\Delta\delta_{av}$(C) values for the analogous IndNi complexes are *ca.* -2 ppm, indicating that the $\eta^5 \rightarrow \eta^3$ distortions in the Ind hapticity are much greater in the Pd complexes.

The chemical shifts of the symmetry-related carbons C1 and C3 (labeling shown in Chart 1 and on ORTEP diagrams) and their respective protons H1 and H3 also help shed light on the character of the Pd-Ind interaction. Inspection of the data in Table 1 shows that H3 resonates upfield of H1 by more than 1 ppm, while C3 resonates upfield of C1 by more than 20 ppm in all compounds. This phenomenon, which has also been observed for the analogous Ni complexes,[4] can be attributed to the relatively large difference in the *trans* influences of PR_3 and Cl ligands;[23] the nonsymmetrical Pd-C interactions resulting from this difference distort the Ind-Pd bonding toward a localized mode (η^1:η^2, Chart 2.1), which is manifested in different hybridizations at C1 (closer to sp^2) and C3 (closer to sp^3).

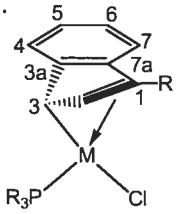

(η^1, η^2)

Chart 2.1

Another consequence of nonsymmetrical Pd-Ind interactions in solution is a high energy barrier for the rotation of the Ind ligand about the Pd-Ind axis. This was measured experimentally by studying the variable temperature ^{1}H NMR spectra for complexes **4**, **7**, and **9**. The coalescence temperature (T_c) and the frequency differences ($\delta\nu$) measured for each pair of exchanging resonances (H1/H3, H4/H7, H5/H6) allowed us to estimate an average energy barrier for the rotation of indenyl rings using the Holmes-Gutowski equation.[24] The $\Delta G^{\ddagger}$ value of ca. 16.5 kcal/mol obtained for the complexes **4**, **7**, and **9** is similar to the values of ca. 16 kcal/mol measured for the analogous Ni-Cl complexes, whereas energy barriers of ca. 10 Kcal/mol have been measured for the corresponding Ni-Me complexes.

The NMR data obtained for complex **10** were very similar to those found for other transition metal η^1-Indenyl complexes that have been reported in the literature.[12a,25] In the ^{1}H NMR spectrum of **10**, the proton on the carbon bonded directly to palladium appeared as a broad signal at 5.85 ppm, whereas the six remaining, nonequivalent Ind protons gave rise to three doublets at 6.77 ppm (H2), 7.32 ppm (H7), 7.89 ppm (H4) and one multiplet between 7.02 and 7.12 ppm for H3, H5 and H6. In the ^{13}C NMR spectrum, the chemical shift of the signal for C1 (44.1 ppm) differs substantially from that of the η-Ind complexes **4**, **5**, and **7-9**.

Solid-state Structural Studies. X-ray crystallographic analyses of the IndPd complexes prepared during the course of this work were undertaken to study the type of Ind-Pd interactions present in each compound (e.g., η^3 versus η^1 in **6** and **10**) and the influence on Ind hapticity of the auxiliary ligands (e.g., μ-Cl in **6** versus PR_3 and Cl in **4**, **5**, **7**, and **9**), phosphine substituents (**4** versus **7** and **9**),[26] and Ind substituent (**4** versus **5**). The ORTEP views for these complexes are shown in Figures 2.1-2.3, while crystal data and details of the diffraction experiments are listed in Table 2.II (for **4**, **5**, **7** and **9**) and 2.III (for **6** and **10**). A selection of bond distances and angles is given in Table 2.IV (for **4**, **5**, **7** and **9**)[27] and Table 2.V (for **6**[28] and **10**); the corresponding data for the compounds IndNi(PPh_3)Cl, **11**,[5a] and (1-Me-Ind)Ni(PPh_3)Cl (**12**)[5c] are also

included in Table 2.IV to facilitate structural comparisons between the Pd and Ni complexes.

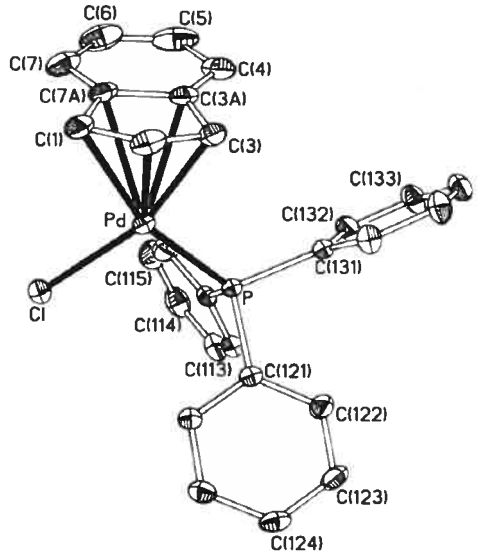

4

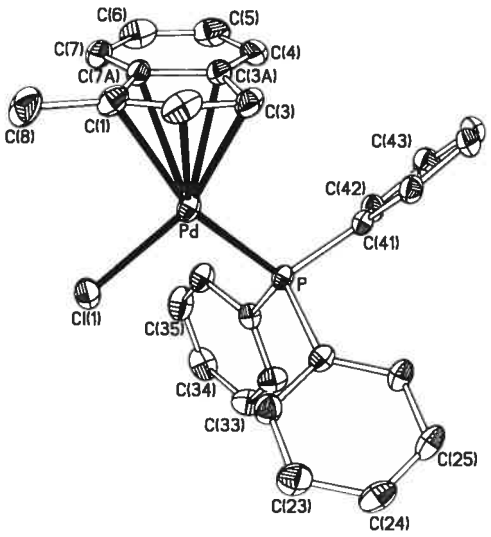

5

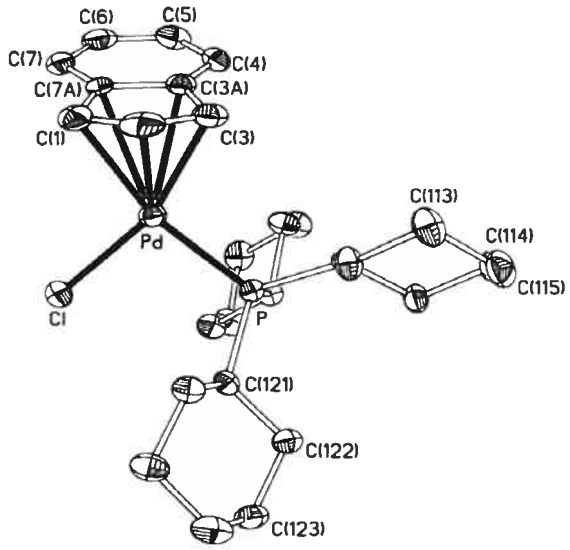

7

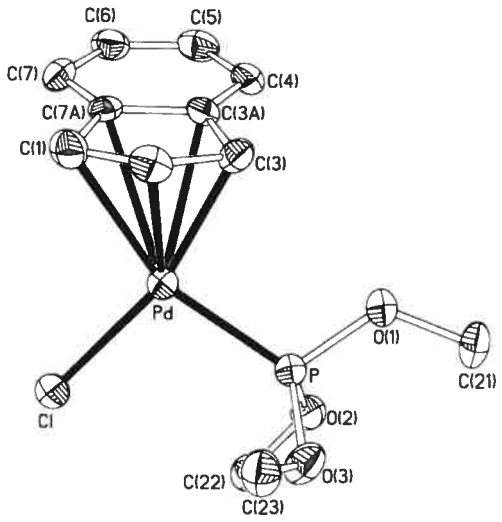

9

Figure 2.1: ORTEP views of complexes **4**, **5**, **7** and **9**. Thermal ellipsoids are shown at 30% probability and hydrogen atoms are omitted for clarity.

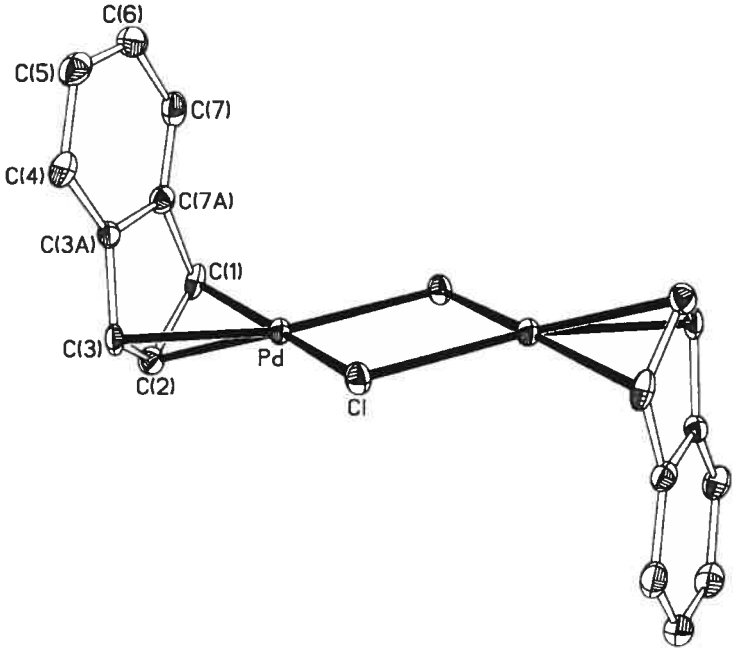

Figure 2.2: ORTEP view of complex **6**. Thermal ellipsoids are shown at 30% probability and hydrogen atoms are omitted for clarity.

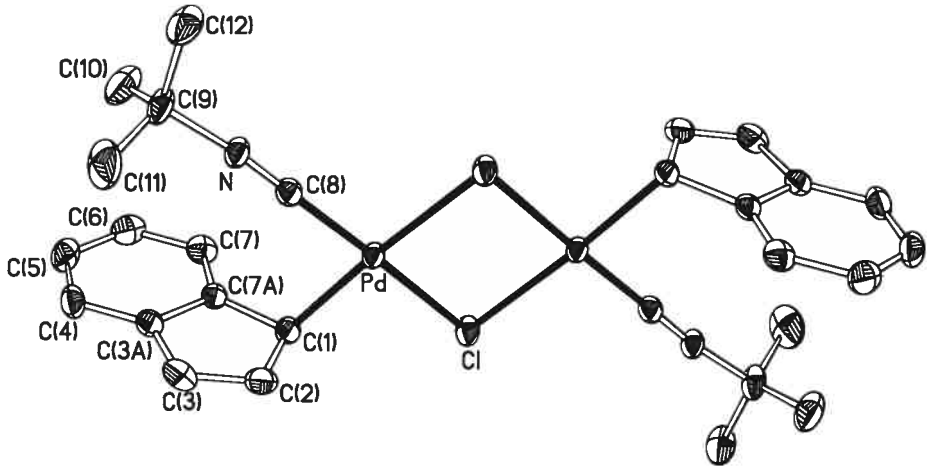

Figure 2.3: ORTEP view of complex **10**. Thermal ellipsoids are shown at 30% probability and hydrogen atoms are omitted for clarity.

Table 2.II. Crystal Data, Data Collection, and Structure Refinement Parameters of **4**, **5**, **7** and **9**

	4	**5**	**7**	**9**
formula	$C_{27}H_{22}ClPPd$	$C_{28}H_{24}ClPPd.CH_2Cl_2$	$C_{27}H_{40}ClPPd$	$C_{12}H_{16}O_3ClPPd$
mol wt	519.27	618.218	537.41	381.07
cryst color, habit	red, block	red, block	orange, plate	red, block
cryst dimens, mm	0.08×0.25×0.33	0.30×0.34×0.47	0.02×0.11×0.65	0.11×0.12×0.18
symmetry	triclinic	monoclinic	monoclinic	monoclinic
space group	P-1	$P2_1/c$	$P2_1$	$P2_1/c$
a, Å	9.9997(1)	14.3388(1)	11.6214(3)	14.8857(4)
b, Å	14.5450(2)	11.0454(1)	19.4114(5)	17.2545(4)
c, Å	17.2588(2)	17.7748(1)	11.8247(3)	11.1260(4)
α, deg	65.630(1)	90	90	90
β, deg	83.151(1)	108.156(1)	102.441(2)	91.905(2)
γ, deg	89.093(1)	90	90	90
Z	4	4	4	8
D(calcd), g cm^{-3}	1.520	1.535	1.370	1.661
diffractometer	Bruker AXS SMART 2K	Bruker AXS SMART 2K	Bruker AXS SMART 2K	Bruker AXS SMART 2K
temp, K	223(2)	223(2)	223(2)	223(2)
λ (Cu Kα), Å	1.54178	1.54178	1.54178	1.54178
μ, mm^{-1}	8.421	9.035	7.336	13.255
scan type	ω scan	ω scan	ω scan	ω scan
F(000)	1048	1248	1120	1520
θ_{max} (deg)	72.90	72.90	72.93	73.03
h,*k*,*l* ranges	$-12 \le h \le 12$	$-17 \le h \le 17$	$-23 \le h \le 23$	$-18 \le h \le 18$
	$-17 \le k \le 17$	$-13 \le k \le 13$	$-14 \le k \le 14$	$-21 \le k \le 21$
	$-21 \le l \le 21$	$-22 \le l \le 21$	$-23 \le l \le 23$	$-10 \le l \le 12$
reflns used ($I > 2\sigma(I)$)	7969	4825	8753	4016
abs correction	multiscan SADABS	multiscan SADABS	multiscan SADABS	multiscan SADABS
T (min, max)	0.1200, 0.5100	0.0630, 0.0670	0.4370, 0.8640	0.1850, 0.2330
$R\ [F^2>2\sigma(F^2)]$, $wR(F^2)$	0.0322, 0.0885	0.0521, 0.1385	0.0426, 0.0994	0.0883, 0.2194
GOF	1.027	1.029	1.012	1.030
Flack param			0.022(7)	

Table 2.III. Crystal data, Data Collection, and Structure Refinement Parameters of **6** and **10**

	6	**10**
formula	$C_{18}H_{14}Cl_2Pd_2$	$C_{14}H_{16}ClNPd$
mol wt	513.99	340.13
cryst color, habit	orange, needle	orange, block
cryst dimens, mm	0.15×0.25×0.50	0.08×0.10×0.39
symmetry	Triclinic	monoclinic
space group	P-1	$P2_1/c$
a, Å	10.2103(6)	6.37760(10)
b, Å	12.5513(7)	13.9174(3)
c, Å	12.7249(7)	16.0809(3)
α, deg	87.970(1)	90
β, deg	78.209(1)	90.260(1)
γ, deg	89.497(1)	90
volume, $Å^3$	1592.32(16)	1427.32(5)
Z	4	4
D(calcd), g cm^{-3}	2.141	1.583
diffractometer	Bruker AXS SMART 1K	Bruker AXS SMART 2K
temp, K	173(2)	223(2)
λ, Å	0.7107	1.54178
μ, mm^{-1}	2.580	12.018
scan type	ω scan	ω scan
F(000)	992	680
θ_{max}, (deg)	29.62	72.88
h,k,l range	$-14 \le h \le 14$ $-17 \le k \le 17$ $-17 \le l \le 17$	$-7 \le h \le 6$ $-17 \le k \le 16$ $-19 \le l \le 19$
reflns used $(I > 2\sigma(I))$	11089	2498
Absorption correction	multi-scan SADABS	multi-scan SADABS
T (min, max)	0.53, 0.86	0.27, 0.38
R $[F^2>2\sigma(F^2)]$, $wR(F^2)$	0.0596, 0.1451	0.0263, 0.0680
GOF	0.894	1.018
BASF, %	17.6	

Table 2.IV. Selected Bond Distances (Å) and Angles (deg) for **4**, **5**, **7**, and **9** and Analogous Nickel Complexes **11** and **12**.

	4[27]		**11**	**7**[27]	**9**[27]	**5**	**12**
M-P	2.2785(6)	2.2673(6)	2.1835(7)	2.2702(14)	2.216(3)	2.2649(8)	2.1782(11)
M-Cl	2.3474(6)	2.3560(7)	2.1822(7)	2.3521(13)	2.355(2)	2.3585(8)	2.1865(10)
M-C1	2.244(2)	2.282(3)	2.094(2)	2.290(7)	2.339(10)	2.314(4)	2.137(2)
M-C2	2.186(2)	2.209(3)	2.061(2)	2.193(6)	2.198(10)	2.228(4)	2.072(2)
M-C3	2.192(2)	2.165(3)	2.042(2)	2.179(6)	2.120(9)	2.144(4)	2.026(3)
M-C3a	2.607(2)	2.544(3)	2.318(2)	2.595(5)	2.570(10)	2.520(3)	2.308(2)
M-C7a	2.610(2)	2.580(2)	2.344(2)	2.647(6)	2.671(10)	2.586(3)	2.351(2)
C1-C2	1.404(4)	1.393(4)	1.399(4)	1.401(12)	1.397(16)	1.392(6)	1.403(4)
C2-C3	1.410(4)	1.413(4)	1.417(4)	1.430(10)	1.436(15)	1.419(6)	1.421(4)
C3-C3a	1.474(4)	1.468(4)	1.449(3)	1.454(9)	1.440(15)	1.479(6)	1.451(4)
C3a-C7a	1.415(4)	1.422(4)	1.422(3)	1.422(8)	1.413(14)	1.417(4)	1.417(4)
C7a-C1	1.464(4)	1.465(4)	1.459(3)	1.434(10)	1.463(15)	1.475(5)	1.457(4)
P-M-Cl	96.23(2)	97.04(2)	98.82(4)	95.89(6)	99.7(9)	97.56(3)	97.43(2)
C3-M-Cl	158.71(7)	160.78(8)	161.51(8)	161.1(2)	163.6(3)	159.4(1)	161.52(7)
C3-M-P	104.91(7)	101.75(8)	99.33(8)	102.5(2)	96.4(3)	102.9(1)	100.69(7)
C1-M-Cl	97.29(7)	99.48(8)	95.48(8)	100.5(2)	103.1(3)	98.1(1)	95.83(8)
C1-M-P	164.25(7)	161.72(8)	165.6(7)	163.4(2)	156.9(3)	132.1(1)	166.34(8)
C1-M-C3	61.4(1)	61.3(1)	66.5(1)	61.3(3)	61.1(4)	61.3(1)	66.3(1)
ΔM-C[a] (Å)	0.39	0.39	0.26	0.39	0.39	0.32	0.25
HA[b] (deg)	15.49	14.58	10.9	15.49	15.54	14.72	11.00
FA[c] (deg)	14.84	14.40	11.7	14.03	15.57	13.32	11.80

[a] Δ(M-C) = 0.5 {(M-C3a + M-C7a)} – 0.5{(M-C1 + M-C3)}.

[b] HA is the angle formed between the planes formed by the atoms C1, C2, C3 and C1, C3, C3a, C7a.

[c] FA is the angle formed between the planes formed by the atoms C1, C2, C3 and C3a, C4, C5, C6, C7 and C7a.

Table 2.V. Selected Bond Distances (Å), and Angles (deg) for **6** and **10**.

6[28]		**10**	
Pd-C1	2.204(6)	Pd-C1	2.063(3)
Pd-C2	2.137(7)	Pd-C8	1.929(3)
Pd-C3	2.165(7)	Pd-Cl	2.3634(7)
Pd-C3a	2.640(7)	Pd-Cl#1	2.4580(7)
Pd-C7a	2.656(6)	C8-N	1.138(4)
C1-C2	1.424(10)	C9-N	1.463(3)
C2-C3	1.404(10)	C1-C2	1.477(5)
C3-C3a	1.491(9)	C1-C7a	1.495(4)
C3a-C7a	1.419(9)	C2-C3	1.349(5)
C7a-C1	1.479(9)	C3-C3a	1.435(4)
C1-Pd-C3	62.4(3)	C3a-C7a	1.408(4)
C1-Pd-Cl	165.88(18)	C1-Pd-C8	87.66(12)
Cl-Pd-Cl#1	87.06(6)	C8-Pd-Cl	177.77(8)
Cl#1-Pd-C3	165.34(18)	C1-Pd-Cl	90.37(9)
Pd-Cl-Pd#1	92.94(6)	C8-Pd-Cl#1	95.22(8)
Δ(M-C)	0.463	C1-Pd-Cl#1	176.25(8)
HA	17.30	Cl-Pd-Cl#1	86.79(2)
FA	16.39	Pd-Cl-Pd#1	93.21(2)
		C8-N-C9	171.3(3)
		N-C8-Pd	179.3(3)

The overall geometry around Pd in **10** is very nearly square planar (less than 5° deviation in all angles) but much more irregular in the remaining compounds. The largest structural distortion in the latter compounds arises from the small C(1)-Pd-C(3) angle of ca. 61°, which is fairly similar to the corresponding value of ca. 66° in the analogous Ni complexes. It is instructive to begin the structural discussion of Ind

hapticity with the structures of the η-Ind complexes; the main structural features of complex **10** will be discussed last.

The metal center in all of the η-Ind complexes is within reasonable bonding distance from the P, Cl, C(1), C(2), and C(3) atoms but considerably farther away from C3a and C7a. The extent of M-Ind interaction can be most conveniently estimated by the relative values of the "slip" parameter Δ(M-C), which corresponds to the difference between the average M-C distances from the two allylic carbons (C1, C3) and the two quaternary carbons (C3a, C7a); the hinge and fold angles (HA, FA, as defined in Table 2.IV) are also useful for this purpose.[29] Interestingly, the Δ(M-C), HA and FA values observed for complex **6** (Table 2.V) are larger than those of all known monomeric Pd complexes (Table 2.IV), implying a larger degree of $\eta^5 \rightarrow \eta^3$ distortion in this complex. Since **6** is the only neutral $Pd^{(II)}$Ind compound not bearing a phosphine ligand, it is tempting to speculate on the importance of Pd→phosphine π-back-bonding in these complexes; however, the closeness of the structural parameters for complexes **4**, **7**, and **9**, bearing phosphines of different π-acidities, seems to discount this possibility.

Let us turn now to comparing the structural features of the monomeric Ni and Pd complexes. The data listed in Table 4 show that the Pd complexes exhibit significantly larger values of Δ(M-C) (*ca.* 0.32-0.39 Å versus 0.25 Å) and HA/FA (ca. 13.3-15.5° versus 10.9-11.8°), implying that $\eta^5 \rightarrow \eta^3$ slip-fold distortions are more pronounced in IndPd complexes relative to their analogous Ni counterparts. The same trend is observed in the reported structural data for previously studied IndPd complexes.[4] For example, the Δ(M-C) values for $IndPd(PMe_3)(CH_2SiMe_3)$[12b] and its close analogue $(1\text{-Me-Ind})Ni(PMe_3)(CH_3)$[8b] are 0.39 and 0.27 Å, respectively. The generally weaker Pd-Ind interaction presumably reflects the more electron rich nature of Pd versus Ni; this assertion is borne out the results of our electrochemical studies (vide infra).

As expected on the basis of the unequal trans influences of PR_3 and Cl ligands, the Pd-Ind interactions in **4**, **5**, **7**, and **9** are also quite nonsymmetrical: Pd-C(3) < Pd-C(1) by about 15-40 times esd values. The net result of this distortion is a partial localization of bonding in the allyl moiety of the Ind ligand (i.e., $\eta^1 : \eta^2$ distortion,

Chart 2.1), which is also reflected in the nominally shorter C(1)-C(2) versus C(2)-C(3) distances. Moreover, the localization of bonding inside the Ind moiety is also reflected in the ^{1}H and $^{13}C\{^{1}H\}$ NMR chemical shifts of these complexes (vide supra); therefore, the solid-state hapticity of the Ind ligand in these Pd complexes is maintained in solution, as observed for the previously studied Ni complexes. Consistent with this correspondence between the solid-state and solution structures, we have noted a correlation between Δ(M-C) and Δδ(^{13}C) parameters of Ni and Pd complexes (Figure 2.4); a similar correlation has also been demonstrated previously for a wide range of Ind complexes.[19]

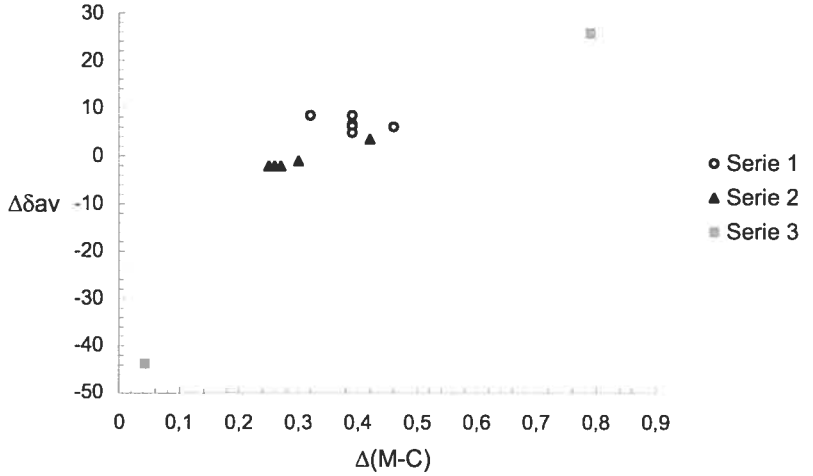

	Complex	(Δ(M-C), Δδ)
Serie 1 ○	(Ind)Pd(PPh_3)Cl	(0.39, 6.7)
	(1-Me-Ind)Pd(PPh_3)Cl	(0.32, 8.5)
	(Ind)Pd(PCy_3)Cl	(0.39, 8.5)
	(Ind)Pd($P(OMe)_3$)Cl	(0.39, 6.3)
	(Ind)Pd(PMe_3)(CH_2-$SiMe_3$) [12b]	(0.39, 5.0)
	{(Ind)Pd(μ-Cl)}$_2$	(0.46, 6.2)
Serie 2 ▲	Ni(Ind)$_2$ [22]	(0.42, 3.6)
	(Ind)Ni(PPh_3)Cl [5a]	(0.25, -2)
	(1-Me-Ind)Ni(PPh_3)Cl [5c]	(0.26, -2)
	(1-Me-Ind)Ni(PCy_3)Cl [5c]	(0.30, -1)
	(1-Me-Ind)Ni(PMe_3)Cl [5c]	(0.27, -2)
Serie 3 ■	(η^5-Ind)$_2$Fe [20]	(0.04, -43)
	(η^3-Ind)Ir(PMe_3)$_3$ [21]	(0.79, 26)

Figure 2.4: Correlation between Δδav (ppm) and Δ(M-C) (Å)

In contrast to the η-Ind complexes discussed above, the Ind ligand in complex **10** adopts a monohapto coordination mode. This compound crystallizes in the centrosymmetric space group $P2_1/c$ and lies on an inversion center. The Pd center is surrounded by η^1-Ind, *t*-BuNC, and two μ-Cl ligands. As expected, the Pd-C8 distance (ca. 1.93 Å) is shorter than the Pd-C1 distance (ca. 2.06 Å). The Pd-Cl bond distances *trans* to the η^1-Ind are longer (by ca. 10 esd. values) than those trans to the *t*-BuNC, indicating that η^1-Ind exerts a larger *trans* influence than *t*-BuNC. The remaining structural parameters for this complex are similar to those found in structurally characterized η^1-Ind complexes.[30] For example, the metal-bound carbon atom is sp^3 hybridized as reflected in the C1-C7a (ca. 1.50 Å) and C1-C2 (ca. 1.48 Å) distances that are in the normal range for single C-C bonds, whereas the C2-C3 distance (*ca.* 1.35 Å) is in the expected range for a $C(sp^2)$-$C(sp^2)$ double bond.

The structural parameters for the isocyanide ligand (C8-N ~ 1.14 Å, C8-N-C9 ~ 171°) and the ν(CN) absorption band in **10** (2204 cm^{-1}), which is at higher energy than the free ligand (2136 cm^{-1}), are consistent with little π-back-bonding. Similar ν(CN) values, Pd-C and C-N distances, and C-N-C angles have been reported for other Pd(II)-isocyanide complexes.[31] The IR data in particular indicates an increased C-N bond order, probably caused by a strong σ donation from the isocyanide ligand's lone pair to Pd with little or no π-back-donation.

Electrochemical Studies. Table 2.I lists the reduction potentials obtained from the cyclic voltammetry (CV) studies carried out on complexes **4**, **5**, **7**, **8**, **11**, and **12**. The CV measurements of these complexes showed that they undergo two successive and irreversible one-electron reductions (presumably $M^{(II)} \rightarrow M^{(I)}$ and $M^{(I)} \rightarrow M^{(0)}$) at potentials ranging from – 0.64 V to – 1.24 V for the first wave and from – 1 .05 V to – 1.64 V for the second. (In the case of complexes **8** and **12**, second reductions were too weak to be observed.) The relative reduction potentials of these complexes indicate that the Ind-Ni complexes are more easily reduced than the Ind-Pd compounds; this is consistent with the solid-state data, which implied more electron rich Pd centers. Inspection of the electrochemical data also shows that the E_{red} values for the species **8**

(E_{red1} = -1.24 V) and **4** (E_{red1} = -0.94 V, E_{red2} = -1.41 V) follow the donor ability of the phosphine (PMe_3 > PPh_3); the reduction potential of the PCy_3 analogue **7** is less negative (E_{red1} = -1.07 V, E_{red2} = -1.64 V) than that of the PMe_3 analogue, presumably due to the a less effective electron donation caused by the greater steric volume of PCy_3.

Catalytic Reactivities of IndPd Complexes. Recent work in our group has shown that the complexes (Ind)Ni(PR_3)Cl are inert toward hydrosilanes and olefins, but they catalyze the dehydrogenative polymerization of $PhSiH_3$,[8a] hydrosilylation of olefins and ketones,[9] and polymerization of olefins[6] in the presence of excess MAO. We have briefly probed the reactivities of some of the IndPd species reported here as a preliminary comparison of their reactivities relative to those of their Ni analogues. Thus, the reaction of complexes **4-7** with excess $PhSiH_3$ led to an instantaneous darkening of the reaction mixture and the evolution of a gas, indicating that the Pd complexes react with this substrate in the absence of cocatalysts. Careful NMR monitoring of mixtures of the complexes **4-6** and 200 equiv of $PhSiH_3$ in a C_6D_6 solution indicated the disappearance of the substrate Si-H and Ph-Si signals (ca. 20% over 20 min); curiously, however, no new ^1H signals were detected for the anticipated products of the reaction (i.e., $(PhSiH)_n$). Monitoring the $^{31}P\{^1H\}$ NMR spectra during the course of the reaction showed only a broad signal at ca. –1.2 ppm (assigned to exchanging PPh_3); the spectrum at the end of the reaction signaled the presence of free PPh_3 (ca. –5 ppm) and $O{=}PPh_3$ (ca. +25 ppm).

Additional information was obtained from monitoring the reaction of the Pd complexes with stoicheometric quantities of $PhSiH_3$. Thus, the ^1H NMR spectrum of the reaction of **4** with $PhSiH_3$ (ca. 1:1) showed free IndH, $(PhSiH_2)_2$ (singlet at ca. 4.46 ppm assigned to Si-*H* of the dimer),[8b] and Ph_2SiH_2 (singlet at ca. 5.1 ppm) in addition to other, unassigned peaks; the $^{31}P\{^1H\}$ NMR spectrum of the final mixture showed only $Pd(PPh_3)_n$ (ca. +24 ppm). On the other hand, the analogous reaction with **6** led to the complete consumption of $PhSiH_3$ and formation of indene and indane (hydrogenated indene), in addition to a number of minor signals; significantly, no trace

of the anticipated Si-containing products (e.g., dimer, oligomer, and Ph_2SiH_2) was observed.

Evidently, these reactions follow a complicated and as yet not well-understood course. The available data allow us, however, to offer the following speculation: (a) initial reaction of $PhSiH_3$ with the Pd precursors results in the elimination of IndH and the formation of $Pd^{(0)}$; (b) in the presence of PPh_3 ligands (reaction with **4**), the resulting $Pd(PPh_3)_n$ can react with unreacted substrate to promote both dehydrogenative Si-Si bond formation and redistribution, whereas these reactions do not seem to occur in the absence of phosphine (reaction with **6**). It is noteworthy that, unlike the case of the Ni complexes, the presence of MAO did not change the course of the reactions involving IndPd complexes. Finally, no hydrosilylation of styrene was observed in the presence of $PhSiH_3$ and the complexes **4**-**6**, with or without MAO.

We have also studied the catalytic activities of our Pd complexes in the polymerization of ethylene. Thus, we found that complexes **4** and **6** produced polyethylene (PE) with modest activities (204 and 124 kg PE/mol of Pd.h, respectively; polymerization conditions: 600 equiv of MAO; ethylene-saturated toluene with $P_{ethylene} \approx 16$ atm; 60 °C; 30 min). It appears, therefore, that these Pd complexes are more active in this reaction relative to their Ni counterparts; for instance, the complex (1-Me-Ind)Ni(PPh_3)Cl showed an activity of about 50 kg PE/mol of Ni.h under similar conditions (except for $P_{ethylene} \approx 5$ atm).

Conclusion

Two routes have been developed for the preparation of indenyl palladium complexes. The first route, involving the reaction of $(PhCN)_2PdCl_2$ with LiInd and PPh_3, gives modest yields, while the second route, the addition of PR_3 to the dimeric compound $\{(\eta^3\text{-Ind})Pd(\mu\text{-Cl})\}_2$ (**6**), gives good yields of $(\eta\text{-Ind})Pd(PR_3)Cl$. The dimeric derivate $\{(\eta^1\text{-Ind})(t\text{-BuNC})Pd(\mu\text{-Cl})\}_2$ (**10**), which is the first example of an isolated $(\eta^1\text{-Ind})Pd$ complex, was obtained from the reaction of *t*-BuNC with **6**. The structural studies have revealed significant differences in the hapticity of the Ind ligand

(both in solution and in the solid state) between the Pd and Ni complexes, with the IndPd complexes displaying greater $\eta^5 \rightarrow \eta^3$ slippage. Electrochemical measurements have confirmed that the Pd centers are relatively more electron rich. Preliminary reactivity studies have shown that the Pd complexes are somewhat more reactive than their Ni analogues, but systematic studies are needed to delineate the exact differences in the chemistry of these complexes. Studies are underway to probe and expand the scope of the reactions catalyzed by the IndPd compounds.

Experimental Section.

General Comments. All manipulations and experiments were performed under an inert atmosphere using standard Schlenk techniques and/or a nitrogen-filled glovebox. Dry, oxygen-free solvents were prepared by distillation from appropriate drying agents and employed throughout. The syntheses of $(PhCN)_2PdCl_2$[32] and $(PMe_3)_2PdCl_2$[33] were carried out according to published procedures; all other reagents used in the experiments were obtained from commercial sources and used as received. The elemental analyses were performed by the Laboratoire d'Analyse Elémentaire (Université de Montréal). Bruker ARX400, AV400, AMX300, AV300 spectrometers were employed for recording ^1H (400 and 300 MHz), $^{13}C\{^1H\}$ (100.56 and 75.42 MHz), and $^{31}P\{^1H\}$ (161.92 MHz) NMR spectra at ambient temperature. The NMR spectra are referenced to a) the residual solvent resonances for the ^1H and $^{13}C\{^1H\}$ spectra, and b) 85% H_3PO_4 (0 ppm) for the $^{31}P\{^1H\}$ spectra. The ethylene polymerization experiments have been realized as described in a recent paper.[6d]

Crystal Structure Determinations. The crystal data for complexes **4**, **5**, **6**, **7**, **9** and **10** were collected on a Bruker AXS Smart 2K and 1K (for **6**) diffractometers using SMART.[34] Graphite-monochromated Cu Kα radiation was used at 223(2) K for all crystals except that of **6** for which the radiation used was Mo Kα at 173 (2) K. Cell refinement and data reduction were done using SAINT.[35] All structures were solved by direct methods using SHELXS97[36] and difmap synthesis using SHELXL97;[37] the

refinements were done on F^2 by full-matrix least squares. All non-hydrogen atoms were refined anisotropically, while the hydrogens (isotropic) were constrained to the parent atom using a riding model. The crystal structure of **6** presented two twin components which have been described by a matrix obtained with the Gemini's program.[38] In the case of complex **9**, the Cu radiation employed resulted in relatively high absorption and gave less satisfactory data; using SADABS[39] improved the results, but the *R* factor for this structure remained fairly high (*ca.* 8.8%). The crystal data and experimental details are listed in Tables 2.II and 2.III, while selected bond distances and angles are listed in Tables 2.IV and 2.V.

Synthesis of {(η^3-Ind)Pd(μ-Cl)}$_2$ (6). The original synthesis of this compound was reported previously;[10] we have used the following procedure, which has been reported by Lin and Boudjouk.[18] Into a Schlenk flask, under nitrogen, Na_2PdCl_4 (6.5 g, 21.9 mmol) and 200 mL of ethanol were heated to reflux until a clear brown solution was obtained. After the solution was cooled to room temperature, 1-$SiMe_3$-Ind (4.7 g, 25 mmol) was added to produce a brown solid, which precipitated gradually. After it was stirred for 20 min, the mixture was filtered and the collected solid washed successively with distilled water, Et_2O, and ethanol to give the compound {(η^3-Ind)Pd(μ-Cl)}$_2$ (**6**) (4.9 g, 87%) as a brown powder. Recrystallization of a small portion of this solid from a cold CH_2Cl_2/Et_2O solution yielded crystals suitable for X-ray diffraction studies. ^{1}H NMR ($CDCl_3$, 300 MHz): 6.88-6.83 (m, $H_{4\text{-}5\text{-}6\text{-}7}$), 5.84 (br, $H_{1\text{-}2\text{-}3}$). ^{13}C {^{1}H} NMR ((Me_2SO-d_6), 75.40 MHz): 136.9 (s, C_{3a}-C_{7a}), 127.4 (s, C_4-C_7), 118.8 (s, $C_{5\text{-}6}$), 114.0 (s, C_2), 85.4 (s, C_1-C_3).

Synthesis of (Ind)Pd(PPh_3)Cl (4). Method A. An Et_2O solution (60 mL) of IndLi (320 mg, 2.61 mmol) was added dropwise to a stirring suspension of $(PhCN)_2PdCl_2$ (1 g, 2.61 mmol) in Et_2O (80 mL) at – 78 °C. The mixture was warmed to room temperature and stirred for 30 min. After PPh_3 was added (410 mg, 1.56 mmol), the resultant dark red mixture was stirred for approximately 30 min, filtered through a

small pad of celite, and concentrated. A red brown powder precipitated and was isolated by filtration (501 mg, 60%).

Method B. PPh_3 (1.14 g, 4.3 mmol) was added to a stirred Et_2O suspension (110 mL) of $\{(\eta^3\text{-Ind})Pd(\mu\text{-Cl})\}_2$ **6** (1.24 g, 2.4 mmol) at room temperature. After stirring for 1h, the resulting red solution was concentrated to ca. 60 mL. A red brown powder precipitated and was isolated by filtration (2.02 g, 89%). Recrystallization of a small portion of this solid from a cold CH_3CN/hexane solution yielded crystals suitable for X-ray diffraction studies and elemental analysis. ^{1}H NMR ($CDCl_3$, 300 MHz): 7.56-7.39 (m, PPh_3), 7.26 (d, $^3J_{H\text{-}H}$ = 7.5 Hz, H_7), 7.07 (t, $^3J_{H\text{-}H}$ = 7.5 Hz, H_6), 6.87 (t, $^3J_{H\text{-}H}$ = 7.4 Hz, H_5), 6.73 (t, $^3J_{H\text{-}H}$ = 6.4 Hz, H_2), 6.51 (d, $^3J_{H\text{-}H}$ = 9.9 Hz, H_1), 6.38 (d, $^3J_{H\text{-}H}$ = 7.2 Hz, H_4), 4.57 (t, $^3J_{H\text{-}H}$ = 2.01 Hz, H_3). ^{13}C $\{^1$H$\}$ NMR ($CDCl_3$, 100.56 MHz): 136.16 (s, C_{7a}), 135.18 (s, C_{3a}), 134.30 (d, $^2J_{C\text{-}P}$ = 12.4 Hz, C_{ortho}), 132.00 (d, $^1J_{C\text{-}P}$ = 45.57 Hz, C_{ipso}), 130.95 (s, C_{para}), 128.96 (d, $^3J_{C\text{-}P}$ = 10.6 Hz, C_{meta}), 127.45 (s, C_6), 126.55 (s, C_5), 119.77 (s, C_7), 116.91 (s, C_4), 111.56 (d, $^2J_{C\text{-}P}$ = 22.7 Hz, C_2), 97.23 (d, $^2J_{C\text{-}P}$ = 22.7 Hz, C_1), 79.88 (s, C_3). ^{31}P $\{^1$H$\}$ NMR ($CDCl_3$, 121.49 MHz): 28.58 (s). ^{31}P $\{^1$H$\}$ NMR (C_6D_6, 121.49 MHz): 27.98 (s). Anal. Calcd for $C_{27}H_{22}Cl_1P_1Pd_1$: C, 62.45; H, 4.27. Found: C, 61.91; H, 4.56.

Synthesis of (1-Me-Ind)Pd(PPh_3)Cl (5). An Et_2O solution (60 mL) of 1-Me-IndLi (355 mg, 2.61 mmol) was added dropwise to a stirring suspension of $(PhCN)_2PdCl_2$ (1 g, 2.61 mmol) in Et_2O (80 mL) at – 78 °C. The mixture was warmed to room temperature and then stirred for 30 min. After adding PPh_3 (410 mg, 1.56 mmol), the resultant dark red mixture was stirred approximately 30 min, filtered through a small pad of celite, and concentrated. A red brown precipitate was isolated by filtration (501 mg, 60%). Recrystallization of a small portion of this solid from a cold CH_2Cl_2/hexane solution yielded crystals suitable for X-ray diffraction studies and elemental analysis. ^{1}H NMR (C_6D_6, 400 MHz): 7.50-7.61 (m, PPh_3), 7.03 (d, $^3J_{H\text{-}H}$ = 7.7 Hz, H_7), 6.90-6.95 (m, PPh_3), 6.94 (t, $^3J_{H\text{-}H}$ = 7.6 Hz, H_6), 6.75 (t, $^3J_{H\text{-}H}$ = 7.4 Hz, H_5), 6.23 (d, $^3J_{H\text{-}H}$ = 7.5 Hz, H_4), 6.12 (d, $^3J_{H\text{-}H}$ = 2.7 Hz, H_2), 4.28 (d, $^3J_{H\text{-}H}$ = 2.7 Hz, H_3), 2.04 (d, $^3J_{H\text{-}P}$ = 10.4 Hz, *Me*). ^{1}H NMR ($CDCl_3$, 400 MHz): 7.39-7.45 (m, PPh_3), 7.19 (d, $^3J_{H\text{-}H}$ = 7.3

Hz, H_7), 7.08 (t, $^3J_{H-H}$ = 7.3 Hz, H_6), 6.86 (t, $^3J_{H-H}$ = 7.6 Hz, H_5), 6.49 (d, $^3J_{H-H}$ = 2.8 Hz, H_2), 6.24 (d, $^3J_{H-H}$ = 7.4 Hz, H_4), 4.46 (d, $^3J_{H-H}$ = 2.8 Hz, H_3), 2.05 (d, $^3J_{H-P}$ = 10.6 Hz, *Me*). $^{13}C\{^1H\}$ NMR (C_6D_6, 100.56 MHz) : 138.96 (d, $^3J_{C-P}$ = 4.1 Hz, C_{7a}), 136.37 (d, $^3J_{C-P}$ = 0.69 Hz, C_{3a}), 135.02 (d, $^2J_{C-P}$ = 12.5 Hz, C_{ortho}), 133.85 (d, $^1J_{C-P}$ = 43.7 Hz, C_{ipso}), 131.01 (s, C_{para}), 129.13 (d, $^3J_{C-P}$ = 10.4 Hz, C_{meta}), 126.95 (s, C_6), 126.84 (s, C_5), 118.70 (s, C_7), 116.48 (s, C_4), 113.33 (d, $^2J_{C-P}$ = 21.5 Hz, C_1), 111.56 (d, $^2J_{C-P}$ = 5.5 Hz, C_2), 76.46 (s, C_3), 13.09 (d, $^3J_{C-P}$ = 5.6 Hz, *Me*). $^{31}P\{^1H\}$ NMR (C_6D_6, 161.92 MHz): 30.03 (s). $^{31}P\{^1H\}$ NMR ($CDCl_3$, 161.92 MHz): 29.67 (s). Anal. Calcd for $C_{28}H_{24}Cl_1P_1Pd_1.2/3LiCl$: C, 59.89; H, 4.54. Found: C, 59.32; H, 4.46.

Synthesis of (Ind)Pd(PCy_3)Cl (7). PCy_3 (490 mg, 1.75 mmol) was added to a stirred Et_2O suspension (30 mL) of $\{(\eta^3\text{-Ind})Pd(\mu\text{-Cl})\}_2$ **6** (500 mg, 0.97 mmol) at room temperature. After it was stirred for 45 min, the resulting orange solution was filtered and then concentrated to 5 mL. After adding 10 mL of hexane, an orange powder precipitated and was isolated by filtration (800 mg, 85%). Recrystallization of a small portion of this solid from a cold CH_3CN/hexane solution yielded crystals suitable for X-ray diffraction studies and elemental analysis. ^1H NMR (C_6D_6, 300 MHz): 7.13 (d, $^3J_{H-H}$ = 7.6 Hz, H_7), 6.92 (t, $^3J_{H-H}$ = 7.2 Hz, H_6), 6.88 (d, $^3J_{H-H}$ = 6.9 Hz, H_4), 6.81 (t, $^3J_{H-H}$ = 7.1 Hz, H_5), 6.33 (t, $^3J_{H-H}$ = 3.06 Hz, H_2), 6.21 (d, $^3J_{H-H}$ = 9.4 Hz, H_1), 5.11 (s, H_3), 1.98-1.08 (m, PCy_3). $^{13}C\{^1H\}$ NMR (C_6D_6, 75.40 MHz): 137.85 (s, C_{7a}), 137.15 (s, C_{3a}), 126.34 (s, C_6), 124.61 (s, C_5), 119.84 (s, C_7), 117.83 (s, C_4), 110.87 (d, $^2J_{C-P}$ = 5.2 Hz, C_2), 94.26 (d, $^2J_{C-P}$ = 21.8 Hz, C_1), 70.94 (d, $^2J_{C-P}$ = 3.4 Hz, C_3), 35.35 (d, $^1J_{C-P}$ = 19.8 Hz, C_{ipso}), 30.2 (d, $^2J_{C-P}$ = 11.1 Hz, C_{ortho}), 27.69 (d, $^3J_{C-P}$ = 11.7 Hz, C_{meta}), 27.61 (d, $^3J_{C-P}$ = 10.9 Hz, C_{meta}), 6.61 (s, C_{para}). $^{31}P\{^1H\}$ NMR (C_6D_6, 161.92 MHz): 49.04 (s). $^{31}P\{^1H\}$ ($CDCl_3$, 161.92 MHz): 48.34 (s). Anal. Calcd for $C_{27}H_{40}Cl_1P_1Pd_1$: C, 60.34; H, 7.50. Found: C, 59.92; H, 7.66.

Synthesis of (Ind)Pd(PMe_3)Cl (8). PMe_3 (161 μL, 1.6 mmol) was syringed into a stirred Et_2O suspension (50 mL) of $\{(\eta^3\text{-Ind})Pd(\mu\text{-Cl})\}_2$ **6** (500 mg, 0.97 mmol) at room temperature. After it was stirred for 45 min, the resulting red solution was

filtered and then concentrated to 60 mL. An orange powder precipitated and was isolated by filtration (380 mg, 73%). Recrystallization of a small portion of this solid from a cold toluene/hexane solution yielded crystals suitable for X-ray diffraction studies and elemental analysis. NMR ^{1}H ($CDCl_3$, 400 MHz): 7.20 (d, $^{3}J_{H\text{-}H}$ = 7.6 Hz, H_7), 7.04 (t, $^{3}J_{H\text{-}H}$ = 7.0 Hz, H_6), 6.98-6.93 (m, H_5 et H_4), 6.64 (t, $^{3}J_{H\text{-}H}$ = 2.9 Hz, H_2), 6.42 (d, $^{3}J_{H\text{-}H}$ = 9.5 Hz, H_1), 5.26 (s, H_3), 1.48 (d, $^{2}J_{H\text{-}P}$ = 11.4 Hz, PMe_3). NMR ^{13}C {^{1}H} (C_6D_6, 75.40 MHz): 136.34 (s, C_{7a}), 134.89 (s, C_{3a}), 126.67 (s, C_6), 125.84 (s, C_5), 119.55 (s, C_7), 116.23 (s, C_4), 111.16 (s, C_2), 97.00 (d, $^{2}J_{C\text{-}P}$ = 24.6 Hz, C_1), 70.23 (s, C_3), 16.68 (d, $^{1}J_{C\text{-}P}$ = 29.4 Hz, PMe_3). NMR ^{31}P {^{1}H} ($CDCl_3$, 161.92 MHz): -6.93. Anal. Calcd for $C_{12}H_{16}Cl_1P_1Pd_1$: C, 43.27; H, 4.84. Found: C, 43.19; H, 4.94.

Synthesis of IndPd(P(OMe)$_3$)Cl (9). P(OMe)$_3$ (175 μL, 1.6 mmol) was syringed into a stirred Et_2O suspension (30 mL) of {η^3-Ind)Pd(μ-Cl)}$_2$ **6** (400 mg, 0.78 mmol) at room temperature. After it was stirred for 2 h, the resulting red solution was filtered and then concentrated to 15 mL. Addition of hexane (15 mL) resulted in the precipitation of an orange powder, which was filtered and washed with hexane to give an orange solid (460 mg, 82%). Recrystallization of a small portion of this solid from an ether solution at room temperature yielded crystals suitable for X-ray diffraction studies and elemental analysis. NMR ^{1}H ($CDCl_3$, 400 MHz): 7.24 (d, $^{3}J_{H\text{-}H}$ = 7.5 Hz, H_7), 7.10-7.06 (m, H_6 and H_4), 6.98 (t, $^{3}J_{H\text{-}H}$ = 7.5 Hz, H_5), 6.58-6.56 (m, H_2), 6.49 (d, $^{3}J_{H\text{-}H}$ = 16.8 Hz, H_1), 5.69 (d, $^{3}J_{H\text{-}H}$ = 2.3 Hz, H_3), 3.64 (d, $^{3}J_{H\text{-}P}$ = 12.9 Hz, P(OMe)$_3$). NMR ^{13}C {^{1}H} ($CDCl_3$, 100.56 MHz): 136.02 (d, $^{3}J_{C\text{-}P}$ = 7.4 Hz, C_{7a}), 134.56 (d, $^{3}J_{C\text{-}P}$ = 4.2 Hz, C_{3a}), 127.64 (s, C_6), 126.56 (s, C_5), 120.09 (s, C_7), 118.25 (s, C_4), 111.16 (d, $^{2}J_{C\text{-}P}$ = 10.6 Hz, C_2), 99.42 (d, $^{2}J_{C\text{-}P}$ = 34.95 Hz, C_1), 73.15 (d, $^{2}J_{C\text{-}P}$ = 7.05 Hz, C_3), 53.24 (s, P(OMe)$_3$). NMR ^{31}P {^{1}H} ($CDCl_3$, 161.92 MHz): 131.2. Anal. Calcd for $C_{12}H_{16}Cl_1O_3P_1Pd_1$: C, 37.82; H, 4.23. Found: C, 37.55; H, 4.29.

Synthesis of [(η^1-Ind)$_2$(t-BuNC)$_2$Pd(μ-Cl)$_2$] (10). A stirred benzene solution (10 mL) of ^{t}-BuNC (161 μL, 1.44 mmol) was added to a stirred benzene solution (25 mL) of {(η^3-Ind)Pd(μ-Cl)}$_2$ 6 (400 mg, 0.78 mmol) at room temperature. The resulting orange

solution was stirred for 45 min, filtered, and evaporated to dryness. The residue was crystallized from Et_2O at 0°C to give the product as orange crystals (300 mg, 57%). NMR ^1H ($CDCl_3$, 300 MHz): 7.89 (d, $^3J_{H-H}$ = 6.9 Hz, H_4), 7.38 (d,$^3J_{H-H}$ = 7.4 z, H_7), 7.13-7.02 (m, H_3, H_5 and H_6), 6.77 (d, $^3J_{H-H}$ = 5.01 Hz, H_2), 5.85 (br, H_1), 0.40 (s, ^{t}-BuNC(CH_3)$_3$). NMR ^{13}C {^1H} (C_6D_6, 75.40 MHz): 153.55 (s, C_{7a}), 142.86 (s, C_{3a}), 141.06 (s, C_3 or C_5 or C_6), 125.75 (s, C_4), 125.25 (s, C_3 or C_5 or C_6), 125.18 (s, C_2), 124.34 (s, C_3 or C_5 or C_6), 121.39 (s, C_7), 57.07 (s, CMe$_3$), 44.11 (s, C_1), 28.90 (s, CMe_3). The missing resonance for CN is probably obscured under the residual solvent resonances at *ca.* 129 ppm.. IR (KBr): 2204 cm^{-1} (s, CN) . Anal. Calcd for $C_{28}H_{32}Cl_2P_2Pd_2$: C, 49.43; H, 4.74; N, 4.12. Found: C, 50.59; H, 4.90; N, 3.94. All our attempts to further purify this material were unsuccessful.

Calculation of the Energy Barrier to the Indenyl Rotation in Complexes 4, 7 and 9.

The Holmes-Gutowski equation for a two site exchange process involving molecular rotation, $\Delta G^{\ddagger} / RT_c = 22.96 + \ln (T_c / \delta\nu)$,[24] can be used to calculate the free energy of activation for the hindered indenyl rotation process. The two variables in this equation, the coalescence temperatures (T_c) and frequency differences ($\delta\nu$) for each pair of exchanging resonances, are listed below along with the corresponding calculated $\Delta G^{\ddagger}$ values.

Complex	Exchanging Protons	Tc (K)	δν (Hz)	$\Delta G^{\ddagger}$ (Kcal/mol)
	H1 / H3	368-373	824	16.2-16.5
4	H4 / H7	358-368	336	16.4-16.8
	H5 / H6	348-358	76	16.9-17.4
	H1 / H3	358-363	409	16.2-16.5
7	H4 / H7	348-358	64	17.0-17.5
	H5 / H6	318-328	29	16.1-16.5
	H1 / H3	358-368	344	16.4-16.8
9	H4 / H7	328-338	68	16.1-16.5
	H5 /H6	318-328	28	16.1-16.9

It should be noted that the temperatures at which the spectra were recorded were not calibrated, and that the temperature increments studied were not sufficiently small to allow the determination of accurate coalescence temperatures. Nevertheless, these uncertainties are relatively insignificant and the average $\Delta G^{\ddagger}$ values thus obtained represent a reliable, qualitative estimate of the energy barrier to the indenyl rotation process.

Cyclic Voltammetry.

Electrochemical measurements were performed on an Epsilon electrochemical analyzer using 0.002 M solutions of the Palladium$^{(II)}$ complexes in a 0.1 M CH_3CN solution of *n*-Bu_4PF_6 (0.1 M). Cyclic voltammograms were obtained in a standard, one compartment electrochemical cell using a graphite disk as the working electrode, a platinum wire as the counter electrode, and a silver wire as the reference electrode. The cyclic voltammetry experiments were performed in the potential range of -2.4 V to 1.2 V using a scan rate of 100 mV/s. Under these conditions, $E_{1/2}$ for the Fc^+-Fc couple was 570 mV.

Acknowledgment.

This work was made possible thanks to the financial support provided by the Natural Sciences and Engineering Research Council of Canada (operating grants to D. Z.) and Université de Montréal (scholarships to C. S.-S.). We are also indebted to Johnson Matthey for the generous loan of $PdCl_2$, to Dr. M. Simard and F. Bélanger-Gariépy for their assistance with the X-ray analyses, and to Dr. Yaofeng Chen for his help in evaluating the catalytic activities of complexes 4 and 6 in the polymerization of ethylene. Prof. Boudjouk is thanked for supplying the experimental details for the reaction of 1-$SiMe_3$-Ind with $Na_2[PdCl_4]$.

Supporting Information Available.

Complete details of the X-ray analysis of **4**, **5**, **6**, **7**, **9** and **10**, including tables of crystal data, collection and refinement parameters, bond distances and angles, anisotropic

thermal parameters, and hydrogen atom coordinates. This material is free of charge via the Internet at http://pubs.acs.org.

References

[1] (a) Rerek, M. E.; Ji, L.-N.; Basolo, F. *J. Chem. Soc., Chem. Commun.* **1983**, 1208. (b) Ji, L. -N.; Rerek, M. E.; Basolo, F. *Organometallics* **1984**, *3*, 740. (c) Casey, C. P.; O'Connor, J. M. *Organometallics* **1985**, *4*, 384. (d) O'Connor, J. M.; Casey, C. P. *Chem. Rev.* **1987**, *87*, 307.

[2] (a) Frankom, T. M.; Green, J. C.; Nagy, A.; Kakkar, A. K.; Marder, T.B. *Organometallics* **1993**, *12*, 3688. (b) Gamasa, M. P.; Gimeno, J.; Gonzalez-Bernado, C.; Martin-Vaca B., M.; Monti, D.; Basseti, M. *Organometallics* **1995**, *15*, 302.

[3] Reactivity differences have also been noted between the Cp/Ind complexes of early transition metals, but since these complexes are generally electronically unsaturated their reactivity differences are less likely to be related to the hapticity of the ligands and more likely influenced by steric and symmetry factors.

[4] For a recent review on the chemistry of group 10 metal indenyl complexes see: Zargarian, D. *Coord. Chem. Rev.* **2002**, *233-234*, 157.

[5] (a) Huber, T. A.; Bélanger-Gariépy, F.; Zargarian, D. *Organometallics* **1995**, *14*, 4997. (b) Bayrakdarian, M.; Davis, M. J.; Dion, S.; Dubuc, I.; Bélanger-Gariépy, F.; Zargarian, D. *Can. J. Chem.* **1996**, *74*, 2115. (c) Huber, T.A.; Bayrakdarian, M.; Dion, S.; Dubuc, I.; Bélanger-Gariépy, F.; Zargarian, D. *Organometallics* **1997**, *16*, 5811. (d) Groux, L.F; Bélanger-Gariépy, F.; Zargarian, D.; Vollmerhaus, R. *Organometallics* **2000**, *19*, 1507. (e) Fontaine, F.-G.; Dubois, M.-A.; Zargarian, D. *Organometallics* **2001**, *20*, 5156.

[6] (a) Vollmerhaus, R.; Bélanger-Gariépy, F.; Zargarian, D. *Organometallics* **1997**, *16*, 4762. (b) Dubois, M.-A.; Wang, R.; Zargarian, D.; Tian, J.; Vollmerhaus, R.; Li, Z.; Collins, S. *Organometallics* **2001**, *20*, 663. (c) Groux, L. F.; Zargarian, D. *Organometallics* **2001**, *20*, 3811. (d) Groux, L. F.; Zargarian, D.; Simon, L. C.; Soares, J. B. P. *J. Mol. Catal. A* **2003**, *193(1-2)*, 51. (e) Groux, L. F.; Zargarian D. *Organometallics* **2003**, *22*, 3124. (f) Groux, L. F.; Zargarian D. *Organometallics* **2003**, *22*, 4759.

[7] (a) Wang, R.; Bélanger-Gariépy, F.; Zargarian, D. *Organometallics* **1999**, *18*, 5548. (b) Wang, R.; Groux, L. F.; Zargarian D. *Organometallics* **2002**, *21*, 5531. (c) Wang, R.; Groux, L. F.; Zargarian, D. *J. Organomet. Chem* **2002**, *660(1)*, 98. (d) Rivera, E.; Wang, R; Zhu, X. X.; Zargarian, D.; Giasson, R. *J. Mol. Catal. A* **2003**, *204-205*, 325.

[8] (a) Fontaine, F. -G.; Kadkhodazadeh, T.; Zargarian, D. *J. Chem. Soc., Chem. Commun.* **1998**, 1253-1254. (b) Fontaine, F.-G.; Zargarian, D. *Organometallics* **2002**, *21*, 401.

[9] Fontaine, F. -G.; Nguyen, R.-V.; Zargarian, D. *Can. J. Chem.* **2003**, *81*, 1299.

[10] (a) Nakasuji, K.; Yamaguchi, M.; Murata, I.; Tatsumi, K.; Natamura, A. *Organometallics* **1984**, *3*, 1257. (b) Samuel, E.; Bigorgne, M. *J. Organomet. Chem.* **1969**, *19*, 9.

[11] Tanase, T.; Nomura, T.; Fukushina, T.; Yamamoto, Y.; Kobayashi, K. *Inorg. Chem.* **1993**, *32*, 4578.

[12] (a) Alias, F. M.; Belderrain, T. R.; Paneque, M.; Poveda, M. L.; Carmona, E. *Organometallics* **1998**, *17*, 5620. (b) Alias, F. M.; Belderrain, T. R.; Carmona, E.; Graiff, C.; Paneque, M.; Poveda, M. L. *J. Organomet. Chem.* **1999**, *577*, 316.

[13] (a) Vicente, J.; Abad, J.-A.; Bergs, R.; Jones, P. G.; De Arellano, M. C. R. *Organometallics* **1996**, *15*, 1422. (b) Vicente, J.; Abad, J.-A.; Bergs, R.; De Arellano, M. C. R.; Martinez-Vivente, E.; Jones, P. G. *Organometallics* **2000**, *19*, 5597.

[14] Fiato, R. A .; Mushak, P.; Battiste, M. A. *J. Chem. Soc., Chem. Commun.* **1975**, 869.

[15] Consistent with this proposal, this side reaction is most prevalent with the Ni precursors containing the weakly labile ligand PMe_3.

[16] Different metal-containing side-products are generated in this side reaction depending on the metallic precursors used. For example, $(PPh_3)_2Ni^{(II)}Cl_2$ generates $(PPh_3)_3Ni^{(I)}Cl$, which is thought to arise from the conproportionation of the $Ni^{(II)}$ precursor and the $(PPh_3)_nNi^{(0)}$ species generated in the coupling reaction. On the other hand, reaction of the analogous $(PMe_3)_2NiCl_2$ gives only $Ni(PMe_3)_4$, which can be detected by its characteristic ^{31}P signal at - 22 ppm (Tolman, C. A. *J. Am. Chem. Soc.* **1970**, *92*, 2956). For the palladium precursor $(PPh_3)_2PdCl_2$, only the species $Pd(PPh_3)_n$ (n= 3 or 4) has been detected by $^{31}P\{^1H\}$ NMR at - 24 ppm.

[17] We have noted that the independently prepared (η-Ind)Pd(PR_3)Cl react much more readily than their Ni counterparts with IndLi to give 1,1'-biindene; this might explain why the metathetic routes involving Ind anions are particularly ineffective for the synthesis of indenyl Pd complexes.

[18] Lin, S.; Boudjouk, P. *J. Chin. Chem. Soc.* **1989**, *36*, 35.

[19] Baker, R. T.; Tulip, T. H. *Organometallics* **1986**, *5*, 839.

[20] Westcott, S. A.; Kakkar. A. K.; Stringer, G.; Taylor, N. J.; Marder, T. B. *J. Organomet. Chem.* **1990**, *394*, 777.

[21] Merda, J. S.; Kacmarcik, R. T.; Engen, D. V. *J. Am. Chem. Soc.* **1986**, *108*, 329.

[22] Kohler, F. H. *Chem. Ber.* **1974**, *107*, 570.

[23] The difference in the chemical shifts of the H1/H3 signals is much larger in **4** (ca. 2 ppm) than in **7**, **8**, and **9** (ca. 1 ppm). This is partially caused by the anisotropic current effects of the PPh_3 phenyl rings. This same phenomenon is clearly evident in the Ni complex **11** for which the chemical shift difference between H1 an H3 signals is greater than 2.5 ppm (Table 2.I). We believe that the reason for the smaller anisotropic shift in the Pd complexes is the longer Pd-PPh_3 and Pd-Ind bond distances, which place H3 farther from the Ph rings of PPh_3 (by ca. 0.2 Å).

[24] Abraham. R. J.; Loftus, P. Proton and Carbon-13 NMR Spectroscopy; Wiley: New York, 1985; Chapter 7, pp 165-168, eq. 7.11: $\Delta G^{\ddagger}/RTc = 22.96 + \ln(T_c/\delta\nu)$.

[25] (a) Casey, C. P.; O' Connor J. M *Organometallics* **1985**, 4, 384. (b) Hermmann, W. A.; Kuhn, F. E.; Romao, C. C. *J. Organomet. Chem.* **1995**, *489*, C56. (c) O' Hare, D *Organometallics* **1987**, *6*, 1766.

[26] We have also studied the solid-state structure of the PMe_3 analogue, complex **8**, but the low quality of the crystal results have precluded their inclusion here.

[27] The unit cells of complexes **4**, **7**, and **9** contain two independent molecules differing from each other by the orientation of the phosphine ligand in each case. In the case of **7** and **9**, the distances and angles are quite similar and have been averaged; in the case of complex **4**, however, the distances and angles of the two molecules are too dissimilar to allow averaging.

[28] The unit cell of complex **6** contains four half independent molecules; the distances and angles are similar and have been averaged.

[29] The Δ(M-C), HA, and FA values for a range of Ind complexes are given in references 19 and 20. The corresponding data for group 10 complexes are given in reference 4.

[30] (a) Guérin, F.; Beddie, C. L.; Stephan, D. W.; v. H. Spence, E.; Wurz, R. *Organometallics* **2001**, *20*, 3466. (b) Deck, P. A.; Fronczek, F. R. *Organometallics* **2000**, *19*, 327. (c) Blenkiron, P; Enright, G. D.; Taylor, N. J.; Carty, A. J. *Organometallics* **1996**, *15*, 2855. (d) Thorn, M. G.; Fanwick, P. E.; Chesnut, R. W.; Rothwell, I. P. *Chem. Commun.* **1999**, 2543. (e) Radius, U.; Sundermeyer, J.; Peters, K.; v. Schering, H. G. Z. *Anorg. Allg. Chem.* **2002**, *628*, 1226.

[31] (a) Otsuka, S.; Nakamura, A.; Yoshida, T. *J. Am. Chem. Soc.* **1969**, *91*, 7196. (b) Crociani, B.; Boschi, T.; Belluco, U. *Inorg. Chem.* **1970**, *9*, 2021. (c) Cherwinski, W. J.; Clark, H. C.; Manzer, L. E. *Inorg. Chem.* **1972**, *11*, 1511. (d) De Munno, G.; Bruno, G.; Grazia Arena, C.; Drommi, D.; Faraone, F. *J. Organomet. Chem.* **1993**, *450*, 263.

[32] Anderson, G. K.; Lin, M. *Inorg. Synth.* **1990**, *28*, 60.

[33] Klein, H-F; Zettel, B; Flörke, U.; Haupt, H. -J. *Chem. Ber.* **1992**, *125*, 9.

[34] *SMART*, Release 5.059; Bruker Molecular Analysis Research Tool, Bruker AXS Inc.: Madison, WI 53719-1173, 1999.

[35] *SAINT*, Release 6.06; Integration Software for Single Crystal Data. Bruker AXS Inc.: Madison, WI 53719-11, 1999.

[36] Sheldrick, G. M. *SHELXS*. Program for the solution of Crystal Structures. University of Goettingen. Germany, 1997.

[37] Sheldrick, G. M. *SHELXL*. Program for the Refinement of Crystal Structures. University of Goettingen. Germany, 1997.

[38] *GEMINI*, version 1.02; Twinning solution Program, Bruker AXS Inc.: Madison, WI 53711-5373, 1999.

[39] Sheldrick, G.M. *SADABS*, Bruker Area Detector Absorption Corrections, Bruker AXS Inc.: Madison, WI 53719-1173, 1997.

Chapitre 3: Synthesis and Reactivities of Neutral and Cationic Indenyl Palladium Complexes

Article 2

Christine Sui-Seng, Laurent F. Groux, and Davit Zargarian*

Département de chimie, Université de Montréal, Montréal, Québec, Canada H3C 3J7

Organometallics **2006**, *25*, 571-579

Abstract

The complexes [(1-R-Ind)Pd(PPh_3)Me] (R = H (**3**), Me (**4**)), [(1-R-Ind)Pd(PPh_3)$_2$]BF_4 (R = H (**5**[BF_4]), Me (**6**)), and [(1-R-Ind)Pd(PPh_3)(OSO_2CF_3)] (R = H (**7**), Me (**8**)) have been prepared by reacting their corresponding Pd-Cl derivatives with MeMgCl, $AgBF_4$/PPh_3, and AgOTf, respectively. These complexes have been characterized by NMR spectroscopy and, in the case of **3**, **5**[BF_4], **6** and **7**, by X-ray crystallography. The triflate moiety in complexes **7** and **8** is displaced readily by various ligands to give [(1-R-Ind)Pd(PPh_3)L][OTf] (L = PPh_3, **5**[OTf]; PMe_3, **9**; CH_3CN, **10**; PhCN, **11**; *t*-BuNC, **12**). Reactions of **7** or **8** with various olefins result in isomerization (1-hexene), dimerization and (or) trimerization (ethylene, styrene, and *p*-fluoro-styrene), oligomerization (*p*-amino- and *p*-methyl-styrene), or polymerization (*p*-methoxy-styrene). Compounds **1-8** promote the addition of $HSiCl_3$ to styrene and phenylacetylene.

Introduction

A number of advantages have favored the use of Ind complexes (Ind = indenyl and its substituted derivatives) in comparison to their Cp analogues in catalytic applications.[1] This is especially true for the Ind complexes of metals from groups 4-9, whereas the catalytic reactivities of group 10 metal-Ind complexes have not been investigated until very recently.[2] Thus, studies on the chemistry of Ni-Ind complexes have led to the discovery of interesting structural and bonding motifs,[3] as well as catalytic reactivities in the oligo- and polymerization of alkenes,[4] alkynes,[5] and $PhSiH_3$,[6] and in the hydrosilylation of alkenes and ketones.[7]

Our interest in the structures and catalytic activities of Ni-Ind complexes prompted us to explore the chemistry of analogous Pd compounds in order to elucidate the influence of the metal center on the chemistry of these compounds. Although a number of Ind-Pd complexes had been reported prior to our studies,[8] there were no general synthetic routes to these compounds. Our initial studies were, therefore, aimed

primarily at identifying reliable synthetic protocols to Ind-Pd complexes. In a previous report,[9] we described a high yield preparation of $[(\eta^3\text{-Ind})Pd(\mu\text{-Cl})]_2$ from the reaction of Me_3Si-Ind with $Na_2[PdCl_4]$ in ethanol, and showed that reacting this dimeric species with PR_3 or *t*-BuNC gives the complexes $[IndPd(PR_3)Cl]$ (R = Ph, Me, OMe, Cy) and $[(\eta^1\text{-Ind})(t\text{-BuNC})Pd(\mu\text{-Cl})]_2$, respectively. Curiously, however, this protocol proved very sensitive to the presence of substituents on the Ind ligand, thus limiting this approach to the synthesis of the parent (unsubstituted) indenyl complexes.

Since the reactivities of Ind complexes are often influenced significantly by the nature of the substituents on the Ind ligand, we sought an alternative synthetic route to variously substituted Pd-Ind complexes. We have explored, with limited success, the metathetic reaction of Li[R-Ind] with suitable Pd precursors, thus preparing a series of 1-Me-Ind derivatives in low yields.[10] Nevertheless, access to the compounds (1-Me-Ind)$Pd(PPh_3)X$ has allowed us to study their structures and reactivities as a function of Ind substituent and X ligand. The present report describes the preparation and characterization of the complexes [(1-R-Ind)$Pd(PPh_3)$Me] (R = H, (**3**); Me, (**4**)), [(1-R-Ind)$Pd(PPh_3)_2][BF_4]$ (R = H, (**5**[BF_4]); Me, (**6**)), and [(1-R-Ind)$Pd(PPh_3)$(OTf)] (R = H, (**7**); Me, (**8**); OTf = OSO_2CF_3), and discusses the reactivities of some of these complexes with $PhSiH_3$, ethylene, 1-hexene, and *p*-X-styrene (X = H, F, Me, NH_2, OMe). The facile substitution of the OTf moiety in complex **7** has given access to the new cationic complexes $[(Ind)Pd(PPh_3)(L)]^+$ (L = PPh_3, (**5**[OTf]); PMe_3, (**9**); CH_3CN, (**10**); PhCN, (**11**); *t*-BuNC, (**12**)), which are also described briefly. The effectiveness of our Ind-Pd(II) complexes in catalyzing the addition of $HSiCl_3$ to styrene and phenylacetylene were also examined.

Results and Discussion

Synthesis and Spectroscopic Characterization. The chloro complexes (1-R-Ind)$Pd(PPh_3)Cl$ (R = H, (**1**); Me, (**2**)) have been prepared by addition of PPh_3 to the dimer $[(\eta^3\text{-Ind})Pd(\mu\text{-Cl})]_2$ (for **1**) or to the mixture of Li[1-Me-Ind] and $[(PhCN)_2PdCl_2]$ (for **2**).[9] Complexes **1** and **2** were then used to prepare the analogous

Pd-Me, Pd-PPh_3 and Pd-OTf derivatives, as follows (Scheme 3.1): reaction with MeMgCl gave (1-R-Ind)Pd(PPh_3)Me (R = H, **3**; Me, **4**) in ca. 25% yield; reaction with $AgBF_4$ in the presence of one equiv of PPh_3 gave the cationic complexes [(1-R-Ind)Pd(PPh_3)$_2$][BF_4] (R = H, **5**[BF_4]; Me, **6**) in ca. 90% yield; reaction with AgOTf gave (1-R-Ind)Pd(PPh_3)(OTf) (R = H, **7**; Me, **8**) in ca. 80% yield. Complexes **3**-**8** are thermally stable in the solid state and can be stored at room temperature; in solution, however, decomposition takes place after a few days with concomitant deposition of Pd metal. Complexes **3**, **5**[BF_4], **6**, and **7** were isolated in pure form, but the purifications of **4** and **8** were not successful.[11] The NMR spectra of these complexes support their proposed structures, as described below.

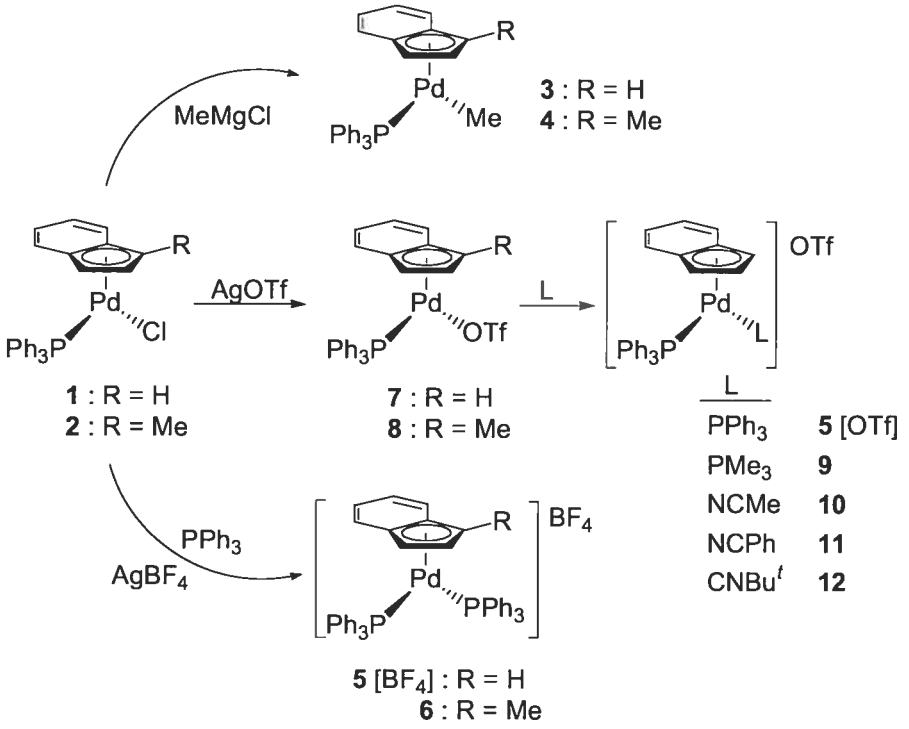

Scheme 3.1

The $^{31}P\{^1H\}$ NMR spectra showed one singlet resonance for the PPh_3 ligand in these complexes (at ca. 40 ppm for **3** and **4**, 29-31 ppm for **7** and **8**, and 28 ppm for

5[BF_4]). On the other hand, the $^{31}P\{^1H\}$ NMR spectrum of complex **6** showed AB doublets at ca. 29 and 30 ppm ($^2J_{P\text{-}P} \sim 59$ Hz), reflecting the inequivalence of the two PPh_3 ligands. This is caused by the presence of the Me substituent, which eliminates the mirror plane normally present in (indenyl)ML_2 complexes, such that the C_s symmetry of **5**[BF_4] is reduced to C_1 for **6** in the absence of a rapid rotation of the Ind ligand.

The ^1H and $^{13}C\{^1H\}$ NMR spectra of these compounds were fairly similar to those of their Ni counterparts and proved particularly informative on the coordination mode of the Ind ligands. For instance, **3** and **5**[BF_4] showed only one resonance for the symmetry-related pairs of protons (H1/H3, H4/H7, and H5/H6) or carbons (C1/C3, C4/C7 and C5/C6); the chemical shifts of these resonances were very similar to the corresponding signals in the high-temperature spectrum of complex **1**.[9] In contrast, the ^1H and $^{13}C\{^1H\}$ NMR spectra of the OTf derivative **7** display distinct signals for these nuclei, much like the ambient temperature spectra of complex **1**.[9] These observations indicate that the rotation of the Ind ligand is similarly hindered in **7** and **1** but is much more facile in **3**.

This conclusion is in accord with the results of variable temperature NMR studies that have allowed us to calculate an energy barrier of ca. 10.6 kcal/mol for the rotation of the Ind ring in **3**, in contrast to a much higher barrier in **1** (ca. 16.5 kcal/mol).[9] On the basis of previously established correlations between Ind hapticity and rotational barriers,[12] we conclude that, in solution, the Ind ligand in **3** is coordinated to Pd in a more symmetrical fashion and with a greater degree of hapticity than in **1** (Chart 3.1).

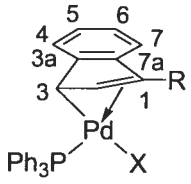

1: R = H, X = Cl
2: R = Me, X = Cl
7: R = H, X = OTf
8: R = Me, X = OTf

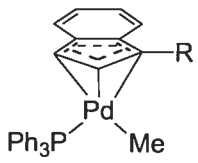

3: R = H
4: R = Me

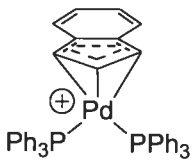

5

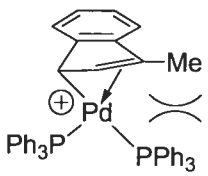

6

Chart 3.1

The stronger Ind-Pd interactions in this Pd-Me complex can be attributed to the more effective bonding between Ind and the softer Pd center in the alkyl derivative, while the more symmetrical coordination is due to the smaller difference between the trans influence of the ancillary ligands PPh_3 and Me in complex **3**.

The ^1H NMR spectral patterns displayed by **4** and **8** were similar to those observed in the ambient temperature spectra of (Ind)Pd(PR_3)Cl (R = Ph, Me, OMe, Cy).[9] For example, the ^1H NMR spectrum of **4** contained two doublets (H4/H7) and two triplets (H5/H6) between ca. 6.8 and 7.2 ppm, a doublet of doublets at ca. 6.4 ppm (H2), a singlet at ca. 5.3 ppm (H3) and a doublet at ca. 2.1 ppm (CH_3-Ind); in addition, a doublet was detected at –0.12 ppm ($^3J_{P\text{-}H} \sim 4$ Hz) for the Pd-Me moiety. The complete absence of symmetry in **4** and **8** means that the proton and carbon nuclei of the 1-Me-Ind ligand cannot be exchanged by Ind rotation, which is contrary with the situation in **3** and **6** wherein the C_1 symmetry becomes C_s as a result of rapid Ind rotation.

Finally, analysis of the Pd-OTf complexes by IR and $^{19}F\{^1H\}$ NMR spectroscopy showed typical resonances for an η^1-coordinated triflate group:[13] asymmetric sulfonyl stretching modes at ca. 1312 cm^{-1} in the IR spectra and singlet resonances at ca. –80 ppm in the $^{19}F\{^1H\}$ NMR spectra.

Solid State Structural Studies. The solid state structures of complexes **3**, **5**[BF_4], **6** and **7** have been studied by X-ray crystallography. The crystal data are presented in Tables 3.I and 3.II, selected structural parameters are presented in Tables 3.III (for **3** and **7**) and 3.IV (for **5**[BF_4] and **6**), and the ORTEP diagrams for these complexes are shown in Figures 3.1-3.4. The overall geometry around Pd in all four complexes is approximately square planar, with the largest distortion arising from the small C1-Pd-C3 angle (ca. 60°). Close inspection of the main structural parameters obtained for these complexes and comparison of their values to those of previously reported Ind-Pd allows an evaluation of the influence of Ind substituents and the Cl, Me, and OTf ligands on the Ind hapticity and overall structures of these complexes, as described below.

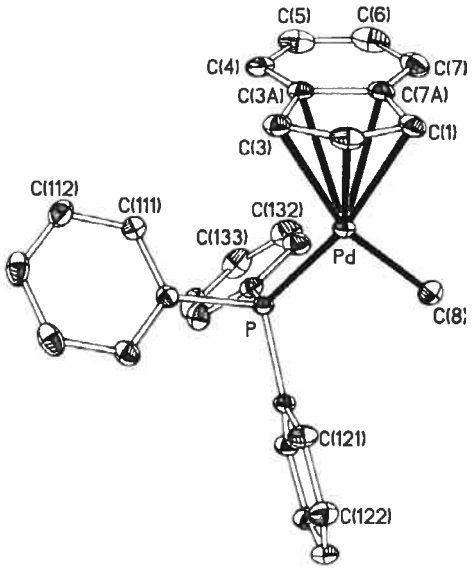

Figure 3.1: ORTEP view of complex **3**. Thermal ellipsoids are shown at 30% probability and hydrogen atoms are omitted for clarity.

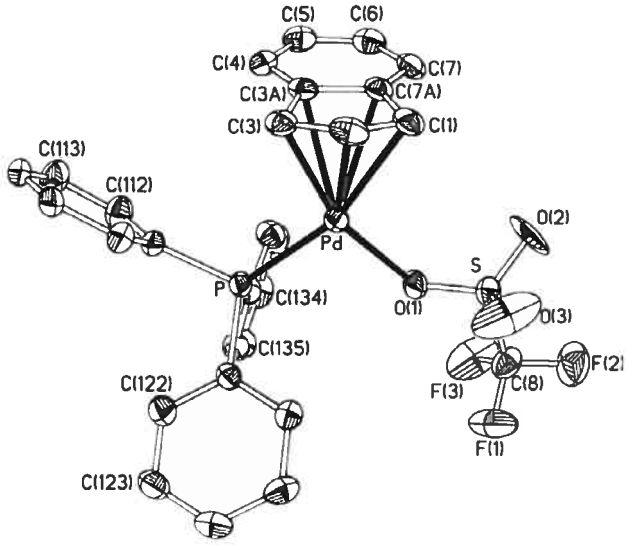

Figure 3.2: ORTEP view of complex **7**. Only one of the two independent molecules is shown. The OTf anion is disordered over two positions; the view shown in this figure represents the major model. Thermal ellipsoids are shown at 30% probability and hydrogen atoms are omitted for clarity.

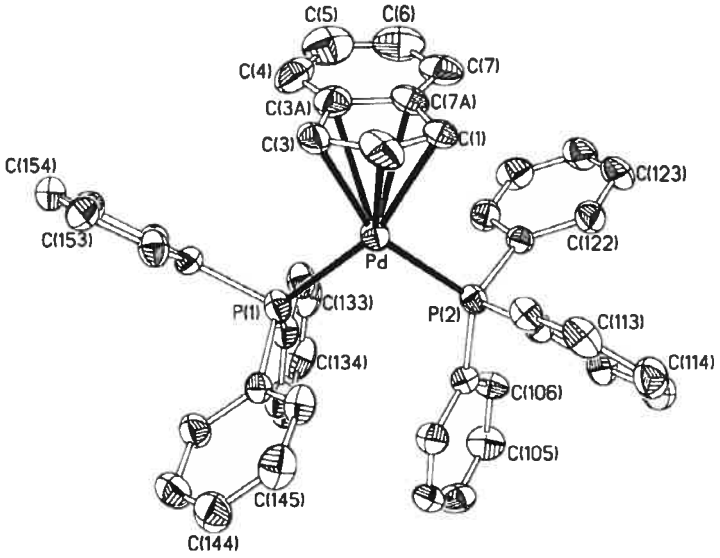

Figure 3.3: ORTEP view of complex **5**[BF_4]. Thermal ellipsoids are shown at 30% probability. The BF_4 anion and the hydrogen atoms are omitted for clarity.

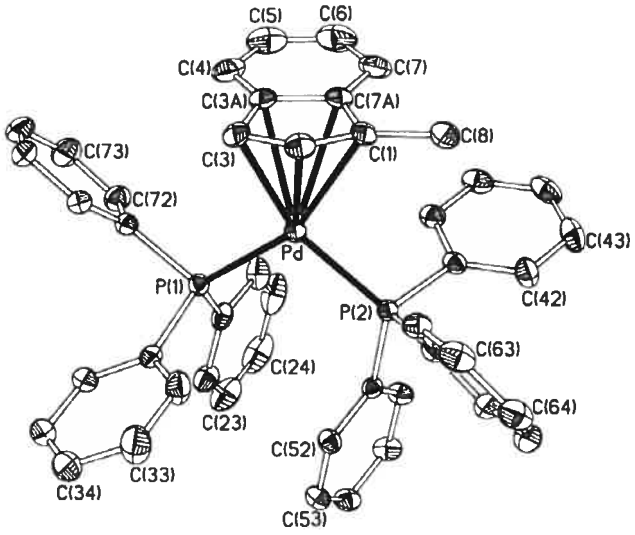

Figure 3.4: ORTEP view of complex **6**·1.5CH_2Cl_2. Thermal ellipsoids are shown at 30% probability. The BF_4 anion, the solvent, and the hydrogen atoms are omitted for clarity.

Table 3.I: Crystal data, Data Collection, and Structure Refinement Parameters of **3** and **7**

	3	**7**
formula	$C_{28}H_{25}PPd$	$C_{28}H_{22}PF_3O_3SPd$
mol wt	498.85	632.89
cryst color, habit	yellow-orange, block	red, block
crystal dimens, mm	0.15×0.19×0.60	0.07×0.10×0.27
cryst syst	triclinic	triclinic
space group	*P*-1	*P*-1
a, Å	7.5169(1)	10.3261(1)
b, Å	11.5414(1)	11.2327(2)
c, Å	13.8896(1)	23.9756(3)
α, deg	93.358(1)	80.607(1)
β, deg	96.272(1)	87.530(1)
γ, deg	107.103(1)	74.077(1)
V, Å^3	1139.53(2)	2638.37(6)
Z	2	4
D(calcd), g cm^{-3}	1.454	1.593
diffractometer	Bruker AXS SMART 2K	Bruker AXS SMART 2K
temp, K	223	223
λ, Å	1.54178	1.54178
μ, mm^{-1}	7.304	7.427
scan type	ω scan	ω scan
F(000)	508	1272
θ_{max} (deg)	72.83	72.65
h,k,l range	$-7 \le h \le 8$	$-12 \le h \le 12$
	$-14 \le k \le 14$	$-13 \le k \le 10$
	$-17 \le l \le 16$	$-29 \le l \le 29$
No. of reflns collected/unique	13683/4319	32097/10061
abs corr	multiscan	multiscan
T (min, max)	0.23, 0.33	0.44, 0.70
R ($F^2 > 2\sigma(F^2)$), $R_w(F^2)$	0.0287, 0.0747	0.0421, 0.1046
GOF	1.053	0.955

Table 3.II. Crystal data, Data Collection, and Structure Refinement Parameters of **5**[BF_4] and **6**

	5[BF_4]	**6**
formula	$C_{45}H_{37}P_2PdBF_4$	$C_{46}H_{39}P_2PdBF_4.1.5CH_2Cl_2$
mol wt	832.90	974.31
cryst color, habit	red-orange, needle	red-orange, block
cryst dimens, mm	0.08×0.14×0.27	0.08×0.15×0.19
cryst syst	monoclinic	triclinic
space group	$P2_1/n$	P-1
a, Å	11.685(5)	11.8930(1)
b, Å	20.765(11)	14.2475(1)
c, Å	15.709(6)	14.2624(3)
α, deg	90	75.970(1)
β, deg	95.89(3)	84.247(1)
γ, deg	90	68.763(1)
V, Å^3	3791(3)	2185.18(3)
Z	4	2
D(calcd), g cm^{-3}	1.459	1.481
Diffractometer	Nonius CAD-4	Bruker AXS SMART 2K
Temperature, K	293	223
λ, Å	1.54178	1.54178
μ, mm^{-1}	5.176	6.225
Scan type	ω scan	ω scan
F(000)	992	990
θ_{max}, (deg)	69.97	72.84
h,k,l range	$-14 \le h \le 14$	$-14 \le h \le 14$
	$-25 \le k \le 25$	$-17 \le k \le 17$
	$-19 \le l \le 19$	$-17 \le l \le 17$
no. of reflns collected/unique	15548/7177	26475/8353
abs cor	Ψ-scan	multiscan
T (min, max)	0.34, 0.69	0.40, 0.73
R ($F^2 > 2\sigma(F^2)$), $R_w(F^2)$	0.0475, 0.0873	0.0435, 0.1186
GOF	0.643	1.003

Table 3.III. Selected Bond Distances (Å) and Angles (deg) for **1**[a], **3** and **7**[b].

	1 (X = Cl)		**3** (X = C8)	**7** (X = O)
Pd-P	2.2785(6)	2.2273(6)	2.2260(5)	2.283(1)
Pd-X	2.3474(6)	2.3560(7)	2.061(3)	2.157(15)
Pd-C1	2.244(2)	2.282(3)	2.273(2)	2.290(4)
Pd-C2	2.186(2)	2.209(3)	2.273(2)	2.196(4)
Pd-C3	2.192(2)	2.165(3)	2.321(2)	2.135(4)
Pd-C3a	2.607(2)	2.544(3)	2.562(2)	2.554(4)
Pd-C7a	2.610(2)	2.580(2)	2.533(2)	2.615(4)
C1-C2	1.404(4)	1.393(4)	1.410(4)	1.390(7)
C2-C3	1.410(4)	1.413(4)	1.403(4)	1.421(7)
C3-C3a	1.474(4)	1.468(4)	1.449(3)	1.478(6)
C3a-C7a	1.415(4)	1.422(4)	1.425(3)	1.419(6)
C7a-C1	2.1.464(4)	1.465(4)	1.460(4)	1.478(6)
S-O1				1.415(9)
S-O2				1.418(10)
S-O3				1.377(11)
S-C8				1.817(10)
C8-F1				1.294(12)
P-Pd-X	96.23(2)	97.04(2)	89.85(9)	92.3(4)
C3-Pd-X	158.71(7)	160.78(8)	160.60(11)	165.0(5)
C3-Pd-P	104.91(7)	101.75(8)	109.45(6)	101.35(13)
C1-Pd-X	97.29(7)	99.48(8)	100.86(11)	104.3(5)
C1-Pd-P	164.25(7)	161.72(8)	168.20(7)	160.95(13)
C1-Pd-C3	61.4(1)	61.3(1)	59.74(9)	61.51(17)
ΔM-C (Å)	0.39	0.39	0.25	0.37
HA (deg)	15.49	14.58	10.17	15.22
FA (deg)	14.84	14.40	9.29	13.61

a) See ref. 9.

b) The structural parameters for the two independent molecules in the unit cell of **7** were quite similar and have been averaged.

Table 3.IV. Selected Bond Distances (Å) and Angles (deg) for **5**[BF_4] and **6**.

	5[BF_4]	**6**
Pd-P1	2.301(2)	2.3095(7)
Pd-P2	2.309(2)	2.3227(7)
Pd-C1	2.270(6)	2.336(3)
Pd-C2	2.230(6)	2.233(3)
Pd-C3	2.223(6)	2.209(3)
Pd-C3a	2.570(9)	2.577(3)
Pd-C7a	2.585(9)	2.645(3)
C1-C2	1.418(9)	1.405(5)
C2-C3	1.434(9)	1.425(5)
C3-C3a	1.443(9)	1.459(5)
C3a-C7a	1.422(10)	1.427(5)
C7a-C1	1.445(10)	1.477(5)
C1-C8		1.500(5)
P1-Pd-P2	104.31(7)	103.72(3)
C3-Pd-C1	60.1(3)	60.59(13)
C3-Pd-P2	156.2(2)	158.82(10)
C3-Pd-P1	99.5(2)	97.34(10)
C1-Pd-P1	159.5(2)	156.14(9)
C1-Pd-P2	96.1(2)	98.92(9)
ΔM-C (Å)	0.33	0.34
HA (deg)	11.86	13.71
FA (deg)	12.18	15.99

The Pd center in each of these complexes is within reasonable bonding distance from the P, C1, C2, C3 and X atoms (X = C8 in **3**, P2 in **5**[BF_4] and **6**, and O in **7**), but considerably farther away from C3a and C7a. This difference in the Pd distances to the allylic and benzo carbons is a reflection of the so-called "slippage" of the Ind ligand. The degree of such slippage away from the idealized η^5 coordination is often measured by calculating parameters such as the slip value (ΔM-C) and the hinge and fold

angles(HA and FA).[14] Inspection of these parameters (Tables 3.III and 3.IV) shows that the degree of slippage in the Pd-OTf complex **7** is similar to those found for the analogous Pd-Cl compounds (1-R-Ind)Pd(PR'$_3$)Cl (R= H, Me; R' = Ph, Cy, Me, OMe),[9] but significantly larger than those found for the Pd-Me derivative **3**; evidently, Ind hapticity in IndPd(PPh$_3$)X is greatly influenced by the nature of the X ligand (Me > Cl ~ OTf). These results also show that the Ind hapticities are much greater (smaller ΔM-C, HA, and FA parameters) in the corresponding Ni complexes; this structural difference is reflected in subtle but important differences in the reactivities of the analogous Ni and Pd complexes (vide infra).

A comparison of the structural parameters found in the cationic complexes **5**[BF$_4$] and **6** on one hand, and the neutral species **1**,[9] **2**,[9] **3**, and **7** on the other, shows again that the most important factor affecting the Pd-Ind interactions is the nature of the X moiety, followed by the overall charge of the complex. Thus, Ind hapticity is reinforced on going from the neutral species **1**, **2**, and **7** (X = Cl and OTf; ΔM-C = 0.32-0.39 Å) to the cationic complexes **5**[BF$_4$] and **6** (X = PPh$_3$; ΔM-C = 0.33 and 0.34 Å), to the neutral Pd-Me compound **3** (ΔM-C = 0.25 Å). The Ind substituent also appears to play a role, especially in the case of the bis(phosphine) complexes, wherein the Me substituent prevents closer approach of the Ind ligand (in **6**) to the Pd center and results in the less symmetrical coordination of the Ind ligand (Chart 3.1): Pd-C1 > Pd-C3 by more than 0.12 Å (40 esd) in **6** compared to less than 0.05 Å (8 esd) in **5**[BF$_4$].

Reactivities of the Pd-triflate species 7 and 8. We have studied the substitution of the triflate moiety in complex **7** by different nucleophiles L as a route for the preparation of new cationic complexes (Scheme 3.1). These ligand substitution reactions were carried out by treating **7** with one equiv of L in $CDCl_3$. NMR spectroscopy showed rapid and clean displacement of the OTf moiety to give the adducts [IndPd(PPh$_3$)(L)][OTf] (L = PPh$_3$ (**5**[OTf]), PMe$_3$ (**9**), CH$_3$CN (**10**), PhCN (**11**), and *t*-BuNC (**12**)). The spectroscopic characterization of these complexes was quite straightforward. For example, the $^{31}P\{^1H\}$ NMR spectra of **5**[OTf] and **10-12** each

showed a new singlet resonance in a narrow chemical shift range (27-31 ppm), attributed to the PPh_3 ligand, whereas the PMe_3 adduct **9** gave rise to an AX set of doublets at 30.0 and –16.6 ppm ($^2J_{P\text{-}P}$ = 60 Hz), as expected. The ^1H and $^{13}C\{^1H\}$ NMR spectra of the new species also displayed the expected signals for Ind and PPh_3 ligands. In addition, the presence of the CH_3CN and $CNC(CH_3)_3$ ligands in complexes **10** and **12**, respectively, was signaled by ^1H NMR resonances at 2.07 and 1.15 ppm, respectively.

The IR spectra of **10-12** proved valuable, because the frequencies of the ν(CN) bands reflect the nature of Pd-L interactions. Thus, the ν(CN) frequencies of free and coordinated CH_3CN (2254 vs. 2247cm^{-1})[15] and PhCN (2230 vs. 2227 cm^{-1}) indicate negligible degree of π-back-bonding between these weakly π-acidic ligands and the cationic Pd center. On the other hand, the corresponding ν(CN) frequencies for the *t*-BuNC ligand (2136 cm^{-1} in the free ligand vs. 2206 cm^{-1} in complex **12**) signal a greater C-N bond order resulting from significant σ donation from the HOMO of the ligand, which has antibonding character with respect to the C-N bond. Similar IR data have been reported for other Pd(II)-isocyanide complexes.[9,16]

The lability of the triflate moiety also allowed us to explore the reactivities of complexes **7** and **8** with olefins. The reactions with ethylene were performed by bubbling $CDCl_3$ solutions of complexes **7** and **8** with ethylene for ca. 5 min. Careful analysis of the reaction mixtures by ^1H and $^{13}C\{^1H\}$ NMR spectroscopy indicated the formation of (*E*)- and (*Z*)-2-butenes (Scheme 3.II). In contrast, methyl methacrylate did not react at all with **7** or **8**, whereas 1-hexene was isomerized to (*E*)- and (*Z*)-2-hexene (ca. 3:1). GC/MS analysis of the isomerization reaction catalyzed by complex **7** showed the presence of trace quantities of (1-hexenyl)indene in the reaction mixture: $M^{\cdot+}$ at *m/z* = 198; $M^{\cdot+}$ - 15 (Me); $M^{\cdot+}$ - 29 (Et); $M^{\cdot+}$ - 43 (Pr); $M^{\cdot+}$ - 57(Bu); etc.

The reactions of variously substituted styrenes with **7** or **8** gave interesting results. Thus, 50-70 equiv of styrene reacted with either complex over 15 h at room temperature to give nearly quantitative conversion of the substrate to the head-to-tail dimer (*Z*)-1,3-diphenyl-1-butene. GC/MS analyses of the reaction mixtures confirmed that the main product was a single isomer of the dimer ($M^{\cdot+}$ at *m/z* 208), but also

revealed the presence of trace quantities (< 2%) of a trimer ($M^{\cdot+}$ at *m/z* 312) and Ind-C(Ph)=CH_2 ($M^{\cdot+}$ at *m/z* 218). Analogous reactions with *p*-fluoro-styrene gave a 65 : 35 mixture of the linear dimer ($M^{\cdot+}$ at *m/z* 244) and trimer ($M^{\cdot+}$ at *m/z* 366); GC/MS analyses showed that the dimer consists of two isomers (ca. 98:2), but structural details could not be established firmly from the ^1H NMR spectra. On the other hand, reactions of complex **7** with electron-rich *p*-X-styrenes (X= NH_2, Me, OMe) gave higher oligomers and polymers, as follows: *p*-amino-styrene was converted quantitatively to an oligomer (M_w ~1050, M_w/M_n ~ 1.3, 100 turnovers) as was *p*-methyl-styrene (M_w ~1250, M_w/M_n ~ 1.4, 885 turnovers), whereas *p*-methoxy-styrene was polymerized (M_w ~ 29000, M_w/M_n ~ 3.2, 970 turnovers).

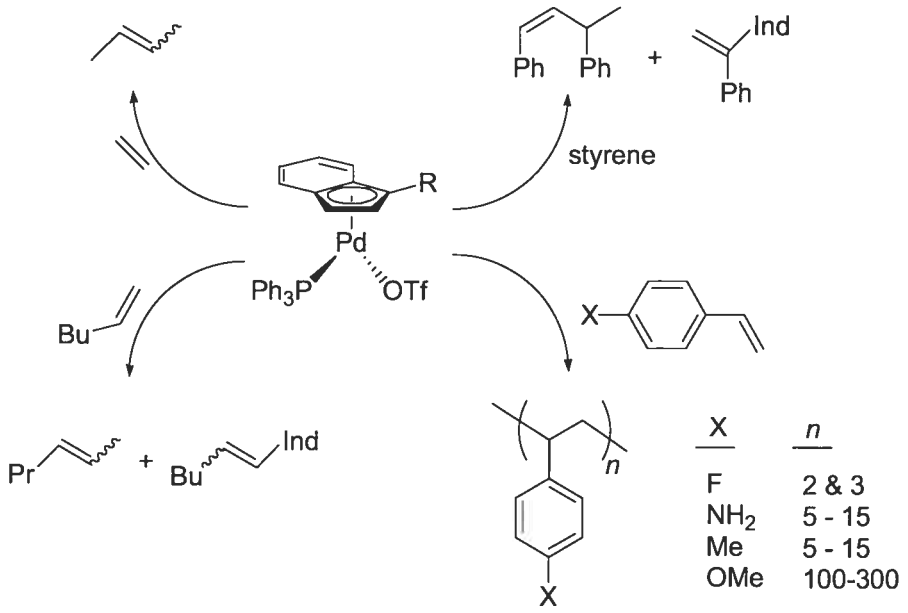

Scheme 3.2

The greater reactivities of styrenes encouraged us to explore their co-oligomerization between themselves and with 1-hexene. Unfortunately, however, all reactions with mixtures of olefins failed to induce hetero-oligomerization reactions. For instance, reacting a 1:1 mixture of styrene and 1-hexene with complex **7** led to the formation of (*Z*)-1,3-diphenyl-1-butene and (*E*)- and (*Z*)-2-hexene only.

Taken together, these results indicate that the reactivities of **7** and **8** with olefins are quite sensitive to the nature of the substrates, ranging from no reaction with methyl methacrylate to isomerization with 1-hexene and oligo- and polymerization with ethylene and *p*-X-styrenes. Comparison of these reactivities to those observed with analogous Ni-Ind complexes demonstrates subtle differences. For example, styrene is converted to mostly poly(styrenes) ($M_w \sim 10^4$-10^5) by in-situ generated cations $[IndNi(PPh_3)]^+$,[4c,e,f,l] whereas the analogous Pd complexes promote a regioselective dimerization. On the other hand, both Ni- and Pd-Ind precursors show the same reactivities with ethylene and 1-hexene. It is worth noting that reaction of ethylene with the complex **1** or $\{(Ind)Pd(\mu\text{-}Cl)\}_2$ or $IndNi(PR_3)Cl$ in the presence of excess MAO gives polyethylene.[4b,9] We propose that the reactions of the Pd-OTf derivatives with olefins proceed through the common hydrido Pd species $[L_nPdH]^+$ (Scheme 3.3), but it is not clear how the specific nature of each olefin can steer the reaction pathway from isomerization to the formation of dimers, oligomers, or polymers.

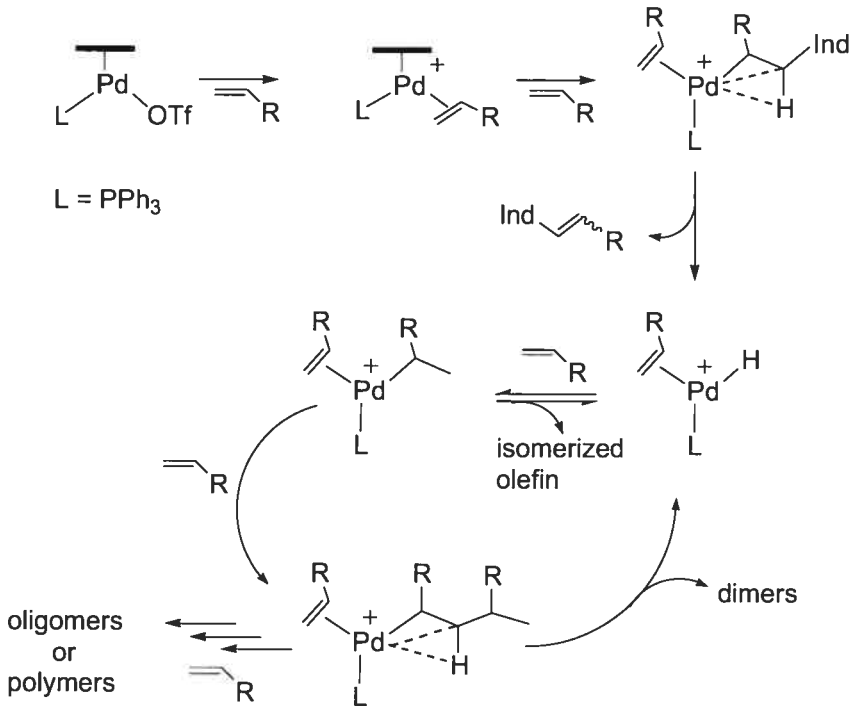

Scheme 3.3

Reactivities of Pd-Ind complexes with silanes. Previous studies have shown that Ni-Ind complexes can promote the dehydrogenative oligomerization of hydrosilanes and their additions to olefins and ketones.[6,7,4f,41,17] Our initial explorations on the reactivities of analogous Pd-Ind complexes indicated that the complexes **1** and **2** promote partial conversion of $PhSiH_3$ to products of a redistribution process (Ph_nSiH_{4-n}) and small amounts of Si-Si bond containing products. These findings motivated us to investigate the reactivities of the Pd-Me and Pd-OTf complexes **3**, **4**, **7**, and **8** with $PhSiH_3$, as follows.

Addition of 100 equiv of $PhSiH_3$ to C_6D_6 solutions of the Pd complexes at room temperature caused an immediate darkening of the reaction mixture and led to a concomitant evolution of gas. Monitoring the reaction mixtures by ^1H NMR spectroscopy indicated that ca. 20% of $PhSiH_3$ was consumed over 20 min, after which the reaction subsided almost completely and an insoluble solid accumulated in the bottom of the NMR tube. The reactions promoted by the Pd-OTf complexes showed new signals characteristic of the dimer $(PhH_2Si)_2$ (< 5%), leading us to conclude that these complexes do activate the Si-H bonds in $PhSiH_3$ and promote the formation of H-H[18] and Si-Si bonds, albeit fairly inefficiently. On the other hand, no new signal was detected in the reactions of the Pd-Me precursors. We speculate that these complexes promote the redistribution of Si-Ph and Si-H bonds in the initially formed $(PhSiH)_n$ to give SiH_4 (gas) and insoluble, cross-linked oligomers.

The low degree of substrate conversion and the difficulties in identification of the products of the above reactions prompted us to shift the focus of our studies away from silane oligomerization and onto hydrosilylation reactions. Initial tests with a range of different olefins and silanes showed that all complexes **1**-**8** can promote the addition of $HSiCl_3$ to styrene with the exclusive formation of 1-phenyl-1-(trichlorosilyl)ethane[19] in good yields (Table 3.V). Addition of $HSiCl_3$ to phenylacetylene was also examined briefly and found to give a mixture of α-and β-addition products $Ph(SiCl_3)C{=}CH_2$ and (*E*)-$PhCH{=}CHSiCl_3$ (Table 3.V, runs 9-11).[20] That these reactions likely proceed by the initial elimination of IndH was indicated by the reaction of the Pd-Me and Pd-Cl precursors with $HSiCl_3$ in the absence of olefin or alkyne substrates: an instantaneous darkening of the mixture was observed and the

formation of IndH was confirmed from the ^{1}H NMR spectra; the ^{31}P NMR spectrum of the mixture contained peaks at 36, 32, and 23 ppm, which remain unidentified.

Table 3.V : Pd-catalyzed hydrosilylation reactions with $HSiCl_3$[a]

entry	Cat.	Substrate	Products (conversion %)
1	**1**	Styrene	$Ph(SiCl_3)CHCH_3$ (92)
2	**2**	Styrene	$Ph(SiCl_3)CHCH_3$ (90)
3[b]	**2**	Styrene	$Ph(SiCl_3)CHCH_3$ (100)
4	**3**	Styrene	$Ph(SiCl_3)CHCH_3$ (84)
5	**5**$[BF_4]$	Styrene	$Ph(SiCl_3)CHCH_3$ (86)
6	**6**	Styrene	$Ph(SiCl_3)CHCH_3$ (93)
7	**7**	Styrene	$Ph(SiCl_3)CHCH_3$ (100)
8	**8**	Styrene	$Ph(SiCl_3)CHCH_3$ (95)
9[c]	**2**	PhC≡CH	(*E*)-PhCH=CH$SiCl_3$ (50)
			$Ph(SiCl_3)C=CH_2$ (50)
10[c]	**5**$[BF_4]$	PhC≡CH	(*E*)-PhCH=CH$SiCl_3$ (52)
			$Ph(SiCl_3)C=CH_2$ (48)
11[c]	**7**	PhC≡CH	(*E*)-PhCH=CH$SiCl_3$ (58)
			$Ph(SiCl_3)C=CH_2$ (42)

[a] Unless otherwise specified, all reactions were run in C_6D_6 at room temperature for 24 hours using a Pd: olefin/alkyne : $HSiCl_3$ ratio of 1: 100: 100.

[b] 150 equiv of $HSiCl_3$ was used in this run.

[c] In $CDCl_3$, room temperature, 24 h.

Finally, addition of $HSiCl_3$ to ketones and esters, and the more difficult hydrosilylation reactions with $PhSiH_3$, $HSiEt_3$, $HSi(OEt)_3$, and $HSiMe_2Cl$ were not catalyzed by our Pd complexes.

Conclusion

We have prepared and characterized the new Ind-Pd complexes [(1-R-Ind)Pd(PPh_3)Me] (R = H (**3**), Me (**4**)), [(1-R-Ind)Pd(PPh_3)$_2$]BF_4 (R = H (**5**[BF_4]), Me (**6**)), and [(1-R-Ind)Pd(PPh_3)(OTf)] (R = H (**7**), Me (**8**)) by reaction of their chloro analogues [(1-R-Ind)Pd(PPh_3)Cl] (R = H (**1**), Me (**2**)) with MeMgCl, $AgBF_4$/PPh_3 and AgOTf, respectively. Single crystal X-ray diffraction studies on complexes **3**, **5**[BF_4], **6**, and **7** have shown that Pd-Ind interactions are influenced by the nature of the X ligands, the overall charge, and, to a lesser extent, the Ind substituents. The lability of the OTf moiety in triflate complex **7** has allowed us to generate the new cationic species [IndPd(PPh_3)(L)]$^+$ (L = PPh_3, PMe_3, CH_3CN, PhCN, *t*-BuNC). Exploring the reactivites of complexes **7** and **8** with olefins has shown that these complexes isomerize 1-hexene, dimerize ethylene and styrene, dimerize and trimerize *p*-fluoro-styrene, oligomerize *p*-X-styrenes (X = NH_2 and Me), and polymerize *p*-methoxy-styrene. A brief examination of the reactivities of these complexes with hydrosilanes has shown that they are inefficient promoters of the dehydrogenative oligomerization of $PhSiH_3$, but catalyze the addition of $HSiCl_3$ to styrene and phenylacetylene.

The results of this study indicate that, contrary to our expectations, the preparation of (R-Ind)M(L)(X) complexes are more difficult for Pd relative to those for Ni, especially those derivatives bearing Ind substituents other than Me. Moreover, although the catalytic properties of the Pd complexes complement those of their Ni counterparts, the reactivities of the Ind-Pd compounds appear to be less easy to control and modulate. On the other hand, recent investigations have pointed out that another difference between these analogous complexes is the fairly easy access to amino(palladium) derivatives of η^3– and η^1–Ind and dimeric (μ–Ind)Pd^I-Pd^I species. Studies are currently underway on the preparation, characterization, and reactivities of new Ind-Pd complexes and will be communicated in due course.

Experimental Section

General Comments. All manipulations and experiments were performed under an inert atmosphere using standard Schlenk techniques and/or a nitrogen-filled glovebox. Dry, oxygen-free solvents were prepared by distillation from appropriate drying agents and employed throughout. The syntheses of (Ind)Pd(PPh_3)Cl (**1**) and (1-Me-Ind)Pd(PPh_3)Cl (**2**) have been reported previously;[9] all other reagents used in the experiments were obtained from commercial sources and used as received. The elemental analyses were performed by the Laboratoire d'Analyse Elémentaire (Université de Montréal). Bruker ARX400, AV400, AMX300, AV300 spectrometers were employed for recording ^{1}H (400 MHz and 300 MHz), $^{13}C\{^{1}H\}$ (100.56 MHz and 75.42 MHz), $^{31}P\{^{1}H\}$ (161.92 MHz and 121.49 MHz) and $^{19}F\{^{1}H\}$ (376.31 MHz and 282.23 MHz) NMR spectra at ambient temperature. The ^{1}H and ^{13}C NMR spectra were referenced to solvent resonances, as follows: 7.26 and 77.16 ppm for $CHCl_3$ and $CDCl_3$, respectively, and 7.16 and 128.06 ppm for C_6D_5H and C_6D_6, respectively. The ^{31}P and ^{19}F NMR spectra were referenced, respectively, to 85% H_3PO_4 (0 ppm) and $C_6H_5CF_3$ (-63.9 ppm). The IR spectra were recorded on a Perkin-Elmer 1750 FTIR instrument (4000-450 cm^{-1}) with samples prepared as KBr pellets.

Crystal Structure Determinations. The crystal data for complex **5**[BF_4] were collected on a Nonius CAD-4 diffractometer with graphite-monochromated Cu Kα radiation at 293 K using the CAD-4 software.[21] Refinement of the cell parameters was done with the CAD-4 software, while the data reduction used NRC-2 and NRC-2A.[22] The crystal data for complexes **3**, **6** and **7** were collected on a Bruker AXS Smart 2K diffractometer using SMART.[23] Graphite-monochromated Cu Kα radiation was used at 223 K. Cell refinement and data reduction were done using SAINT.[24] All structures were solved by direct methods using SHELXS97[25] and difmap synthesis using SHELXL97;[26] the refinements were done on F^2 by full-matrix least squares methods. All non hydrogen atoms were refined anisotropically, while the hydrogens (isotropic) were constrained to the parent atom using a riding model. The Crystal data and experimental details are listed in Tables 3.I and 3.II, while selected bond distances and

angles are listed in Tables 3.III and 3.IV . The OTf moiety in the crystal structure of **7** was disordered over two positions, with occupancies of 0.54 and 0.46. Two positions were also found for the counterion BF_4 in the structures of **5**[BF_4] and **6** with occupancy factors of 0.54/0.46 and 0.50/0.50, respectively. One of the solvent molecules (CH_2Cl_2) present within the crystal structure of **6** was also disordered over two positions (occupancies of 0.62 and 0.38). Each of the disorders was refined anisotropically using restraints (SAME/SADI/EADP/DFIX) applied in order to improve the model.

Synthesis of (Ind)Pd(PPh_3)(Me), (3). A solution of MeMgCl (256 μL of a 3 M solution in THF) was added dropwise to a solution of (Ind)Pd(PPh_3)Cl (**1**) (400 mg, 0.77 mmol) in Et_2O (80 mL) at room temperature. The resulting orange mixture was stirred for approximately 1.5 h, filtered, and concentrated to give an orange precipitate, which was isolated by filtration (110 mg, 29%). Recrystallization of this solid from a cold Et_2O/hexane solution yielded crystals suitable for X-ray diffraction studies and elemental analysis. NMR ^{1}H (C_6D_6, 300 MHz): δ 7.32-7.26 (m, PPh_3), 7.21 (pseudo dd, $^3J_{H\text{-}H}$ = 2.9 Hz, H_4 and H_7), 7.08 (pseudo dd, $^3J_{H\text{-}H}$ = 2.9 Hz, H_5 and H_6), 6.99-6.96 (m, PPh_3), 6.62 (t, $^3J_{H\text{-}H}$ = 3.1 Hz, H_2), 5.26 (pseudo t, $^3J_{H\text{-}H}$ = 3.5 Hz, H_1 and H_3), 0.57 (d, $^2J_{H\text{-}P}$ = 4.8 Hz, Pd-CH_3). ^{13}C{^{1}H} NMR (C_6D_6, 100.56 MHz): δ 134.19 (d, $^2J_{C\text{-}P}$ = 13.5 Hz, C_{ortho}), 133.8, 132.45, 131.79, 131.54, 130.22 (s, C_{para}), 128.51 (d, $^3J_{C\text{-}P}$ = 11.8 Hz, C_{meta}), 126.62, 124.00, 122.20 (s, C_5 and C_6), 117.21 (s, C_4 and C_7), 108.59 (s, C_2), 83.37 (s, C_1 and C_3), -18.33 (d, $^2J_{C\text{-}P}$ = 12.6 Hz, Pd-*Me*). ^{31}P {^{1}H} NMR ($CDCl_3$, 161.92 MHz): δ 39.81 (s). ^{31}P {^{1}H} NMR (C_6D_6, 121.49 MHz): δ 40.61 (s). Anal. Calcd for $C_{28}H_{25}P_1Pd.H_2O$: C, 65.06; H, 5.26. Found: C, 65.63; H, 5.19.

Synthesis of (1-Me-Ind)Pd(PPh_3)Me, (4). A solution of MeMgCl (93 μL of 3 M solution in THF) was added dropwise to a solution of (1-Me-Ind)Pd(PPh_3)Cl (**2**) (165 mg, 0.309 mmol) in benzene (25 mL) at 10 °C. The resulting brown mixture was stirred for approximately 45 min, filtered, and evaporated to dryness. The residue was precipitated from Et_2O/hexane at –22 °C to give an orange powder (35 mg, 22%).

NMR ^{1}H ($CDCl_3$, 300 MHz): δ 7.35-7.30 (m, PPh_3), 7.15 (m, PPh_3 and H_7), 7.00 (t, $^{3}J_{H\text{-}H}$ = 7.3 Hz, H_6), 6.88 (t, $^{3}J_{H\text{-}H}$ = 7.1 Hz, H_5), 6.78 (d, $^{3}J_{H\text{-}H}$ = 6.9 Hz, H_4), 6.41 (d, $^{3}J_{H\text{-}H}$ = 2.7 Hz, H_2), 5.34 (s, H_3), 2.07 (d, $^{4}J_{H\text{-}P}$ = 5.7 Hz, 1-*Me*-Ind), -0.12 (d, $^{2}J_{H\text{-}P}$ = 4.1 Hz, CH_3-Pd). ^{13}C{^{1}H} NMR (C_6D_6, 100.56 MHz): δ 138.19, 134.61 (d, $^{2}J_{C\text{-}P}$ = 14.7 Hz, C_{ortho}), 132.11, 131.43, 129.99 (s, C_{para}), 128.76 (d, $^{3}J_{C\text{-}P}$ = 10.2 Hz, C_{meta}), 126.46, 124.92, 123.91, 122.40 (s, C_6), 121.64 (s, C_5), 119.25 (s, C_1), 116.61 (s, C_7), 115.53 (s, C_4), 109.42 (s, C_2), 81.52 (s, C_3), -9.32 (br, Pd-*Me*). ^{31}P {^{1}H} NMR (C_6D_6, 161.92 MHz): δ 40.24 (s).

Synthesis of [(Ind)Pd(PPh_3)$_2$]BF_4, (5[BF_4]). A mixture of (Ind)Pd(PPh_3)Cl (**1**) (130 mg, 0.25 mmol), $AgBF_4$ (49 mg, 0.25 mmol), and PPh_3 (60 mg, 0.25 mmol) was stirred in CH_2Cl_2 (15 mL) for 1.5 h at room temperature and filtered to remove AgCl. Concentration of the filtrate to ca. 5 mL, followed by addition of 10 mL of Et_2O gave a red-orange precipitate, which was isolated by filtration (180 mg, 87%). Recrystallization of a small portion of this solid from a cold CH_2Cl_2/Et_2O solution yielded crystals suitable for X-ray diffraction studies and elemental analysis. ^{1}H NMR ($CDCl_3$, 300 MHz): δ 7.74-7.21 (m, PPh_3 and protons of Ind), 7.10-7.04 (m, PPh_3 and protons of Ind), 6.21 (dd, $^{3}J_{H\text{-}H}$ = 2.8 Hz, H_4 and H_7), 5.48 (q, $^{3}J_{H\text{-}H}$ = 3.9 Hz, H_1 and H_3). ^{13}C {^{1}H} NMR ($CDCl_3$, 75.40 MHz): δ 133.54 (t, $^{2}J_{C\text{-}P}$ = 5.9 Hz, C_{ortho}), 131.43 (s, C_{para}), 130.16 (d, $^{1}J_{C\text{-}P}$ = 46 Hz, C_{ipso}), 130.17(s, C_5 and C_6), 129.06 (pseudo t, $^{3}J_{C\text{-}P}$ = 5.3 Hz, C_{meta}), 127.94 (s, C_4 and C_7), 118.83 (s, C_2), 95.46 (pseudo t, $^{2}J_{C\text{-}P}$ = 11.6 Hz, C_1 and C_3). ^{31}P {^{1}H} NMR ($CDCl_3$, 121.49 MHz): δ 27.66 (s). Anal. Calcd for $C_{45}H_{37}B_1F_4P_2Pd$: C, 64.89; H, 4.48. Found: C, 64.36; H, 4.29.

Synthesis of [(1-Me-Ind)Pd(PPh_3)$_2$]BF_4, (6). A mixture of (1-Me-Ind)Pd(PPh_3)Cl (**2**) (100 mg, 0.19 mmol), $AgBF_4$ (37 mg, 0.19 mmol) and PPh_3 (50 mg, 0.19 mmol) was stirred in CH_2Cl_2 (15 mL) for 3 h at room temperature and filtered to remove AgCl. Concentration of the filtrate to ca. 5 mL, followed by addition of ca. 15 mL of Et_2O gave an orange precipitate, which was isolated by filtration (144 mg, 90%). Recrystallization of a small portion of this solid from a cold CH_2Cl_2/hexane solution

yielded crystals suitable for X-ray diffraction studies and elemental analysis. ^{1}H NMR ($CDCl_3$, 400 MHz): δ 7.42-6.92 (m, PPh_3 and protons of Ind), 6.53 (d, $^{3}J_{H-H}$ = 7.3 Hz, H_4 or H_7), 6.23 (d, $^{3}J_{H-H}$ = 7.7 Hz, H_7 or H_4), 5.08 (dd, $^{3}J_{H-P}$ = 3 Hz, H_3), 1.29 (dd, $^{3}J_{H-H}$ = 11.4 et 11.5 Hz, 1-*Me*-Ind). ^{13}C {^{1}H} NMR ($CDCl_3$, 100.56 MHz): δ 133.46 (dd, $^{2}J_{C-P}$ = 26.7 Hz, $^{4}J_{C-P}$ = 11.8 Hz, C_{ortho}), 131.45 (dd, $^{3}J_{C-P}$ = 4.8 Hz, $^{4}J_{C-P}$ = 2.1 Hz, C_{3a}), 131.11 (dd, $^{4}J_{C-P}$ = 11.1 Hz, $^{6}J_{C-P}$ = 2.8 Hz, C_{para}), 130.19 (dd, $^{1}J_{C-P}$ = 45.4 Hz, $^{3}J_{C-P}$ = 2.1 Hz, C_{ipso}), 128.70 (dd, $^{3}J_{C-P}$ = 11.1 Hz, $^{5}J_{C-P}$ = 2.1 Hz, C_{meta}), 128.38 (dd, $^{3}J_{C-P}$ = 42.9 Hz, $^{3}J_{C-P}$ = 1.4 Hz, C_{7a}), 128.07 (s, C_5 or C_6), 126.96 (s, C_6 or C_5), 118.24 (s, C_4 ou C_7), 117.38 (s, C_7 or C_4), 114.06 (dd, $^{2}J_{C-P}$ = 19.4 Hz, $^{2}J_{C-P}$ = 4.2 Hz, C_1), 112.26 (t, $^{2}J_{C-P}$ = 6.2 Hz, C_2), 90.15 (dd, $^{2}J_{C-P}$ = 19.4 Hz, $^{2}J_{C-P}$ = 4.9 Hz, C_3), 11.67 (d, $^{3}J_{C-P}$ = 4.8 Hz, *Me*). ^{31}P {^{1}H} NMR ($CDCl_3$, 121.49 MHz): δ 29.94 (d, $^{2}J_{P-P}$ = 58.5 Hz, PPh_3), 28.60 (d, $^{2}J_{P-P}$ = 58.5 Hz, PPh_3). Anal. Calcd for $C_{46}H_{39}P_2BF_4Pd.1.5CH_2Cl_2$: C, 58.55; H, 4.34. Found: C, 58.16; H, 4.28.

Synthesis of (Ind)Pd(PPh_3)(OTf), (7). A mixture of (Ind)Pd(PPh_3)Cl (**1**) (250 mg, 0.48 mmol) and AgOTf (186 mg, 0.72 mmol) was stirred in CH_2Cl_2 (50 mL) for 2 h at room temperature and filtered to remove AgCl. Evaporation of the filtrate to dryness and crystallization of the residue from C_6H_6/hexane at room temperature gave the product as a brown red precipitate (250 mg, 83%). Recrystallization of a small portion of this solid from a C_6H_6/hexane solution yielded crystals suitable for X-ray diffraction studies and elemental analysis. ^{1}H NMR ($CDCl_3$, 400 MHz): δ 7.42-7.34 (m, PPh_3), 7.32 (d, $^{2}J_{H-H}$ = 7.3 Hz, H_7), 7.15 (t, $^{3}J_{H-H}$ = 7.4 Hz, H_6), 7.04 (d, $^{3}J_{H-H}$ = 8.9 Hz, H_1), 6.87 (t, $^{3}J_{H-H}$ = 7.4 Hz, H_5), 6.77 (br, H_2), 6.29 (d, $^{3}J_{H-H}$ = 7.4 Hz, H_4), 4.68 (s, H_3). ^{13}C {^{1}H} NMR ($CDCl_3$, 100.56 MHz): δ 136.74 (s, C_{7a}), 135.57 (s, C_{3a}), 133.72 (d, $^{2}J_{C-P}$ = 12.3 Hz, C_{ortho}), 131.42 (s, C_{para}), 130.09 (d, $^{1}J_{C-P}$ = 45.5 Hz, C_{ipso}), 129.06 (d, $^{3}J_{C-P}$ = 9.9 Hz, C_{meta}), 128.65 (s, C_6), 127.65 (s, C_5), 121.24 (s, C_7), 117.65 (s, C_4), 111.78 (s, C_2), 102.51 (s, C_1), 73.18 (s, C_3). The ^{13}C NMR resonance of the triflate group could not be detected. ^{31}P {^{1}H} NMR ($CDCl_3$, 161.92 MHz): δ 29.12 (s). ^{19}F {^{1}H} NMR ($CDCl_3$, 376.31 MHz): δ -80.06 (s). Anal. Calcd for $C_{28}H_{22}O_3F_3P_1S_1Pd_1$: C, 53.13; H, 3.50; S, 5.07. Found: C, 53.06; H, 3.31; S, 4.69.

Synthesis of (1-Me-Ind)Pd(PPh_3)(OTf), (8). A mixture of (1-Me-Ind)Pd(PPh_3)Cl (**2**) (450 mg, 0.84 mmol) and AgOTf (325 mg, 1.27 mmol) was stirred in CH_2Cl_2 (50 mL) for 2 h at room temperature and filtered to remove AgCl. Evaporation of the filtrate to dryness and crystallization of the residue from C_6H_6/hexane at room temperature gave a brown-red powder (430 mg, 79%). ^{1}H NMR ($CDCl_3$, 400 MHz): δ 7.43-7.37 (m, PPh_3), 7.32 (d, $^2J_{H-H}$ = 7.7 Hz, H_7), 7.16 (t, $^3J_{H-H}$ = 7.8 Hz, H_6), 6.87 (t, $^3J_{H-H}$ = 7.5 Hz, H_5), 6.55 (br, H_2), 6.13 (d, $^3J_{H-H}$ = 7.3 Hz, H_4), 4.54 (s, H_3), 2.09 (d, $^4J_{H-P}$ = 11.3 Hz, CH_3). ^{31}P {^{1}H} NMR ($CDCl_3$, 161.92 MHz): δ 31.39 (s). ^{19}F {^{1}H} NMR ($CDCl_3$, 376.31 MHz): δ -80.51 (s).

Ligand substitution reactions with 7. Substitution of the OTf ligand in **7** by L was monitored by spectroscopy, without isolating the resulting adducts. These reactions were carried out by adding 1 equiv of L to a 0.5 mL $CDCl_3$ solution of **7** (ca. 0.03 mmol) in an NMR tube. The NMR spectra of these samples were then measured at room temperature. The data are given below.

[(Ind)Pd(PPh_3)$_2$][OTf], (5[OTf]). ^{1}H NMR ($CDCl_3$, 300 MHz): δ 7.43-7.26 (m, PPh_3 and protons of Ind), 7.12-7.02 (m, PPh_3 and protons of Ind), 6.19-6.22 (m, H_4 and H_7), 5.48-5.44 (m, H_1 and H_3). ^{13}C {^{1}H} NMR ($CDCl_3$, 75.40 MHz): δ 133.77 (t, $^2J_{C-P}$ = 5.9 Hz, C_{ortho}), 131.68 (s, C_{para}), 130.04 (d, $^1J_{C-P}$ = 46 Hz, C_{ipso}), 129.38 (pseudo t, $^3J_{C-P}$ = 5.3 Hz, C_{meta}), 128.38 (s, C_5 and C_6), 118.88 (s, C_4 and C_7), 113.11 (s, C_2), 95.35 (pseudo t, $^2J_{C-P}$ = 11.6 Hz, C_1 and C_3). ^{31}P {^{1}H} NMR ($CDCl_3$, 121.49 MHz): δ 27.73 (s). ^{19}F {^{1}H} NMR ($CDCl_3$, 282.23 MHz): δ -78.19 (s).

[(Ind)Pd(PPh_3)(PMe_3)][OTf], (9). ^{31}P {^{1}H} NMR (C_6D_6, 161.92 MHz): δ 30.05 (d, $^2J_{P-P}$ = 59.7 Hz), -16.66 (d, $^2J_{P-P}$ = 59.7 Hz). ^{19}F {^{1}H} NMR ($CDCl_3$, 376.31 MHz): δ -80.9 (s).

[(Ind)Pd(PPh$_3$)(CH$_3$CN)][OTf], (10). ^{1}H NMR (CDCl$_3$, 400 MHz): δ 7.55-7.45 (m, PPh$_3$), 7.36-7.27 (m, PPh$_3$), 7.16 (t, $^3J_{H\text{-}H}$ = 7.6 Hz, H_6), 7.05 (br, H_1 and H_7), 6.92 (t, $^3J_{H\text{-}H}$ = 7.6 Hz, H_5), 6.72 (pseudo t, $^3J_{H\text{-}H}$ = 3.6 Hz, H_2), 6.24 (d, $^3J_{H\text{-}H}$ = 7.6 Hz, H_4), 5.04 (br, H_3), 2.07 (s, *Me*CN). ^{13}C {^{1}H} NMR (CDCl$_3$, 100.56 MHz): δ 135.47 (s, C_{7a}), 134.59 (s, C_{3a}), 133.77 (d, $^2J_{C\text{-}P}$ = 12.5 Hz, C_{ortho}), 131.61 (s, C_{para}), 129.28 (d, $^3J_{C\text{-}P}$ = 11.09 Hz, C_{meta}), 128.97 (s, C_6), 128.04 (s, C_5), 122.34 (s, C_7), 118.92 (s, C_4), 112.09 (s, C_2), 101.14 (d, $^2J_{C\text{-}P}$ = 18.6 Hz, C_1), 77.17 (s, C_3), 3.14 (s, CH$_3$CN). ^{31}P {^{1}H} NMR (C$_6$D$_6$, 121.49 MHz): δ 31.05 (s). ^{19}F {^{1}H} NMR (CDCl$_3$, 376.31 MHz): δ -80.8 (s). IR (KBr, cm^{-1}): 2291 (w), 2247 (w), 2186 (w).

[(Ind)Pd(PPh$_3$)(PhCN)][OTf], (11). ^{1}H NMR (CDCl$_3$, 400 MHz): δ 7.63-7.34 (m, PPh$_3$ and protons of Ind), 7.31-7.27 (m, protons of Ind and PhCN), 7.19-7.15 (m, protons of Ind and PhCN), 7.09-7.04 (m, protons of Ind and PhCN), 6.94 (t, $^3J_{H\text{-}H}$ = 7.6 Hz, H_5), 6.87 (pseudo t, $^3J_{H\text{-}H}$ = 2.7 Hz, H_2), 6.24 (d, $^3J_{H\text{-}H}$ = 7.6 Hz, H_4), 5.07 (br, H_3). ^{31}P {^{1}H} NMR (C$_6$D$_6$, 121.49 MHz): δ 30.97 (s). ^{19}F {^{1}H} NMR (CDCl$_3$, 376.31 MHz): δ -80.6 (s). IR (KBr, cm^{-1}): 2227 (m).

[(Ind)Pd(PPh$_3$)(*t*-BuNC)][OTf], (12). ^{1}H NMR (CDCl$_3$, 300 MHz): δ 7.62-7.24 (m, protons of Ind and PPh$_3$), 7.22-7.12 (m, protons of Ind and PPh$_3$), 7.10-6.95 (m, protons of Ind), 6.69 (br, H_2), 6.32 (d, $^3J_{H\text{-}H}$ = 7.5 Hz, H_4), 5.35 (br, H_3), 1.15 (s, CNC(CH_3)$_3$). ^{31}P {^{1}H} NMR (CDCl$_3$, 121.49 MHz): δ 30.05. ^{19}F {^{1}H} NMR (CDCl$_3$, 282.23 MHz): δ -78.2 (s). IR (KBr, cm^{-1}): 2206 (s).

Dimerization of Ethylene Catalyzed by Complexes 7 and 8. Ethylene was bubbled through CDCl$_3$ solutions of **7** or **8** (20 mg in 1 mL) for ca. 5 min prior to analysis by NMR. ^{1}H NMR (CDCl$_3$, 400 MHz): 1.61 (d, $^3J_{H\text{-}H}$ = 5.0, CH$_3$ of *Z*-butene), 1.64 (dd, $^3J_{H\text{-}H}$ = 5.0, $^4J_{H\text{-}H}$ = 1.2, CH$_3$ of *E*-butene), 5.44 (m, vinylic H for both *Z*- and *E*-butenes).

Dimerization of Styrene Catalyzed by Complex 7 and 8. Styrene (125 μL, 1 mmol) was added to a $CDCl_3$ solution of **7** or **8** (10 mg in 1 mL) and the sample was placed in an ultra-sonic bath for 15 h to ensure mixing. Analysis by ^1H NMR showed a near complete conversion of styrene to the dimer (Z)-1,3-diphenyl-1-butene. ^1H NMR ($CDCl_3$, 400 MHz): δ 7.18-6.98 (m, protons of Ph), 6.29 (br, Ph-C*H*=), 6.26 (dd, $^3J_{H\text{-}H}$ = 1 Hz and 6.1 Hz), 3.38 (quintuplet, $J_{H\text{-}H}$ = 6.74 Hz, C*H*), 1.27 (d, $J_{H\text{-}H}$ = 7.1 Hz, C*H*$_3$). The GC/MS analysis of the NMR mixtures showed the presence of the dimer 1,3-diphenyl-1-butene ($M^{\cdot+}$ = 208; $M^{\cdot+}$ - $CH_3^{\cdot}$ = 193; $M^{\cdot+}$ - PhH = 130; $M^{\cdot+}$ - (PhH + $CH_3^{\cdot}$) = 115, etc.) and traces of the trimer of the styrene for which the fragmentation pattern was nearly identical to that of the dimer, with the exception of the parent ion peak ($M^{\cdot+}$ = 312).

Reaction of complex 7 with *p*-F-styrene. This reaction was carried out in $CDCl_3$ at room temperature using 100 equiv of *p*-fluoro-styrene. After the sample was agitated in an ultra-sonic bath for 24 h, the mixture was subjected to NMR and GC/MS analyses that showed complete conversion of the monomer to dimeric and trimeric species. ^1H NMR ($CDCl_3$, 400 MHz): δ 7.39-7.01 (m, protons of Ph), 6.45-6.31 (m, C*H*=), 3.69 (quintuplet, $J_{H\text{-}H}$ = 6.9 Hz, C*H*), 1.52, 1.34 (d, $J_{H\text{-}H}$ = 7.1 Hz, C*H*$_3$). The GC/MS analysis of the sample showed the presence of the dimer (two isomers, totaling 66%) and a trimer (34%). The fragmentation patterns for the two isomers of the dimer were nearly identical: $M^{\cdot+}$ at *m/z* 244; $M^{\cdot+}$ - $CH_3^{\cdot}$ at *m/z* 229; $M^{\cdot+}$ - ($CH_3^{\cdot}$ + C_6H_5F) at *m/z* 133; $[FC_6H_4CH_2]^{\cdot+}$ at *m/z* 109. The fragmentation pattern for the trimer was nearly identical to that of the dimers, with the exception of the parent ion peak ($M^{\cdot+}$ at *m/z* 366).

Reaction of complex 7 with *p*-X-styrenes (X = NH_2, Me, OMe). The reaction of *p*-amino-styrene was carried out on NMR scale using 100 equiv of substrate (148 μL) in $CDCl_3$, at room temperature, for 24 h. The reactions with X = Me and OMe were carried out by stirring a mixture of **7** (ca. 20 mg, 0.0316 mmol) and a large excess of the olefin (4.25 mL, 1000 equiv) in toluene (4 mL) for 24 hours at room temperature.

Evaporation of the solvent and unreacted styrene gave a gray-yellow white solid. These were isolated and subjected to NMR and GPC analyses (in THF, relative to poly(styrene) standards), as follows. X = NH_2: 150 mg, 100 % yield, M_w ~1050, M_w/M_n ~ 1.3, M_w ~1250, ^{1}H NMR ($CDCl_3$): 7.08 (br), 6.72-6.48 (m), 4.49 (br), 3.79 (br) 2.49 (br), 1.87 (br), 1.32 (br); X = Me: 3.7 g, 88% yield, M_w/M_n ~ 1.4, ^{1}H NMR ($CDCl_3$): 7.33 (br), 6.59 (br), 2.55 (br), 1.46 (br); X = OMe: 4.1 g, 96% yield, M_w ~ 29000, M_w/M_n ~ 3.2, ^{1}H NMR ($CDCl_3$): 6.62 (br), 3.79 (br), 1.82 (br), 1.42 (br).

Reactivities of Complexes 7 and 8 with 1-Hexene. Monitoring the reaction of 1-hexene (0.1 mL, 0.80 mmol, 1.6 M in $CDCl_3$) with complexes **7** or **8** (ca. 10 mg, 0.016 mmol, 0.032 M in $CDCl_3$) by ^{1}H and $^{13}C\{^1H\}$ NMR spectroscopy indicated the slow formation of (*E*)- and (*Z*)-2-hexenes (75:25) over 24 h. $^{13}C\{^1H\}$ NMR data for *E*-2-hexene: δ 13.8, 18.0, 22.7, 34.9, 124.8 and 131.5; $^{13}C\{^1H\}$ NMR data for *Z*-2-hexene: δ 12.8, 14.1, 25.7, 29.1, 123.9, 131.0. The GC/MS analysis of the NMR mixture for the reaction with complex **7** showed the presence of hexenes and traces of 1,3-(hexenyl)-indene: $M^{\cdot+}$, *m/z* 198; $M^{\cdot+}$ – 15 (CH_3); $M^{\cdot+}$ – 29 (CH_2CH_3); $M^{\cdot+}$ – 43 (Pr); $M^{\cdot+}$ – 57 (Bu); etc..

Hydrosilylation of Styrene. The following general procedure was followed for the NMR-scale hydrosilylation experiments: To a $CDCl_3$ solution of styrene and $HSiCl_3$ (180-230 μL, 100 equiv of each) was added the Ind-Pd complex (ca. 10 mg, 0.02 mmol) and the sample was kept in an ultra-sonic bath for 24 h to ensure agitation and homogeneity. Analysis by ^{1}H NMR ($CDCl_3$, 400 MHz) showed the formation of (1-phenyl-1-trichlorosilyl)ethane: 7.19-7.11 (m, protons of the Ph), 2.56 (q, $^3J_{H-H}$ = 7.5 Hz, C*H*), 1.41 (q, $^3J_{H-H}$ = 7.5 Hz, C*H*$_3$). These data matches literature values (ref. 18a). The GC/MS analysis of the NMR mixtures showed only the hydrosilylation product ($M^{\cdot+}$ = 239). The conversions were determined on the basis of the ^{1}H NMR spectra of the reaction mixture; this was deemed as a reliable measure of the yields because no other products were detected in these reactions.

Hydrosilylation of Phenylacetylene. The following general procedure was followed for the NMR-scale hydrosilylation experiments: To a $CDCl_3$ solution of PhC≡CH and $HSiCl_3$ (190-210 μL, 100 equiv of each) was added the precursor complex (**1**-**8**, ca. 10 mg) and the sample placed in an ultra-sonic bath for the duration of the reaction to ensure agitation and homogeneity. Analysis by ^1H NMR (C_6D_6, 400 MHz) showed that phenylacetylene had been completely hydrosilylated into a 1:1 mixture of 1-(phenyl)-2-(trichlorosilyl)-ethylene and 1-(phenyl)-1-(trichlorosilyl)-ethylene. For 1-(phenyl)-2-(trichlorosilyl)-ethylene: 7.85 (d, $^3J_{H\text{-}H}$ = 16 Hz, Ph-C*H*=), 7.70-7.50 (m, protons of Ph), 6.93 (d, $^3J_{H\text{-}H}$ = 16 Hz, =C*H*-$SiCl_3$); for 1-(phenyl)-1-(trichlorosilyl)-ethylene: 7.70-7.50 (m, protons of Ph), 6.28 & 6.04 (s, =CH_2). The GC/MS analysis of the NMR mixtures showed the presence of the hydrosilylation product ($M^{\cdot+}$, *m/z* 237).

Acknowledgment.

This work was made possible thanks to the financial support provided by the Natural Sciences and Engineering Research Council of Canada (operating grants to D. Z.) and Université de Montréal (scholarships to C. S.-S.). We are also indebted to Julie Boivin for help with the GPC analyses, to Johnson Matthey for the generous loan of $PdCl_2$, and to Dr. M. Simard and Mme F. Bélanger-Gariépy for their assistance with the X-ray diffraction studies, and to Prof. F. Schaper for helpful discussions.

Supporting Information Available.

Complete details of the X-ray analysis of **3**, **5**, **6**, and **7** including tables of crystal data, collection and refinement parameters, bond distances and angles, anisotropic thermal parameters, and hydrogen atoms coordinates have been deposited at the Cambridge Crystallographic Data Centre (CCDC 283700 – 283703). These data can be obtained free of charge via www.ccdc.cam.ac.uk/data_request/cif, or by emailing data_request@ccdc.cam.ac.uk, or by contacting the Cambridge Crystallographic Data Centre, 12, Union Road, Cambridge CB2 1EZ, UK; fax: +44 1223 336033.

References

[1] (a) Frankom, T. M.; Green, J. C.; Nagy, A.; Kakkar, A. K.; Marder, T. B. *Organometallics* **1993**, *12*, 3688. (b) Gamasa, M. P.; Gimeno, J.; Gonzalez-Bernado, C.; Martin-Vaca B., M.; Monti, D.; Basseti, M. *Organometallics* **1995**, *15*, 302. (c) O'Connor, J. M.; Casey, C. P. *Chem. Rev.* **1987**, *87*, 307.

[2] For a recent review on the chemistry of group 10 metal indenyl complexes see: Zargarian, D. *Coord. Chem. Rev.* **2002**, *233-234*, 157.

[3] (a) Huber, T. A.; Bélanger-Gariépy, F.; Zargarian, D. *Organometallics* **1995**, *14*, 4997. (b) Bayrakdarian, M.; Davis, M. J.; Dion, S.; Dubuc, I.; Bélanger-Gariépy, F.; Zargarian, D. *Can. J. Chem.* **1996**, *74*, 2115. (c) Huber, T. A.; Bayrakdarian, M.; Dion, S.; Dubuc, I.; Bélanger-Gariépy, F.; Zargarian, D. *Organometallics* **1997**, *16*, 5811. (d) Groux, L. F; Bélanger-Gariépy, F.; Zargarian, D.; Vollmerhaus, R. *Organometallics* **2000**, *19*, 1507. (e) Fontaine, F.-G.; Dubois, M.-A.; Zargarian, D. *Organometallics* **2001**, *20*, 5156.

[4] (a) Vollmerhaus, R.; Bélanger-Gariépy, F.; Zargarian, D. *Organometallics* **1997**, *16*, 4762. (b) Dubois, M.-A.; Wang, R.; Zargarian, D.; Tian, J.; Vollmerhaus, R.; Li, Z.; Collins, S. *Organometallics* **2001**, *20*, 663. (c) Groux, L. F.; Zargarian, D. *Organometallics* **2001**, *20*, 3811. (d) Groux, L. F.; Zargarian, D.; Simon, L. C.; Soares, J. B. P. *J. Mol. Catal. A* **2003**, *193(1-2)*, 51. (e) Groux, L. F.; Zargarian D. *Organometallics* **2003**, *22*, 3124. (f) Groux, L. F.; Zargarian D. *Organometallics* **2003**, *22*, 4759. (h) Sun, H.; Li, W.; Han, X.; Shen, Q.; Zhang, Y. *J. Organomet. Chem.* **2003**, *688*, 132. (i) Li, W.-F.; Sun, H.-M.; Shen, Q.; Zhang, Y.; Yu, K.-B. *Polyhedron* **2004**, *23*, 1473. (j) Jimenez-Tenorio, M.; Puerta, M. C.; Salcedo, I.; Valerga, P.; Costa, S. I.; Silva, L. C.; Gomes, P. T. *Organometallics* **2004**, *23*, 3139. (k) Sun, H. M.; Shao, Q.; Hu, D. M.; Li, W. F.; Shen, Q.; Zhang, Y. *Organometallics* **2005**, *24*, 331. (l) Gareau, D.; Sui-Seng, C.; Groux, L. F.; Brisse, F.; Zargarian, D. *Organometallics* **2005**, *24*, 4003.

[5] (a) Wang, R.; Bélanger-Gariépy, F.; Zargarian, D. *Organometallics* **1999**, *18*, 5548. (b) Wang, R.; Groux, L. F.; Zargarian D. *Organometallics* **2002**, *21*, 5531. (c) Wang,

R.; Groux, L. F.; Zargarian, D. *J. Organomet. Chem* **2002**, *660*, 98. (d) Rivera, E.; Wang, R; Zhu, X. X.; Zargarian, D.; Giasson, R. *J. Molec. Catal. A* **2003**, *204-205*, 325.

[6] (a) Fontaine, F. -G.; Kadkhodazadeh, T.; Zargarian, D. *J. Chem. Soc., Chem. Commun.* **1998**, 1253. (b) Fontaine, F.-G.; Zargarian, D. *Organometallics* **2002**, *21*, 401.

[7] Fontaine, F.-G.; Nguyen, R.-V.; Zargarian, D. *Can. J. Chem.* **2003**, *81*, 1299.

[8] The following compounds have been reported: $[(\eta^3\text{-Ind})Pd(\mu\text{-Cl})]_2$ (Nakasuji, K.; Yamaguchi, M.; Murata, I.; Tatsumi, K.; Natamura, A. *Organometallics* **1984**, *3*, 1257; Samuel, E.; Bigorgne, M. *J. Organomet. Chem.* **1969**, *19*, 9); $[(\mu\text{-}\eta^3\text{-Ind})Pd(CNR)]_2$ (R = *t*-Bu, 2,6-$(CH_3)_2C_6H_3$; 2,4,6-$(CH_3)_3C_6H_2$; 2,4,6-(*t*-Bu)$_3C_6H_2$) (Tanase, T.; Nomura, T.; Fukushina, T.; Yamamoto, Y.; Kobayashi, K. *Inorg. Chem.* **1993**, *32*, 4578); $[(\eta^3\text{-Ind})Pd(PMe_3)(CH(SiMe_3)_2)]$ (Alias, F. M.; Belderrain, T. R.; Panequivue, M.; Poveda, M. L.; Carmona, E. *Organometallics* **1998**, *17*, 5620; Alias, F. M.; Belderrain, T. R.; Carmona, E.; Graiff, C.; Panequivue, M.; Poveda, M. L. *J. Organomet. Chem.* **1999**, *577*, 316); $[(\eta^3\text{-Ind})PdL_2]^+$ with L_2 = bipy, tmeda (Vicente, J.; Abad, J.-A.; Bergs, R.; Jones, P. G.; De Arellano, M. C. R. *Organometallics* **1996**, *15*, 1422; Vicente, J.; Abad, J.-A.; Bergs, R.; De Arellano, M. C. R.; Martinez-Vivente, E.; Jones, P. G. *Organometallics* **2000**, *19*, 5597). In addition, a preliminary communication has appeared on the preparation of a series of Ind derivates from the reaction of cyclopropene and $(PhCN)_2PdCl_2$ (Fiato, R. A .; Mushak, P.; Battiste, M. A. *Chem. Commun.* **1975**, 869).

[9] Sui-Seng, C.; Enright, G. D.; Zargarian, D. *Organometallics* **2004**, *23*, 1236.

[10] The Pd-promoted coupling of Li[R-Ind] is a major side reaction that leads to very low yields of the desired complexes. See ref. 9.

[11] Isolating pure samples of complexes **3** and **7** was less complicated than that of their 1-Me-Ind analogues **4** and **8** because of the greater solubility of the latter in common solvents. In addition, the Pd-OTf complex **8** slowly decomposes to $[(1\text{-Me-Ind})Pd(PPh_3)_2]^+$ during recrystallization.

[12] (a) Baker, T.; Tulip, T. H. *Organometallics* **1986**, *5*, 839. (b) Barr, R. D.; Green, M.; Marder, T. B.; Stone, F. G. A. *J. Chem. Soc., Dalton. Trans.* **1984**, 1261. (c) Kakkar, A. K.; Taylor, N. J.; Calabrese, J. C.; Nugent, W. A.; Roe, D. C.; Connaway, E. A.; Marder, T. B. *J. Chem. Soc.; Chem Commun.* **1989**, 990. (d) Westcott, Kakkar, A. K., S. A.; Taylor, N. J.; Roe, D. C.; Marder, T. B. *Can. J. Chem.* **1999**, *77*, 205.

[13] (a) Lawrence, G. A. *Chem. Rev.* **1986**, *86*, 17. (b) Braun, T.; Parsons, S.; Perutz, R. N.; Voith, M *Organometallics* **1999**, *18*, 1710.

[14] Δ(M-C) = 0.5 {(M-C3a + M-C7a)} – 0.5{(M-C1 + M-C3). HA is the angle between the planes encompassing the atoms C1, C2, C3 and C1, C3, C3a, C7a. FA is the angle between the planes encompassing the atoms C1, C2, C3 and C3a, C4, C5, C6, C7 and C7a. The Δ(M-C), HA and FA values for a range of Ind complexes are given in ref 12a and the following report: Westcott, S. A.; Kakkar, A. K.; Stringer, G.; Taylor, N. J.; Marder, T. B. *J. Organomet. Chem.* **1990**, *394*, 777. The corresponding data for group 10 complexes are given in reference 2.

[15] The assignment of the band at 2247 cm^{-1} to ν(CN) should be considered tentative, because the IR spectrum of complex **10** also showed two equivually weak bands at 2291 and 2186 cm^{-1}.

[16] (a) Otsuka, S.; Nakamura, A.; Yoshida, T. *J. Am. Chem. Soc.* **1969**, *91*, 7196. (b) Crociani, B.; Boschi, T.; Belluco, U. *Inorg. Chem.* **1970**, *9*, 2021. (c) Cherwinski, W. J.; Clark, H. C.; Manzer, L. E. *Inorg. Chem.* **1972**, *11*, 1511. (d) De Munno, G.; Bruno, G.; Grazia Arena, C.; Drommi, D.; Faraone, F. *J. Organomet. Chem.* **1993**, *450*, 263.

[17] Chen, Y.; Sui-Seng, C.; Zargarian, D. *Organometallics* **2005**, *24*, 149.

[18] It is worth noting that the evolution of H_2 from the reactions of $PhSiH_3$ with Ind-Ni complexes has been observed previously (ref. 6b).

[19] (a) Hayashi, T.; Hirate, S.; Kitayama, K.; Tsuji, H.; Torii, A.; Uozomi, Y. *J. Org. Chem.* **2001**, *66*, 1441. (b) Bringmann, G.; Wuzik, A.; Breuning, M.; Henschel, P.; Peters, K.; Peters, E.-M. *Tetrahedron: Asymmetry* **1999**, *10*, 3025. (c) Uozomi, Y.; Tsuji, H.; Hayashi, T. *J. Org. Chem.* **1998**, *63*, 6137. (d) Ricard, L.; Marinetti, A.

Organometallics **1994**, *13*, 3956. (e) Marinetti, A. *Tetrahedron Lett.* **1994**, *35*, 5861. (f) Tsuji, J.; Hara, M.; Ohno, K. *Tetrahedron* **1974**, *30*, 2143.

[20] (a) Brook, M. A.; Neuy, A. *J. Org. Chem.* **1990**, *55*, 3609. (b) Tamao, K.; Yoshida, J.-I; Yamamoto, H.; Kakui, T; Matsumoto, H.; Takahashi, M.; Kurita, A; Murata, M.; Kumada, M. *Organometallics* **1982**, *1*, 355. (c) Auner, N.; Wagner, C.; Ziche, W. *Z. Naturforsch*, **1994**, *49b*, 831.

[21] *CAD-4 Software*, Version 5.0; Enraf-Nonius: Delft, The Netherlands, 1989.

[22] Gabe, E. J.; Le Page, Y.; Charlant, J.-P.; Lee, F. L.; White, P. S. *J. Appl Crystallogr.* **1989**, *22*, 384.

[23] *SMART*, Release 5.059; Bruker Molecular Analysis Research Tool, Bruker AXS Inc.: Madison, WI 53719-1173, 1999.

[24] *SAINT*, Release 6.06; Integration Software for Single Crystal Data. Bruker AXS Inc.: Madison, WI 53719-11, 1999.

[25] Sheldrick, G. M. *SHELXS*. Program for the solution of Crystal Structures. University of Goettingen. Germany, 1997.

[26] Sheldrick, G. M. *SHELXL*. Program for the Refinement of Crystal Structures. University of Goettingen. Germany, 1997.

Chapitre 4: New Palladium(II)-(η^{3-5}- or η^1-Indenyl) and Dipalladium(I)-(μ,η^3-Indenyl) Complexes

Article 3

Christine Sui-Seng,[a] Gary D. Enright,[b] and Davit Zargarian*[a]

[a] Département de chimie, Université de Montréal, Québec, Canada H3C 3J7

[b] Steacie Institute for Molecular Sciences, National Research Council, Ottawa, Ontario, Canada K1A 0R6

Journal of the American Chemical Society **2006**, *128*, 6508-6519.

Abstract

Reaction of the dimeric species $[(\eta^3\text{-Ind})Pd(\mu\text{-Cl})]_2$ (**1**) (Ind = indenyl) with NEt_3 gives the new amino(palladium) complex $(\eta^{3\text{-}5}\text{-Ind})Pd(NEt_3)Cl$ (**3**), whereas the analogous reactions with $BnNH_2$ (Bn = $PhCH_2$) or pyridine (py) afford the complexes *trans*-$L_2Pd(\eta^1\text{-Ind})Cl$ (L = $BnNH_2$ (**4**), py (**5**)). Similarly, the one-pot reaction of **1** with a mixture of $BnNH_2$ and the phosphine ligands PR_3 gives the mixed-ligand, amino and phosphine species $(PR_3)(BnNH_2)Pd(\eta^1\text{-Ind})Cl$, (R = Cy (**6a**), Ph (**6b**)); the latter complexes can also be prepared by addition of $BnNH_2$ to $(\eta^{3\text{-}5}\text{-Ind})Pd(PR_3)Cl$ (R = Cy (**2a**), Ph (**2b**)). Complexes **6** undergo a gradual decomposition in solution to generate the dinuclear Pd^I compounds $(\mu,\eta^3\text{-Ind})(\mu\text{-Cl})Pd_2(PR_3)_2$ (R = Cy (**7a**), Ph (**7b**)) and the Pd^{II} compounds $(BnNH_2)(PR_3)PdCl_2$ (R = Cy (**8a**), Ph (**8b**)), along with 1,1'-biindene. The formation of **7** is proposed to proceed by a comproportionation reaction between in-situ generated Pd^{II} and Pd^0 intermediates. Interestingly, the reverse of this reaction, disproportionation, also occurs spontaneously to give **2**. All new compounds have been characterized by NMR spectroscopy and, in the case of **3**, **4**, **5**, **6a**, **7a**, **7b**, and **8a**, by X-ray crystallography.

Introduction

Studies on the structures and reactivities of Ind complexes (Ind = indenyl and its substituted or functionalized derivatives) have shown that the bonding mode adopted by the Ind ligand in a given complex and its net electronic contribution to the metal center depend strongly on the electronic configuration of the metal (d^n) and its formal electron count. Thus, the formally electron-deficient complexes of early metals ($d^{0\text{-}5}$, up to 18 valence electrons) generally favor greater hapticities (η^5-Ind),[1] whereas the more electron-rich late metal centers ($d^{6\text{-}8}$, 16-18 valence electrons) favor lower hapticities and display various degrees of "slip-fold" distortions ($\eta^{1\text{-}5}$-Ind). This flexible and responsive nature of M-Ind bonding, the so-called "indenyl effect", is believed to facilitate a number of interesting stoichiometric and catalytic reactions.[2]

Most of the studies carried out to date on Ind complexes have focused on compounds of groups 4-9 transition metals, such that the chemistry of group 10 metal indenyl complexes is much less explored. Nevertheless, a number of studies carried out over the past decade on Ni^{II}-Ind complexes IndNi(L)X and $[IndNi(L)L']^+$ have shown that the Ind ligand is more slip-folded in these complexes in comparison to the complexes Ind-M^{I}(L)L' of group 9 metals despite the similar (formal) electron counts of the metal centers in these complexes (d^8, 18 electrons).[3] Some of these Ni-Ind complexes are also competent precatalysts for the oligo- and polymerization of alkenes,[4] alkynes,[5] and $PhSiH_3$,[6] and for the hydrosilylation of olefins.[4f,4k,7]

The interesting structural characteristics and catalytic reactivities promoted by Ni-Ind compounds and the relatively unexplored chemistry of their Pd analogues[8] have motivated us to initiate a systematic study of Pd-Ind compounds in order to elucidate the influence of the metal center on structures and reactivities. Our initial studies showed significantly lower Ind hapticities (more "slippage") in the compounds (η^{3-5}-Ind)Pd(PR_3)Cl (R= Ph, Cy, Me, and OMe); moreover, replacing the PR_3 in these compounds by *t*-BuNC gave $[(\eta^1\text{-Ind})(t\text{-BuNC}))Pd(\mu\text{-Cl})]_2$.[9] Subsequently, we undertook to synthesize a new series of complexes bearing Lewis bases other than phosphines and isocyanides to allow a comparison of structural and reactivity features as a function of both metal and the Lewis base ligand.

The present contribution reports on the syntheses of the Ind-Pd^{II}(amine) complexes ($\eta^{3\text{-}5}$-Ind)Pd(NEt_3)Cl, (η^1-Ind)Pd($BnNH_2$)$_2$Cl (Bn = $PhCH_2$), and (η^1-Ind)Pd(py)$_2$Cl (py = pyridine). The subsequent reaction of these complexes with phosphines has given access to new Pd^{I}-Pd^{I} complexes bearing a bridging indenyl ligand, i.e., (μ-η^3-Ind)(μ-Cl)$Pd_2(PR_3)_2$ (R = Ph, Cy). Several dinuclear Pd^{I}-Pd^{I} complexes featuring μ-allyl or μ-cyclopentadienyl ligands are known,[10] whereas [(μ-η^3-Ind)Pd(CNR)]$_2$ represent the only μ-Ind complexes reported previously.[8c,8d]

Results and Discussion

Reaction of the dimer [(η^3-Ind)Pd(μ-Cl)]$_2$ (1) with amines. The synthetic route developed for the preparation of phosphine and isocyanide complexes (η-Ind)Pd(PR_3)Cl (**2**) and [(η^1-Ind)(t-BuNC)Pd(μ-Cl)]$_2$ (Scheme 4.1)[9a] was used to prepare the target amino complexes. Thus, stirring a suspension of **1**[11] in benzene with NEt_3 gave the complex (η-Ind)Pd(NEt_3)Cl (**3**), whereas the analogous reactions with $BnNH_2$ and py gave the η^1-Ind complexes (η^1-Ind)Pd($BnNH_2$)$_2$Cl (**4**) and (η^1-Ind)Pd(py)$_2$Cl (**5**), respectively (Scheme 4.1). The new complexes were isolated in 70-75% yields as brown (**3**) or yellow-brown (**4** and **5**) solids; the latter compounds were also prepared in ca. 85% yield via the reaction of **3** with 1 or 2 equivalents of $BnNH_2$ or py (Scheme 4.1). All three complexes are thermally stable and can be handled in air, both in the solid state and in solution, without appreciable decomposition. Their identities were deduced from their NMR spectra and confirmed by the results of elemental analyses and single crystal X-ray diffraction studies, as described below.

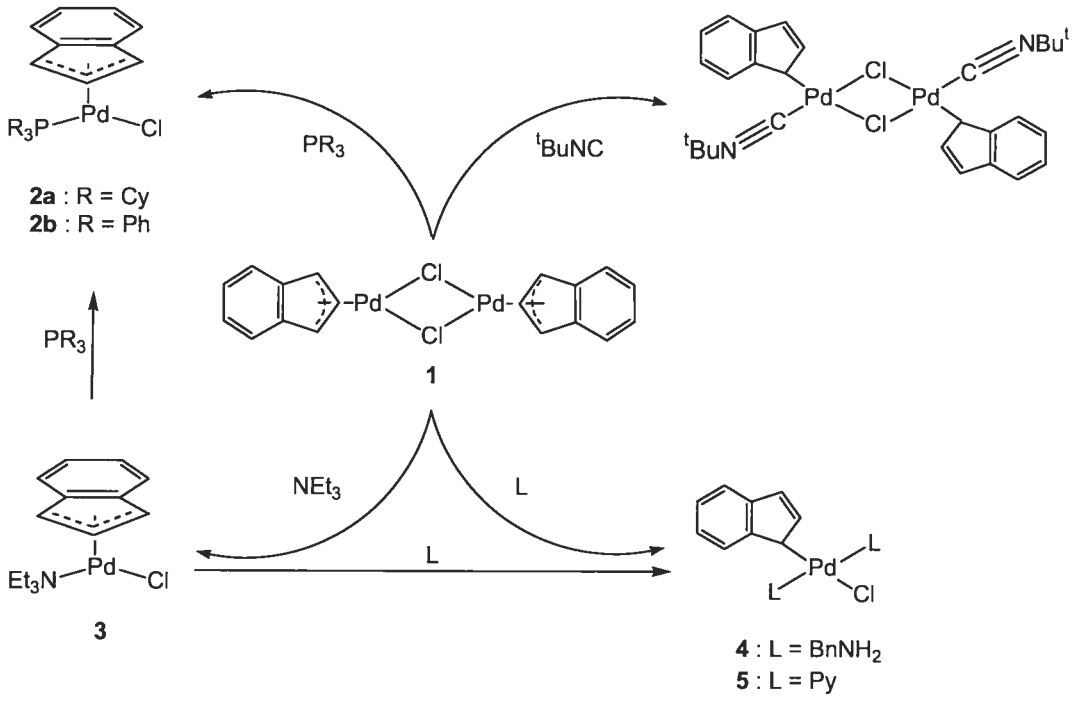

Scheme 4.1

Characterization of 3-5 by NMR. The ambient temperature ^{1}H NMR spectrum of (η-Ind)Pd(NEt_3)Cl (**3**) displayed relatively broad signals for all Ind protons, but a better resolution was obtained at -10 °C. The assignment of the ^{1}H and ^{13}C {^{1}H} NMR spectra was facilitated by selective homodecoupling, inverse-gated decoupling, COSY and HMQC experiments. The selective 1D NOESY experiment correlated H3 and H4 at 4.61 and 6.45 ppm, respectively, with the methylene groups of NEt_3 (see Figure 4.2 for the numbering scheme). Moreover, the high resolution of the ^{1}H NMR spectrum of **3** allowed us to observe the detailed multiplicities of these signals and to determine the various H-H coupling constants, as follows: $^3J_{H1\text{-}H2} \sim {}^3J_{H2\text{-}H3} \sim {}^4J_{H1\text{-}H3} \sim 2.4$ Hz; $^4J_{H1\text{-}H7} \sim {}^4J_{H3\text{-}H4} \sim 0.8$ Hz; $^5J_{H3\text{-}H5} \sim {}^5J_{H1\text{-}H6} \sim 1.2$ Hz.

Overall, the chemical shifts and the multiplicities of the signals for the Ind protons in **3** follow a pattern commonly observed for the previously studied (η-Ind)Pd(PR_3)Cl analogues.[9] For instance, the signals for H1 (5.59 ppm) and H3 (4.61 ppm) are both strongly shielded in comparison to the other Ind signals (6.31-6.93 ppm). On the other hand, the ^{13}C chemical shifts of C1 and C3 (ca. 73 vs. 82 ppm) indicate a somewhat higher shielding for C1, which is the opposite of our previous observations for Ni- and Pd-Ind complexes bearing phosphines. For example, the chemical shifts of these nuclei in (η-Ind)Pd(PR_3)Cl are in the range of 94-113 ppm for C1 and 70-80 ppm for C3, indicating that the hybridization is more sp^2-like at C1 and more sp^3-like at C3; we have argued that these observations are consistent with the larger trans influence of PR_3 versus Cl.[9a] Accordingly, we attribute the observation of a more shielded C1 in **3** to a more sp^3-like hybridization at C1 arising from the weaker trans influence of NEt_3 versus Cl. The latter phenomenon is reflected in the solid state structure of this complex, which shows that Pd-C1 < Pd-C3 (vide infra), but the fairly downfield chemical shift of H1 (ca. 5.6 ppm) is not consistent with sp^3-C1.

The ^{1}H and ^{13}C{^{1}H} NMR spectra of complexes **4** and **5** showed only one set of signals, indicating that only one isomer, *cis* or *trans*, was obtained in each case; we have assumed that these complexes adopt the thermodynamically more stable *trans* geometry, as in bis(amine)dihalogenopalladium(II) complexes.[12] The NMR data for the indenyl fragment were very similar to those found in previously reported transition-

metal η^1-indenyl complexes.[8e,9a,13] In the ^{13}C NMR spectra, for instance, the chemical shift of C1 is significantly upfield of the corresponding signals in η-Ind complexes **2** (40 vs. 94-113 ppm). The signals for the diastereotopic PhCH_2NH_2 protons in complex **4** appear as four triplets of doublets centered at 3.84, 3.34, 2.37 and 1.61 ppm (Figure 3.1a). The H,H-COSY spectrum indicates that these signals form an ABCD spin system. The vicinal and geminal coupling constants were estimated at ca. 3 and 12 Hz, respectively. Unambiguous assignment of the amine protons was achieved by adding a few drops of D_2O to the NMR sample, which caused the two multiplets observed for NH_2 at 2.37 and 1.61 ppm to disappear (Figure 4.1b). The NH/ND exchange also reduced the two CH_2 signals into an AB doublet, and this allowed us to determine the geminal coupling constant for these protons ($^2J_{AB}$ ~ 12 Hz).

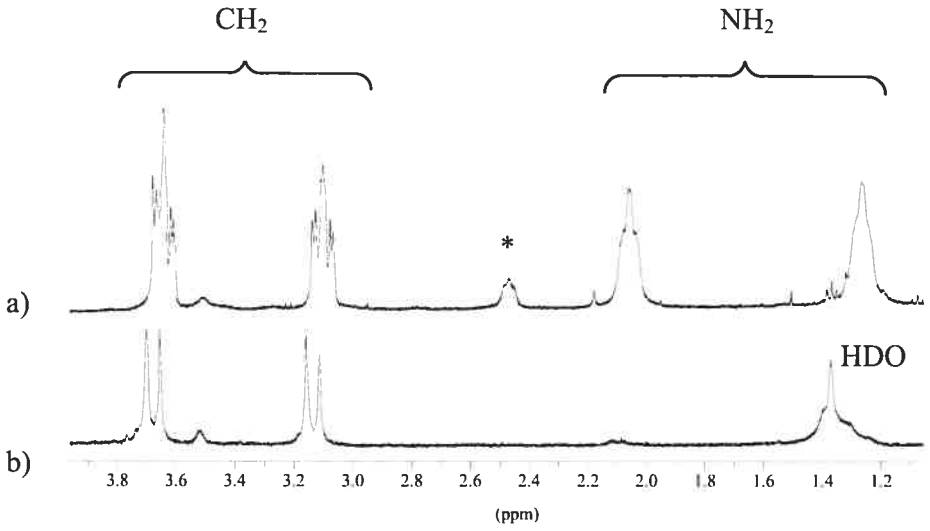

Figure 4.1: a) 400 MHz ^1H NMR spectrum of complex **4** in C_6D_6 showing the four multiplets of the CH_2NH_2 protons. (*: impurities) b) The ^1H NMR spectrum of complex **4** in C_6D_6/D_2O.

Solid State Structures of 3-5. The X-ray analyses of **3-5** have confirmed the spectral assignments and provided valuable structural information for these first Ind-Pd complexes bearing amine ligands. The crystal data and selected structural parameters

are presented in Tables 4.I and 4.II and the ORTEP diagrams are shown in Figures 4.2 and 4.3, respectively.

Table 4.I: Crystal data, Data Collection, and Structure Refinement Parameters of **3-5** and **6a** (The data of **6a** have been corrected with PLATON/SQUEEZE).

	3	**4**	**5**	**6a**
formula	$C_{15}H_{22}NClPd$	$C_{23}H_{25}N_2ClPd.0.5C_6H_6$	$C_{19}H_{17}N_2ClPd$	$C_{34}H_{49}NPClPd$
mol wt	358.19	510.35	415.20	644.56
cryst color, habit	brown-orange, block	yellow, plate	orange, block	orange, block
cryst dimens, mm	0.08×0.23×0.53	0.06×0.15×0.15	0.19×0.28×0.38	0.11×0.15×0.30
system	Monoclinic	Triclinic	Orthorombic	Triclinic
space group	$P2_1/c$	$P\bar{1}$	$Pbca$	$P\bar{1}$
a, Å	8.7756(1)	8.1918(13)	13.2654(2)	10.3658(1)
b, Å	13.9797(2)	10.3940(16)	13.3187(2)	12.3444(1)
c, Å	12.4209(1)	14.768(16)	19.3102(4)	14.4307(2)
α, deg	90	83.970(3)	90	91.696(1)
β, deg	95.397(1)	76.233(3)	90	109.563(1)
γ, deg	90	69.495(3)	90	100.612(1)
volume, Å^3	1517.04(3)	1143.6(3)	3411.69(10)	1701.87(3)
D(calcd), g cm^{-1}	1.568	1.482	1.617	1.258
Z	4	2	8	2
diffractometer	Bruker AXS SMART 2K	Bruker AXS SMART 1K	Bruker AXS SMART 2K	Bruker AXS SMART 2K
temp, K	100	125	100	100
λ	1.54178 Å	0.71073 Å	1.54178 Å	1.54178 Å
μ, mm^{-1}	11.331	0.943	10.201	5.709
scan type	ω scan	ω scan	ω scan	ω scan
F(000)	728	522	1664	676
θ_{max}, (deg)	72.91	29.22	72.92	72.85
h,k,l range	$-10 \le h \le 10$ $-17 \le k \le 17$ $-15 \le l \le 14$	$-11 \le h \le 11$ $-14 \le k \le 14$ $-20 \le l \le 20$	$-16 \le h \le 15$ $-15 \le k \le 16$ $-23 \le l \le 23$	$-12 \le h \le 12$ $-14 \le k \le 15$ $-17 \le l \le 17$
No. of reflns collected/unique	18428/3002	14017/6119	26119/3389	20599/6482
Absorption correction	multi-scan SADABS	multi-scan SADABS	multi-scan SADABS	multi-scan SADABS
T (min, max)	0.16, 0.56	0.86, 0.94	0.09, 0.31	0.43, 0.64
R [$F^2 > 2\sigma(F^2)$], $R_w(F^2)$	0.0280, 0.0735	0.0370, 0.0951	0.0470, 0.1275	0.0478, 0.1459
GOF	1.043	1.053	0.967	1.139

Table 4.II. Selected Bond Distances (Å) and Angles (deg) for **3-5** and **6a**.

	3 (X = N, Y = C3)	**4** (X = N1, Y = N3)		**5** (X = N1, Y = N2)		**6a** (X = N, Y = P)
Pd-X	2.1674(18)	2.066(3)	2.061(3)	2.031(4)		2.129(3)
Pd-Cl	2.3598(5)	2.3996(8)		2.479(4)	2.278(4)	2.3812(9)
Pd-Y	2.225(2)	2.066(2)		2.036(4)		2.2752(9)
Pd-C1	2.151(2)	2.086(3)		2.054(10)	2.145(12)	2.110(4)
Pd-C2	2.171(2)					
Pd-C3a	2.608(2)					
Pd-C7a	2.548(2)					
C1-C2	1.403(4)	1.473(4)		1.465(12)	1.481(14)	1.490(5)
C2-C3	1.406(3)	1.352(5)		1.35(2)	1.35(3)	1.359(6)
C3-C3a	1.474(3)	1.457(4)		1.45(2)	1.37(5)	1.456(6)
C3a-C7a	1.422(3)	1.414(4)		1.423(10)	1.43(3)	1.426(5)
C7a-C1	1.480(3)	1.482(4)		1.493(14)	1.494(14)	1.472(5)
C3a-C4	1.383(4)	1.394(4)		1.341(13)	1.360(14)	1.391(5)
C4-C5	1.396(3)	1.386(5)		1.465(12)	1.461(15)	1.387(6)
C5-C6	1.386(4)	1.396(5)		1.372(13)	1.362(16)	1.408(7)
C6-C7	1.399(4)	1.390(5)		1.40(2)	1.41(2)	1.395(6)
C7-C7a	1.385(3)	1.390(4)		1.39(2)	1.41(2)	1.395(5)
X-Pd-Cl	93.19(5)	92.39(11)	81.32(18)	91.23(14)	86.67(14)	82.84(9)
C1-Pd-X	166.93(8)	87.11(14)	98.2(2)	91.9(3)	91.0(3)	89.84(14)
C1-Pd-Y	62.32(9)	91.6(1)		89.2(3)	88.9(3)	95.15(11)
Cl-Pd-Y	159.79(7)	88.91(7)		87.90(15)	93.27(16)	92.22(3)
C3-Pd-N	106.42(8)					
C1-Pd-Cl	97.61(7)					
ΔM-C (Å)[a]	0.39					
HA (deg)[b]	16.46					
FA (deg)[c]	12.71					

[a] $\Delta(M\text{-}C) = 0.5\ \{(M\text{-}C3a + M\text{-}C7a)\} - 0.5\{(M\text{-}C1 + M\text{-}C3)\}$.

[b] HA is the angle formed between the planes formed by the atoms C1, C2, C3 and C1, C3, C3a, C7a.

[c] FA is the angle formed between the planes formed by the atoms C1, C2, C3 and C3a, C4, C5, C6, C7 and C7a.

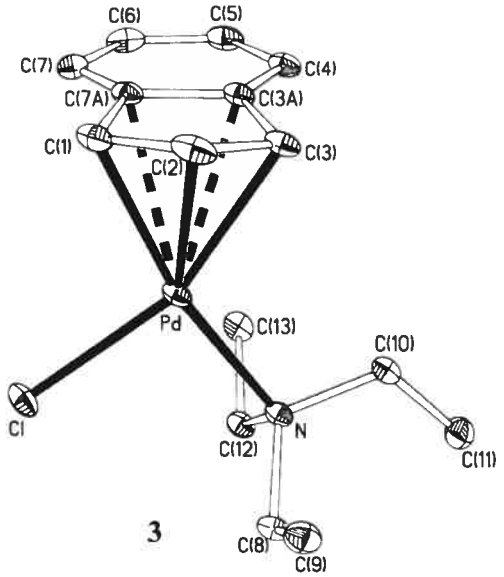

3

Figure 4.2: ORTEP view of complex **3**. Thermal ellipsoids are shown at 30% probability and hydrogen atoms are omitted for clarity.

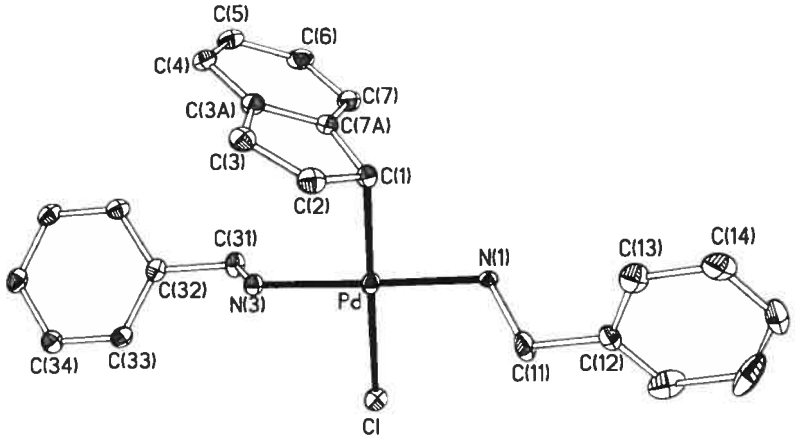

4

Figure 4.3: ORTEP view of complex **4**. Thermal ellipsoids are shown at 30% probability, and hydrogen atoms and the solvent molecule are omitted for clarity. The $BnNH_2$ is disordered over two positions; the views shown in this figure represent the major model.

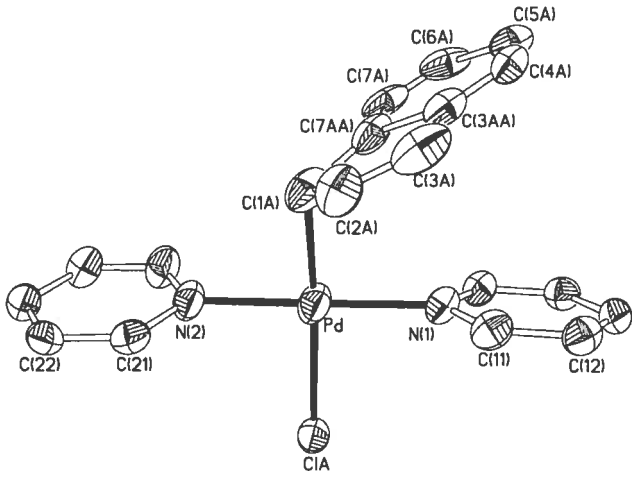

5

Figure 4.3: ORTEP view of complex **5**. Thermal ellipsoids are shown at 30% probability, and hydrogen atoms are omitted for clarity. The Ind and Cl ligands are each disordered over two positions; the views shown in this figure represent the major model.

The overall geometry is approximately square planar in complex **3**, with the largest distortion arising from the small C1-Pd-C3 angle of 62°. The Pd-N distance of 2.225(2) Å is in the range of Pd-N bond lengths reported to date for Pd-NEt_3 complexes.[14] The fairly long Pd-C3a and Pd-C7a distances indicate that the Ind-Pd interaction is primarily through the allylic carbons C1, C2, and C3. The significant difference in the Pd-C bond lengths is a reflection of the so-called "slippage" of the Ind ligand, which can be measured by calculating the parameters such as the slip value (ΔM-C) and the hinge and fold angles (HA and FA).[15] The calculated values of these parameters in **3**, 0.39 Å and ca. 16 and 12 °, respectively, are similar to those found for the phosphine analogues ($\eta^{3\text{-}5}$-Ind)Pd(PR_3)Cl (**2**) but significantly smaller than those of [(η^3-Ind)Pd(μ-Cl)]$_2$ (**1**) (ΔM-C = 0.46 Å, HA = 17°, FA = 16°).[9a] On the other hand, the significant asymmetry in the Pd-C(allyl) bond lengths (Pd-C1 < Pd-C3) is the opposite of the generally observed trend in phosphine complexes (Pd-C1 > Pd-C3),

thus confirming the trans influence order deduced from the NMR spectra (PR_3 > Cl > NEt_3).

X-ray crystal structure analyses of complexes **4** and **5** have confirmed the *trans* square planar geometry around Pd (Figure 4.3). The structural parameters for these complexes are similar to those found in the only other structurally characterized (η^1-Ind)Pd complex,[9a] as well as those of other η^1-Ind compounds reported previously.[16, 17] For example, the sp^3 hybridized character of the Pd-bound carbon atom is reflected in the C1-C7a (*ca.* 1.50 Å) and C1-C2 (*ca.* 1.47 Å) distances that are in the normal range for C-C single bonds, whereas the C2-C3 distance (*ca.* 1.35 Å) is in the expected range for a $C(sp^2)$-$C(sp^2)$ double bond. The Pd-N bond lengths (ca. 2.06 Å for **4** and 2.03 Å for **5**) lie well within the range of distances reported previously for analogous compounds.[18] The coordinated pyridine rings in complex **5** form a dihedral angle of ca. 15° and are oriented nearly orthogonal to the Pd square plane, which serves, presumably, to maximize Pd→py backbonding and minimize steric interactions.

New monometallic (η^1-Ind)Pd^{II} and bimetallic (μ,η^3-Ind)Pd^{I}_2 complexes. That complexes featuring $\eta^{3\text{-}5}$- or η^1-Ind ligands can be prepared from the reaction of the common precursor **1** with various ligands L (PR_3, NEt_3, *t*-BuNC, $BnNH_2$, py; Scheme 4.1) shows unambiguously that the nature of the incoming ligand L has a direct bearing on Ind hapticity in the product. To determine how the Ind hapticity would change with a mixture of ligands, we added 2 equivalents of PR_3 to a CH_2Cl_2 solution of **4**, generated in-situ by addition of 2 equivalents of $BnNH_2$ to **1**. The reaction with PCy_3 gave an orange brown solution from which we isolated an orange powder that was identified as the mixed-ligand species (η^1-Ind)Pd(PCy_3)($BnNH_2$) Cl, **6a** (Scheme 4.2, Method A, 85% yield). The analogous reaction with PPh_3 gave (η^1-Ind)Pd(PPh_3)($BnNH_2$) Cl, **6b**, which was characterized by NMR but could not be isolated and purified because it decomposed to two new products that will be discussed later (Scheme 4.2). Complexes **6a** and **6b** were also obtained by adding one equivalent of $BnNH_2$ to (η-Ind)Pd(PCy_3)Cl (**2a**) or its PPh_3 analogue **2b**, respectively (Scheme 4.2, Method B, ca. 78% yield for **6a**).

The new η^1-Ind complexes **6** can be considered to be suitable models for the postulated intermediate in the ligand displacement reaction (η-Ind)M(L)Cl + L' → (η-Ind)M(L')Cl + L proceeding by an associative mechanism. It is interesting to note that associative ligand substitutions of the closely related complexes (η-Ind)M(L)$_2$ of group 9 metals are believed to proceed via η^3-Ind intermediates (e.g., (η^3-Ind)Ir(PMe$_2$Ph)$_3$).[19] One possible explanation for the apparently different behaviors of these d^8 metal centers is that in each case the intermediate species maintains the electronic configuration of its precursor complex; thus, the (η^1-Ind)Pd^{II} and (η^3-Ind)Ir^{I} species both maintain the (nearly) 16- and 18-electron configurations of their respective predecessors.

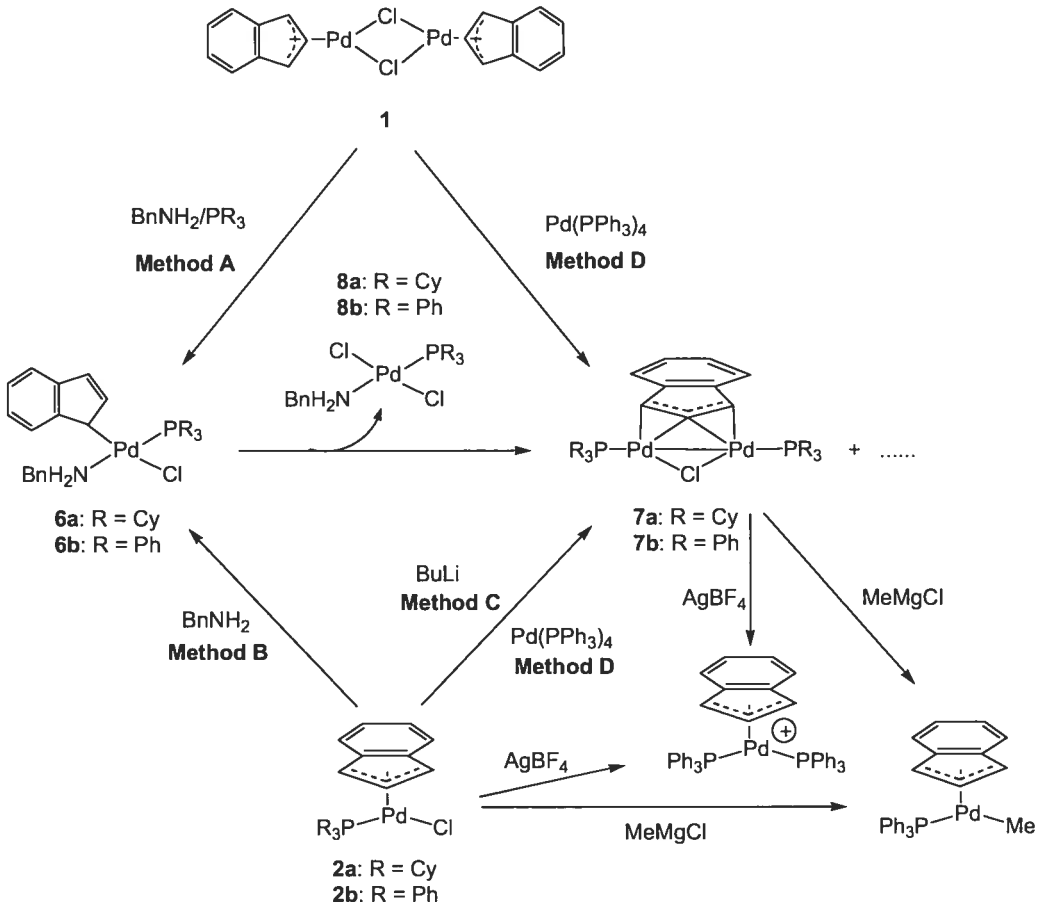

Scheme 4.2

As mentioned above, after a few hours, complex **6b** decomposes fairly rapidly to give two new products. Complex **6a** was found to have greater thermal stability, but it too decomposed gradually (over 24 h) to give a solid residue which gave a mixture of crystals upon recrystallization. Visual inspection of this mixture under a microscope showed two different crystals, orange microcrystals and larger yellow-orange crystals, which were separated mechanically and identified by X-ray diffraction analyses as $(\mu,\eta^3\text{-Ind})(\mu\text{-Cl})Pd_2(PCy_3)_2$, **7a**, and $(BnNH_2)(PCy_3)PdCl_2$, **8a**, respectively. The products arising from the decomposition of **6b** were found to be PPh_3 analogues of **7a** and **8a**. In this case, recrystallization of the solid residues from CH_2Cl_2/hexane did furnish pure samples of $(\mu,\eta^3\text{-Ind})(\mu\text{-Cl})Pd_2(PPh_3)_2$, **7b**, in ca. 50% yield, but samples of the second product, **8b**, were always contaminated with **7b** and could not be obtained in pure form. We have probed the various reaction pathways that convert **1**, **2**, or **6** into complexes **7** and **8**, and have examined briefly the stabilities and reactivities of the latter; these studies are discussed next. The characterization of the new complexes **6-8** will be discussed in the following section.

The analogous reactions of **5** with phosphines or the reaction of **2** with py gave complex mixtures, which were analyzed by NMR and shown to contain the following species: **2a**, $(\eta^1\text{-Ind})Pd(PCy_3)(py)Cl$, $(PCy_3)_2PdCl_2$, **7a**, and biindene in the PCy_3 reactions; $(PPh_3)_2PdCl_2$, **7b**, and biindene in the PPh_3 reactions. The isolation of the products from these mixture was not pursued.

The bimetallic $(\mu,\eta^3\text{-Ind})Pd^I_2$ compounds **7** are reminiscent of the analogous Cp complex $(\mu,\eta^3\text{-Cp})(\mu\text{-Cl})Pd_2(P^iPr_3)_2$, which are prepared by reacting $CpPd(P^iPr_3)Cl$ with the reducing agent Mg, the hydrides $LiAlH_4$ or $NaBH_4$, or the alkylating agent *n*-BuMgBr.[20] By analogy to the latter route, we reacted **2a** and **2b** with 0.5 equiv of BuLi in NMR scale reactions to test whether bimetallic **7** could be obtained thus. The ^1H NMR spectra of these reactions contained the expected signals for **7**, in addition to signals attributed to 1-butene and free indene (Method C, Scheme 4.2). Monitoring the reaction by $^{31}P\{^1H\}$ NMR spectroscopy showed the appearance, during the initial stages of the reaction, of new signals at ca. δ 49 ppm (PCy_3 species) and 41 ppm (PPh_3 species), followed by a gradual disappearance of these signals and the emergence of

the corresponding signals for **7**. We propose that these species are Pd^{II}-Bu intermediates whose decomposition by β-H elimination gives 1-butene and Pd^{II}-H species. The latter are not detected due to a rapid reductive elimination that generates free indene and $Pd^0(PR_3)_n$ species. The formation of **7** likely proceeds by a comproportionation reaction between the in-situ generated Pd^0 species and the Pd^{II} precursors **2** (Scheme 4.3). It is noteworthy that direct comproportionation reactions between organopalladium(II) and Pd^0 species have been used to prepare many different Pd^I species, including dipalladium(I) compounds featuring (μ:η^3-Cp) and (μ:η^3-allyl) ligands.[10] Accordingly, we found that a direct reaction between $Pd(PPh_3)_4$ and **1** or **2b** gives **7b** (Method D, Scheme 4.2), thus confirming that a comproportionation reaction can lead to analogous (μ:η^3-Ind) compounds.

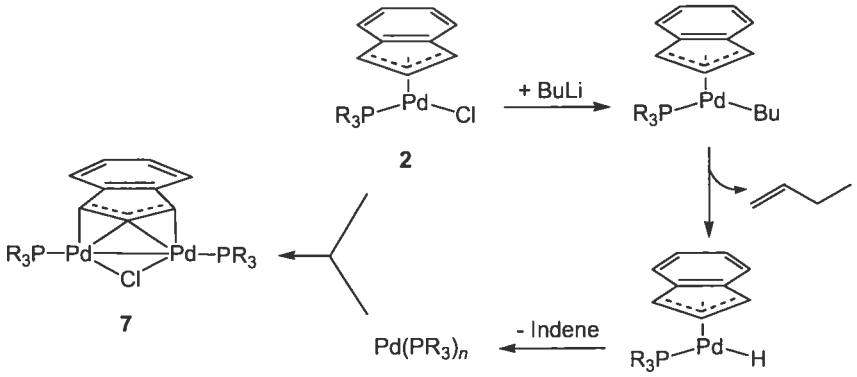

Scheme 4.3

The above observations allow us to rationalize the unanticipated formation of **7** and **8** from **6** via the sequence of steps shown in Scheme 4.4. First, **6** undergoes a ligand redistribution process to give the bis(chloro) compounds $(BnNH_2)(PR_3)PdCl_2$, **8**, and the bis(η^1-Ind) complexes $(\eta^1\text{-Ind})_2Pd(PR_3)(BnNH_2)$ (step a); the latter decompose via reductive elimination to give 1,1'-biindene (Ind-Ind) and $Pd^0(PR_3)_n(BnNH_2)_m$ (step b); a comproportionation reaction between the latter and **6** generates the (μ:η^3-Ind)Pd^I_2 species **7** (step c). The side-product Ind-Ind has been detected in the reaction mixtures by ^{1}H NMR of the solutions of **6** (over 24 h) and GC/MS analyses has confirmed its

presence (M^+ at *m/z* 230). Moreover, some of this side-product gets dehydrogenated to *trans*-1,1'-bis(indenylidene) (Ind=Ind),[21] which co-crystallized with **7a** (vide infra). We speculate that this dehydrogenation proceeds by addition of the benzylic C-H bond of Ind-Ind to the in-situ generated Pd^0 species to give (η^1-(1-Ind-Ind))Pd(H)(PR_3)($BnNH_2$) (step d); β-H elimination of the latter generates Ind=Ind and a bis(hydrido) species (step e) that regenerates the original Pd^0 species by eliminating H_2 (step f).

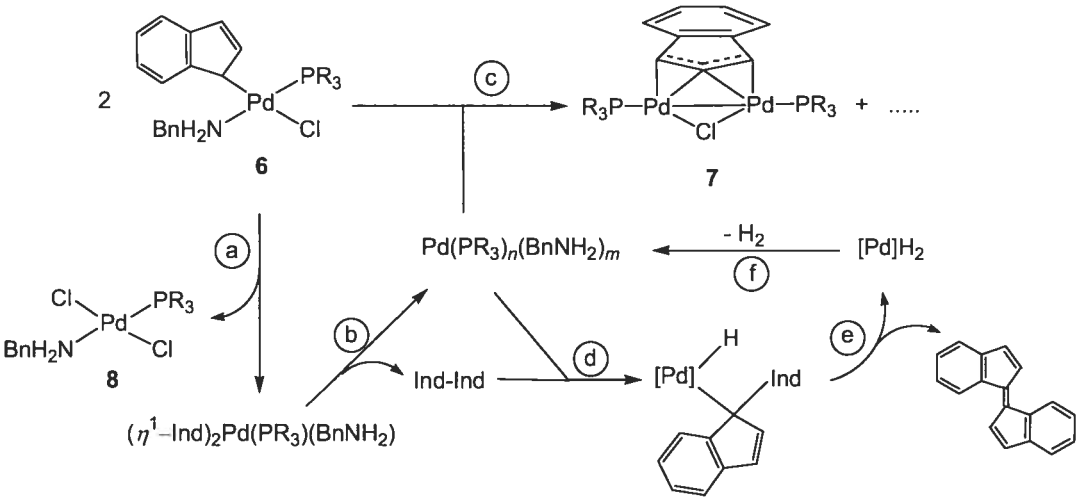

Scheme 4.4

Solid samples of the μ-η^3-Ind compounds **7** can be handled in air indefinitely, but in solution they undergo a gradual and irreversible transformation (over several weeks) into the corresponding monomeric Pd^{II}-phosphine species (η-Ind)Pd(PR_3)Cl (**2**). This observation seemed to indicate that complexes **7** behave as if they are simple combinations of the Pd^{II} compounds **2** and the $Pd^0(PR_3)$ fragment, rather than "real" dipalladium(I) species. Indeed, our preliminary results indicate that complexes **7** demonstrate virtually identical reactivities compared to **2**. For instance, reacting **7b** with $AgBF_4$ results in the formation of some black Pd residues and the monomeric complex [(η-Ind)Pd(PPh_3)$_2$][BF_4] in 46% isolated yield; the latter compound is also obtained from the reaction of (η-Ind)Pd(PPh_3)Cl (**2b**) with $AgBF_4$ (Scheme 4.2).[9b] Similarly, reacting MeMgCl with either **7b** or **2b** gives the same product, namely (η-

Ind)Pd(PPh_3)Me.[9b] It appears, therefore, that the comproportionation reaction that generates complexes **7** can proceed in the reverse sense (disproportionation) to give complexes **2** and $Pd^0(PR_3)_n$.

Characterization of complexes 6-8. Complexes **6a**, **7a**, **7b**, and **8a** were characterized by NMR spectroscopy, elemental analyses (except for **8a**), and single-crystal X-Ray diffraction studies, whereas complexes **6b** and **8b** were identified by comparing their NMR spectra to those of their fully characterized PCy_3 analogues.

The ambient temperature NMR spectra of **6a** and **6b** gave indications of a slow exchange process. For example, the $^{31}P\{^1H\}$ NMR spectra showed a broad singlet at 41.5 and 37.1 ppm, respectively; similarly, some of the ^1H and ^{13}C NMR signals were broadened and some missing. Cooling the NMR sample to -10 °C resulted in the sharpening of the ^{31}P signals and the emergence in the ^1H and ^{13}C NMR spectra of new signals due to the PCy_3, $BnNH_2$, and the η^1-Ind ligands (e.g., δ_{H1} = 4.94 ppm for **6a** (d, $^3J_{H\text{-}P}$ = 5.4 Hz) and 4.47 ppm for **6b** (d, $^3J_{H\text{-}P}$ = 7.6 Hz); δ_{C1} = 38.9 ppm for **6a** and 46.6 for **6b**).

X-Ray diffraction studies helped establish the identity of **6a** unambiguously. The ORTEP diagram for **6a** is shown in Figure 4.4, while Tables 4.I and 4.II list the crystallographic data and selected bond distances and angles.

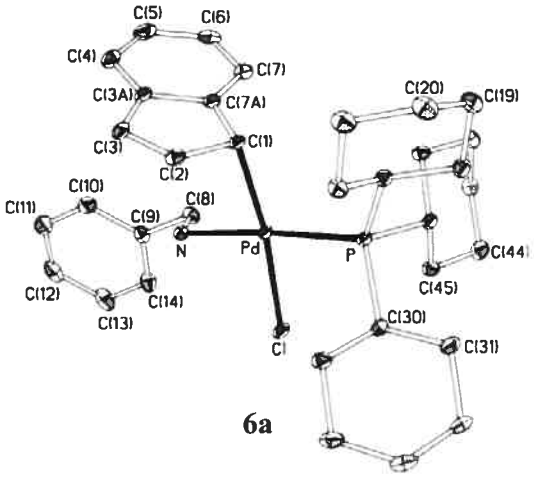

6a

Figure 4.4: ORTEP view of complex **6a**. Thermal ellipsoids are shown at 30% probability and hydrogen atoms are omitted for clarity.

The essentially square planar geometry adopted by the Pd center in **6a** shows a slight tetrahedral distortion (e.g., C1-Pd-Cl ~ 172°), which serves, presumably, to minimize steric interactions between the Ind and PCy_3 ligands. The Pd-N distance is much longer than the corresponding distance in **4**, presumably because of the much greater trans influence of PCy_3 versus $BnNH_2$. All the other distances and angles are comparable to those found in the η^1-Ind complexes **4** and **5**. Similarly, in the X-ray molecular structure of complex **8a** (Table 4.III, Figure 4.5) the Pd center adopts a distorted square planar geometry (e.g., Cl1-Pd-Cl2 ~ 176°) and the Pd-N and Pd-P distances are very close to those observed for complex **6a**.

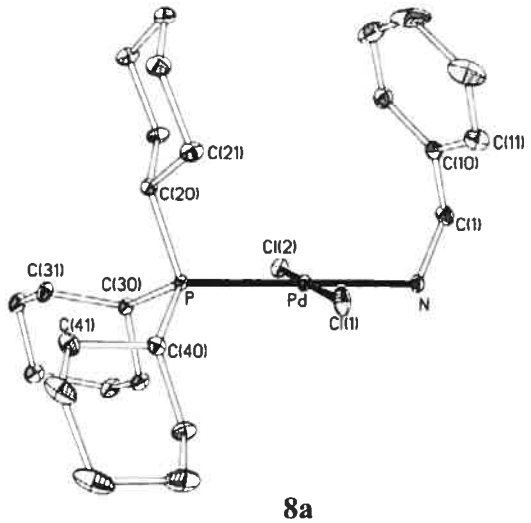

8a

Figure 4.5: ORTEP view of complex **8a**. Thermal ellipsoids are shown at 30% probability and hydrogen atoms are omitted for clarity. Selected bond lengths (Å) and angles (deg): Pd-Cl1 = 2.2951(5), Pd-Cl2 = 2.3068(5), Pd-N = 2.126(2), Pd-P = 2.2665(5), N-C1 = 1.489(3), P-Pd-Cl1 = 91.08(2), Cl1-Pd-N = 86.97(5), N-Pd-Cl2 = 88.85(5), Cl2-Pd-P = 93.09(2).

The decomposition of **6** to new compounds was signaled by the appearance in the $^{31}P\{^1H\}$ NMR spectrum of new signals at δ 38.5 (**7a**), 25.7 (**7b**), 44.1 (**8a**), and 28.6 (**8b**). The spectral patterns observed in the ^1H and $^{13}C\{^1H\}$ NMR spectra of the μ-η^3-Ind moiety in **7a** and **7b** were very different from those of (η-Ind)Pd(PR_3)Cl

complexes, but quite similar to the corresponding signals of the previously studied complexes $[(\mu,\eta^3\text{-Ind})Pd(CNR)]_2$.[8c,d] For instance, a set of signals corresponding to an AX_2 system was observed for H2 (4.22 ppm, quintuplet, $^3J_{H\text{-}H} = {}^3J_{H\text{-}P} = 3.6$ Hz) and H1/H3 (triplets of doublets at δ 5.81 ppm (**7a**) and 5.12 ppm (**7b**), $^3J_{H\text{-}P} = 7.3$ Hz, $^3J_{H\text{-}H} = 3.6$ Hz),[22] while H4-H7 displayed an AA'BB' system ($\delta_{H4,7} = 7.04$ ppm and $\delta_{H5,6} = 7.35$ ppm for **7a**; $\delta_{H4,7} = 5.98$ ppm and $\delta_{H5,6} = 6.52$ ppm for **7b**). This segment of the ^{1}H NMR spectrum for **7b** is shown in Figure 3.6. It should be noted that the chemical shifts for H4 and H7 in complex **7b** are much more upfield than those of H5 and H6 anticipated, while the opposite trend is observed in **7a**. Inspection of the solid structure of **7b** has shown that H4 and H7 are fairly close to the center of one of the PPh_3 phenyl rings (vide infra), which indicates that the upfield shifts are likely caused by the anisotropy cone of the Ph rings. The $^{13}C\{^1H\}$ NMR spectra showed only five resonances assigned to the symmetry-related pairs of carbons C1/C3, C5/C6, C4/C7, C3a/C7a and C2; the assignments were facilitated by the HMQC spectra.

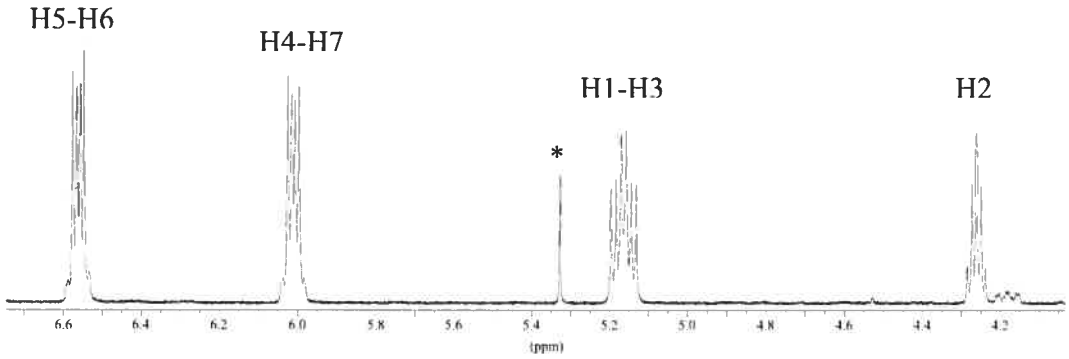

Figure 4.6: 300-MHz ^{1}H NMR spectrum of complex **7b** in $CDCl_3$. (*: trace CH_2Cl_2)

The X-ray molecular structures obtained for **7a** and **7b** are consistent with the NMR spectra observed in solution. The ORTEP diagrams for these compounds are shown in Figure 4.7, and the crystallographic data and selected bond distances and angles are listed in Tables 4.III and 4.IV.

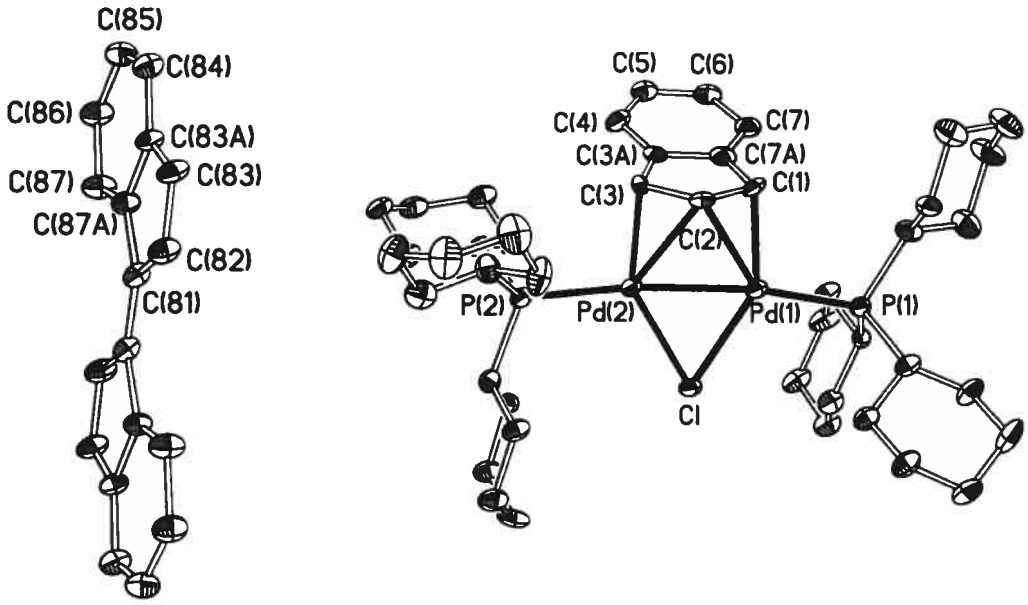

7a

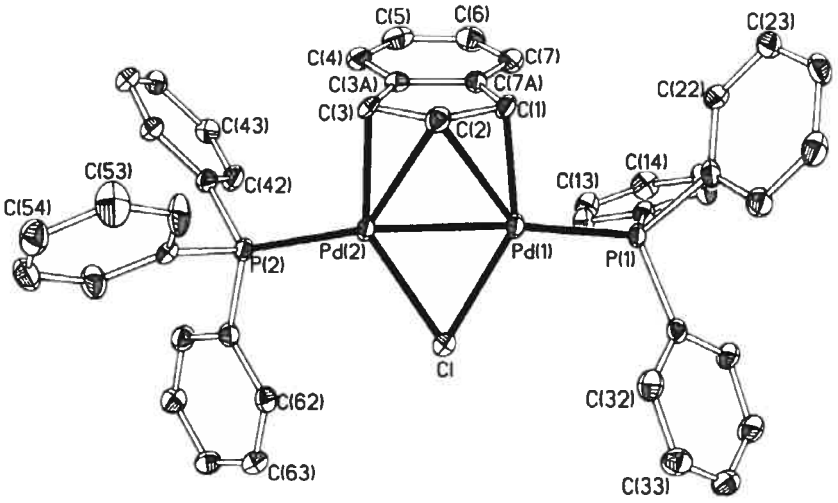

7b

Figure 4.7: ORTEP views of complexes **7a** and **7b**. Thermal ellipsoids are shown at 30% probability and hydrogen atoms are omitted for clarity.

Table 4.III. Crystal data, Data Collection, and Structure Refinement Parameters of **7a**, **7b** and **8a**.

	7a	**7b**	**8a**
formula	$C_{54}H_{79}ClP_2Pd_2$	$C_{45}H_{37}ClP_2Pd_2$	$C_{25}H_{42}Cl_2NPPd$
mol wt	1038.36	887.94	564.87
cryst color, habit	orange, block	red, block	yellow, block
cryst dimens, mm	0.12×0.17×0.34	0.29×0.30×0.51	0.20×0.30×0.42
system	monoclinic	monoclinic	monoclinic
space group	$P2_1/n$	Cc	$P2_1/c$
a, Å	17.481(3)	13.8689(3)	17.0179(2)
b, Å	16.598(3)	14.2117(3)	9.4258(1)
c, Å	17.740(3)	19.1372(6)	18.1497(3)
α, deg	90	90	90
β, deg	109.518(7)	104.345(2)	115.208(1)
γ, deg	90	90	90
volume, Å^3	4851.6(13)	3654.35(16)	2634.09(6)
Z	4	4	4
D(calcd), g cm^{-1}	1.422	1.614	1.424
diffractometer	Bruker AXS Smart 2K	Bruker AXS Smart 2K	Bruker AXS Smart 2K
temp, K	100	220	100
λ	1.54178 Å	1.54178 Å	1.54178 Å
μ, mm^{-1}	7.363	9.684	8.201
scan type	ω scan	ω scan	ω scan
F(000)	2168	1784	1176
θ_{max}, (deg)	53.43	72.95	72.84
h,k,l range	$-18 \le h \le 18$	$-16 \le h \le 17$	$-20 \le h \le 21$
	$-17 \le k \le 17$	$-17 \le k \le 17$	$-11 \le k \le 11$
	$-18 \le l \le 18$	$-22 \le l \le 19$	$-21 \le l \le 19$
no. of reflns collected/unique	59157/5653	14769/5858	21228/5049
Absorption correction	multi-scans SADABS	multi-scans SADABS	multi-scans SADABS
T (min, max)	0.08, 0.29	0.06, 0.22	0.19, 0.37
R [$F^2 > 2\sigma(F^2)$], $R_w(F^2)$	0.0549, 0.1253	0.0535, 0.1369	0.0308, 0.0798
GOF	0.976	1.041	1.039

Table 4.IV. Selected Bond Distances (Å) and Angles (deg) for **7a** and **7b**.

	7a	**7b**
Pd1-Cl	2.4301(19)	2.411(2)
Pd1-P1	2.293(2)	2.260(2)
Pd1-C1	2.107(7)	2.072(7)
Pd1-C2	2.425(7)	2.405(7)
Pd2-Cl	2.4207(19)	2.432(2)
Pd2-P2	2.280(2)	2.274(2)
Pd2-C2	2.412(7)	2.401(8)
Pd2-C3	2.106(7)	2.122(7)
Pd1-C7a	2.988(7)	2.929(8)
Pd2-C3a	2.974(7)	2.930(7)
Pd1-Pd2	2.5971(8)	2.6031(6)
C1-C2	1.418(10)	1.422(11)
C2-C3	1.415(10)	1.427(11)
C3-C3a	1.496(10)	1.480(12)
C3a-C7a	1.429(11)	1.419(11)
C7a-C1	1.476(10)	1.502(11)
C3a-C4	1.403(10)	1.392(12)
C4-C5	1.379(11)	1.400(15)
C5-C6	1.377(10)	1.391(14)
C6-C7	1.417(10)	1.399(14)
C7-C7a	1.389(10)	1.379(12)
C1-Pd1-P1	103.1(2)	99.9(2)
P1-Pd1-Cl	113.52(7)	115.60(6)
Cl-Pd1-P2	57.45(5)	57.89(5)
Pd2-Pd1-C1	86.0(2)	86.5(2)
C3-Pd2-P2	99.5(2)	101.5(2)
P2-Pd2-Cl	115.42(7)	114.34(7)
Cl-Pd2-Pd1	57.80(5)	57.10(5)
Pd1-Pd2-C3	87.4(2)	87.2(2)
Pd1-Cl-Pd2	64.74(5)	65.01(5)
ΔM-C (Å)[a]	0.87	0.83
HA (deg)	5.61	1.92
FA (deg)	12.49	4.69

[a] $\Delta(M\text{-}C) = 0.5\ \{(Pd1\text{-}C7a + Pd2\text{-}C3a)\} - 0.5\ \{(Pd1\text{-}C1 + Pd2\text{-}C3)\}$.

The coordination geometry around the Pd atoms in both complexes is square planar, displaying angular distortions of 5-30°. The structures consist of two Pd^{I} centers coordinated by a terminal phosphine ligand (Pd-P ~ 2.26-2.29 Å) and bridged by a μ,η^3-Ind and a μ-Cl. The diamagnetism of these d^9 complexes implies a Pd-Pd bond, which is reflected in the relatively short bond distance of ca. 2.60 Å; this is similar to analogous distances of 2.61-2.72 Å found in (μ-allyl)(μ-X)Pd(PPh_3)$_2$ (X = Cl,[23] I,[24] Cp,[25] allyl[26]) and lies within the expected range of 2.53-2.70 Å for Pd^{I}-Pd^{I} bond distances found in a large number of compounds.[27] As was alluded to above, H4 and H7 are fairly close to one of the Ph rings of the PPh_3 ligand in **7b**,[28] which helps explain the unusually upfield signals of these protons in the ^{1}NMR spectrum of **7b** (vide supra).

The most notable feature of these complexes is the unusual bonding mode of the indenyl moiety: although there are many precedents for complexes featuring μ-allyl or μ-Cp ligands on a Pd^{I}-Pd^{I} framework,[10] the only precedents for the analogous μ,η^3-Ind complexes are the compounds [(μ,η^3-Ind)Pd(CNR)]$_2$ (R = *t*-Bu; 2,6-$(CH_3)_2C_6H_3$; 2,4,6-$(CH_3)_3C_6H_2$; 2,4,6-(*t*-Bu)$_3C_6H_2$).[8c,d] The μ,η^3-Ind ligands in **7a** and **7b** are symmetrically bonded to the two Pd^{I} centers and show Pd-C distances identical to those observed in the [(μ,η^3-Ind)Pd(CNR)]$_2$ analogues (Pd1-C1 ~ Pd2-C3 ~ 2.1 Å and Pd1-C2 ~ Pd2-C2 ~ 2.4 Å). The relatively long Pd1-C7a and Pd2-C3a distances of ca. 2.9 Å are out of the normal bonding range and support the trihapto designation. Indeed, the Δ(M-C) values observed for **7a** and **7b** (0.83 and 0.87 Å, respectively; Table 4.IV) are in the same range as those found previously in η^3-Ind complexes[29] and much larger than those of the previously described monomeric ($\eta^{3\text{-}5}$-Ind)Pd^{II} complexes **2**. On the other hand, the HA and FA angles in **7** are fairly small, representing only small planar distortions for the Ind ligands (**7a**: HA ~ 6°, FA ~ 12°; **7b**: HA ~ 2°, FA ~ 5°).

Another interesting feature of the crystal structure in complex **7a** is the presence of a co-crystallized half molecule of *trans*-1,1'-bis(indenylidene) (Figure 3.7). The two Ind moieties in this molecule are linked by a double bond (C81=C81^{i})[30] involving a *trans* configuration imposed by the inversion center. The distances and angles are comparable to those obtained for the recently published structure of *trans*-

1,1'-bis(indenylidene).[31] As mentioned earlier, we believe that this side-product arises from the Pd^0-catalyzed dehydrogenation of Ind-Ind, which is generated in-situ during the formation of **7**.

Conclusion

The reaction of the dimer $[(\eta^3\text{-Ind})Pd(\mu\text{-Cl})]_2$ (**1**) with a variety of ligands has resulted in the formation of complexes featuring Ind ligands of different hapticities, underlining the influence of the auxiliary ligand(s) on the hapticity of Ind. Thus, reaction with phosphines or NEt_3 gives $(\eta^{3\text{-}5}\text{-Ind})Pd(L)Cl$, (**2** and **3**), whereas ^{t}BuNC, $BnNH_2$, and pyridine give the η^1-Ind complexes $[(\eta^1\text{-Ind})(t\text{-BuNC})Pd(\mu\text{-Cl})]_2$ or *trans*-$(\eta^1\text{-Ind})PdL_2Cl$ (L = $BnNH_2$ (**4**), py (**5**)). On the other hand, the one-pot reaction of **1** with a mixture of $BnNH_2$ and the phosphine ligands PCy_3 or PPh_3 gave the mixed-ligand, amino and phosphine species $(\eta^1\text{-Ind})Pd(PR_3)(BnNH_2)Cl$, (**6**), which can also be prepared by addition of $BnNH_2$ to $(\eta\text{-Ind})Pd(PR_3)Cl$ (**2**). Compounds **6** serve as models for the postulated intermediates in the associative ligand displacement reactions $(\eta\text{-Ind})M(L)Cl + L' \rightarrow (\eta\text{-Ind})M(L')Cl + L$.

Gradual decomposition of **6** in solution generates the dinuclear Pd^I compounds $(\mu,\eta^3\text{-Ind})(\mu\text{-Cl})Pd_2(PR_3)_2$ (**7**) displaying a rare mode of Ind hapticity. A brief examination of the reactivities of these new species with $AgBF_4$ or MeMgCl has shown that they give, respectively, the monomeric products $[(\eta\text{-Ind})Pd(PPh_3)_2][BF_4]$ and $(\eta\text{-Ind})Pd(PPh_3)Me$ plus the (undetected) fragment $Pd(PR_3)_n$. Our preliminary observations suggest that complexes **7** are formed via a comproportionation reaction from $Ind\text{-}Pd^{II}$ and $Pd^0(PR_3)_n$ species and undergo spontaneous disproportionation reaction to regenerate these precursors. These results suggest that the possibility of such disproportionation reactions occurring in other $Pd^I\text{-}Pd^I$ complexes should be taken into account, especially in view of the recent reports on the catalytic reactivities exhibited by some of these complexes.[32] We continue to probe further this issue, in particular, and the chemistry of these μ,η^3-Ind compounds in general.

Experimental Section

General Comments. All manipulations and experiments were performed under inert atmosphere using standard Schlenk techniques and/or a nitrogen-filled glovebox. Dry, oxygen-free solvents were prepared by distillation from appropriate drying agents and employed throughout. The syntheses of $[(\eta^3\text{-Ind})Pd(\mu\text{-Cl})]_2$ (**1**), $(\eta\text{-Ind})Pd(PR_3)Cl$ (**2**), $(\eta\text{-Ind})Pd(PPh_3)Me$ and $[(\eta\text{-Ind})Pd(PPh_3)_2][BF_4]$ have been reported previously;[8] all other reagents used in the experiments were obtained from commercial sources and used as received. The elemental analyses were performed by the Laboratoire d'Analyse Elémentaire (Université de Montréal). Bruker AV500, ARX400, AV400, AMX300, AV300 spectrometers were employed for recording ^1H (500 MHz, 400 MHz and 300 MHz), $^{13}C\{^1H\}$ (126 MHz, 100 MHz and 75 MHz), and $^{31}P\{^1H\}$ (202 MHz, 161 MHz and 121 MHz) NMR spectra at ambient temperature, unless otherwise specified. The ^1H and ^{13}C NMR spectra were referenced to solvent resonances, as follows: 7.26 and 77.16 ppm for $CHCl_3$ and $CDCl_3$, 7.16 and 128.06 ppm for C_6D_5H and C_6D_6, 5.30 and 53.52 for $CDHCl_2$ and CD_2Cl_2, 2.11 and 21.10 for C_7D_7H and C_7D_8. The ^{31}P NMR spectra were referenced to 85% H_3PO_4 (0 ppm).

Crystal Structure Determinations

The crystal data for complexes **3**, **4**, **5**, **6a**, **7a**, **7b** and **8a** were collected on a Bruker AXS Smart 2K and 1K (for **4**) diffractometers using SMART.[33] Graphite-monochromated Cu Kα radiation was used at 100 K for all crystals except that of **7b** for which the temperature was 220 K, and **4** for which the radiation used was Mo Kα at 125 K. Cell refinement and data reduction were done using SAINT.[34] All structures were solved by direct methods using SHELXS97[35] and difmap synthesis using SHELXL97;[36] the refinements were done on F^2 by full-matrix least squares. All non hydrogen atoms were refined anisotropically, while the hydrogens (isotropic) were constrained to the parent atom using a riding model. The crystal data and experimental details are listed in Tables 4.I and 4.III, while selected bond distances and angles are listed in Tables 4.II and 4.IV. The Ind moiety and the Cl atom in the crystal structure of **5** were disordered over two positions, with respectives occupancies factors of

(0.58/0.42) and (0.61/0.39). One of the $BnNH_2$ present within the crystal structure of **4** was also disordered over two positions (0.69/0.31). Each of the disorders was refined anisotropically using restraints (SAME/SADI/EADP/DFIX) applied in order to improve the model. The reported structure of **6a** is based on the PLATON/SQUEEZE[37] corrected data (volume of the potential solvent = 168Å^3; improvement of 4.1% in R1 while correcting for 41 electrons/cell).

Synthesis of (η-Ind)Pd(NEt_3)Cl, (3). NEt_3 (441 μL, 3.2 mmol) was added to a stirred C_6H_6 suspension (30 mL) of [(η^3-Ind)Pd(μ-Cl)]$_2$ (**1**; 650 mg, 1.3 mmol) at room temperature. After stirring for 2h, the resulting brown solution was concentrated to *ca.* 5 mL and 15 mL of hexane were added. A brown powder precipitated and was isolated by filtration and washed with hexane (650 mg, 72%). Recrystallization of a small portion of this solid from a C_6H_6/hexane solution yielded crystals suitable for X-ray diffraction studies and elemental analysis. ^{1}H NMR (C_6D_6, 400 MHz): δ 6.91 (d, $^3J_{H\text{-}H}$ = 6.3 Hz, H_7), 6.69 (br, H_5 and H_6), 6.48 (d, $^3J_{H\text{-}H}$ = 6.2 Hz, H_4), 6.34 (br, H_2), 5.62 (br, H_1), 4.68 (br, H_3), 2.63-2.49 (m, CH_2), 0.73 (t, $^3J_{H\text{-}H}$ = 6.9 Hz, CH_3). ^{1}H NMR (C_7D_8, 500 MHz, 263 K): δ 6.93-6.91 (dd, $^3J_{H7\text{-}H6}$ = 7.2 Hz, $^4J_{H7\text{-}H1}$ = 0.9 Hz, H_7), 6.69 (quintuplet of doublet, $^3J_{H\text{-}H}$ = 7.5 Hz, $^5J_{H\text{-}H}$ = 1.2 Hz, H_5 and H_6), 6.45 (dd, $^3J_{H4\text{-}H5}$ = 7.3 Hz, $^4J_{H4\text{-}H3}$ = 0.9 Hz, H_4), 6.31 (t, $^3J_{H\text{-}H}$ = 3.1 Hz, H_2), 5.59 (td, $^3J_{H1\text{-}H2}$ = $^4J_{H1\text{-}H3}$ = 2.4 Hz, $^4J_{H1\text{-}H7}$ = 0.7 Hz, H_1), 4.61 (td, $^3J_{H3\text{-}H2}$ = $^4J_{H3\text{-}H1}$ = 2.5 Hz, $^4J_{H3\text{-}H4}$ = 0.8 Hz, H_3), 2.54 (q, $^3J_{H\text{-}H}$ = 6.9 Hz, CH_2), 0.73 (t, $^3J_{H\text{-}H}$ = 6.9 Hz, CH_3).^{13}C{^{1}H} NMR ($CDCl_3$, 75 MHz): δ 139.86 (s, C_{3a} or C_{7a}), 128.50 (s, C_5), 126.62 (s, C_6), 119.33 (s, C_7), 115.97 (s, C_4), 111.22 (s, C_2), 81.56 (s, C_3), 72.72 (s, C_1), 50.02 (s, CH_2), 10.64 (s, CH_3). The missing resonance for C3a or C7a is probably obscured under the residual solvent resonances at ca. 129 ppm. Anal. Calcd for $C_{15}H_{22}N_1Cl_1Pd_1$: C, 50.29; H, 6.19; N, 3.91. Found: C, 50.15; H, 6.27; N, 3.76.

Synthesis of (η^1-Ind)Pd($BnNH_2$)$_2$Cl, (4). Method A. Benzylamine (127 μL, 1.2 mmol) was added to a stirred C_6H_6 suspension (15 mL) of [(η^3-Ind)Pd(μ-Cl)]$_2$ (**1**; 150

mg, 0.29 mmol) at room temperature. The yellow green mixture was stirred approximately 2 h, filtered and evaporated to dryness to give a yellow solid which was washed with hexane (200 mg, 73%). Recrystallization of a small portion of this solid from a C_6H_6/hexane solution yielded crystals suitable for X-ray diffraction studies.

Method B. Benzylamine (61 μL, 0.56 mmol) was added to a stirred C_6H_6 solution (15 mL) of (Ind)Pd(NEt_3)Cl (**3**; 100 mg, 0.28 mmol) at room temperature. After stirring for 2h, the resulting brown-green mixture was concentrated to *ca.* 5 mL. A yellow powder precipitated and was isolated by filtration and washing with hexane (110 mg, 84%). ^{1}H NMR ($CDCl_3$, 400 MHz): δ 7.64 (d, $^3J_{H\text{-}H}$ = 7.3 Hz, H_4 or H_7), 7.45 (d, $^3J_{H\text{-}H}$ = 7.3 Hz, H_7 or H_4), 7.36-7.28, (m, Ph), 7.23 (t, $^3J_{H\text{-}H}$ = 7.4 Hz, H_6 or H_5), 7.17 (t, $^3J_{H\text{-}H}$ = 7.4 Hz, H_5 or H_6), 7.11-7.08 (m, Ph), 6.82 (d, $^3J_{H\text{-}H}$ = 5.0 Hz, H_3), 6.62 (dd, $^3J_{H\text{-}H}$ = 5.0 Hz and $^3J_{H\text{-}H}$ = 1.9 Hz , H_2), 4.72 (d, $^3J_{H\text{-}H}$ = 1.8 Hz, H_1) 3.84, 3.34 (td, $^3J_{H\text{-}H}$ = 12.4 Hz and $^2J_{H\text{-}H}$ = 3.9 Hz, CH_2), 2.37, 1.61 (brt, $^3J_{H\text{-}H}$ = 11.1 Hz, NH_2). ^{1}H NMR (C_6D_6, 400 MHz): δ 7.70 (d, $^3J_{H\text{-}H}$ = 7.3 Hz, H_4 or H_7), 7.40 (d, $^3J_{H\text{-}H}$ = 7.3 Hz, H_7 or H_4), 7.19-7.16, 7.04-6.90 (m, Ph, H_5 and H_6), 6.67 (d, $^3J_{H\text{-}H}$ = 5.0 Hz, H_3), 6.60 (dd, $^3J_{H\text{-}H}$ = 4.9 Hz and 2.1 Hz , H_2), 4.52 (br, H_1) 3.68, 3.13 (td, $^3J_{H\text{-}H}$ = 11.8 and $^2J_{H\text{-}H}$ = 3.7 Hz, CH_2), 2.13, 1.33 (brt, $^3J_{H\text{-}H}$ = 10.0 Hz NH_2). ^{13}C{^{1}H} NMR ($CDCl_3$, 100 MHz): δ 149.62 (s, C_{7a} or C_{3a}), 141.72 (s, C_{3a} or C_{7a}), 138.94 (s, C_{ipso}), 138.76 (s, C_2), 128.97 (s, C_{ortho}), 128.66 (s, C_6 or C_5) 128.22 (s, C_{meta} and C_{para}), 124.44 (s, C_5 or C_6), 123.76 (s, C_4 or C_7), 121.25 (s, C_7 or C_4), 120.75 (s, C_3), 49.44 (s, CH_2), 40.08 (s, C_1). Anal. Calcd for $C_{23}H_{25}Cl_1N_2Pd_1$: C, 58.61; H, 5.35; N, 5.94. Found: C, 59.04; H, 5.28; N, 5.37.

Synthesis of (η^1-Ind)Pd(Py)$_2$Cl, (5).

Method A. Pyridine (82 μL, 1.0 mmol) was added to a stirred C_6H_6 suspension (25 mL) of [(η^3-Ind)Pd(μ-Cl)]$_2$ (**1**; 130 mg, 0.25 mmol) at room temperature. The yellow brown mixture was stirred for approximately 2 h, filtered, and evaporated to dryness to give a yellow solid (160 mg, 76%).

Method B. Pyridine (207 μL, 2.6 mmol) was added to a stirred C_6H_6 solution (20 mL) of (Ind)Pd(NEt_3)Cl (**3**; 460 mg, 1.3 mmol) at room temperature. After stirring for 3h, the resulting brown-green mixture was concentrated to *ca.* 10 mL. A yellow powder

precipitated and was isolated by filtration and washing with hexane (450 mg, 84%). Recrystallization of a small portion of this solid from a C_6H_6/hexane solution yielded crystals suitable for X-ray diffraction studies.

^{1}H NMR ($CDCl_3$, 400 MHz): δ 8.38 (d, $^3J_{H\text{-}H}$ = 6.9 Hz, H_{ortho}), 7.45 (t, $^3J_{H\text{-}H}$ = 7.6 Hz, H_{para}), 7.01 (t, $^3J_{H\text{-}H}$ = 6.9 Hz, H_{meta}), 6.93-6.72 (m, $H_{4\text{-}7}$), 6.68 (dd, $^3J_{H\text{-}H}$ = 4.1 Hz and 1.6 Hz, H_2), 6.45 (d, $^3J_{H\text{-}H}$ = 5.1 Hz, H_3), 4.77 (br, H_1). ^{13}C{^{1}H} NMR ($CDCl_3$, 100 MHz): δ 151.72 (s, C_{ortho}), 150.58 (s, C_{7a} or C_{3a}), 142.54 (s, C_{3a} or C_{7a}), 137.28 (s, C_2), 136.94 (s, C_{para}), 124.33 (s, C_{meta}), 123.55 (s, C_3), 127.24, 124.93, 122.84, 120.50 (s, $C_{4\text{-}7}$), 42.54 (s, C_1). Anal. Calcd for $C_{19}H_{17}Cl_1N_2Pd_1.H_2O$: C, 52.67; H, 4.42; N, 6.47. Found: C, 52.69; H, 3.89; N, 5.97.

Synthesis of (η^1-Ind)Pd(PCy_3)($BnNH_2$)Cl, (6a).

Method A. Benzylamine (170 μL, 1.56 mmol) was added to a solution of [(η^3-Ind)Pd(μ-Cl)]$_2$ (**1**; 400 mg, 0.78 mmol) in CH_2Cl_2 (30 mL) at room temperature. The brown mixture was stirred for 30 min and PCy_3 (436 mg, 1.56 mmol) was added. The orange brown mixture was stirred for approximately 1 h, filtered and evaporated to dryness to give an orange solid (850 mg, 85%).

Method B. $BnNH_2$ (76 μL, 0.7 mmol) was added to a stirred C_6H_6 solution (20 mL) of (Ind)Pd(PCy_3)Cl (**2a**; 375 mg, 0.7 mmol) at room temperature. After stirring for 2h, the resulting orange solution was evaporated to dryness and 10 mL of hexane were added. An orange powder precipitated and was isolated by filtration (350 mg, 78%). Recrystallization of this solid from a cold hexane solution yielded crystals of (η^1-Ind)Pd(PCy_3)($BnNH_2$)Cl (**6a**), (μ,η^3-Ind)(μ-Cl)Pd_2(PCy_3)$_2$ (**7a**), and ($BnNH_2$)(PCy_3)$PdCl_2$ (**8a**) suitable for X-ray diffraction studies and elemental analysis.

6a: ^{1}H NMR (C_6D_6, 300 MHz): δ 7.95, 7.41, 6.98, 6.82, 6.66 (br, $H_{2\text{-}7}$), 5.03 (br, H_1), 3.85 (br, CH_2), 2.44-1.20 (m, NH_2 and PCy_3). ^{31}P{^{1}H} NMR (C_6D_6, 121 MHz): δ 41.5 (s). ^{1}H NMR (C_7D_8, 500 MHz, 263 K): δ 7.96-7.94, 7.50-7.48, 7.23-6.95 (m, Ph and $H_{4\text{-}7}$), 6.83 (d, $^3J_{H\text{-}H}$ = 5.0 Hz, H_2), 6.80-6.78 (m, $H_{4\text{-}7}$), 6.68 (d, $^3J_{H\text{-}H}$ = 4.9 Hz, H_3), 4.94 (d, $^3J_{H\text{-}P}$ = 5.4 Hz, H_1), 3.82 (t, $^3J_{H\text{-}H}$ = 12.9 Hz, CH_2), 3.53 (s, CH_2), 2.44-1.24 (m,

NH_2 and PCy_3). $^{13}C\{^1H\}$ NMR (C_7D_8, 126 MHz, 263 K): δ 151.76 (s, C_{7a}), 144.68 (s, C_{3a}), 138.94 (s, C_{ipso}), 129.53, 129.02, 128.83, 128.69, 128.60, 128.49, 127.82, 127.65, 127.06, 125.77, 124.84, 124.62, 123.94, 121.74, 121.69 (s, Ph and $C_{2\text{-}7}$), 48.77, 47.26 (s, CH_2), 38.85 (s, C_1), 34.61(d, $^1J_{C\text{-}P}$ = 22.6 Hz, C_{ipso}), 31.09 (d, $^2J_{C\text{-}P}$ = 9.4 Hz, C_{ortho}), 28.41 (t, $^3J_{C\text{-}P}$ = 9.4 Hz, C_{meta}), 27.48 (s, C_{para}). $^{31}P\{^1H\}$ NMR (C_7D_8, 202 MHz, 263 K): δ 40.5 (s). Anal. Calcd for $C_{34}H_{49}Cl_1N_1Pd_1$: C, 63.35; H, 7.66; N, 2.17. Found: C, 63.48; H, 7.88; N, 2.05.

Synthesis of (μ,η^3-Ind)(μ-Cl)$Pd_2(PCy_3)_2$, (7a). After several hours in solution, the complex ($BnNH_2$)(PCy_3)PdCl(η^1-Ind) (**6a**) gave (μ-η^3-Ind)(μ-Cl)Pd(PCy_3)$_2$ (**7a**), as an orange solid. Recrystallization of this solid from a cold hexane solution yielded crystals suitable for X-ray diffraction studies and elemental analysis. ^1H NMR (C_6D_6, 400 MHz): δ 7.35 (dd, $^3J_{H\text{-}H}$ = 5.6 Hz and $^4J_{H\text{-}H}$ = 3.1 Hz, H_5 and H_6), 7.04 (dd, $^3J_{H\text{-}H}$ = 5.6 Hz and $^4J_{H\text{-}H}$ = 3.1 Hz, H_4 and H_7), 5.81 (td, $^3J_{H\text{-}P}$ = 7.3 Hz and $^3J_{H\text{-}H}$ = 3.8 Hz , H_1 and H_3), 4.22 (quintuplet, $^3J_{H\text{-}H}$ = $^3J_{H\text{-}P}$ = 3.6 Hz, H_2), 2.04-1.05 (m, PCy_3). $^{31}P\{^1H\}$ NMR (C_6D_6, 161.92 MHz): δ 38.5 (s). ^1H NMR (CD_2Cl_2, 500 MHz, 263 K): δ 6.97 (dd, $^4J_{H\text{-}H}$ = 3.0 Hz and $^3J_{H\text{-}H}$ = 5.5 Hz, H_5 and H_6), 6.72 (dd, $^3J_{H\text{-}H}$ = 5.4 Hz and $^4J_{H\text{-}H}$ = 3.1 Hz, H_4 and H_7), 5.44 (td, $^3J_{H\text{-}P}$ = 7.2 Hz and $^3J_{H\text{-}H}$ = 3.9 Hz, H_1 and H_3), 3.75 (quintuplet, $^3J_{H\text{-}H}$ = $^3J_{H\text{-}P}$ = 3.5 Hz, H_2), 2.01-0.83 (m, PCy_3). $^{13}C\{^1H\}$ NMR (CD_2Cl_2, 126 MHz, 263 K): δ 145.68 (s, C_{7a} and C_{3a}), 122.84 (s, C_4 and C_7), 121.82 (s, C_5 and C_6), 71.19 (s, C_2), 48.99 (s, C_1 and C_3), 34.64 (t, $^1J_{C\text{-}P}$ = 7.6 Hz, C_{ipso}), 30.11 (s, C_{ortho}), 27.35 (s, C_{meta}), 26.15 (s, C_{para}). $^{31}P\{^1H\}$ NMR (CD_2Cl_2, 202 MHz, 263 K): δ 37.7 (s). Anal. Calcd for $C_{45}H_{73}Cl_1P_2Pd_2.0.5C_{18}H_{12}$: C, 62.46; H, 7.67. Found: C, 62.39; H, 7.93.

Synthesis of ($BnNH_2$)(PCy_3)$PdCl_2$, (8a). Recrystallization of (η^1-Ind)Pd(PCy_3)($BnNH_2$)Cl (**6a**) in hexane gave yellow crystals, which were identified as the complex ($BnNH_2$)(PCy_3)$PdCl_2$ (**8a**), on the basis of the NMR spectra and X-Ray analysis. ^1H NMR (C_6D_6, 300 MHz): δ 7.40, 6.98, 6.87 (br, C_6H_5), 3.83 (br, CH_2), 2.54-1.22 (m, NH_2 and PCy_3). $^{31}P\{^1H\}$ NMR (C_6D_6, 121 MHz): δ 44.11 (s).

(η^1-Ind)Pd($BnNH_2$)(PPh_3)Cl (6b), (μ,η^3-Ind)(μ-Cl)$Pd_2(PPh_3)_2$ (7b), and ($BnNH_2$)(PPh_3)$PdCl_2$ (8b). NMR scale preparation of **6b** (C_6D_6), either by the reaction of **1** (10 mg, 0.0019 mmol) with a mixture of $BnNH_2$ (4 μL, 0.0039 mmol) and PPh_3 (10 mg, 0.0039 mmol) or by the reaction of **2b** (30 mg, 0.058 mmol) with $BnNH_2$ (8 μL, 0.058 mmol), showed formation of **6b**. Monitoring these samples indicated that the initially formed **6b** is gradually converted to **7b** and **8b** after a few hours. All attempts at purifying the mixtures obtained from large-scale reactions led to the isolation of pure samples of **7b** only. Therefore, **7b** has been characterized fully (vide infra), whereas **6b** and **8b** were characterized by NMR spectra only, as described below.

6b. ^{1}H NMR (C_6D_6, 300 MHz): δ 8.01-7.97 (m, PPh_3), 7.48, 7.31 (d, $^3J_{H-H}$ = 7.0 Hz, H_4 and H_7), 7.1-6.8 (m, PPh_3, H_5 and H_6), 6.55 (d, $^3J_{H-H}$ = 5.1 Hz, H_3), 6.44 (d, $^3J_{H-H}$ = 6.1 Hz, H_2), 4.55 (d, $^3J_{H-P}$ = 6.0 Hz, H_1), 3.86, 3.38 (br, NH_2), 2.53, 2.13 (br, CH_2). ^{1}H NMR (C_7D_8, 126 MHz, 263 K): δ 8.00-7.96 (m, PPh_3), 7.46 (d, $^3J_{H-H}$ = 6.7 Hz, H_4 or H_7), 7.38 (d, $^3J_{H-H}$ = 7.2 Hz, H_7 or H_4), 7.2-6.9 (m, PPh_3 and H_{5-6}), 6.80 (d, $^3J_{H-H}$ = 4.6 Hz, Ph and H_{5-6}) 6.56 (d, $^3J_{H-H}$ = 4.6 Hz, H_3), 6.42 (d, $^3J_{H-H}$ = 3.7 Hz, H_2), 4.47 (d, $^3J_{H-P}$ = 7.6 Hz, H_1), 3.92, 3.54, 2.28 (br, CH_2), 3.28, 0.74, 0.25 (br, NH_2). $^{13}C\{^1H\}$ NMR (C_7D_8, 126 MHz, 263 K): δ 150.8 (s, C_{7a}), 143.00 (s, C_{3a}), 141.19 (s, C_{ipso} $BnNH_2$), 139.78 (s, C_2), 135.71 (d, $^2J_{C-P}$ = 11.3 Hz, C_{ortho} PPh_3), 132.33 (d, $^1J_{C-P}$ = 49.0 Hz, C_{ipso} PPh_3), 131.27 (s, C_{para} PPh_3), 129.34 (s, C_{ortho} $BnNH_2$), 129.16 (d, $^3J_{C-P}$ = 10.4 Hz, C_{meta} PPh_3), 129.00 (s, C_{meta} $BnNH_2$), 127.93 (s, C_{para} $BnNH_2$), 124.93, 124.78, 124.30, 122.00, 121.85 (s, C_{3-7}), 48.99 (s, CH_2), 46.60 (s, C_1). $^1P\{^1H\}$ NMR (C_6D_6, 161 MHz): δ 37.1 (s). $^{31}P\{^1H\}$ NMR (C_7D_8, 202 MHz, 263 K): δ 37.0 (s).

Isolation of 7b. Method A. Benzylamine (127 μL, 1.16 mmol) was added to a solution of [(η^3-Ind)Pd(μ-Cl)]$_2$ (**1**; 300 mg, 0.58 mmol) in CH_2Cl_2 (25 mL) at room temperature. The brown mixture was stirred for 10 min and PPh_3 (303 mg, 1.16 mmol) was added. The resulting brown red mixture was stirred for approximately 1 h, filtered, and evaporated to dryness. The orange residue was dissolved in CH_2Cl_2 (15 mL) and layered with hexane (10 mL) to give an orange precipitate, which was isolated as a fine powder by filtration (250 mg, 48%). Recrystallization of a small portion of this powder

from a $CHCl_3$/hexane solution yielded crystals suitable for X-ray diffraction studies and elemental analysis.

Method B. $BnNH_2$ (31 μL, 0.29 mmol) was added to a stirred C_6H_6 solution (15 mL) of (Ind)Pd(PPh_3)Cl (**2b**; 150 mg, 0.29 mmol) at room temperature. After stirring for 2h, the resulting orange solution was evaporated to dryness and 10 mL of hexane were added. An orange powder precipitated and was isolated by filtration (70 mg, 55%). ^{1}H NMR ($CDCl_3$, 400 MHz): δ 7.69-7.64 (m, PPh_3), 7.48-7.38 (m, PPh_3), 6.52 (dd, $^3J_{H\text{-}H}$ = 5.4 Hz and $^4J_{H\text{-}H}$ = 3.1 Hz, H_5 and H_6), 5.98 (dd, $^3J_{H\text{-}H}$ = 5.4 Hz and $^4J_{H\text{-}H}$ = 3.1 Hz, H_4 and H_7), 5.12 (td, $^3J_{H\text{-}P}$ = 7.7 Hz and $^3J_{H\text{-}H}$ = 3.7 Hz , H_1 and H_3), 4.22 (quintuplet, $^3J_{H\text{-}H}$ = 3.4 Hz, H_2). $^{13}C\{^1H\}$ NMR ($CDCl_3$, 100 MHz): δ 143.68 (s, C_{7a} and C_{3a}), 134.69 (t, $^2J_{C\text{-}P}$ = 7.4 Hz, C_{ortho}), 134.62 (d, $^1J_{C\text{-}P}$ = 43.1 Hz, C_{ipso}), 130.29 (s, C_{para}), 129.00 (t, $^3J_{C\text{-}P}$ = 4.9 Hz, C_{meta}), 124.09 (s, C_5 and C_6), 121.62 (s, C_4 and C_7), 78.36 (s, C_2), 57.75 (s, C_1 and C_3). $^{31}P\{^1H\}$ NMR ($CDCl_3$, 121 MHz): δ 25.7 (s). Anal. Calcd for $C_{45}H_{37}Cl_1P_2Pd_2$: C, 60.86; H, 4.20. Found: C, 60.32; H, 4.13.

8b. ^{1}H NMR (C_6D_6, 300 MHz): δ 7.73-7.27 (m, C_6H_5), 4.13 (br, CH_2), 3.02 (br, NH_2). $^{31}P\{^1H\}$ NMR (C_6D_6, 121 MHz): δ 28.59 (s).

Reaction of complex 7b with $AgBF_4$. A mixture of (μ,η^3-Ind)(μ-Cl)$Pd_2(PPh_3)_2$, (**7b**) (140 mg, 0.16 mmol) and $AgBF_4$ (31 mg, 0.16 mmol) was stirred in CH_2Cl_2 (20 mL) for 2 h at room temperature and filtered to remove AgCl. Concentration of the filtrate to ca. 5 mL, followed by addition of ca. 15 mL of Et_2O gave [(η-Ind)Pd(PPh_3)$_2$]BF_4, as an orange precipitate, which was isolated by filtration (60 mg, 46%).

Reaction of complex 7b with MeMgCl. This reaction was monitored by spectroscopy, without isolating the resulting products. A solution of MeMgCl (4 μL of a 3 M solution in THF) was added at room temperature to a 1 mL C_6D_6 solution of (μ,η^3-Ind)(μ-Cl)$Pd_2(PPh_3)_2$, (**7b**) (10 mg, 0.011 mmol) in an NMR tube. The NMR spectra of this sample showed the complete conversion of **7b** to (η-Ind)Pd(PPh_3)Me.

Acknowledgments

This work was made possible thanks to the financial support provided by the Natural Sciences and Engineering Research Council of Canada (operating grants to D. Z.) and Université de Montréal (scholarships to C. S.-S.). We are also indebted to Johnson Matthey for the generous loan of $PdCl_2$, and to Dr. M. Simard and F. Bélanger-Gariépy for their assistance with the X-ray analyses.

Supporting Information Available

Complete details of the X-ray analysis of **3**, **4**, **5**, **6a**, **7a**, **7b** and **8a** including tables of crystal data, collection and refinement parameters, bond distances and angles, anisotropic thermal parameters, and hydrogen atoms coordinates have been deposited at the Cambridge Crystallographic Data Centre (CCDC 296295-296301). These data can be obtained free of charge via www.ccdc.cam.ac.uk/data_request/cif, or by emailing data_request@ccdc.cam.ac.uk, or by contacting the Cambridge Crystallographic Data Centre, 12, Union Road, Cambridge CB2 1EZ, UK; fax: +44 1223 336033.

References

[1] For representative reports on Ind complexes featuring unusually large hapticities see: (a) Bradley, A. C.; Lobkovsky, E.; Chirik, P. J. *J. Am. Chem. Soc.* **2003**, *125*, 8110. (b) Bradley, A. C.; Keresztes, I.; Lobkovsky, E.; Young, V. G.; Chirik, P. J. *J. Am. Chem. Soc.* **2004**, *126*, 16937. (c) Bradley, A. C.; Lobkovsky, E.; Keresztes, I.; Chirik, P. J. *J. Am. Chem. Soc.* **2005**, *127*, 10291.

[2] For representative reactivities of indenyl complexes see the following reports and references therein: (a) Frankom, T. M.; Green, J. C.; Nagy, A.; Kakkar, A. K.; Marder, T.B. *Organometallics* **1993**, *12*, 3688. (b) Gamasa, N. P.; Gimeno, J.; Gonzalez-Bernado, C.; Martin-Vaca, B. M.; Monti, D.; Basseti *Organometallics* **1996**, *15*, 302. (c) Foo, T.; Bergman, R. G. *Organometallics* **1992**, *11*, 1801. (d) Trost, B. M.; Kulawiec, R. J. *J. Am. Chem. Soc.* **1993**, *115*, 2027. (e) O'Connor, J. M.; Casey, C. P. *Chem. Rev.* **1987**, *87*, 307. (f) Marder, T. B.; Roe, C. D.; Milstein, D. *Organometallics* **1988**, *7*, 1451. (g) Halterman, R. L. *Chem. Rev.* **1992**, *92*, 965. (h) Hauptman, E.; Sabo-Etienne, S.; White, P. S.; Brookhart, M.; Garner, J. M.; Fagan, P. J.; Calabrese, J. C. *J. Am. Chem. Soc.* **1994**, *116*, 8038.

[3] For a recent review on the chemistry of group 10 metal indenyl complexes see: Zargarian, D. *Coord. Chem. Rev.* **2002**, *233-234*, 157.

[4] (a) Vollmerhaus, R.; Bélanger-Gariépy, F.; Zargarian, D. *Organometallics* **1997**, *16*, 4762. (b) Dubois, M.-A.; Wang, R.; Zargarian, D.; Tian, J.; Vollmerhaus, R.; Li, Z; Collins, S. *Organometallics* **2001**, *20*, 663. (c) Groux, L. F.; Zargarian, D. *Organometallics* **2001**, *20*, 3811. (d) Groux, L. F.; Zargarian, D.; Simon, L. C.; Soares, J. B. P. *J. Mol. Catal. A* **2003**, *193(1-2)*, 51. (e) Groux, L. F.; Zargarian D. *Organometallics* **2003**, *22*, 3124. (f) Groux, L. F.; Zargarian D. *Organometallics* **2003**, *22*, 4759. (g) Sun, H.; Li, W.; Han, X.; Shen, Q.; Zhang, Y. *J. Organomet. Chem.* **2003**, *688*, 132. (h) Li, W.-F.; Sun, H.-M.; Shen, Q.; Zhang, Y.; Yu, K.-B. *Polyhedron* **2004**, *23*, 1473. (i) Jimenez-Tenorio, M.; Puerta, M. C.; Salcedo, I.; Valerga, P.; Costa, S. I.; Silva, L. C.; Gomes, P. T. *Organometallics* **2004**, *23*, 3139. (j) Sun, H. M.; Shao, Q.; Hu, D. M.; Li, W. F.; Shen, Q.; Zhang, Y. *Organometallics*

2005, *24*, 331. (k) Gareau, D.; Sui-Seng, C.; Groux, L. F.; Brisse, F.; Zargarian, D. *Organometallics* **2005**, *24*, 4003.

[5] (a) Wang, R.; Bélanger-Gariépy, F.; Zargarian, D. *Organometallics* **1999**, *18*, 5548. (b) Wang, R.; Groux, L. F.; Zargarian D. *Organometallics* **2002**, *21*, 5531. (c) Wang, R.; Groux, L. F.; Zargarian, D. *J. Organomet. Chem* **2002**, *660*, 98. (d) Rivera, E.; Wang, R; Zhu, X. X.; Zargarian, D.; Giasson, R. *J. Mol. Catal. A* **2003**, *204-205*, 325.

[6] (a) Fontaine, F. -G.; Kadkhodazadeh, T.; Zargarian, D. *J. Chem. Soc., Chem. Commun.* **1998**, 1253. (b) Fontaine, F.-G.; Zargarian, D. *Organometallics* **2002**, *21*, 401.

[7] Fontaine, F.-G.; Nguyen, R.-V.; Zargarian, D. *Can. J. Chem.* **2003**, *81*, 1299.

[8] To our knowledge, the following are the only Pd-Ind compounds reported prior to our studies: $[(\eta^3\text{-Ind})Pd(\mu\text{-Cl})]_2$,[8a,8b] $[(\mu,\eta^3\text{-Ind})Pd(CNR)]_2$ (R = *t*-Bu, 2,6-$(CH_3)_2C_6H_3$; 2,4,6-$(CH_3)_3C_6H_2$; 2,4,6-(*t*-Bu)$_3C_6H_2$),[8c,8d] $(\eta^3\text{-Ind})Pd(PMe_3)(CH(SiMe_3)_2)$,[8e,8f] $[(\eta^3\text{-Ind})PdL_2]^+$ (L_2 = bipy, tmeda).[8g,8h] A preliminary communication has also appeared on the preparation of a series of Ind derivates from the reaction of cyclopropene and $(PhCN)_2PdCl_2$.[8i] (a) Nakasuji, K.; Yamaguchi, M.; Murata, I.; Tatsumi, K.; Natamura, A. *Organometallics* **1984**, *3*, 1257. (b) Samuel, E.; Bigorgne, M. *J. Organomet. Chem.* **1969**, *19*, 9. (c) Tanase, T.; Nomura, T; Yamamoto, Y.; Kobayashi, K. *J. Organomet. Chem.* **1991**, *410*, C25. (d) Tanase, T.; Nomura, T.; Fukushina, T.; Yamamoto, Y.; Kobayashi, K. *Inorg. Chem.* **1993**, *32*, 4578. (e) Alias, F. M.; Belderrain, T. R.; Paneque, M.; Poveda, M. L.; Carmona, E. *Organometallics* **1998**, *17*, 5620. (f) Alias, F. M.; Belderrain, T. R.; Carmona, E.; Graiff, C.; Paneque, M.; Poveda, M. L. *J. Organomet. Chem.* **1999**, *577*, 316. (g) Vicente, J.; Abad, J.-A.; Bergs, R.; Jones, P. G.; De Arellano, M. C. R. *Organometallics* **1996**, *15*, 1422. (h) Vicente, J.; Abad, J.-A.; Bergs, R.; De Arellano, M. C. R.; Martinez-Vivente, E.; Jones, P. G. *Organometallics* **2000**, *19*, 5597. (i) Fiato, R. A.; Mushak, P.; Battiste, M. A. *Chem. Comm.* **1975**, 869.

[9] (a) Sui-Seng, C.; Enright, G. D.; Zargarian, D. *Organometallics* **2004**, *23*, 1236. (b) Sui-Seng, C.; Groux, L. F.; Zargarian, D., *Organometallics* **2006**, *25*, 571.

[10] For reviews on Pd(I)-Pd(I) compounds see: (a) Murahashi, T.; Kurosawa, H. *Coord. Chem. Rev.* **2002**, *231*, 207. (b) Werner, *Adv. Organomet. Chem.* **1981**, *19*, 155.

[11] For the original synthesis of this dimeric compound see ref. 8(a) and 8(b) above. For a revised synthesis see ref. 9(a).

[12] Coe, J. C.; Lyons, R. J. *Inorg Chem.* **1970**, *9*, 1775.

[13] (a) Casey, C. P.; O' Connor J. M *Organometallics* **1985**, *4*, 384. (b) Hermmann, W. A.; Kuhn, F. E.; Romao, C. C. *J. Organomet. Chem.* **1995**, *489*, C56. (c) O' Hare, D *Organometallics* **1987**, *6*, 1766.

[14] To our knowledge, only two examples of Pd-NEt_3 complexes were characterized by single-crystal X-ray crystallography: $(Et_3N)_2PdCl_2$ (Timokhin, V. I.; Anastasi, N. R.; Stahl, S. S. *J. Am. Chem. Soc.* **2003**, *125*, 12996) and $[Pd(dmpe)(Me)(NEt_3)][BPh_4]$ (Seligson, A. L.; Trogler, W. C. *J. Am. Chem. Soc.* **1991**, *113*, 2520).

[15] $\Delta(M\text{-}C) = 0.5\ \{(M\text{-}C3a + M\text{-}C7a)\} - 0.5\{(M\text{-}C1 + M\text{-}C3)$. HA is the angle between the planes encompassing the atoms C1, C2, C3 and C1, C3, C3a, C7a. FA is the angle between the planes encompassing the atoms C1, C2, C3 and C3a, C4, C5, C6, C7 and C7a. The Δ(M-C), HA and FA values for a range of Ind complexes are given in the following reports: (a) Baker, T.; Tulip, T. H. *Organometallics* **1986**, *5*, 839. (b)Westcott, S. A.; Kakkar, A. K.; Stringer, G.; Taylor, N. J.; Marder, T. B. *J. Organomet. Chem.* **1990**, *394*, 777. The corresponding data for group 10 complexes are given in reference 3.

[16] (a) Guérin, F.; Beddie, C. L.; Stephan, D. W.; v. H. Spence, E.; Wurz, R. *Organometallics* **2001**, *20*, 3466. (b) Deck, P. A.; Fronczek, F. R. *Organometallics* **2000**, *19*, 327. (c) Blenkiron, P; Enright, G. D.; Taylor, N. J.; Carty, A. J. *Organometallics* **1996**, *15*, 2855. (d) Thorn, M. G.; Fanwick, P. E.; Chesnut, R. W.; Rothwell, I. P. *Chem. Comm.* **1999**, 2543. (e) Radius, U.; Sundermeyer, J.; Peters, K.; v. Schering, H. G. Z. *Anorg. Allg. Chem.* **2002**, *628*, 1226.

[17] For a detailed discussion of η^1-Ind complexes, see: Stradiotto, M.; McGlinchey, M. J. *Coord. Chem. Rev.* **2001**, *219*-221, 311.

[18] For examples on X-ray structures of *trans*-Bis(benzylamine)palladium(II) complexes, see: (a) Sui-Seng, C.; Zargarian, D. *Acta Cryst.* **2003**, *E59*, m957. (b) Decken, A.; Pisegna, G. L.; Vogels, C. M.; Westcott, S. A. *Acta Cryst.* **2000**, *C56*, 1071. For examples on X-ray structures of *trans*-Bis(pyridine)palladium(II) complexes, see: (c) Viossat, B.; Dung, N. -H.; Robert, F. *Acta Cryst.* **1993**, *C49*, 84. (d) Cheshkov, D. A.; Belyaev, B. A.; Belov, A. P.; Rybakov, V. B. *Acta Cryst.* **2004**, *E60*, m300.

[19] Merola, J. S.; Kacmarcik, R. T.; Van Engen, D. *J. Am. Chem. Soc.* **1986**, *108*, 329.

[20] Felkin, H.; Turner, G. K. *J. Organomet. Chem.* **1977**, *129*, 429.

[21] Strictly speaking, the designation of *trans*-1,1'-bis(indenylidene) as Ind=Ind is not consistent with the definition of Ind as the indenyl radical C_9H_7, but this designation has been adopted for its simplicity and intuitive appeal.

[22] In the $^1H\{^{31}P\}$ NMR spectra, the signal for H2 appears as a triplet ($^3J_{H\text{-}H}$ = 3.6 Hz) while that of H1 and H3 appears as a doublet ($^3J_{H\text{-}H}$ = 3.5 Hz).

[23] Sieller, J.; Svensson, A.; Lindqvist, O. *J. Organomet. Chem.* **1987**, *320*, 129.

[24] Kobayashi, Y.; Iataka, Y.; Yamazaki, H. *Acta Cryst.* **1972**, *B28*, 899.

[25] (a) Werner, H.; Kuhn, A.; Tune, D. J. Kruger, C.; Brauer, D. J.; Sekutowski, J. C.; Tsay, Yi. –H *Chem. Ber.* **1977**, *110*, 1763. (b) Werner, H.; Tune, D.; Parker, G.; Kruger, C.; Brauer, D. J. *Angew. Chem., Int. Ed. Eng.* **1975**, *14*, 185.

[26] Jolly, P. W.; Kruger, C.; Schick, K. –P.; Wilke, G. *Z. Naturforsch.* **1985**, *35b*, 926.

[27] (a) Yamamoto, Y.; Yamakazi, H. *Bull. Chem. Soc. Jpn.* **1985**, *58*, 1843. (b) Yamamoto, Y.; Yamakazi, H. *Inorg. Chem.* **1986**, *25*, 3327. (c) Holloway, R. G.; Penfold, B. R.; Colton, R.; McCormich, M. J. *J. Chem. Soc. Chem. Comm.* **1976**, 485. (d) Kullberg, M. L.; Lemke, F. R.; Powell, D. R.; Kubiak, C. P. *Inorg. Chem.* **1985**, *24*, 3589.

[28] The distance from H4 to the Ph group (C41-C42-C43-C44-C45-C46) is 2.771 Å and that from H7 to the Ph group (C11-C12-C13-C14-C15-C16) is 3.347 Å. By comparison, the distance from H1 to the Ph group (C21-C22-C23-C24-C25-C26) is 3.511 Å and that from H3 to the Ph group (C41-C42-C43-C44-C45-C46) is 3.968 Å. Protons H5 and H6 are too far from the closest Ph group (>4 Å).

[29] Examples include (η^5-Ind)(η^3-Ind)W(CO)$_2$ (Δ(M-C) = 0.07 and 0.72 Å) (Nesmeyanov, A. W.; Ustynyuk, N. A.; Makarova, L. G.; Andrianov, V. G.; Struchkov, Y. T.; Andrae, S.; Ustynyuk, Y. A.; Malyugina, S. G. *J. Organomet. Chem.* **1978**, *159*, 189 and (η^3-Ind)Ir(PMe$_3$)$_3$ (Δ(M-C) = 0.79 Å) (ref. 19). For detailed discussions of Ind hapticity see references 15a and 15b.

[30] Symmetry code: (i) –x + 1, – y, – z + 2

[31] Caparelli, M. V.; Machado, R.; De Sanctis, Y.; Arce, A. J. *Acta Cryst.* **1996**, *C52*, 947.

[32] (a) Stambouli, J. P. ; Kuwano, R.; Hartwig J. F. *Angew. Chem. Int. Ed. Engl.* **2002**, *41*, 4746. (b) Prashad, M.; Mak, X. Y.; Liu, Y.; Repic, O. *J. Org. Chem.* **2003**, *68*, 1163 (c) Christmann, U.; Vilar, R.; White, A. J. P.; Williams, D. J. *Chem. Soc., Chem. Commun.* **2004**, 1294.

[33] *SMART*, Release 5.059; Bruker Molecular Analysis Research Tool, Bruker AXS Inc.: Madison, WI 53719-1173, 1999.

[34] *SAINT*, Release 6.06; Integration Software for Single Crystal Data. Bruker AXS Inc.: Madison, WI 53719-11, 1999.

[35] Sheldrick, G. M. *SHELXS*. Program for the solution of Crystal Structures. University of Goettingen. Germany, 1997.

[36] Sheldrick, G. M. *SHELXL*. Program for the Refinement of Crystal Structures. University of Goettingen. Germany, 1997.

[37] A. L. Spek, *PLATON* 2002 University of Utrecht, Utrecht, The Netherlands.

Chapitre 5: Structure et Réactivité du Complexe (1-$SiMe_3$-Ind)Pd(PPh_3)Cl

Introduction

Dans les chapitres précédents, les préparations des différents composés indényles de Pd(II) du type (1-R-Ind)Pd(PPh_3)(X) (R = H, Me ; X = Cl, Me, OTf) ont permis d'examiner l'influence d'un substituant sur le ligand indényle et le rôle du ligand X sur les structures et les réactivités de ces complexes.[1] Il a ainsi été démontré au cours du chapitre 2, qu'au niveau structural, la présence du Me sur l'Ind impliquait une distorsion supplémentaire dans la coordination de l'Ind sur le centre métallique (Pd-C1 > Pd-C3), tandis qu'au niveau de la réactivité envers les silanes et les oléfines, aucun changement majeur n'avait lieu. Le présent chapitre s'inscrit dans la continuité de cette étude et décrit la préparation d'un nouveau complexe comportant un ligand indényle plus encombré, le dérivé (1-$SiMe_3$-Ind)Pd(PPh_3)Cl (**1**) ainsi que les études préliminaires de sa réactivité.

Résultats et Discussion

Synthèse et caractérisation du composé (1-$SiMe_3$-Ind)Pd(PPh_3)Cl, (1). Le complexe (1-$SiMe_3$-Ind)Pd(PPh_3)Cl, (**1**) a été synthétisé suivant la procédure établie dans notre récent article pour l'obtention des complexes (1-R-Ind)Pd(PPh_3)Cl (R = H, Me),[1a] par addition d'un équiv. de (1-Me_3Si-Ind)Li et de 0.5 équiv. de PPh_3 sur le précurseur $(PhCN)_2PdCl_2$ (Schéma 5.1).

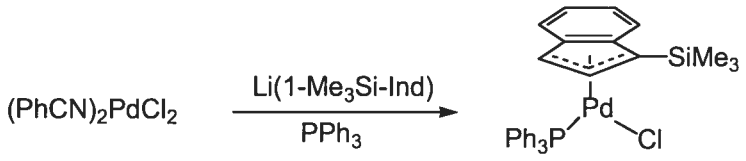

Figure 5.1

Le complexe **1** a été isolé sous forme d'un solide orange avec un rendement de 29%. Thermiquement stable à l'air et en solution, il a pu facilement être recristallisé et analysé par spectroscopie RMN, analyse élémentaire et diffraction des rayons X (vide infra). Son spectre RMN $^{31}P\{^1H\}$ consiste en une seule résonance à 29.3 ppm tandis que ses spectres RMN ^1H et $^{13}C\{^1H\}$ présentent les mêmes caractéristiques que celles déjà obtenues pour le complexe (1-Me-Ind)Pd(PPh_3)Cl analogue.[1a] Par exemple, son spectre RMN ^1H contient deux doublets et deux triplets entre 6.42 et 7.41 ppm attribuables aux protons H4/H7 et H5/H6 respectivement, un doublet de doublet à 6.51 ppm dû à H2 et un autre à 4.39 ppm pour H3, ainsi qu'un singulet à 0.63 ppm attribuable au $SiMe_3$ de l'indényle. Comme attendu, son spectre RMN $^{13}C\{^1H\}$ présente une résonance à plus haut champ (d'au moins 25 ppm) pour le carbone C3 comparativement à C1, ce qui provient de la différence d'influence trans entre les ligands PPh_3 et Cl (PPh_3 > Cl). Il en résulte une interaction Pd-C dissymétrique qui se traduit par une localisation partielle dans la partie allylique du ligand indényle (distorsion η^1:η^2), se manifestant par des hybridations différentes pour les carbones C1 (semblable à un Csp^2) et C3 (semblable à un Csp^3).

L'étude cristallographique du complexe **1** (Annexe 2) a permis d'obtenir de nouvelles informations sur l'hapticité de l'indényle. La figure 5.2 représente le dessin ORTEP du complexe **1**, et les tableaux 5.I et 5.II, les données et paramètres structuraux. La géométrie autour du Pd est pseudo plan carré et la plus grande distorsion résulte de l'angle C1-Pd-C3 (~ 61°). Les distances Pd-C7a et Pd-C3a sont supérieures aux longueurs des liaisons Pd-C1, Pd-C2 et Pd-C3, ce qui traduit une distorsion ($\eta^3 \leftrightarrow \eta^5$) dans la coordination de l'indényle. Cette distorsion se reflète également dans la valeur des paramètres Δ(M-C) (0.33 Å), HA (13.58°) et FA (12.28°) qui sont du même ordre de grandeur que ceux obtenus pour les complexes du type (η-Ind)Pd(PR_3)Cl (R = Ph, Cy, Me, OMe).[1a] De plus, cette étude cristallographique a permis de confirmer la distorsion de type η^1:η^2, déjà mise en évidence en solution d'après l'étude RMN (vide supra), reflétée par des distances différentes pour les liaisons Pd-C (Pd-C1 > Pd-C2 > Pd-C3 et Pd-C7a > Pd-C3a) (Tableau 5.II).

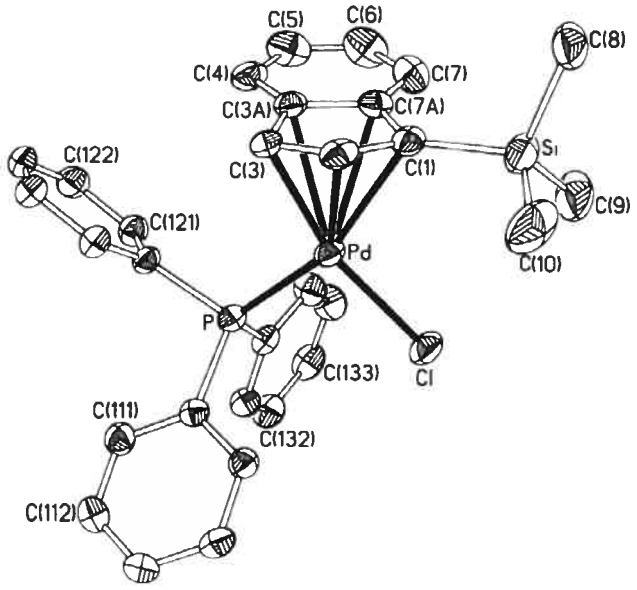

Figure 5.2: Dessin ORTEP du complexe **1** représenté avec des ellipsoïdes thermiques à 30% de probabilité et sans les atomes d'hydrogène.

Table 5.I: Données cristallographiques du composé **1** (Les données présentées ont été corrigées avec la fonction SQUEEZE du logiciel PLATON).

	1
formule	$C_{30}H_{30}PClSiPd$
masse moléculaire	591,45
couleur, forme	rouge, bloc
dimens, mm	0,05×0,18×0,39
système	Triclinique
groupe d'espace	*P*-1
a, Å	15,8783(4)
b, Å	17,4154(4)
c, Å	17,9389(5)
α, deg	82,496(2)
β, deg	65,690(2)
γ, deg	81,820(2)
volume, Å^3	4460,5(2)
Z	6

	1
D(calc), g cm^{-1}	1,321
diffractomètre	Bruker AXS SMART 2K
temp, K	293(2)
λ	1,54178 Å
μ, mm^{-1}	6,861
scan type	ω scan
F(000)	1812
θ_{max}, (deg)	73,10
h,k,l range	$-19 \leq h \leq 18$ $-21 \leq k \leq 21$ $-22 \leq l \leq 21$
No. de réflns collectées	12651
Correction d'absorption	multi-scan SADABS
T (min, max)	0,27, 0,71
$R\ [F^2 > 2\sigma(F^2)]$, $R_w(F^2)$	0,0379, 0,0859
GOF	0,926

Table 5.II. Distances (Å) et Angles (deg) Sélectionnés du Composé **1**.

	1
Pd-P	2,2685(9)
Pd-Cl	2,3382(9)
Pd-C1	2,319(3)
Pd-C2	2,191(3)
Pd-C3	2,172(3)
Pd-C3a	2,571(3)
Pd-C7a	2,623(5)
C1-C2	1,415(4)
C2-C3	1,416(5)
C3-C3a	1,457(5)
C3a-C7a	1,427(4)
C7a-C1	1,479(5)
C1-Si	1,871(4)
P-Pd-Cl	95,35(3)
C3-Pd-Cl	162,32(10)
C3-Pd-P	101,34(10)
C1-Pd-Cl	101,49(9)
C1-Pd-P	161,05(9)
C1-Pd-C3	61,75(12)
ΔM-C (Å)	0,33
HA (deg)	13,58
FA (deg)	12,28

Réactivité du complexe 1 avec les silanes. Afin de pouvoir évaluer l'influence de l'encombrement de l'indényle sur la réactivité des composés Ind de Pd(II), le comportement du complexe (1-Me_3Si-Ind)Pd(PPh_3)Cl envers les silanes a été étudié. Comme observée dans le cas des complexes (1-R-Ind)Pd(PPh_3)Cl (R = H, Me),[1] la réaction de **1** en présence de 100 équivalents de $PhSiH_3$ dans C_6D_6 indique qu'environ 20% de $PhSiH_3$ sont consommés au bout de 20 minutes pour former probablement des oligo- ou polymères insolubles de silanes, non détectables pas RMN ^1H. De plus, la réaction d'hydrosilylation du styrène en présence de $PhSiH_3$ n'est pas catalysée par le complexe **1**, et ne se produit qu'en présence de trichlorosilane pour donner quantitativement du 1-phényl-1-(trichlorosilyl)éthane.[2]

Réactivité catalytique du complexe 1 dans les réactions de couplage de Heck et d'arylamination.[3] Au cours de nos études portant sur l'exploration des propriétés catalytiques du complexe **1**, sa réactivité dans la formation de liens C-C et C-N a brièvement été explorée. La réaction de **1** avec le styrène et un halogénure d'aryle Ar-X (X = I, Br, Cl), en présence de Na_2CO_3 ou de NaOAc dans le N,N-diméthylformamide (couplage de Heck, figure 5.3), a démontré la presque quantitative conversion du styrène (~ 95-100 %) en *E*- et *Z*-stilbène (ca 9 :1) avec l'iodo- et le bromo-benzène, tandis qu'avec le chloro-benzène, des rendements plus faibles ont été obtenus (~ 35%).

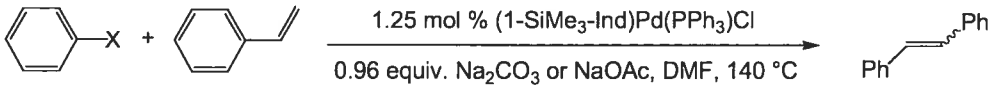

Figure 5.3

La réactivité du complexe **1** dans l'amination catalytique d'halogénures d'aryles avec l'aniline et la morpholine (Figure 5.4) a aussi été brièvement explorée. Selon les conditions expérimentales rapportées par Nolan,[4] l'*ortho*- et le *para*- bromo- et chloro-toluène sont quantitativement convertis en produits de couplage correspondants avec l'aniline, tandis que les réactions de couplage avec la morpholine mènent à des pourcentages de conversion plus bas (*p*-bromotoluène 53%; *p*-chlorotoluène 19%; *o*-bromotoluène 20%; *o*-chlorotoluène 0%).

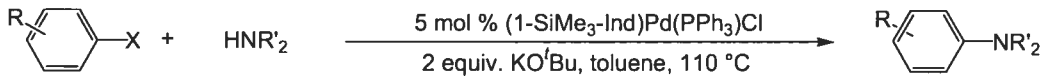

Figure 5.4

Conclusion

La préparation du complexe (1-Me_3Si-Ind)Pd(PPh_3)Cl a pu être effectuée selon une procédure précédemment établie pour l'obtention de composés (1-R-Ind)Pd(PPh_3)Cl (R = H, Me),[1a] par addition de (1-Me_3Si-Ind)Li et PPh_3 sur le

précurseur halogéné $(PhCN)_2PdCl_2$. Ses caractéristiques structurales, en solution comme à l'état solide, démontrent que l'indényle adopte le mode de coordination ($\eta^3 \leftrightarrow \eta^5$) habituellement observé pour ce type de complexes et qu'il présente également la distorsion de type $\eta^1 : \eta^2$, causée par la différence d'influence trans entre les ligands PPh_3 et Cl. La présence du substituant Me_3Si sur l'indényle ne semble donc pas influencer davantage les propriétés structurales de ce type de composés, ni même sa réactivité envers les silanes. Finalement, l'exploration brève de sa réactivité en ce qui a trait à la formation de liens C-C et C-N a mené à des résultats encourageants qui méritent d'être approfondis.

Partie Expérimentale

Remarques générales. Les manipulations et les expériences ont été effectuées sous atmosphère inerte d'azote en utilisant les techniques standards de Schlenk ainsi qu'une boîte à gants. Tous les solvants utilisés ont été préalablement séchés et désoxygénés par distillation sur sodium/benzophénone (*n*-hexane, toluène, Et_2O) ou sur CaH_2 (DMF) sous azote. Ils ont ensuite été conservés sur tamis moléculaire, sous atmosphère inerte et anhydre. La synthèse du composé $(PhCN)_2PdCl_2$[5] a été rapportée précédemment; les autres réactifs proviennent de source commerciale et ont été utilisés tels que reçus. Les protocoles expérimentaux utilisés pour les réactions du complexe **1** en présence de $PhSiH_3$ ou de $HSiCl_3$/styrène ont déjà été décrits dans le chapitre 3.[1] La CG/SM a été effectuée à l'aide d'un appareil AGILENT TECHNOLOGIES 6890 équipé d'une colonne capillaire HP-5MS muni d'un détecteur 5973. Les analyses élémentaires ont été effectuées au Laboratoire d'Analyse Élémentaire de l'Université de Montréal. Les spectres RMN ^1H (400 MHz et 300 MHz), $^{13}C\{^1H\}$ (100 MHz et 75 MHz), et $^{31}P\{^1H\}$ (161 MHz et 121 MHz) à température ambiante ont été enregistrés à l'aide de spectromètres Bruker ARX400, AV400, AMX300, AV300. Les signaux résiduels des solvants deutérés ont été utilisés pour calibrer les spectres de RMN ^1H (C_6D_5H: 7.16 ppm; $CHCl_3$: 7.26 ppm; C_7D_7H: 2.11) et $^{13}C\{^1H\}$ (C_6D_6: 128.06 ppm).[6] Le H_3PO_4 (85%) a été utilisé comme référence externe pour les spectres RMN ^{31}P.

Études cristallographiques.

Les données cristallographiques du composé **1** ont été collectées à 293 K à l'aide d'un diffractomètre Bruker AXS Smart 2K équipé d'une source au graphite et d'un monochromateur de radiation Kα du Cu. La collection, l'affinement de la maille et la réduction des données, la résolution et le raffinement, ont été effectués avec les logiciels SMART,[7] SAINT,[8] SHELXS[9] et SHELXL97,[10] respectivement. La résolution de la structure a été accomplie grâce aux méthodes directes en affinant sur F^2 par la méthode des moindres carrés. Tous les atomes ont été affinés anisotropiquement (en tenant compte des paramètres d'agitation thermique) à l'exception des atomes d'hydrogène qui ont été affinés isotropiquement (en les contraignant à leur atome parent). Les données cristallographiques des composés et les longueurs de liaison et angles sont présentés dans les tableaux 5.I et 5.II, respectivement. Le détail de ces études structurales à l'état solide se trouve également dans l'annexe 3 de cette thèse. L'option SQUEEZE du logiciel PLATON[11] a été utilisée afin de supprimer la contribution du solvant désordonné (425 $Å^3$, 71 électrons/maille) et d'améliorer les données de la structure du complexe **1**. De plus, ce dernier contient 3 molécules par maille et les distances et angles présentés dans le tableau 5.II sont une moyenne de l'ensemble des paramètres de chaque molécule.

Synthèse du (1-SiMe$_3$-Ind)Pd(PPh$_3$)Cl (1). Une solution de 1-SiMe$_3$-IndLi (450 mg, 2.35 mmol) dans l'Et$_2$O (40 mL) est ajoutée goutte à goutte à une suspension de (PhCN)$_2$PdCl$_2$ (900 mg, 2.35 mmol) dans l'Et$_2$O (40 mL) à – 40 °C. Après retour à température ambiante, le mélange noir-rouge résultant est agité pendant 40 minutes et PPh$_3$ (308 mg, 1.17 mmol) est alors ajoutée. Le mélange rouge foncé obtenu est agité pendant environ 30 minutes puis filtré sur célite et évaporé à sec. Il en résulte un résidu huileux rouge brun qui est extrait à l'Et$_2$O (35 mL) et 40 mL d'hexane lui sont ajoutés. La solution rouge est alors concentrée, un solide orange se forme et est isolé par filtration (200 mg, 29%). La recristallisation d'une portion de ce solide dans un mélange 1:1 d'Et$_2$O/hexane conduit à la formation de monocristaux qui ont pu être analysés par diffraction des rayons X et par analyse élémentaire. RMN ^{1}H (C_6D_6, 300

MHz): δ 7.65-7.56 (m, PPh_3), 7.41 (d, $^3J_{H-H}$ = 7.6 Hz, H_7), 6.99 (t, $^3J_{H-H}$ = 7.6 Hz, H_6), 6.97-6.92 (m, PPh_3), 6.80 (t, $^3J_{H-H}$ = 7.5 Hz, H_5), 6.51 (dd, $^3J_{H-H}$ = 3.6 Hz and 1.08 Hz, H_2), 6.42 (d, $^3J_{H-H}$ = 7.5 Hz, H_4), 4.39 (dd, $^3J_{H-H}$ = 2.7 and 0.7 Hz, H_3), 0.63 (s, Me_3Si). $^{13}C\{^1H\}$ NMR (C_6D_6, 100.56 MHz): δ 141.07 (s, C_{7a}), 138.00 (s, C_{3a}), 135.02 (d, $^2J_{C-P}$ = 15.8 Hz, C_{ortho}), 132.85 (d, $^1J_{C-P}$ = 59.8 Hz, C_{ipso}), 130.61 (s, C_{para}), 128.70 (d, $^3J_{C-P}$ = 10.4 Hz, $C_{méta}$), 126.75 (s, C_6), 125.79 (s, C_5), 120.68 (s, C_7), 116.76 (s, C_4), 116.45 (s, C_2), 111.56 (s, C_1), 82.07 (s, C_3), -0.44 (s, Me_3Si). $^{31}P\{^1H\}$ NMR (C_6D_6, 121.49 MHz): δ 29.30 (s). Analyse élémentaire calculée pour $C_{30}H_{30}Si_1Cl_1P_1Pd_1$: C, 60.92; H, 5.11. Obtenue: C, 60.97; H, 5.23.

Procédure générale pour les réactions de couplage de Heck. Un mélange de styrène (1.35 mmol, 1.0 equiv), d'halogénure d'aryle (1.1 mmol, 0.8 equiv), de base (1.3 mmol, 0.96 equiv), et 0.0125 équiv de complexe **1** (1.25 mol %) est agité dans le DMF à 140 °C pendant 24 heures sous atmosphère de N_2. Le mélange réactionnel a ensuite été hydrolysé à 0°C à l'aide d'une solution de HCl aqueux (5%) et extrait à l'hexane. Les phases organiques réunies sont alors neutralisées avec une solution aqueuse de $NaHCO_3$, séchées sur $MgSO_4$ et évaporées. Les produits ont été caractérisés par spectroscopie RMN ^1H et CG/SM. Les rendements ont été calculés par CG/SM, en se basant sur le pourcentage de conversion du styrène.

Procédure générale pour les réactions d'amination. Un mélange d'halogénure d'aryle (0.27 mmol, 1 équiv.), d'amine (0.40 mmol, 1.5 équiv.), de complexe **1** (8 mg, 0.013 mmol, 5 mol %), de KO^{t}Bu (61 mg, 0.54 mmol, 2 équiv) et de toluène (2 mL) est agité et chauffés à 110 °C pendant 17 heures sous atmosphère de N_2. Après évaporation à sec du solvant, la caractérisation par CG/SM et par spectroscopie RMN a permis l'identification des produits de la réaction, par comparaison avec les données précédemment reportées pour les composés tels que le *N*-(2-methylphenyl)morpholine,[12] le *N*-(4-methylphenyl)morpholine,[13] le *N*-(2-methylphenyl)aniline[14] et le *N*-(4-methylphenyl)aniline.[15] Les rendements ont été calculés par rapport au pourcentage de conversion de l'halogénure d'aryle.

Références

[1] (a) Sui-Seng, C.; Enright, G. D.; Zargarian, D. *Organometallics* **2004**, *23*, 1236. (b) Sui-Seng, C.; Groux, L. F.; Zargarian, D. *Organometallics* **2006**, *25*, 571.

[2] (a) Hayashi, T.; Hirate, S.; Kitayama, K.; Tsuji, H.; Torii, A.; Uozomi, Y. *J. Org. Chem.* **2001**, *66*, 1441. (b) Bringmann, G.; Wuzik, A.; Breuning, M.; Henschel, P.; Peters, K.; Peters, E.-M. *Tetrahedron : Asymmetry* **1999**, *10*, 3025. (c) Uozomi, Y.; Tsuji, H.; Hayashi, T. *J. Org. Chem.* **1998**, *63*, 6137. (d) Ricard, L.; Marinetti, A. *Organometallics* **1994**, *13*, 3956. (e) Marinetti, A. *Tetrahedron Lett.* **1994**, *35*, 5861. (f) Tsuji, J.; Hara, M.; Ohno, K. *Tetrahedron* **1974**, *30*, 2143.

[3] Sui-Seng, C.; Castonguay, A.; Chen, Y.; Gareau, D.; Groux, L. F., Zargarian, D. *Topics in Catalysis* **2006**, sous presse.

[4] R. A. Kelly, N. M. Scott, S. Diez-Gonzalez, E. D. Stevens and S. P. Nolan, *Organometallics* **2005**, *24*, 3442.

[5] Anderson, G. K.; Lin, M. *Inorg. Synth.* **1990**, *28*, 60.

[6] Gottlieb, H. E.; Kotlyar, V.; Nudelman, A. *J. Org. Chem.* **1997**, *62*, 7512.

[7] *SMART*, Release 5.059; Bruker Molecular Analysis Research Tool, Bruker AXS Inc.: Madison, WI 53719-1173, 1999.

[8] *SMART*, Release 5.059; Bruker Molecular Analysis Research Tool, Bruker AXS Inc.: Madison, WI 53719-1173, 1999.

[9] Sheldrick, G. M. *SHELXS*. Program for the solution of Crystal Structures. University of Goettingen. Germany, 1997.

[10] Sheldrick, G. M. *SHELXL*. Program for the Refinement of Crystal Structures. University of Goettingen. Germany, 1997.

[11] Spek, A. L. *Acta. Cryst.* A46, C34. *PLATON*, A Multipurpose Crystallographic Tool. Utrecht University, Utrecht, The Netherlands, 2002.

[12] Hartwig, J. F.; Kawatsura, M.; Hauck, S. I.; Shaughnessy, K. H.; Alcazar-Roman, L. M. *J. Org. Chem.* **1999**, *64*, 5575.

[13] Wolfe, J. P.; Buchwald, S. L. *J. Org. Chem.* **1996**, *61*, 1133.

[14] Kataoka, N.; Shelby, Q.; Stambuli, J. P.; Hartwig, J. F. *J. Org. Chem.* **2002**, *67*, 5553.

[15] Kuwano, R.; Utsonomiya, M.; Hartwig, J. F. *J. Org. Chem.* **2002**, *67*, 6479.

Chapitre 6: Préparation et Réactivité de Complexes η^1- et ($\eta^3 \leftrightarrow \eta^5$)-Indényle-platine.

Introduction

Les quelques travaux rapportés dans la bibliographie concernant les complexes indényle-platine portent essentiellement sur leur synthèse et leur caractérisation, sans que leur réactivité n'ait été étudiée. La préparation de dérivés η^1- et $\eta^{3\text{-}5}$-Ind a été examinée par O'Hare en 1987.[1a] Le traitement du précurseur halogéné (COD)$PtCl_2$ avec 1.0 ou 2.5 équivalent(s) d'IndNa à T.A. dans le THF a conduit à la formation des complexes (COD)Pt(η^1-Ind)Cl (**1**) et (COD)Pt(η^1-Ind)$_2$ (**2**) (Figure 6.1). Ces composés ont été isolés avec un rendement d'environ 70 % et ont été caractérisés uniquement par spectroscopie RMN.[1] Contrairement à son analogue η^1-C_5Me_5, le composé **1** est remarquablement stable, même dans les solvants polaires et n'a pas tendance à s'isomériser vers le complexe $\eta^{3\text{-}5}$-Ind correspondant. En présence de $AgBF_4$, cependant, il se transforme en un complexe cationique η-Ind (**3**), qui peut aussi être formé par protonation du composé **2** avec 1 équivalent de HBF_4 (Figure 6.1).

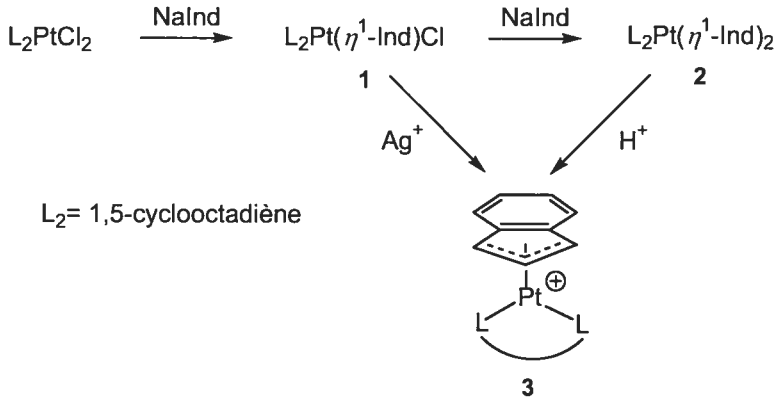

Figure 6.1

En 1999, Ackermann et al. ont rapporté un autre exemple de complexe Ind de Pt(II) obtenu par réarrangement en solution du précurseur η^1-propargylique correspondant:[2]

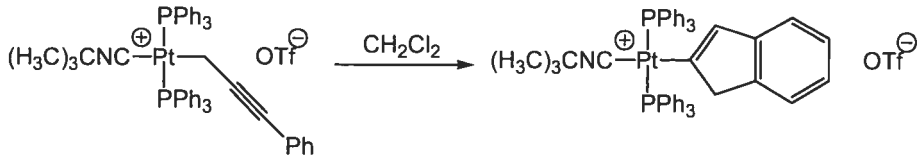

Figure 6.2

Ces exemples de composés platine-indényle constituent, à notre connaissance, les seuls existants dans la littérature. L'objectif de ce travail s'inscrit donc dans la continuité et consistera à mettre au point des voies d'accès aux composés Ind-Pt et d'explorer leur réactivité.

Résultats et Discussion

Synthèse et caractérisation spectroscopique. L'approche proposée par O'Hare pour l'obtention de complexes Ind-Pt(II)[1a] a tout d'abord été envisagée. L'addition d'un équivalent d'IndLi à une solution de (COD)PtClX (X = Cl, Me) dans l'Et_2O ou le THF permet d'obtenir, avec des rendements satisfaisants (75-85 %), les complexes (COD)Pt(η^1-Ind)X (X = Cl (**1**), Me (**4**)), tandis que l'addition de 2 équivalents d'IndLi sur le (COD)$PtCl_2$ donne le complexe (COD)Pt(η^1-Ind)$_2$ (**2**) avec un rendement de 70 %. Ce dernier a ensuite été utilisé pour la préparation du complexe cationique [(η-Ind)Pt(COD)]$^+$ (**3**) par réaction avec 1 équivalent de HBF_4 (rendement = 85 %) (Figure 6.3).

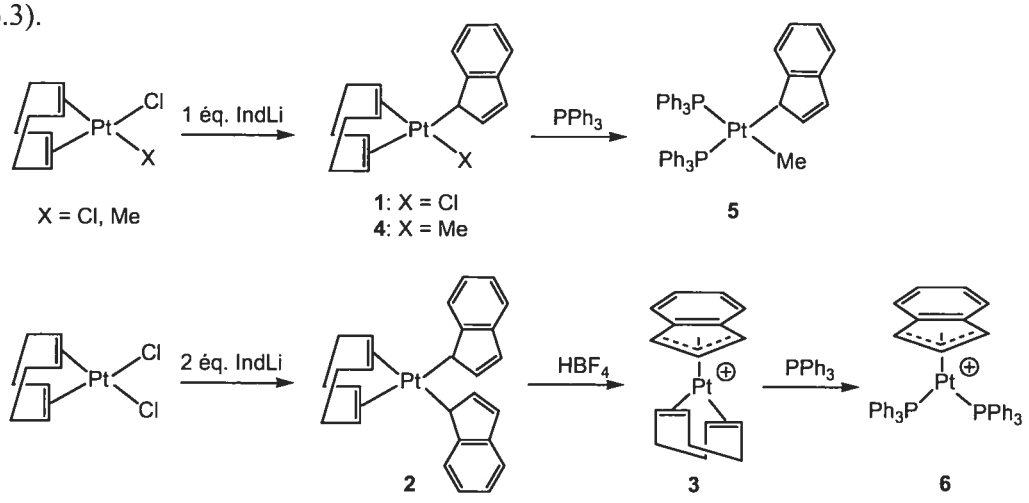

Figure 6.3

L'addition de HBF_4 sur le complexe (COD)Pt(η^1-Ind)Me (**4**) conduit quant à elle à la protonation du ligand indényle et les seuls produits de décomposition formés détectables par RMN sont l'indène et le COD. En présence de phosphines encombrées, telles que PCy_3 ou P(*o*-tolyl)$_3$, le composé **4** aurait pu parvenir à s'isomériser vers le complexe (η-Ind)Pt(PR_3)Cl correspondant, par dissociation du ligand COD, mais étant donné l'encombrement stérique de la phosphine, aucune réaction ne s'est produite. Néanmoins, en présence de PPh_3, la réaction de substitution du COD a été complète et on assiste à la formation du composé $(PPh_3)_2$Pt(η^1-Ind)Me (**5**). Similairement, la réaction du cation $[(\eta\text{-Ind})Pt(COD)]^+$ (**3**) avec PPh_3 a donné le composé bis(phosphine) correspondant $[(\eta\text{-Ind})Pt(PPh_3)_2]^+$ (**6**) (Figure 6.3).

Par la suite, conformément à la synthèse des composés Ind-Ni précédemment établie dans le groupe,[3] une autre tentative de synthèse des complexes Ind de Pt(II) a consisté à additionner un équivalent de (1-R-Ind)Li (R = H, Me_3Si) sur le précurseur $(PPh_3)_2PtCl_2$. Comme ce fut le cas pour le Pd,[4] la réaction a cependant favorisé la formation du produit d'homocouplage pour donner majoritairement du 1,1'-biindène. L'une des stratégies alors utilisée fut d'avoir recours à un précurseur contenant des ligands plus labiles, tel que le $(PhCN)_2PtCl_2$, afin de favoriser la dissociation du ligand L de l'intermédiaire L_2Pt(η^1-Ind)Cl, par rapport à l'étape d'addition d'un second équivalent d'IndLi, et permettre ainsi sa conversion en un complexe (η-Ind)Pt(L)Cl. Néanmoins, ici également, la réaction mène à la formation de 1,1'-biindène (Figure 6.4).

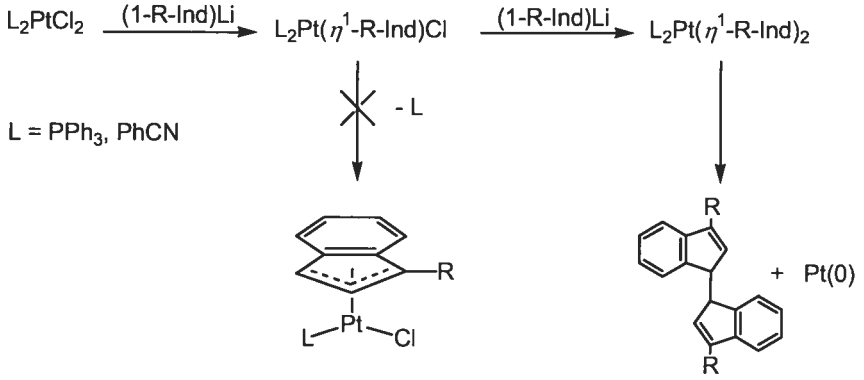

Figure 6.4

S'inspirant de récents travaux publiés par notre groupe et permettant la synthèse du complexe (η^3-Ind)Ni(PPh_3)Br par addition oxydante du 1-Br-IndH sur le $Ni(PPh_3)_4$,[5] une autre tentative d'obtention d'un complexe Ind-Pt a consisté à additionner 1 équivalent de 1-Br-IndH sur $Pt(PPh_3)_4$. Toutefois, du $(PPh_3)_2PtBr_2$ et du 1,1'-biindène furent à nouveau obtenus.

Les complexes **1-6**, tous de couleur beige-jaune, sont thermiquement stables à l'air et en solution et peuvent être conservés à température ambiante. Ils ont été caractérisés par spectroscopie RMN, analyse élémentaire et diffraction des rayons X (sauf pour le composé **5**). Ces études ont apporté de pertinentes informations sur les caractéristiques structurales de ces composés et seront décrites dans les paragraphes suivants.

Les spectres RMN du composé (COD)Pt(η^1-Ind)Me (**4**) et $(PPh_3)_2$Pt(η^1-Ind)Me (**5**) présentent des caractéristiques similaires à celles décrites par O'Hare pour les composés η^1-Ind-Pt analogues (COD)Pt(η^1-Ind)Cl (**1**) et (COD)Pt(η^1-Ind)$_2$ (**2**).[1] L'enregistrement de spectres DQPH-COSY avait notamment permis l'attribution et le calcul de toutes les constantes de couplage existantes au sein des composés **1**-**2**,[1] ce qui n'a pas été effectué dans le cas des composés **4** et **5**. Néanmoins, la résolution des spectres RMN a été suffisante pour permettre d'en calculer la majorité. Par exemple, les spectres RMN ^1H et $^{13}C\{^1H\}$ du composé **4** montrent respectivement des signaux à 5.12 ppm ($^2J_{H\text{-}Pt}$ = 182 Hz) et à 54.13 ppm ($^1J_{C\text{-}Pt}$ = 581 Hz), correspondant respectivement au H1 et C1 du ligand Ind (pour le complexe **5**, δ_{H1} = 5.17 ppm, $^2J_{H\text{-}Pt}$ = 180 Hz), ce qui est très semblable aux valeurs observées pour **1** et **2**. Ces valeurs sont également proches de celles obtenues pour les complexes η^1-Ind de métaux de transitions déjà rapportés.[4,6] De plus, les spectres RMN présentent également des signaux caractéristiques de la présence d'une liaison Pt-Me:[7] δ_{H1} = 1.17 ppm ($^2J_{H\text{-}Pt}$ = 76 Hz), δ_{C1} = 7.07 ppm ($^1J_{C\text{-}Pt}$ = 745 Hz) pour le composé **4**; et δ_{H1} = 0.0 ppm ($^2J_{H\text{-}Pt}$ = 63 Hz) pour le composé **5**. Le spectre RMN $^{31}P\{^1H\}$du composé **5** montre aussi 2 doublets à 29.6 et 30.5 ppm ($^2J_{P\text{-}P}$ = 8.3 Hz, $^1J_{P\text{-}Pt}$ = 2486 et 1938 Hz) reflétant ainsi

l'inéquivalence des deux phosphines et confirmant la structure *cis* du composé. Quant au spectre RMN $^{31}P\{^{1}H\}$ du composé **6**, étant donné sa symétrie C_s, une seule résonance à 2.77 ppm ($^{1}J_{P\text{-}Pt}$ = 4333 Hz) est observée. De même, ses spectres RMN ^{1}H et $^{13}C\{^{1}H\}$ ne montrent qu'une seule résonance pour les paires de protons (H1/H3, H4/H7, et H5/H6) et de carbones (C1/C3, C4/C7, et C5/C6) équivalents par symétrie, ce qui avait déjà été observé pour le complexe analogue de Pd [(η-Ind)$Pd(PPh_3)_2$][BF_4].[8]

Études structurales à l'état solide. Les structures à l'état solide des composés **1**, **2**, **3**, **4** et **6** ont été résolues par diffraction des rayons X. Les diagrammes ORTEP sont représentés dans les figures 6.5 et 6.6, tandis que les données cristallographiques et les paramètres structuraux sont présentés dans les tableaux 6.I et 6.II.

Les composés **1, 2** et **4** présentent une géométrie autour du centre métallique pseudo plan carré. Les paramètres structuraux de ces composés sont semblables à ceux observés dans les structures des autres complexes η^1-Ind de métaux de transition.[4,8-9] Par exemple, le caractère sp^3 du carbone de la liaison Pt-C1 se reflète dans les distances C1-C2 (*ca.* 1.48 Å) et C1-C7a (*ca.* 1.50 Å) qui sont de l'ordre de grandeur des distances obtenues pour une liaison simple C-C, tandis que la distance C2-C3 (*ca.* 1.35 Å) correspond bien à celle d'une liaison $C(sp^2)$-$C(sp^2)$. Au niveau des distances Pt-X (X = Cl (**1**), η^1-Ind (**2**), Me (**4**)), il est intéressant de constater que Pt-C8 (**4**) < Pt-C(1) (**4**) ~ Pt-C11 (**2**) < Pt-Cl (**1**). De même, dans le cas du complexe **4,** on constate que la distance Pt-oléfine en trans du ligand X est plus allongée que celle en trans de l'atome C1 du ligand η^1-Ind, tandis que dans le composé **1**, elle est plus courte. Ces observations nous amènent à conclure que l'influence trans du groupement Cl < η^1-Ind < CH_3.[10] D'autre part, on remarque que l'élongation des doubles liaisons oléfiniques C21=C22 et C25=C26 (1.365 et 1.403 Å) correspond à l'allongement qui est généralement observé dans les complexes (COD)Pt analogues.[7a,11]

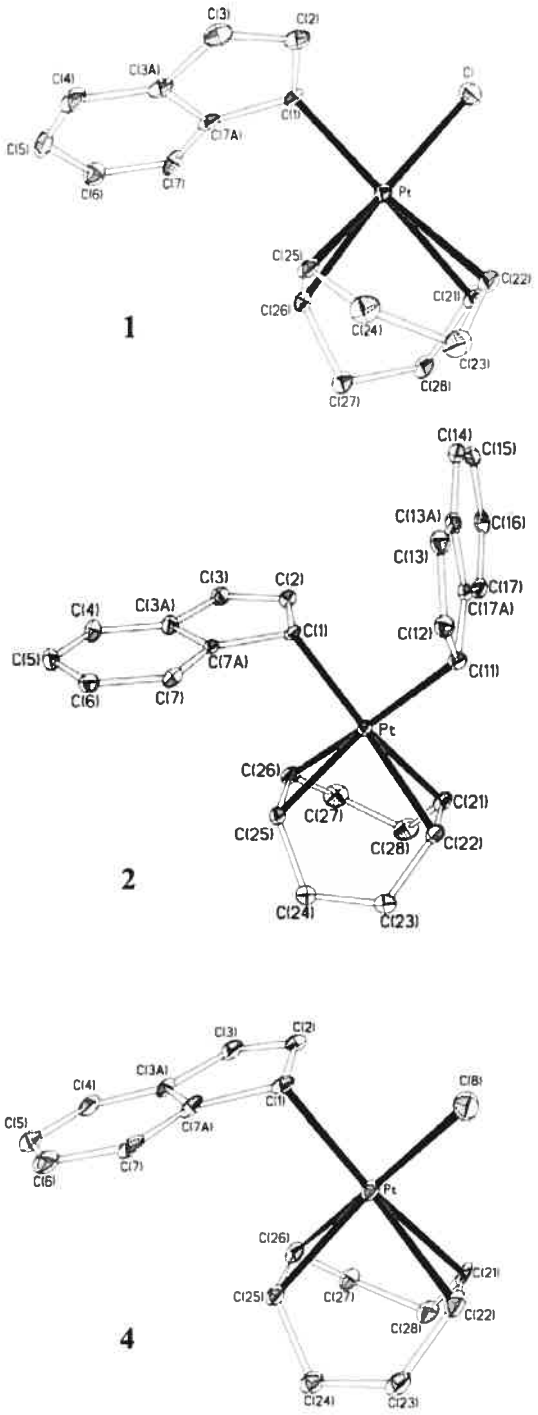

Figure 6.5: Dessins ORTEP des complexes **1**, **2** et **4** représentés avec des ellipsoïdes thermiques à 30% de probabilité et sans les atomes d'hydrogène.

Table 6.I: Données cristallographiques des composés 1, 2, 3, 4 et 6.

	1	2	3	4	6
formule	$C_{17}H_{19}ClPt$	$C_{26}H_{26}Pt$	$C_{17}H_{19}BF_4Pt$	$C_{28}H_{22}Pt$	$C_{45}H_{37}BF_4P_2Pt$
masse moléculaire	453,86	533,56	505,22	433,45	921,59
couleur, forme	jaune, bloc	jaune, plaque	jaune, plaque	jaune, bloc	jaune, plaque
dimens, mm	0,12×0,14×0,32	0,05×0,09×0,12	0,06×0,25×0,45	0,08×0,23×0,30	0,08×0,10×0,20
système	Monoclinique	Triclinique	Orthorhombique	Monoclinique	Monoclinique
groupe d'espace	*C*2/c	*P*-1	*A*ba2	$P2_1/n$	$P2_1/n$
a, Å	22,6640(5)	8,3210(11)	12,2596(11)	9,5752(3)	11,6602(3)
b, Å	8,2185(2)	10,5075(14)	23,111(2)	13,3133(4)	20,6255(5)
c, Å	17,9396(4)	12,5313(17)	11,0481(10)	11,7387(4)	15,7548(4)
α, deg	90	71,156(2)	90	90	90
β, deg	119,999(1)	75,883(2)	90	106,562(2)	95,883(1)
γ, deg	90	69,848(2)	90	90	90
volume, $Å^3$	2893,85(11)	962,5(2)	3130,2(5)	1434,4(6)	3725,9(2)
Z	8	2	8	4	4
D(calc), g cm^{-1}	2,083	1,841	2,144	2,007	1,643
diffractomètre	Bruker AXS SMART 2K	Bruker AXS SMART 1K	Bruker AXS SMART 1K	Bruker AXS SMART 2K	Bruker AXS SMART 2K
temp, K	200	125	125	100	200
λ	1,54178 Å	0,71073 Å	0,71073 Å	1,54178 Å	1,54178 Å
μ, mm^{-1}	19,678	7,296	9,001	18,136	18,136
scan type	ω scan	ω scan	ω scan	ω scan	ω scan
F(000)	1728	520	1920	832	1824
θ_{max}, (deg)	71,99	29,14	29,12	72,91	68,92
h,k,l range	$-27 \le h \le 27$	$-11 \le h \le 10$	$-16 \le h \le 16$	$-11 \le h \le 11$	$-12 \le h \le 13$
	$-10 \le k \le 9$	$-14 \le k \le 14$	$-31 \le k \le 31$	$-16 \le k \le 15$	$-24 \le k \le 24$
	$-21 \le l \le 21$	$-16 \le l \le 17$	$-15 \le l \le 15$	$-14 \le l \le 13$	$-18 \le l \le 18$
No. de réflns collectées/unique	11374/2822	9852/5035	19174/4189	11374/2822	50471/6829
Correction d'absorption	multi-scan SADABS	multi-scan SADABS	multi-scan SADABS	multi-scan SADABS	multi-scan SADABS
T (min, max)	0,350, 1,000	0,408, 0,694	0,084, 0,583	0,017, 0,234	0,78, 1,00
$R\,[F^2 > 2\sigma(F^2)]$, $R_w(F^2)$	0,0421, 0,1032	0,0290, 0,0580	0,0141, 0,0324	0,0432, 0,1078	0,0280, 0,0812
GOF	1,089	1,032	0,982	1,105	1,037

Table 6.II. Distances (Å) et Angles (deg) Sélectionnés des Composés 1, 2, 3, 4 et 6.

	1 (X=Cl)	2 (X=C11)		4 (X=C8)	3 (X=C3)	6 (X=C3)
Pt-C1	2,115(4)	2,116(4)		2,117(5)	2,216(3)	2,223(4)
Pt-X	2,274(5)	2,113(4)		2,060(6)		
Pt-C2					2,218(3)	2,202(3)
Pt-C3					2,192(4)	2,254(3)
Pt-C3a					2,467(2)	2,653(4)
Pt-C7a					2,480(2)	2,624(4)
Pt-P1						2,2621(8)
Pt-P2						2,2714(8)
Pt-C21	2,260(5)	2,207(4)		2,212(5)	2,180(3)	
Pt-C22	2,274(5)	2,228(4)		2,188(5)	2,155(4)	
Pt-C25	2,125(5)	2,248(4)		2,277(4)	2,178(2)	
Pt-C26	2,148(5)	2,212(4)		2,238(5)	2,174(2)	
C1-C2	1,494(7)	1,501(6)	1,520(9)	1,483(3)	1,427(4)	1,412(6)
C2-C3	1,352(9)	1,342(6)	1,353(8)	1,360(6)	1,441(5)	1,414(6)
C3-C3a	1,468(9)	1,458(6)	1,462(7)	1,452(6)	1,470(5)	1,466(6)
C7a-C1	1,487(6)	1,481(5)	1,471(8)	1,484(6)	1,470(4)	1,459(7)
C21-C22	1,367(8)	1,371(7)		1,368(9)	1,405(5)	
C25-C26	1,403(7)	1,365(7)		1,380(7)	1,408(4)	
C1-Pt-X	86,79(14)	88,64(16)		85,6(2)	62,99(13)	60,94(14)
X-Pt-C26	162,15(14)	160,23(18)		162,1(2)	102,8(2)	
C26-Pt-C25	38,35(19)	35,65(18)		35,59(18)	37,76(10)	
X-Pt-C25	159,34(14)	163,19(17)		161,8(2)	102,65(14)	
C25-Pt-C22	81,00(19)	79,37(16)		80,82(17)	82,47(14)	
C22-Pt-C1	160,2(2)	166,59(17)		160,7(2)	99,55(12)	
C22-Pt-C21	35,1(2)	36,00(17)		36,2(2)	37,83(14)	
C21-Pt-C1	164,6(2)	157,37(18)		162,6(3)	110,16(11)	
C1-Pt-C26	97,48(18)	91,03(16)		94,7(2)	161,86(18)	
C1-Pt-C25	91,54(18)	98,68(16)		98,73(9)	151,16(11)	
X-Pt-C21	90,11(15)	91,46(17)		93,4(2)	164,81(13)	
X-Pt-C22	93,77(15)	89,99(16)		89,1(2)	152,24(11)	
C3-Pt-P2						95,62(10)
P2-Pt-P1						103,57(3)
P1-Pt-C1						99,73(10)
ΔM-C (Å)					0,27	0,40
HA (deg)					13,03	15,74
FA (deg)					11,85	14,19

La géométrie autour du centre métallique dans les complexes **3** et **6** est également plan carré et la plus grande distorsion résulte de l'angle C1-Pt-C3 (ca. 60°). Le ligand COD du composé **3** et les phosphines du composé **6** sont coordonnés d'une manière symétrique sur le Pt et présentent des distances similaires (Pt-C21 ~ Pt-C22 ~ Pt-C25 ~ Pt-C26 ~ 2.17Å pour **3**; Pt-P1 = Pt-P2 = 2.26 Å pour **6**). De plus, les longueurs des liens entre le Pt et les carbones C3a et C7a sont beaucoup plus grandes que les liens formés par le Pt avec les carbones C1, C2 et C3, ce qui traduit une distorsion ($\eta^3 \leftrightarrow \eta^5$) dans la coordination de l'indényle. Cette distorsion se reflète également dans la valeur des paramètres Δ(M-C), HA et FA qui sont d'ailleurs beaucoup plus grands dans le cas du composé **6** en comparaison avec **3**. Cette différence pourrait être le résultat de l'exigence stérique des phosphines versus le ligand COD, qui empêche l'indényle de se rapprocher du Pt et d'adopter une hapticité davantage η^5, mais aussi et surtout de la rétroliaison du Pt envers les doubles liaisons oléfiniques du COD dans le composé **3**, qui se compense par une hapticité de l'indényle η^3 plus prononcée. D'autre part, on constate que les paramètres Δ(M-C) (0.40 Å), HA (15.74°) et FA (14.19°) du composé **6** sont plus grands que ceux obtenus pour le composé de Pd analogue [(η-Ind)Pd(PPh_3)$_2$][BF_4] (Δ(M-C) = 0.33 Å, HA = 11.86° et FA = 12.18°)[8] et que les interactions M-Ind et M-P sont légèrement plus fortes dans le cas du Pt comparativement au Pd.

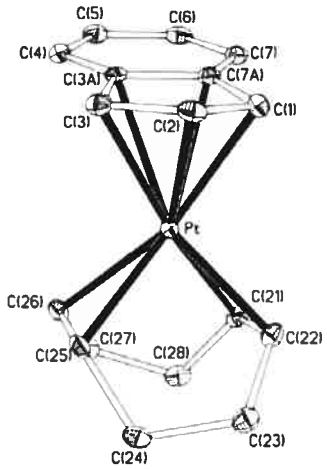

Figure 6.6: Dessin ORTEP du complexe **3** représenté avec des ellipsoïdes thermiques à 30% de probabilité, sans les atomes d'hydrogène et l'anion BF_4

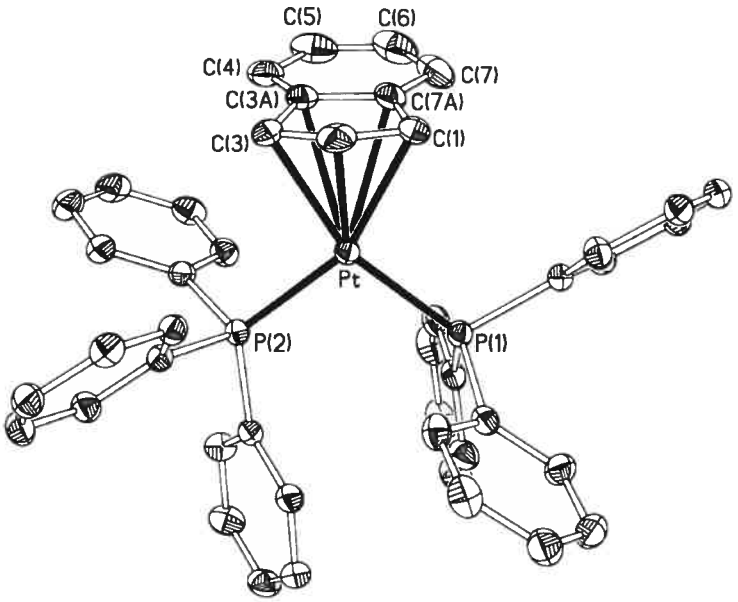

Figure 6.6: Dessin ORTEP du complexe **6** représenté avec des ellipsoïdes thermiques à 30% de probabilité, sans les atomes d'hydrogène et l'anion BF_4

Réactivités catalytiques des complexes Ind-Pt. Des études précédentes ont démontré que les complexes Ind du Ni(II) sont relativement actifs envers le couplage déshydrogénatif du $PhSiH_3$ pour produire des oligomères linéaires et cycliques de type $(PhSiH)_n$, ainsi qu'envers l'hydrosilylation d'oléfines et de cétones.[12] L'exploration de la réactivité des complexes Ind de Pd(II) a ensuite permis de montrer qu'ils étaient également réactifs envers le $PhSiH_3$, avec une activité très modeste par rapport à celle des composés Ind-Ni, et qu'ils pouvaient également promouvoir, uniquement en présence d'hydrosilane très activé, tel que le $HSiCl_3$, l'hydrosilylation du styrène et du phénylacétylène.[4,8] Ces résultats nous ont donc incité à explorer les réactivités des complexes Ind-Pt obtenus, en présence de $PhSiH_3$. L'addition de $PhSiH_3$ (ca. 100 équiv) sur une solution de C_6D_6 des complexes **3** ou **4** à T.A. provoque un dégagement gazeux, qui s'estompe progressivement, et un noircissement de la solution. Les spectres RMN ^1H de ces réactions démontrent qu'après quelques heures environ, 20% du $PhSiH_3$ a été consommé et converti en Ph_2SiH_2. L'analyse GC/MS des mélanges réactionnels résultants confirme que le Ph_2SiH_2 ($M^{+\cdot}$ à m/z 184) et le $PhSiH_3$ ($M^{+\cdot}$ à m/z

108) restant constituent bien les produits majoritaires de cette réaction, mais révèle aussi la présence de traces de Ph_3SiH ($M^{+\cdot}$ à m/z 260) et de $(PhH_2Si)_2$ ($M^{+\cdot}$ à m/z 214). Ces résultats nous amènent à conclure que les complexes Ind-Pt peuvent activer la liaison Si-H du $PhSiH_3$ et promouvoir ainsi sa redistribution et la formation de liaison Si-Si. De plus, la réaction des complexes **3** ou **4**, en solution dans C_6D_6, en présence de $PhSiH_3$ (50 équiv) et de styrène (50 équiv) simultanément, produit majoritairement du $PhCH_2CH_2SiH_2Ph$[13] (~ 35%), ainsi que du $PhSiH_2$ (~ 30%). Des traces du produit d'addition Markovnikov, le $PhCH(SiH_2Ph)Me$, et des produits de redistribution, le Ph_2SiH_2 et le Ph_3SiH, ont également été observés par GC/MS.

Conclusion

Les résultats de ce chapitre ont permis de développer une voie de synthèse fiable pour l'obtention des composés (COD)Pt(η^1-Ind)X (X = Cl, Me) et (COD)Pt(η^1-Ind)$_2$ par addition d'un ou deux équivalents d'IndLi sur les précurseurs (COD)PtXCl (X = Cl, Me). L'addition d'HBF_4 sur le complexe (COD)Pt(η^1-Ind)$_2$ a ensuite permis d'obtenir l'espèce cationique [(η-Ind)Pt(COD)]$^+$. Ces complexes ont été isolés avec de bons rendements et pour la première fois entièrement caractérisés. Les études cristallographiques ont démontré que les longueurs des distances Pt-oléfine (COD) dans les complexes neutre de type (COD)Pt(η^1-Ind)X (X = Cl, Me, η^1-Ind) variaient en fonction de la nature du ligand positionné en trans de celles-ci et ont permis d'établir le classement suivant: influence trans Cl < η^1-Ind < Me. De plus, les structures à l'état solide des complexes cationiques [(η-Ind)PtL$_2$]$^+$ (L$_2$ = COD, $(PPh_3)_2$) ont permis de mettre en évidence la distorsion $\eta^3 \leftrightarrow \eta^5$ de l'Ind qui dans le cas du COD est davantage prononcée. Les études préliminaires de réactivité de ces composés ont démontré qu'ils pouvaient promouvoir la redistribution du $PhSiH_3$ ainsi que son addition sur le styrène avec de modestes rendements.

Partie Expérimentale

Remarques générales. Les manipulations et expériences ont été effectuées sous atmosphère inerte d'azote en utilisant les techniques standards de Schlenk ainsi qu'une boîte à gants. Tous les solvants utilisés ont préalablement été séchés et désoxygénés par distillation sur sodium/benzophénone (*n*-hexane, benzène, toluène, Et_2O et THF) ou sur CaH_2 (CH_2Cl_2, $CHCl_3$ et CH_3CN) sous azote. Ils ont ensuite été conservés sur tamis moléculaire, sous atmosphère inerte et anhydre. Les synthèses des composés $(COD)PtCl_2$,[14] $(COD)_2PtMeCl$[15], $(COD)Pt(\eta^1\text{-Ind})Cl$,[1a] $(COD)Pt(\eta^1\text{-Ind})_2$[1a] et $[(COD)Pt(\eta\text{-Ind})][BF_4]$[1a] ont été rapportés précédemment; les autres réactifs proviennent de source commerciale et ont été utilisés tels que reçus. Les analyses élémentaires ont été effectuées au Laboratoire d'Analyse Élémentaire de l'Université de Montréal. Les spectres RMN ^1H (400 MHz et 300 MHz), $^{13}C\{^1H\}$ (100 MHz et 75 MHz), et $^{31}P\{^1H\}$ (161 MHz et 121 MHz) à température ambiante ont été enregistrés à l'aide de spectromètres Bruker ARX400, AV400, AMX300, AV300. Les signaux résiduels des solvants deutérés ont été utilisés pour calibrer les spectres de RMN ^1H (C_6D_5H: 7.16 ppm; $CHCl_3$: 7.26 ppm; $CDHCl_2$: 5.30; C_7D_7H: 2.11) et $^{13}C\{^1H\}$ (C_6D_6: 128.06 ppm; $CDCl_3$: 77.16 ppm; CD_2Cl_2: 53.52; C_7D_8: 21.10).[16] Le H_3PO_4 (85%) a été utilisé comme référence externe pour les spectres RMN ^{31}P.

Etudes cristallographiques.

Les données cristallographiques des composés **1**, **2**, **3**, **4** et **6** ont été collectées à l'aide d'un diffractomètre Bruker AXS Smart 2K et 1K (pour **2** et **3**), équipé d'une source au graphite et d'un monochromateur de radiation Kα du Cu à 223 K pour les composés **1** et **6**, et à 100 K pour **4**, et de radiation Kα du Mo à 125 K pour **2** et **3**. La collection, l'affinement de la maille et la réduction des données, la résolution et l'affinement des paramètres structuraux ont été effectués avec les logiciels SMART,[17] SAINT,[18] SHELXS[19] et SHELXL97,[20] respectivement. La résolution des structures a été accomplie grâce aux méthodes directes en affinant sur F^2 par la méthode des moindres carrés. Tous les atomes ont été affinés anisotropiquement à l'exception des atomes d'hydrogène qui ont été affinés isotropiquement (en les contraignant à leur atome

parent). Les données cristallographiques des composés et les longueurs de liaison et angles sont présentés dans les tableaux 6.I et 6.II, respectivement. Le détail de ces études structurales à l'état solide se trouve également dans l'annexe 3 de cette thèse.

Préparation du (COD)Pt(η^1-Ind)Cl, (1). La procédure de synthèse ainsi que les caractéristiques RMN de ce composé ont précédemment été décrites par O'Hare.[1] La recristallisation d'une portion du solide jaune obtenu dans un mélange froid 1:1 d'Et_2O/hexane conduit à la formation de monocristaux qui ont pu être analysés par diffraction des rayons X et par analyse élémentaire. Analyse élémentaire calculée pour $C_{17}H_{19}Pt_1Cl_1$: C, 44.99; H, 4.22. Obtenue: C, 44.87; H, 3.99.

Préparation du (COD)Pt(η^1-Ind)$_2$, (2). Selon une procédure modifiée du protocole décrit par O'Hare,[1] une solution d'IndLi (310 mg; 2.52 mmol) dans l'Et_2O (20 mL) est ajoutée goutte à goutte à une suspension de $(COD)_2PtCl_2$ (470 mg, 1.25 mmol) dans l'Et_2O (20 mL) à température ambiante. Après 4h d'agitation, le mélange jaune résultant est filtré. Le filtrat obtenu est ensuite concentré jusqu'à environ 5 mL. Après addition de 5 mL d'hexane, un solide beige précipite et est isolé par filtration (640 mg, 95%). La recristallisation d'une portion du solide jaune obtenu dans un mélange froid 1:1 d'Et_2O/hexane conduit à la formation de monocristaux qui ont pu être analysés par diffraction des rayons X et par analyse élémentaire. Les caractéristiques RMN de ce composé ont précédemment été décrites par O'Hare.[1] Analyse élémentaire calculée pour $C_{26}H_{26}Pt_1$: C, 58.53; H, 4.91. Obtenue: C, 57.87; H, 5.05.

Préparation du [(η-Ind)Pt(COD)][BF_4], (3). La procédure de synthèse ainsi que les caractéristiques RMN de ce composé ont précédemment été décrites par O'Hare.[1] La recristallisation d'une portion du solide beige obtenu dans un mélange froid 1:1 de THF/CH_2Cl_2 conduit à la formation de monocristaux qui ont pu être analysés par diffraction des rayons X et par analyse élémentaire. Analyse élémentaire calculée pour $C_{17}H_{19}B_1F_4Pt_1$: C, 40.41; H, 3.79. Obtenue: C, 40.37; H, 3.60.

Préparation du (COD)Pt(η^1-Ind)(Me), (4).

Une solution d'IndLi (396 mg; 3.22 mmol) dans l'Et_2O (50 mL) est ajoutée goutte à goutte à une suspension de $(COD)_2PtMeCl$ (1 g, 2.83 mmol) dans l'Et_2O (100 mL) à température ambiante. Après 4h d'agitation, le mélange orange-rosé est filtré. Le filtrat obtenu est ensuite concentré jusqu'à environ 5 mL. Après addition de 5 mL d'hexane, un solide beige précipite et est isolé par filtration (1.1 g, 85%). La recristallisation d'une portion de ce solide dans un mélange froid 1:1 d'Et_2O/hexane conduit à la formation de monocristaux qui ont pu être analysés par diffraction des rayons X et par analyse élémentaire. RMN ^1H (C_6D_6, 400 MHz): δ 7.67-7.62, 7.25-7.24 (m, H_{4-7}), 6.88 (br s, H_2 et H_3), 5.12 (s, $^2J_{H-Pt}$ = 182 Hz, H_1), 4.34-3.98, 3.62-3.54 (m, C*H*=), 1.85-1.40 (m, CH_2), 1.17 (s, $^2J_{H-Pt}$ = 76 Hz, Pt-CH_3). RMN $^{13}C\{^1H\}$ (C_6D_6, 100 MHz): δ 152.03 (s, C_{7a} ou C_{3a}), 144.63 (s, C_{3a} ou C_{7a}), 139.00 (s, $^2J_{C-Pt}$ = 63 Hz, C_2), 123.95, 123.78, 122.17, 120.78 (s, C_{4-7}), 121.60 (s, $^3J_{C-Pt}$ = 47 Hz, C_3), 104.48, 104.19 (s, $^1J_{C-Pt}$ = 85 Hz, *C*H=), 95.02, 94.78 (s, $^1J_{C-Pt}$ = 85 Hz, *C*H=), 54.13 (s, $^1J_{C-Pt}$ = 581 Hz, C_1), 31.34, 29.88, 29.16, 27.89 (s, *C*H_2), 7.07 (s, $^1J_{C-Pt}$ = 745 Hz, Pt-*Me*). Analyse élémentaire calculée pour $C_{18}H_{22}Pt_1$: C, 49.88; H, 5.12. Obtenue: C, 49.32; H, 5.32.

Préparation du $(PPh_3)_2Pt(\eta^1$-Ind)(Me), (5). La substitution du ligand COD du composé **4** par PPh_3 a été effectuée à l'échelle RMN, sans isoler l'adduit résultant, par addition de 2 équiv de PPh_3 à 0.5 mL d'une solution de **4** (ca. 0.03 mmol) dans C_6D_6. Les spectres RMN ont ensuite été enregistrés à température ambiante. RMN ^1H (C_6D_6, 300 MHz): δ 7.88-6.78 (m, PPh_3 et H_{2-7}), 5.17 (t, $^3J_{H-P}$ = 16.3 Hz, $^2J_{H-Pt}$ = 180 Hz, H_1) 0.00 (t, $^3J_{H-P}$ = 7.2 Hz, $^2J_{H-Pt}$ = 63.4 Hz, Pt-CH_3). RMN $^{31}P\{^1H\}$ (C_6D_6, 121 MHz): δ30.57 (d, $^2J_{P-P}$ = 8.3 Hz, $^1J_{P-Pt}$ = 1938 Hz, PPh_3), 29.61 (d, $^2J_{P-P}$ = 8.3 Hz, $^1J_{P-Pt}$ = 2486 Hz, PPh_3).

Préparation du $[(\eta$-Ind)Pt$(PPh_3)_2][BF_4]$, (6). La substitution du ligand COD du composé **3** par PPh_3 a été effectuée à l'échelle RMN, sans isoler l'adduit résultant, par addition de 2 équiv de PPh_3 à 0.5 mL d'une solution de **3** (ca. 0.03 mmol) dans $CDCl_3$.

Les spectres RMN ont ensuite été enregistrés à température ambiante. Après évaporation lente à l'air du solvant, des monocristaux jaunes se sont formés et ont pu être analysés par diffraction des rayons X et par analyse élémentaire. RMN ^{1}H ($CDCl_3$, 400 MHz): δ 7.30-7.17 (m, PPh_3 et H_2 de Ind), 7.08 (dd, $^{3}J_{H\text{-}H}$ = 3.1 Hz, H_5 et H_6), 6.99-6.97 (m, PPh_3), 6.28 (dd, $^{3}J_{H\text{-}H}$ = 3.1 Hz, H_4 et H_7), 5.02 (q, $^{3}J_{H\text{-}H}$ = 2.7 Hz, H_1 et H_3). RMN $^{31}P\{^{1}H\}$ ($CDCl_3$, 162 MHz): δ 2.77 (s, $^{1}J_{P\text{-}Pt}$ = 4333 Hz, PPh_3). Analyse élémentaire calculée pour $C_{45}H_{37}B_1F_4P_2Pt_1$: C, 58.65; H, 4.05. Obtenue: C, 58.31 ; H, 3.77.

Références

[1] (a) O'Hare, D. *Organometallics* **1987**, *6*, 1766. (b) O'Hare, D. *J. Organomet. Chem.* **1987**, *323*, C13-C17.O'Hare, D. *Organometallics* **1987**, *6*, 1766.

[2] Ackermann, M. N.; Ajmera, R. K.; Barnes, H. E.; Gallucci, J. C.; Wojicicki, A. *Organometallics* **1999**, *18*, 787.

[3] Zargarian, D. *Coord. Chem. Rev.* **2002**, *233-234*, 157.

[4] Sui-Seng, C.; Enright, G. D.; Zargarian, D. *Organometallics* **2004**, *23*, 1236.

[5] (a) Boucher, S. ; Zargarian. D. *Can. J. Chem.* **2006**, 84, sous presse. (b) Boucher, S. Mémoire de Maîtrise, Université de Montréal, **2006**.

[6] (a) Alias, F. M.; Belderrain, T. R.; Paneque, M.; Poveda, M. L.; Carmona, E. *Organometallics* **1998**, *17*, 5620. (b) Casey, C. P.; O' Connor J. M *Organometallics* **1985**, *4*, 384. (c) Hermmann, W. A.; Kuhn, F. E.; Romao, C. C. *J. Organomet. Chem.* **1995**, *489*, C56.

[7] voir les références suivantes pour les détails des caractéristiques RMN de certains composés à liaison Pt-Me: (a) Klein, A. ; Klinkhammer, K. –W. ; Scheiring, T. *J. Organomet. Chem.* **1999**, *592*, 128. (b) Shaver, A.; Hamer, G. *Can. J. Chem.* **1980**, *58*, 2011.

[8] Sui-Seng, C.; Groux, L. F.; Zargarian, D. *Organometallics* **2006**, *25*, 571.

[9] (a) Sui-Seng, C.; Enright, G. D.; Zargarian, D. *J. Am. Chem. Soc.*, accepted with minor revisions. (b) Guérin, F.; Beddie, C. L.; Stephan, D. W.; v. H. Spence, E.; Wurz, R. *Organometallics* **2001**, *20*, 3466. (c) Deck, P. A.; Fronczek, F. R. *Organometallics* **2000**, *19*, 327. (d) Blenkiron, P; Enright, G. D.; Taylor, N. J.; Carty, A. J. *Organometallics* **1996**, *15*, 2855. (e) Thorn, M. G.; Fanwick, P. E.; Chesnut, R. W.; Rothwell, I. P. *Chem. Comm.* **1999**, 2543. (f) Radius, U.; Sundermeyer, J.; Peters, K.; v. Schering, H. G. Z. *Anorg. Allg. Chem.* **2002**, *628*, 1226.

[10] Une étude similaire sur le composé (COD)Pt(η^1-Cp)Me avait également permis de montrer par comparaison des distances platine-carbone que le Cp possédait une

influence trans inférieure à celle du Me: Day, C. S. ; Day, V. D. ; Shaver, A. ; Clark, H. C. *Inorg. Chem.* **1981**, *20*, 2188.

[11] (a) Syed, A.; Stevens, E. D.; Cruz, S. G. *Inorg. Chem.* **1984**, *23*, 3673. (b) Howard, J. A. K. *Acta Cryst.* **1982**, *B38*, 2896. (c) Chetcuti, M.; Howard, J. A. K.; Pfeffer, M.; Spencer, J. L.; Stone, F. G. A. *J. Chem. Soc. Dalton Trans.* **1981**, 276.

[12] (a) Fontaine, F. -G.; Kadkhodazadeh, T.; Zargarian, D. *J. Chem. Soc., Chem. Commun.* **1998**, 1253. (b) Fontaine, F.-G.; Zargarian, D. *Organometallics* **2002**, *21*, 401. (c) Fontaine, F.-G.; Nguyen, R.-V.; Zargarian, D. *Can. J. Chem.* **2003**, *81*, 1299. Chen, Y.; Sui-Seng, C.; Zargarian, D. *Organometallics* **2005**, *24*, 149. (d) Groux, L. F.; Zargarian D. *Organometallics* **2003**, *22*, 4759. (e) Gareau, D.; Sui-Seng, C.; Groux, L. F.; Brisse, F.; Zargarian, D. *Organometallics* **2005**, *24*, 4003.

[13] Fu, P.-F.; Brard, L.; Li, Y.; Marks, T. J. *J. Am. Chem. Soc.* **1995**, *117*, 7157.

[14] McDermott, J. X.; White, J. F.; Whitesides, G. M. *J. Am. Chem. Soc.* **1976**, *98*, 6521.

[15] Manzer, L. E.; Clark. H. C. *J. Organomet. Chem.* **1973**, *59*, 411.

[16] Gottlieb, H. E.; Kotlyar, V.; Nudelman, A. *J. Org. Chem.* **1997**, *62*, 7512.

[17] *SMART*, Release 5.059; Bruker Molecular Analysis Research Tool, Bruker AXS Inc.: Madison, WI 53719-1173, 1999.

[18] *SMART*, Release 5.059; Bruker Molecular Analysis Research Tool, Bruker AXS Inc.: Madison, WI 53719-1173, 1999.

[19] Sheldrick, G. M. *SHELXS*. Program for the solution of Crystal Structures. University of Goettingen. Germany, 1997.

[20] Sheldrick, G. M. *SHELXL*. Program for the Refinement of Crystal Structures. University of Goettingen. Germany, 1997.

Chapitre 7: Conclusion générale et perspectives

Contrairement à la chimie des complexes indényles du nickel, qui a connu un important développement ces dernières années et a permis de mettre en évidence l'étendue de leur potentiel catalytique, celle des composés indényles de palladium et de platine est restée relativement peu explorée et ne compte que quelques exemples dans la littérature, obtenus pour la plupart de manière fortuite.[1] L'objectif principal de cette thèse consiste donc à mettre au point des voies d'accès fiables pour l'obtention des composés indényles du palladium et du platine, à explorer leurs réactivités, et ainsi à mieux cerner l'influence du centre métallique sur la chimie de ces composés indényles.

Une vaste gamme de nouveaux complexes Ind de Pd et de Pt comportant des ligands phosphines, halogénures, alkyles ou encore isocyanures et amines a ainsi été préparée, ce qui avait déjà été réalisé dans le cas du Ni. L'étude de leurs réactivités a ensuite permis de souligner les différences de comportement existantes au sein de cette famille de composés, envers les oléfines et les silanes.

Ce chapitre de conclusion consistera donc à faire le point sur les méthodes établies pour la préparation des complexes Ind de Pd et de Pt. Les points saillants de leurs caractéristiques structurales en solution et à l'état solide seront discutés, de même que leurs réactivités. Quelques perspectives de travaux futurs y seront également présentées.

Synthèse et caractérisation des composés indényles de palladium.

Plusieurs méthodes de synthèse ont été établies au cours de ce travail et ont permis l'obtention d'une vingtaine de nouveaux composés indényles de palladium. Les méthodes employées habituellement pour la préparation des composés Ind-Ni, telles que l'addition d'IndLi sur $(PPh_3)_2PdCl_2$ ou l'addition oxydante du 1-Br-IndH sur $Pd(PPh_3)_4$ se sont avérées infructueuses dans le cas du Pd et ont toutes deux conduit à la formation de 1,1'-biindène. L'addition métathétique du (1-R-Ind)Li, (R = H, Me) sur

le précurseur halogéné $(PhCN)_2PdCl_2$ a permis d'éviter cette réaction d'homocouplage, et après addition de phosphine PR'$_3$ (R' = Ph, Cy, Me, OMe), des composés du type (1-R-Ind)Pd(PR'$_3$)Cl ont pu être isolés (Figure 7.1). L'inconvénient majeur de cette méthode est que les rendements obtenus sont modestes et ne s'élèvent pas à plus de 30%, ce qui est dû à la décomposition graduelle du précurseur métallique sous l'action de l'IndLi. Cette approche, initialement développée dans le cadre du chapitre 2, a ensuite été mise à profit pour l'obtention d'un dérivé comportant un ligand Ind stériquement plus encombré, le (1-Me_3Si-Ind)Pd(PPh_3)Cl (chapitre 5). Étant donné les faibles rendements obtenus selon cette méthode, une autre voie synthétique hautement efficace pour la préparation d'un complexe Ind de Pd(II), n'impliquant plus une source anionique d'indényle, a été développée par addition oxydante du 1-Me_3Si-IndH sur le Na_2PdCl_4, et a mené à la formation du dimère [(η^3-Ind)Pd(μ-Cl)]$_2$. Ce dernier s'est ensuite avéré être un excellent précurseur pour l'obtention d'autres types de complexes η^1- ou ($\eta^3 \leftrightarrow \eta^5$)-Ind de Pd par simple addition de deux équivalents de ligand L (L = PR'$_3$, *t*-BuNC, NEt_3, $BnNH_2$, py) (Figures 7.1 et 7.2). Cependant, cette méthode se limite à l'obtention de complexes comportant un Ind non substitué puisque la préparation du dimère analogue substitué [(η^3-1-R-Ind)Pd(μ-Cl)]$_2$ n'a pas pu être effectuée par addition oxydante du (1,3-R-Me_3Si-Ind)H sur Na_2PdCl_4.

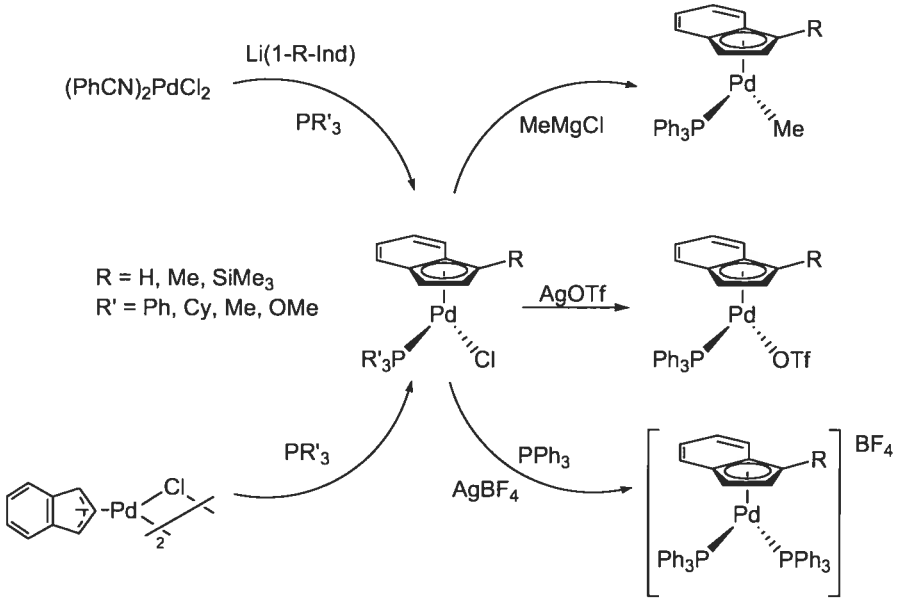

Figure 7.1

Au cours du chapitre 3, nous nous sommes intéressés à l'influence du ligand anionique X sur les structures et réactivités des composés. Dans ce cadre, les dérivés (1-R-Ind)Pd(PPh_3)X (X = Me, OTf, PPh_3) ont donc été préparés par addition respective de MeMgCl, AgOTf et $AgBF_4/PPh_3$ sur les composés (1-R-Ind)Pd(PPh_3)Cl (Figure 7.1). La substitution du ligand triflate du complexe (η-Ind)Pd(PPh_3)(OTf) a ensuite permis de générer de nouvelles espèces cationiques aisément [(η-Ind)Pd(PPh_3)(L)][OTf] (L = PR_3, CH_3CN, PhCN, t-BuNC).

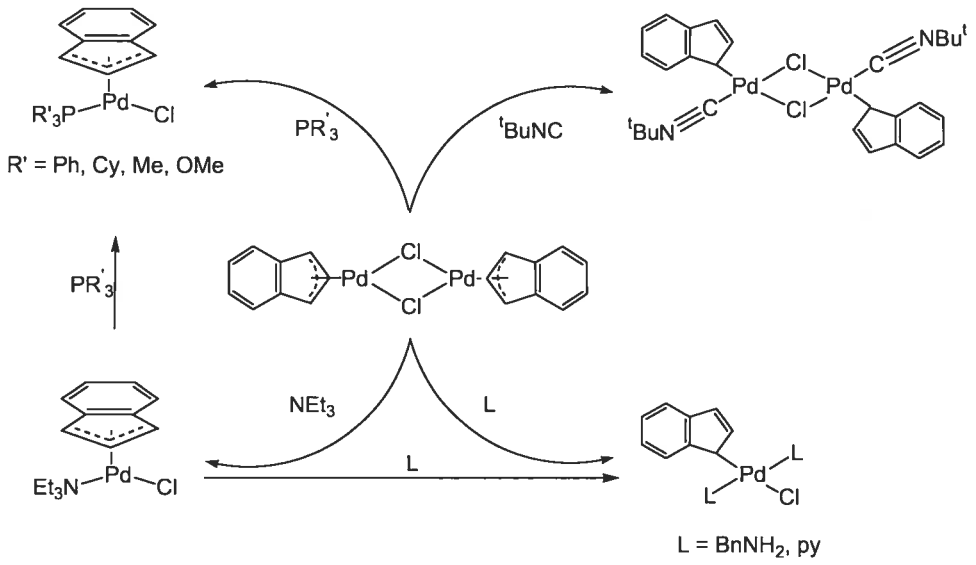

Figure 7.2

Un aspect important à souligner dans ces réactions est l'impact de la nature du ligand L ajouté au dimère précurseur [(η^3-Ind)Pd(μ-Cl)]$_2$ sur l'hapticité de l'indényle dans le nouveau complexe formé. Il apparaît qu'en présence de phosphines et triéthylamine, les complexes résultants comportent un ligand Ind d'hapticité ($\eta^3 \leftrightarrow \eta^5$) tandis qu'avec la benzylamine, la pyridine ou le *t*-butylisocyanure, une hapticité η^1 est favorisée. L'addition simultanée de PR'$_3$ (R' = Ph, Cy) et de $BnNH_2$ sur le dimère [(η^3-Ind)Pd(μ-Cl)]$_2$ a quant à elle permis d'isoler les espèces η^1-Ind mixtes de formule (PR'$_3$)($BnNH_2$)Pd(η^1-Ind)Cl, qui ont également été formées par addition de $BnNH_2$ sur les complexes (η-Ind)Pd(PR'$_3$)Cl correspondants. En solution, il a été démontré que

ces complexes subissaient alors une transformation graduelle pour générer des composés dinucléaires de Pd(I), (μ,η^3-Ind)(μ-Cl)$Pd_2(PR'_3)_2$ qui contiennent un ligand indényle et chlorure pontant sur les deux centres métalliques, ainsi que les composés $(BnNH_2)(PR'_3)PdCl_2$ et du 1,1'-biindène (Chapitre 4). Ces espèces dinucléaires de Pd(I) sont le résultat d'une réaction de comproportionnation entre les complexes Ind-Pd(II) et des espèces de $Pd(0)(PR_3)_n$ générées in situ et se disproportionnent lentement en solution pour régénérer leur précurseur (Figure 7.3).

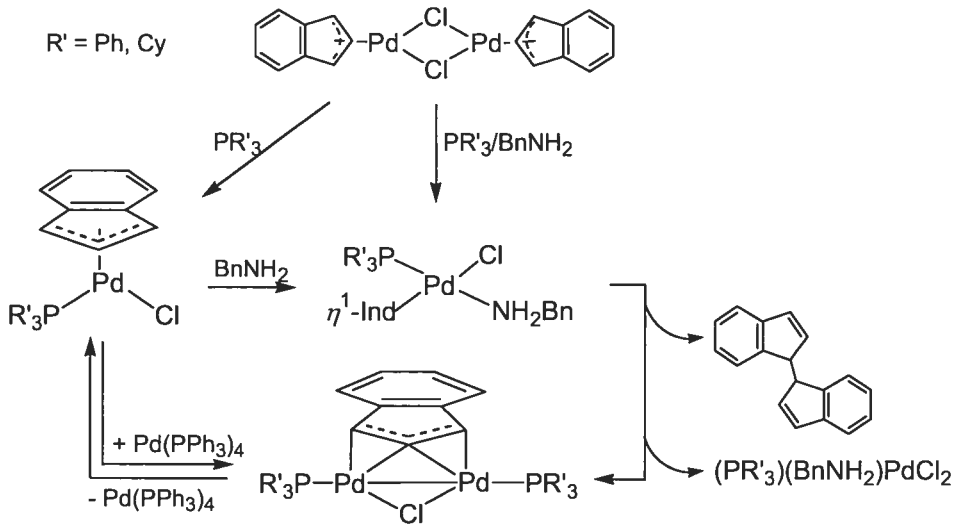

Figure 7.3

La plupart des composés Ind de Pd préparés au cours de ces travaux sont thermiquement stables à l'air et en solution, contrairement aux composés Ind-Ni, et ont pu être caractérisés par voltammétrie cyclique, spectroscopie RMN, analyse élémentaire et diffraction des rayons X. Comme attendu, les études électrochimiques ont démontré que les potentiels de réduction des composés Ind de Pd variaient en fonction de la richesse électronique du centre métallique et présentaient en conséquence pour E_{red} des valeurs inférieures à celles obtenues pour les composés Ind-Ni analogues. Il serait donc intuitif de prévoir que les composés Ind-Pd étant plus riches en électrons présentent des hapticités inférieures à celles des composés Ind-Ni analogues. De nombreuses informations sur l'hapticité de l'indényle dans ces

composés ont pu être extraites des analyses RMN et des études cristallographiques. En solution, les spectres RMN des composés η^1-Ind se différenciaient aisément de ceux des composés η-Ind notamment par les valeurs de déplacements chimiques observées pour les carbones C1 directement liés au Pd pour les complexes η^1-Ind (pour un complexe η^1-Ind, $\delta_{C1} \sim 40$ ppm versus 95-115 ppm pour un complexe η-Ind). De plus, le calcul du paramètre $\Delta\delta^{13}C$ a permis d'identifier pour chacun des composés le type d'interaction métal-indényle. Les composés étudiés de formule (η-Ind)Pd(L)(X) (L = PR_3, NEt_3; X = Cl, Me, OTf) présentent des valeurs de $\Delta\delta^{13}C$ variant entre 6.3 et 8.8 ppm, ce qui traduit une distorsion $\eta^3 \leftrightarrow \eta^5$ dans la coordination de l'indényle sur le centre métallique. Cette interaction dissymétrique en solution fut également confirmée par la suite à l'état solide, grâce aux études cristallographiques (Figure 7.4).

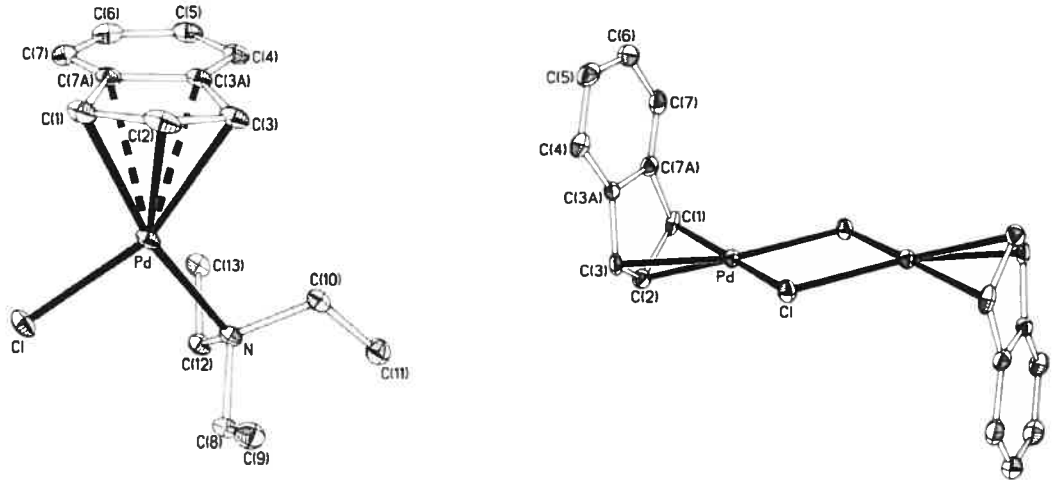

Figure 7.4: Dessins ORTEP du (η-Ind)Pd(NEt_3)Cl et du [(η^3-Ind)Pd(μ-Cl)$_2$]

Le Pd adopte une géométrie pseudo plan-carrée avec des distances Pd-C3a et Pd-C7a plus longues que les distances Pd-C1, Pd-C2 et Pd-C3, confirmant l'hapticité $\eta^3 \leftrightarrow \eta^5$ déjà observée en solution. Les valeurs des paramètres Δ(M-C), HA, et FA correspondent eux aussi à des situations intermédiaires de coordination $\eta^3 \leftrightarrow \eta^5$ ($\Delta M\text{-}C_{moy} = 0.35$ Å, $HA_{moy} = 14.2°$ et $FA_{moy} = 13.5°$) avec une tendance vers un état η^3 plus prononcé dans le cas du complexe [(η^3-Ind)Pd(μ-Cl)$_2$] (ΔM-C = 0.46 Å, HA = 17.3° et FA = 16.4°) (Figure 7.4), ce qui est bien supérieur à la distorsion observée pour les

complexes Ind de Ni(II) analogues (ΔM-C_{moy} = 0.25 Å, HA_{moy} = 11.0° et FA_{moy} = 11.7°). Dans le cas des complexes (μ,η^3-Ind)(μ-Cl)$Pd_2(PR'_3)_2$ (R' = Ph, Cy), le ligand indényle adopte par contre un mode de coordination η^3 peu commun et ponte sur les deux centres métalliques simultanément (Figure 7.5). Bien que plusieurs exemples de complexes dinucléaires de Pd(I) comportant des ligands pontants μ-Cp ou μ-allyl aient déjà été rapportés dans la littérature,[2] seul un exemple de complexe (μ,η^3-Ind) de Pd(I) avait été décrit.[3] Les valeurs des paramètres Δ(M-C) obtenus pour ces complexes confirment par ailleurs leur trihapticité (Δ(M-C) ~ 0.85 Å).

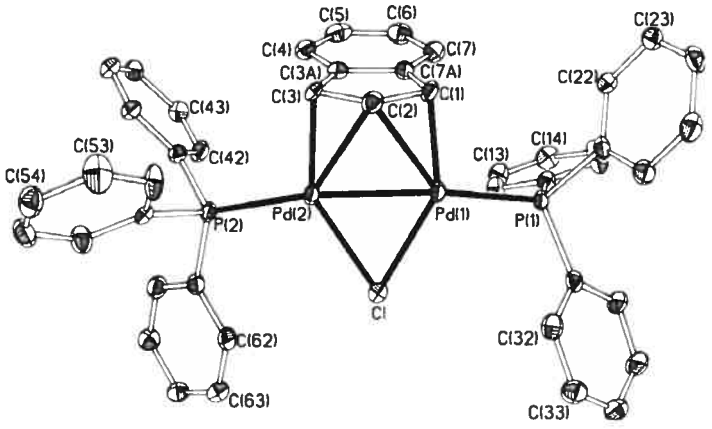

Figure 7.5: Dessin ORTEP du (μ,η^3-Ind)(μ-Cl)$Pd_2(PPh_3)_2$

Réactivité des composés indényles de palladium.

L'exploration de la réactivité des complexes Ind de Pd(II) obtenus, dans les réactions avec les oléfines a démontré qu'ils possédaient une activité catalytique supérieure à celle des complexes Ind de Ni(II), notamment dans la polymérisation de l'éthylène, en présence de MAO (activité catalytique du composé (η-Ind)Pd(PPh_3)Cl = 204 kg de PE mol^{-1} h^{-1} versus 50 kg de PE mol^{-1} h^{-1} pour le complexe (1-Me-Ind)Ni(PPh_3)Cl).

En contrepartie, les études de réactivité des composés Ind de Pd(II) en présence de silanes, en particulier le $PhSiH_3$, ont démontré qu'ils possédaient des activités bien plus modestes (environ 20% de $PhSiH_3$ consommé pour les complexes (η-Ind)Pd(L)(X) (L = PR_3; X = Cl, Me, OTf), que celles obtenues avec les complexes Ind-Ni (conversion quasi quantitative du $PhSiH_3$ en polyphénylsilanes linéaires et cycliques). L'ajout d'un substituant plus encombrant sur l'Ind a donc été envisagé, mais le composé résultant, le (1-Me_3Si-Ind)Pd(PPh_3)Cl, n'a guère présenté d'activité supérieure. Il serait maintenant intéressant d'étudier l'effet qu'apporterait la présence d'un indényle disubstitué sur les complexes Ind de Pd(II), comme le (1,3-$(Me_3Si)_2$-Ind) et de constater si, comme dans le cas des composés du Ni,[4] on assisterait à une amélioration considérable des activités catalytiques. Les complexes Ind de Pd(II) se sont également avérés très efficaces comme catalyseur dans l'addition du $HSiCl_3$ au styrène pour donner du 1-phényl-1-(trichlorosilyl)éthane, et au phénylacétylène pour donner les produits d'addition α, $Ph(SiCl_3)C{=}CH_2$, et β, (*E*)-$PhCH{=}CHSiCl_3$. Par contre, contrairement aux composés Ind-Ni analogues, en présence de $PhSiH_3$, $HSiEt_3$, $HSi(OEt)_3$ ou $HSiMe_2Cl$, les réactions d'hydrosilylation du styrène ont été infructueuses.

L'obtention de complexes triflates de Pd(II) (1-R-Ind)Pd(PPh_3)(OTf) nous a ensuite incité à tester leur comportement envers les oléfines. Cette étude a permis de montrer que tout comme les complexes (1-R-Ind)Ni(PPh_3)(OTf), ils constituaient d'efficaces catalyseurs pour l'isomérisation du 1-hexène en *E*- et *Z*-2-hexène (ca. 3:1), et pour la dimérisation de l'éthylène en *E*- et *Z*-2-butènes (Figure 7.6). Cependant, Les réactions envers différents dérivés du styrène ont également été examinées, ce qui a donné les résultats suivants: le styrène est quantitativement et exclusivement converti en l'isomère tête à queue du dimère, le (*Z*)-1,3-diphényl-1-butène; le *p*-fluoro-styrène est converti en un mélange 65 : 35 de dimère et trimère linéaires; le *p*-NH_2-styrène et le *p*-Me-styrène sont quantitativement oligomérisés (M_w ~1050, M_w/M_n ~ 1.3, 100 turnovers pour le premier et M_w ~1250, M_w/M_n ~ 1.4, 885 turnovers pour le second),

tandis que le *p*-MeO-styrene est polymérisé (M_w ~ 29000, M_w/M_n ~ 3.2, 970 turnovers) (Figure 7.6).

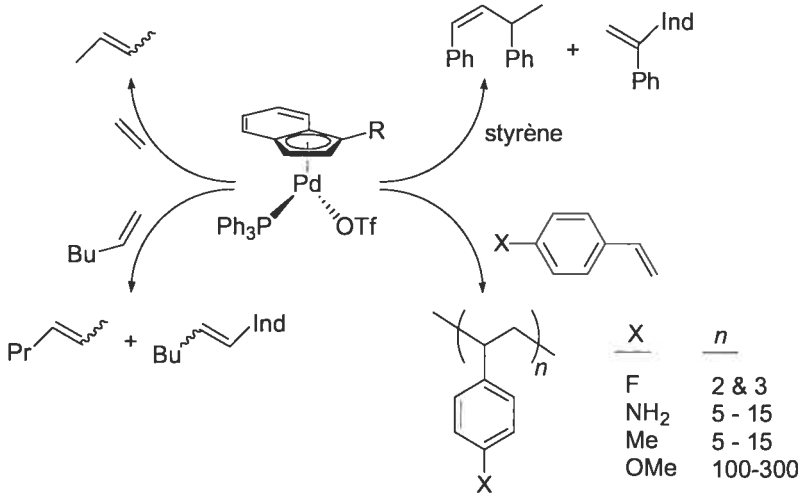

Figure 7.6

Comme l'illustre la figure 7.7, un mécanisme impliquant une espèce active Pd-H cationique a été proposé pour expliquer l'ensemble de ces réactions:

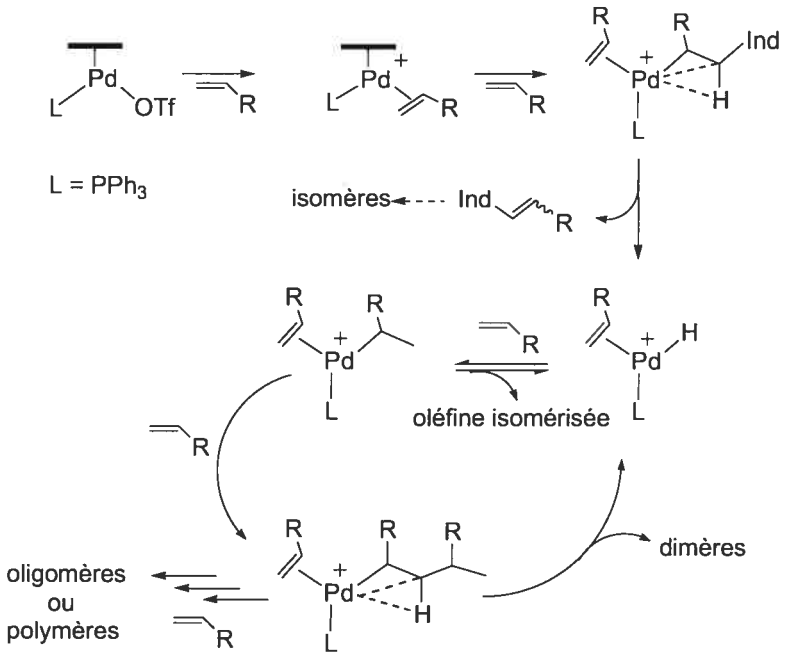

Figure 7.7

Enfin, les études préliminaires de la réactivité du composé (1-Me_3Si-Ind)Pd(PPh_3)Cl en ce qui a trait à la formation de liens C-C et C-N a permis de démontrer que celui-ci catalysait efficacement le couplage dit de Heck, du styrène avec l'iodo- et le bromo-benzène, ainsi que l'amination d'halogénures d'aryles. Il serait maintenant de mise de vérifier l'applicabilité de ces systèmes catalytiques pour les réactions de couplage d'autres substrats organiques afin d'en définir les limites. Il faudrait ensuite optimiser les conditions expérimentales en faisant varier les quantités de substrat, de catalyseur, le solvant et la température.

Un autre aspect intéressant à développer pour compléter cette étude, serait d'explorer les réactivités des composés (η^1-Ind) de Pd obtenus, tels que le $L_2Pd(\eta^1$-Ind)Cl (L = $BnNH_2$, py) et le (PR_3)($BnNH_2$)Pd(η^1-Ind)Cl, ainsi que celles du composé amino-Pd, (η-Ind)Pd(NEt_3)Cl, afin de pouvoir comparer leurs réactivités catalytiques à celles des composés phosphines.

Préparation et réactivité des composés indényles de platine.

Le protocole mis au point pour l'obtention de complexes Ind du Pt(II) repose sur l'addition métathétique d'IndLi sur des précurseurs du type (COD)PtClX (X = Cl, Me). Des composés η^1-Ind de formule (COD)Pt(η^1-Ind)X (X = Cl, η^1-Ind, Me) ont ainsi été isolés avec des rendements satisfaisants. La conversion du complexe (COD)Pt(η^1-Ind)$_2$ en [(η-Ind)Pt(COD)][BF_4] a ensuite été effectuée par addition de HBF_4. Un point important soulevé par cette étude met en évidence la tendance des complexes Ind de Pt à adopter un mode de coordination η^1. Contrairement au Ni, où les composés Ind obtenus jusqu'à lors comportent un ligand ($\eta^5 \leftrightarrow \eta^3$)-Ind, les composés Ind de Pd et Pt, plus riches en électrons, semblent adopter plus fréquemment une monohapticité. Une perspective envisageable pour inciter une hapticité supérieure pourrait être d'utiliser des ligands indényles comportant des substituants électroattracteurs et ainsi persuader le platine à se lier plus fortement à l'indényle. Pour la première fois, ces complexes ont pu être entièrement caractérisés, y compris par

diffraction des rayons X, ce qui a permis d'obtenir des informations sur les interactions M-Ind. En effet, les structures à l'état solide des complexes cationiques $[(\eta\text{-Ind})PtL_2]^+$ (L_2 = COD, $(PPh_3)_2$) ont permis de mettre en évidence la distorsion $\eta^5 \leftrightarrow \eta^3$ de l'Ind, qui dans le cas du COD est plus prononcée. Les études préliminaires des réactivités de ces composés ont montré qu'ils pouvaient promouvoir la redistribution du $PhSiH_3$ et son addition sur le styrène. Il serait donc pertinent d'examiner quelles sont les limites de ce système et d'essayer d'autres substrats tels que les alcynes, les cétones et les imines ainsi que divers silanes autres que le $PhSiH_3$.

L'obtention de complexes Ind de Pt(IV) constitue également un défi intéressant à relever qui n'a pu être exploré au cours de cette thèse. L'isolation de tels composés permettrait de voir l'influence du degré d'oxydation du centre métallique sur les réactivités et structures des complexes. Quelques méthodes de synthèse impliquant par exemple le complexe (COD)Pt(η^1-Ind)Me en présence d'agents oxydants tels que Me-X (X = Br,[5] I,[5] OTf[6]), Ph_2IOTf[7] pourraient se révéler efficaces.

Références

[1] Zargarian, D. *Coord. Chem. Rev.* **2002**, *233-234*, 157.

[2] Pour une revue portant sur les composés dinucléaires de Pd(I), voir: (a) Murahashi, T.; Kurosawa, H. *Coord. Chem. Rev.* **2002**, *231*, 207. (b) Werner, *Adv. Organomet. Chem.* **1981**, *19*, 155.

[3] (a) Tanase, T.; Nomura, T; Yamamoto, Y.; Kobayashi, K. *J. Organomet. Chem.* **1991**, *410*, C25. (b) Tanase, T.; Nomura, T.; Fukushina, T.; Yamamoto, Y.; Kobayashi, K. *Inorg. Chem.* **1993**, *32*, 4578.

[4] Chen, Y.; Sui-Seng, C.; Boucher, S.; Zargarian, D. *Organometallics* **2005**, *24*, 149.

[5] Felice, V. D.; Giovannitti, B.; Renzi, A. D.; Tesauro, D.; Panunzi, A. *J. Organomet. Chem.* **2000**, *593-594*, 445.

[6] Bayler, A.; Canty, A. J.; Edwards, P.; Skelton, B. W.; White, A. H. *J. Chem. Soc., Dalton Trans.* **2000**, 3325.

[7] Canty, A. J.; Patel, J.; Rodermann, T.; Ryan, J. H.; Skelton, B. W.; White, A. H. *Organometallics* **2004**, *23*, 3466.

Annexes

Annexe 1: Informations supplémentaires des chapitres II, III et IV

Les rapports cristallographiques et les fichiers cif des structures des composés parus dans les chapitres II, III et IV sont téléchargeables à partir du site internet suivant: http://pubs.acs.org. Ces données ont été déposées au 'Cambridge Crystallographic Data Centre' (CCDC) et sont également téléchargeables via le site internet de CCDC: www.ccdc.cam.ac.uk/data_request/cif, ou en envoyant un message électronique à: data_request@ccdc.cam.ac.uk, ou par courrier, en contactant the Cambridge Crystallographic Data Centre, 12, Union Road, Cambridge CB2 1EZ, UK; fax: +44 1223 336033.

	Composé	N° CCDC
Chapitre II	(Ind)Pd(PPh_3)Cl (**4**)	236386
	(1-Me-Ind)Pd(PPh_3)Cl (**5**)	236387
	{(η^3-Ind)Pd(μ-Cl)}$_2$ (**6**)	236388
	(Ind)Pd(PCy_3)Cl (**7**)	236389
	IndPd($P(OMe)_3$)Cl (**9**)	236390
	[(η^1-Ind)$_2$(t-BuNC)$_2$Pd(μ-Cl)$_2$] (**10**)	236385
Chapitre III	(Ind)Pd(PPh_3)(Me) (**3**)	283700
	[(Ind)Pd(PPh_3)$_2$]BF_4 (**5**)	283701
	[(1-Me-Ind)Pd(PPh_3)$_2$]BF_4 (**6**)	283702
	(Ind)Pd(PPh_3)(OTf) (**7**)	283703
Chapitre IV	(η-Ind)Pd(NEt_3)Cl, (**3**)	296295
	(η^1-Ind)Pd($BnNH_2$)$_2$Cl, (**4**)	296296
	(η^1-Ind)Pd(Py)$_2$Cl, (**5**)	296297
	(η^1-Ind)Pd(PCy_3)($BnNH_2$)Cl, (**6a**)	296298
	(μ,η^3-Ind)(μ-Cl)Pd$_2$(PCy_3)$_2$, (**7a**)	296299
	. (μ,η^3-Ind)(μ-Cl)Pd$_2$(PPh_3)$_2$ (**7b**)	296300
	($BnNH_2$)(PCy_3)$PdCl_2$, (**8a**)	296301

Annexe 2: Informations supplémentaires du chapitre V

Rapport cristallographique de la structure du composé (1-$SiMe_3$-Ind)Pd(PPh_3)Cl (**1**).

Table 1. Crystal data and structure refinement for C30 H30 Cl P Pd Si.

Identification code	suse20
Empirical formula	C30 H30 Cl P Pd Si
Formula weight	591.45
Temperature	293(2)K
Wavelength	1.54178 Å
Crystal system	Triclinic
Space group	P-1
Unit cell dimensions	a = 15.8783(4) Å α = 82.496(2)° b = 17.4154(4) Å β = 65.690(2)° c = 17.9389(5) Å γ = 81.820(2)°
Volume	4460.5(2)$Å^3$
Z	6
Density (calculated)	1.321 Mg/m^3
Absorption coefficient	6.861 mm^{-1}
F(000)	1812
Crystal size	0.39 x 0.18 x 0.05 mm
Theta range for data collection	2.57 to 73.10°
Index ranges	$-19 \le h \le 18$, $-21 \le k \le 21$, $-22 \le \lambda \le 21$
Reflections collected	55033
Independent reflections	17093 [R_{int} = 0.030]
Absorption correction	Semi-empirical from equivalents
Max. and min. transmission	0.7700 and 0.4300
Refinement method	Full-matrix least-squares on F^2
Data / restraints / parameters	17093 / 0 / 928
Goodness-of-fit on F^2	0.926
Final R indices [I>2sigma(I)]	R_1 = 0.0379, wR_2 = 0.0859
R indices (all data)	R_1 = 0.0526, wR_2 = 0.0895
Largest diff. peak and hole	0.615 and -0.309 e/$Å^3$

Table 2. Atomic coordinates (x 10^4) and equivalent isotropic displacement parameters ($Å^2$ x 10^3) for C30 H30 Cl P Pd Si.

U_{eq} is defined as one third of the trace of the orthogonalized Uij tensor.

	x	y	z	U_{eq}
Pd	6185(1)	1316(1)	850(1)	43(1)
P	6087(1)	2370(1)	-10(1)	40(1)
Cl	6935(1)	1930(1)	1457(1)	68(1)
C(1)	5751(3)	210(2)	1734(2)	50(1)
C(3)	5543(3)	466(2)	528(2)	49(1)
C(3A)	4662(3)	703(2)	1171(2)	48(1)
C(4)	3817(3)	1039(2)	1169(3)	64(1)
C(5)	3112(3)	1224(3)	1896(4)	84(2)
C(6)	3216(3)	1086(3)	2625(3)	90(2)
C(7)	4056(3)	758(3)	2649(3)	73(1)
C(7A)	4785(3)	563(2)	1925(2)	50(1)
Si	6291(1)	-138(1)	2484(1)	76(1)
C(8)	5780(4)	-1040(3)	3086(3)	111(2)
C(9)	6061(4)	607(3)	3215(3)	122(2)
C(22)	7561(3)	-359(3)	1874(4)	120(2)
C(110)	7136(2)	2675(2)	-841(2)	39(1)
C(111)	7125(3)	3096(2)	-1553(2)	52(1)
C(112)	7921(3)	3360(2)	-2149(3)	62(1)
C(113)	8739(3)	3215(2)	-2047(3)	61(1)
C(114)	8767(3)	2796(2)	-1353(3)	57(1)
C(115)	7963(2)	2525(2)	-748(2)	44(1)
C(120)	5311(2)	2291(2)	-503(2)	42(1)
C(121)	4435(2)	2692(2)	-270(2)	51(1)
C(122)	3841(3)	2552(2)	-620(3)	61(1)
C(123)	4118(3)	2027(2)	-1202(2)	60(1)
C(124)	4999(3)	1639(2)	-1450(2)	56(1)
C(125)	5593(2)	1763(2)	-1107(2)	49(1)
C(130)	5585(2)	3222(2)	573(2)	43(1)
C(131)	5846(3)	3958(2)	259(2)	50(1)
C(132)	5414(3)	4587(2)	720(3)	63(1)
C(133)	4719(3)	4498(3)	1478(3)	67(1)
C(134)	4459(3)	3768(3)	1801(3)	71(1)
C(135)	4891(3)	3127(2)	1356(2)	61(1)
Pd(1)	450(1)	1727(1)	1009(1)	38(1)
P(1)	467(1)	2974(1)	460(1)	38(1)
Cl(1)	2025(1)	1367(1)	265(1)	56(1)
C(21)	38(2)	635(2)	1890(2)	41(1)
C(28)	-685(2)	981(2)	1658(2)	48(1)
C(27)	-971(2)	1735(2)	1933(2)	48(1)
C(13A)	-577(2)	1808(2)	2523(2)	44(1)
C(26)	-676(3)	2393(2)	3016(2)	57(1)
C(25)	-156(3)	2309(3)	3480(3)	67(1)
C(24)	467(3)	1675(3)	3453(2)	62(1)
C(23)	580(3)	1065(2)	2962(2)	52(1)
C(17A)	56(2)	1131(2)	2490(2)	42(1)
Si(1)	629(1)	-372(1)	1648(1)	51(1)
C(18)	-90(3)	-1040(2)	2507(3)	72(1)
C(19)	1838(3)	-484(2)	1586(3)	69(1)
C(20)	624(3)	-565(2)	656(3)	83(2)
C(2)	6131(3)	62(2)	899(3)	50(1)

C(140)	-647(2)	3549(2)	901(2)	36(1)
C(141)	-1383(2)	3359(2)	749(2)	49(1)
C(142)	-2268(3)	3725(2)	1117(3)	59(1)
C(143)	-2428(3)	4281(2)	1651(3)	57(1)
C(144)	-1712(3)	4483(2)	1801(2)	56(1)
C(145)	-821(2)	4116(2)	1427(2)	46(1)
C(150)	755(2)	3116(2)	-642(2)	40(1)
C(151)	454(3)	3792(2)	-999(2)	51(1)
C(152)	674(3)	3866(2)	-1834(2)	55(1)
C(153)	1188(3)	3279(2)	-2316(2)	57(1)
C(154)	1481(3)	2608(2)	-1962(2)	55(1)
C(155)	1264(2)	2516(2)	-1134(2)	48(1)
C(160)	1263(2)	3498(2)	659(2)	41(1)
C(161)	1551(3)	4200(2)	244(3)	61(1)
C(162)	2108(3)	4594(3)	454(3)	81(2)
C(163)	2382(3)	4299(3)	1076(3)	76(1)
C(164)	2097(3)	3601(3)	1487(3)	66(1)
C(165)	1547(2)	3193(2)	1275(2)	52(1)
Pd(2)	7108(1)	5020(1)	5361(1)	38(1)
P(2)	6516(1)	3858(1)	5584(1)	38(1)
Cl(2)	7183(1)	4978(1)	6642(1)	53(1)
C(21)	7768(2)	6179(2)	4721(2)	44(1)
C(22)	7091(2)	5990(2)	4460(2)	47(1)
C(23)	7410(3)	5285(2)	4069(2)	48(1)
C(23A)	8399(3)	5110(2)	3902(2)	45(1)
C(24)	9086(3)	4549(2)	3467(2)	62(1)
C(25)	9968(3)	4546(3)	3423(3)	71(1)
C(26)	10182(3)	5073(3)	3810(3)	69(1)
C(27)	9516(3)	5625(2)	4258(2)	56(1)
C(27A)	8613(3)	5659(2)	4306(2)	45(1)
Si(2)	7651(1)	7062(1)	5251(1)	61(1)
C(28)	8271(4)	7809(3)	4432(3)	119(2)
C(29)	8191(3)	6860(3)	6016(3)	82(1)
C(30)	6399(3)	7392(3)	5779(3)	103(2)
C(170)	5351(2)	3790(2)	6392(2)	41(1)
C(171)	5106(3)	4164(2)	7098(2)	56(1)
C(172)	4247(3)	4095(2)	7729(3)	64(1)
C(173)	3614(3)	3679(2)	7671(3)	59(1)
C(174)	3855(3)	3312(2)	6972(3)	59(1)
C(175)	4723(2)	3355(2)	6339(2)	50(1)
C(180)	6408(2)	3527(2)	4708(2)	42(1)
C(181)	5811(2)	3976(2)	4383(2)	52(1)
C(182)	5693(3)	3751(3)	3727(2)	61(1)
C(183)	6165(3)	3089(3)	3373(3)	68(1)
C(184)	6752(3)	2647(3)	3675(3)	73(1)
C(185)	6882(3)	2859(2)	4345(2)	56(1)
C(190)	7252(2)	3089(2)	5886(2)	43(1)
C(191)	6888(3)	2469(2)	6438(3)	64(1)
C(192)	7464(3)	1899(3)	6648(3)	87(2)
C(193)	8402(4)	1951(3)	6323(3)	85(2)
C(194)	8770(3)	2563(3)	5776(3)	76(1)
C(195)	8193(3)	3138(2)	5562(3)	61(1)

Table 3. Hydrogen coordinates (x 10^4) and isotropic displacement parameters ($Å^2$ x 10^3) for C30 H30 Cl P Pd Si.

	x	y	z	U_{eq}
H(2)	6677	-249	634	60
H(3)	5697	562	-33	58
H(4)	3733	1136	681	77
H(5)	2545	1449	1896	100
H(6)	2718	1215	3110	108
H(7)	4126	670	3144	87
H(8A)	5116	-940	3336	166
H(8B)	6014	-1193	3504	166
H(8C)	5946	-1450	2726	166
H(9A)	6484	999	2958	182
H(9B)	6146	365	3695	182
H(9C)	5435	844	3370	182
H(10A)	7654	-743	1501	181
H(10B)	7861	-556	2237	181
H(10C)	7820	107	1569	181
H(111)	6571	3199	-1625	63
H(112)	7907	3638	-2624	75
H(113)	9276	3401	-2449	73
H(114)	9325	2692	-1289	68
H(115)	7983	2242	-278	53
H(121)	4245	3055	119	62
H(122)	3250	2817	-457	73
H(123)	3716	1932	-1430	72
H(124)	5191	1291	-1854	67
H(125)	6183	1495	-1275	58
H(131)	6312	4031	-263	60
H(132)	5602	5080	507	75
H(133)	4423	4929	1776	80
H(134)	3988	3704	2322	86
H(135)	4717	2632	1582	73
H(12)	-936	748	1368	58
H(13)	-1344	2118	1768	57
H(14)	-1087	2835	3033	68
H(15)	-231	2696	3820	81
H(16)	821	1644	3762	74
H(17)	995	629	2953	62
H(18A)	-694	-1021	2501	107
H(18B)	-150	-880	3020	107
H(18C)	206	-1562	2441	107
H(19A)	2120	-998	1438	104
H(19B)	1829	-406	2110	104
H(19C)	2190	-106	1180	104
H(20A)	969	-1058	492	125
H(20B)	905	-161	245	125
H(20C)	-4	-577	718	125
H(141)	-1276	2978	393	59
H(142)	-2751	3598	1004	70
H(143)	-3024	4521	1912	69
H(144)	-1823	4867	2155	67
H(145)	-339	4254	1534	55
H(151)	105	4196	-678	61
H(152)	470	4320	-2071	66
H(153)	1337	3334	-2878	69
H(154)	1831	2208	-2288	66

H(155)	1458	2054	-901	57
H(161)	1371	4409	-178	73
H(162)	2300	5067	170	97
H(163)	2756	4568	1215	91
H(164)	2273	3398	1913	79
H(165)	1371	2713	1549	62
H(22)	6529	6283	4536	56
H(23)	7054	4987	3940	58
H(24)	8946	4183	3211	74
H(25)	10432	4181	3125	85
H(26)	10787	5057	3769	82
H(27)	9667	5971	4526	67
H(28A)	7949	7955	4076	178
H(28B)	8893	7598	4119	178
H(28C)	8289	8260	4680	178
H(29A)	8052	7303	6328	123
H(29B)	8852	6758	5734	123
H(29C)	7946	6414	6379	123
H(30A)	6139	7549	5378	154
H(30B)	6329	7824	6088	154
H(30C)	6082	6973	6143	154
H(171)	5522	4462	7146	67
H(172)	4096	4338	8207	77
H(173)	3031	3645	8097	70
H(174)	3429	3029	6922	71
H(175)	4882	3089	5875	60
H(181)	5489	4434	4616	62
H(182)	5289	4053	3525	74
H(183)	6088	2938	2928	82
H(184)	7074	2195	3431	88
H(185)	7285	2550	4543	68
H(191)	6251	2436	6669	77
H(192)	7217	1478	7012	105
H(193)	8789	1570	6474	102
H(194)	9408	2593	5547	91
H(195)	8443	3559	5198	74

Table 4. Anisotropic parameters ($Å^2 \times 10^3$) for C30 H30 Cl P Pd Si.

The anisotropic displacement factor exponent takes the form:

$$-2\pi^2 [h^2 a^{*2} U_{11} + \ldots + 2 h k a^* b^* U_{12}]$$

	U11	U22	U33	U23	U13	U12
Pd	46(1)	36(1)	54(1)	-4(1)	-27(1)	-8(1)
P	40(1)	37(1)	46(1)	-6(1)	-20(1)	-5(1)
Cl	90(1)	58(1)	86(1)	4(1)	-61(1)	-29(1)
C(1)	62(2)	31(2)	66(3)	-3(2)	-34(2)	-10(2)
C(2)	57(2)	24(2)	76(3)	-8(2)	-32(2)	-5(2)
C(3)	60(2)	42(2)	53(2)	-2(2)	-27(2)	-20(2)
C(3A)	50(2)	39(2)	62(3)	3(2)	-27(2)	-15(2)
C(4)	54(2)	59(2)	93(4)	12(2)	-45(3)	-16(2)
C(5)	52(3)	77(3)	111(5)	11(3)	-29(3)	-1(2)
C(6)	64(3)	96(4)	82(4)	-6(3)	-5(3)	1(3)
C(7)	76(3)	74(3)	61(3)	-2(2)	-21(3)	-8(3)
C(7A)	53(2)	40(2)	58(3)	1(2)	-20(2)	-13(2)
Si	112(1)	50(1)	103(1)	7(1)	-80(1)	-16(1)
C(8)	197(6)	69(3)	120(5)	27(3)	-118(5)	-43(4)
C(9)	218(7)	80(4)	122(5)	2(3)	-118(5)	-42(4)
C(22)	105(4)	101(4)	199(7)	1(4)	-112(5)	1(4)
C(110)	39(2)	35(2)	41(2)	-11(2)	-14(2)	-3(1)
C(111)	47(2)	61(2)	52(2)	-3(2)	-23(2)	-2(2)
C(112)	69(3)	68(3)	51(3)	5(2)	-26(2)	-13(2)
C(113)	54(2)	72(3)	55(3)	5(2)	-17(2)	-23(2)
C(114)	44(2)	65(3)	66(3)	-3(2)	-26(2)	-14(2)
C(115)	45(2)	43(2)	46(2)	-4(2)	-20(2)	-6(2)
C(120)	39(2)	44(2)	49(2)	-2(2)	-24(2)	-7(2)
C(121)	48(2)	54(2)	55(2)	-4(2)	-24(2)	-5(2)
C(122)	46(2)	71(3)	69(3)	6(2)	-28(2)	-8(2)
C(123)	65(3)	72(3)	59(3)	8(2)	-40(2)	-24(2)
C(124)	62(3)	59(2)	56(3)	-5(2)	-29(2)	-16(2)
C(125)	48(2)	52(2)	51(2)	-9(2)	-24(2)	-4(2)
C(130)	39(2)	48(2)	48(2)	-14(2)	-21(2)	1(2)
C(131)	52(2)	45(2)	54(2)	-9(2)	-22(2)	-4(2)
C(132)	74(3)	48(2)	73(3)	-17(2)	-34(3)	0(2)
C(133)	70(3)	64(3)	74(3)	-35(3)	-34(3)	10(2)
C(134)	66(3)	85(3)	50(3)	-22(3)	-7(2)	-2(3)
C(135)	65(3)	59(3)	52(3)	-13(2)	-15(2)	-5(2)
Pd(1)	40(1)	31(1)	43(1)	1(1)	-18(1)	-3(1)
P(1)	42(1)	31(1)	40(1)	1(1)	-19(1)	-5(1)
Cl(1)	44(1)	55(1)	58(1)	-1(1)	-14(1)	4(1)
C(21)	44(2)	33(2)	46(2)	8(2)	-19(2)	-9(2)
C(28)	46(2)	43(2)	58(2)	9(2)	-21(2)	-20(2)
C(27)	39(2)	46(2)	53(2)	10(2)	-17(2)	-4(2)
C(13A)	36(2)	43(2)	40(2)	4(2)	-4(2)	-7(2)
C(26)	53(2)	50(2)	53(3)	-12(2)	-6(2)	-2(2)
C(25)	77(3)	65(3)	54(3)	-14(2)	-15(2)	-16(2)
C(24)	59(3)	87(3)	44(2)	-1(2)	-21(2)	-21(2)
C(23)	51(2)	56(2)	48(2)	6(2)	-20(2)	-10(2)
C(17A)	42(2)	39(2)	39(2)	6(2)	-12(2)	-11(2)
Si(1)	64(1)	34(1)	61(1)	2(1)	-35(1)	-3(1)
C(18)	87(3)	44(2)	91(4)	14(2)	-47(3)	-14(2)
C(19)	64(3)	51(2)	97(4)	-4(2)	-41(3)	11(2)
C(20)	121(4)	58(3)	87(4)	-14(3)	-65(3)	22(3)

C(140)	41(2)	31(2)	39(2)	4(1)	-20(2)	-4(1)
C(141)	58(2)	36(2)	65(3)	-7(2)	-36(2)	-3(2)
C(142)	54(2)	46(2)	85(3)	5(2)	-39(2)	-7(2)
C(143)	45(2)	45(2)	70(3)	-3(2)	-15(2)	3(2)
C(144)	59(2)	52(2)	52(3)	-13(2)	-15(2)	-4(2)
C(145)	48(2)	43(2)	47(2)	-6(2)	-19(2)	-9(2)
C(150)	47(2)	37(2)	40(2)	4(2)	-20(2)	-15(2)
C(151)	68(3)	39(2)	51(2)	2(2)	-29(2)	-10(2)
C(152)	68(3)	49(2)	55(3)	15(2)	-32(2)	-21(2)
C(153)	59(2)	75(3)	38(2)	10(2)	-16(2)	-32(2)
C(154)	56(2)	61(2)	44(2)	-4(2)	-13(2)	-11(2)
C(155)	49(2)	49(2)	42(2)	3(2)	-17(2)	-5(2)
C(160)	40(2)	40(2)	46(2)	0(2)	-20(2)	-6(2)
C(161)	65(3)	56(2)	71(3)	16(2)	-38(2)	-22(2)
C(162)	86(3)	68(3)	109(4)	29(3)	-58(3)	-43(3)
C(163)	76(3)	77(3)	102(4)	9(3)	-59(3)	-34(3)
C(164)	66(3)	74(3)	74(3)	2(2)	-44(3)	-14(2)
C(165)	55(2)	51(2)	53(2)	7(2)	-25(2)	-15(2)
Pd(2)	41(1)	40(1)	37(1)	-4(1)	-17(1)	-7(1)
P(2)	39(1)	36(1)	38(1)	-5(1)	-14(1)	-5(1)
Cl(2)	55(1)	70(1)	39(1)	-8(1)	-20(1)	-12(1)
C(21)	49(2)	38(2)	46(2)	7(2)	-22(2)	-12(2)
C(22)	47(2)	44(2)	52(2)	14(2)	-27(2)	-7(2)
C(23)	61(2)	52(2)	38(2)	5(2)	-26(2)	-17(2)
C(23A)	58(2)	47(2)	29(2)	8(2)	-18(2)	-11(2)
C(24)	88(3)	50(2)	36(2)	-3(2)	-15(2)	-3(2)
C(25)	69(3)	69(3)	51(3)	4(2)	-8(2)	11(2)
C(26)	49(2)	78(3)	66(3)	13(3)	-17(2)	-2(2)
C(27)	49(2)	61(2)	56(3)	7(2)	-20(2)	-15(2)
C(27A)	53(2)	40(2)	38(2)	5(2)	-15(2)	-12(2)
Si(2)	69(1)	41(1)	78(1)	-8(1)	-31(1)	-11(1)
C(28)	171(6)	67(3)	115(5)	12(3)	-45(4)	-57(4)
C(29)	97(4)	73(3)	92(4)	-23(3)	-46(3)	-18(3)
C(30)	81(4)	92(4)	139(5)	-55(4)	-42(4)	14(3)
C(170)	38(2)	36(2)	45(2)	1(2)	-14(2)	-4(1)
C(171)	50(2)	60(2)	52(3)	-16(2)	-7(2)	-18(2)
C(172)	59(3)	65(3)	56(3)	-16(2)	-8(2)	-6(2)
C(173)	42(2)	61(3)	56(3)	7(2)	-8(2)	-2(2)
C(174)	47(2)	66(3)	64(3)	11(2)	-25(2)	-16(2)
C(175)	47(2)	57(2)	48(2)	1(2)	-20(2)	-12(2)
C(180)	44(2)	42(2)	39(2)	-7(2)	-12(2)	-12(2)
C(181)	55(2)	51(2)	54(3)	-5(2)	-27(2)	-7(2)
C(182)	65(3)	73(3)	56(3)	-3(2)	-31(2)	-19(2)
C(183)	71(3)	93(4)	51(3)	-19(3)	-25(2)	-24(3)
C(184)	73(3)	77(3)	72(3)	-44(3)	-22(3)	-2(2)
C(185)	51(2)	60(2)	58(3)	-19(2)	-20(2)	2(2)
C(190)	43(2)	46(2)	39(2)	-9(2)	-16(2)	3(2)
C(191)	56(2)	63(3)	63(3)	8(2)	-20(2)	3(2)
C(192)	82(3)	82(3)	80(4)	26(3)	-30(3)	13(3)
C(193)	87(4)	96(4)	71(3)	-7(3)	-45(3)	39(3)
C(194)	55(3)	103(4)	71(3)	-13(3)	-32(3)	19(3)
C(195)	51(2)	65(3)	66(3)	-1(2)	-26(2)	4(2)

Table 5. Bond lengths [Å] and angles [°] for C30 H30 Cl P Pd Si

Pd-C(3)	2.170(3)	C(25)-C(24)	1.366(6)
Pd-C(2)	2.188(3)	C(24)-C(23)	1.412(5)
Pd-P	2.2699(9)	C(23)-C(17a)	1.397(5)
Pd-C(1)	2.320(4)	Si(1)-C(20)	1.857(4)
Pd-Cl	2.3401(9)	Si(1)-C(19)	1.861(4)
Pd-C(3a)	2.599(3)	Si(1)-C(18)	1.869(4)
P-C(110)	1.811(3)	C(140)-C(145)	1.376(4)
P-C(120)	1.815(3)	C(140)-C(141)	1.395(4)
P-C(130)	1.821(3)	C(141)-C(142)	1.382(5)
C(1)-C(2)	1.410(5)	C(142)-C(143)	1.376(5)
C(1)-C(7a)	1.485(5)	C(143)-C(144)	1.370(5)
C(1)-Si	1.872(4)	C(144)-C(145)	1.391(5)
C(2)-C(3)	1.419(5)	C(150)-C(151)	1.385(4)
C(3)-C(3a)	1.446(5)	C(150)-C(155)	1.392(5)
C(3a)-C(4)	1.385(5)	C(151)-C(152)	1.383(5)
C(3a)-C(7a)	1.430(5)	C(152)-C(153)	1.368(5)
C(4)-C(5)	1.365(6)	C(153)-C(154)	1.371(5)
C(5)-C(6)	1.372(7)	C(154)-C(155)	1.372(5)
C(6)-C(7)	1.389(6)	C(160)-C(165)	1.376(5)
C(7)-C(7a)	1.381(5)	C(160)-C(161)	1.378(5)
Si-C(9)	1.858(5)	C(161)-C(162)	1.382(5)
Si-C(22)	1.866(5)	C(162)-C(163)	1.372(6)
Si-C(8)	1.868(5)	C(163)-C(164)	1.369(6)
C(110)-C(115)	1.376(4)	C(164)-C(165)	1.390(5)
C(110)-C(111)	1.392(5)	Pd(2)-C(23)	2.165(3)
C(111)-C(112)	1.371(5)	Pd(2)-C(22)	2.186(3)
C(112)-C(113)	1.368(5)	Pd(2)-P(2)	2.2709(9)
C(113)-C(114)	1.372(5)	Pd(2)-Cl(2)	2.3395(9)
C(114)-C(115)	1.388(5)	Pd(2)-C(21)	2.345(3)
C(120)-C(121)	1.385(4)	Pd(2)-C(23a)	2.578(3)
C(120)-C(125)	1.401(5)	Pd(2)-C(27a)	2.649(3)
C(121)-C(122)	1.392(5)	P(2)-C(180)	1.823(3)
C(122)-C(123)	1.370(5)	P(2)-C(190)	1.827(3)
C(123)-C(124)	1.380(5)	P(2)-C(170)	1.829(3)
C(124)-C(125)	1.374(5)	C(21)-C(22)	1.427(4)
C(130)-C(131)	1.379(5)	C(21)-C(27a)	1.477(5)
C(130)-C(135)	1.390(5)	C(21)-Si(2)	1.860(4)
C(131)-C(132)	1.383(5)	C(22)-C(23)	1.418(5)
C(132)-C(133)	1.360(6)	C(23)-C(23a)	1.466(5)
C(133)-C(134)	1.372(6)	C(23a)-C(24)	1.396(5)
C(134)-C(135)	1.386(5)	C(23a)-C(27a)	1.426(5)
Pd(1)-C(27)	2.181(3)	C(24)-C(25)	1.370(6)
Pd(1)-C(28)	2.199(3)	C(25)-C(26)	1.374(6)
Pd(1)-P(1)	2.2646(8)	C(26)-C(27)	1.379(5)
Pd(1)-C(21)	2.293(3)	C(27)-C(27a)	1.393(5)
Pd(1)-Cl(1)	2.3349(9)	Si(2)-C(30)	1.857(4)
Pd(1)-C(13a)	2.537(3)	Si(2)-C(29)	1.870(5)
Pd(1)-C(17a)	2.572(3)	Si(2)-C(28)	1.871(5)
P(1)-C(140)	1.819(3)	C(170)-C(175)	1.373(4)
P(1)-C(150)	1.827(3)	C(170)-C(171)	1.386(5)
P(1)-C(160)	1.830(3)	C(171)-C(172)	1.377(5)
C(21)-C(28)	1.409(5)	C(172)-C(173)	1.365(5)
C(21)-C(17a)	1.477(5)	C(173)-C(174)	1.368(5)
C(21)-Si(1)	1.880(3)	C(174)-C(175)	1.384(5)
C(28)-C(27)	1.411(5)	C(180)-C(185)	1.373(5)
C(27)-C(13a)	1.459(5)	C(180)-C(181)	1.406(5)
C(13a)-C(26)	1.386(5)	C(181)-C(182)	1.377(5)
C(13a)-C(17a)	1.426(4)	C(182)-C(183)	1.360(6)
C(26)-C(25)	1.377(5)	C(183)-C(184)	1.362(6)

C(184)-C(185)	1.402(5)
C(190)-C(195)	1.373(5)
C(190)-C(191)	1.381(5)
C(191)-C(192)	1.375(5)
C(192)-C(193)	1.368(6)
C(193)-C(194)	1.369(6)
C(194)-C(195)	1.384(5)
C(3)-PD-C(2)	38.00(13)
C(3)-PD-P	102.31(10)
C(2)-PD-P	136.32(11)
C(3)-PD-C(1)	61.50(13)
C(2)-PD-C(1)	36.31(13)
P-PD-C(1)	158.75(9)
C(3)-PD-CL	163.36(10)
C(2)-PD-CL	126.19(10)
P-PD-CL	94.31(3)
C(1)-PD-CL	102.47(9)
C(3)-PD-C(3A)	33.80(12)
C(2)-PD-C(3A)	57.26(12)
P-PD-C(3A)	101.97(8)
C(1)-PD-C(3A)	56.83(12)
CL-PD-C(3A)	142.39(9)
C(110)-P-C(120)	104.38(16)
C(110)-P-C(130)	104.35(15)
C(120)-P-C(130)	104.40(16)
C(110)-P-PD	119.33(11)
C(120)-P-PD	113.50(11)
C(130)-P-PD	109.53(12)
C(2)-C(1)-C(7A)	106.3(3)
C(2)-C(1)-SI	125.9(3)
C(7A)-C(1)-SI	126.9(3)
C(2)-C(1)-PD	66.73(19)
C(7A)-C(1)-PD	85.3(2)
SI-C(1)-PD	121.14(17)
C(1)-C(2)-C(3)	108.7(3)
C(1)-C(2)-PD	76.96(19)
C(3)-C(2)-PD	70.33(18)
C(2)-C(3)-C(3A)	108.3(3)
C(2)-C(3)-PD	71.68(18)
C(3A)-C(3)-PD	89.6(2)
C(4)-C(3A)-C(7A)	119.9(4)
C(4)-C(3A)-C(3)	133.2(4)
C(7A)-C(3A)-C(3)	106.8(3)
C(4)-C(3A)-PD	130.8(3)
C(7A)-C(3A)-PD	76.2(2)
C(3)-C(3A)-PD	56.62(17)
C(5)-C(4)-C(3A)	118.9(4)
C(4)-C(5)-C(6)	121.9(5)
C(5)-C(6)-C(7)	120.8(5)
C(7A)-C(7)-C(6)	118.9(5)
C(7)-C(7A)-C(3A)	119.6(4)
C(7)-C(7A)-C(1)	132.7(4)
C(3A)-C(7A)-C(1)	107.7(3)
C(9)-SI-C(22)	111.6(3)
C(9)-SI-C(8)	108.2(3)
C(22)-SI-C(8)	109.9(3)
C(9)-SI-C(1)	110.9(2)
C(22)-SI-C(1)	106.9(2)
C(8)-SI-C(1)	109.27(19)
C(115)-C(110)-C(111)	118.8(3)
C(115)-C(110)-P	119.0(3)
C(111)-C(110)-P	122.1(3)
C(112)-C(111)-C(110)	120.7(4)
C(113)-C(112)-C(111)	120.0(4)
C(112)-C(113)-C(114)	120.2(4)
C(113)-C(114)-C(115)	120.0(4)
C(110)-C(115)-C(114)	120.2(3)
C(121)-C(120)-C(125)	119.1(3)
C(121)-C(120)-P	122.7(3)
C(125)-C(120)-P	118.1(3)
C(120)-C(121)-C(122)	119.9(4)
C(123)-C(122)-C(121)	120.6(4)
C(122)-C(123)-C(124)	119.7(4)
C(125)-C(124)-C(123)	120.7(4)
C(124)-C(125)-C(120)	120.0(3)
C(131)-C(130)-C(135)	119.0(3)
C(131)-C(130)-P	122.6(3)
C(135)-C(130)-P	118.4(3)
C(130)-C(131)-C(132)	119.9(4)
C(133)-C(132)-C(131)	121.2(4)
C(132)-C(133)-C(134)	119.4(4)
C(133)-C(134)-C(135)	120.5(4)
C(134)-C(135)-C(130)	119.9(4)
C(27)-PD1-C(28)	37.59(12)
C(27)-PD1-P(1)	101.18(9)
C(28)-PD1-P(1)	132.12(9)
C(27)-PD1-C(21)	61.96(12)
C(28)-PD1-C(21)	36.49(12)
P(1)-PD1-C(21)	162.07(9)
C(27)-PD1-CL1	162.29(10)
C(28)-PD1-CL1	128.99(10)
P(1)-PD1-CL1	95.77(3)
C(21)-PD1-CL1	100.60(9)
C(27)-PD1-C(13A)	35.00(12)
C(28)-PD1-C(13A)	58.14(13)
P(1)-PD1-C(13A)	104.85(8)
C(21)-PD1-C(13A)	58.08(12)
CL1-PD1-C(13A)	134.50(9)
C(27)-PD1-C(17A)	57.48(12)
C(28)-PD1-C(17A)	57.14(12)
P(1)-PD1-C(17A)	132.23(8)
C(21)-PD1-C(17A)	34.76(11)
CL1-PD1-C(17A)	106.80(8)
C(13A)-PD1-C(17A)	32.41(10)
C(140)-P(1)-C(150)	103.31(15)
C(140)-P(1)-C(160)	103.85(15)
C(150)-P(1)-C(160)	107.16(15)
C(140)-P(1)-PD1	113.27(10)
C(150)-P(1)-PD1	116.42(11)
C(160)-P(1)-PD1	111.74(11)
C(28)-C(21)-C(17A)	106.0(3)
C(28)-C(21)-SI1	124.0(3)
C(17A)-C(21)-SI1	128.6(3)
C(28)-C(21)-PD1	68.12(18)
C(17A)-C(21)-PD1	83.02(19)
SI1-C(21)-PD1	124.10(17)
C(21)-C(28)-C(27)	109.6(3)
C(21)-C(28)-PD1	75.39(19)
C(27)-C(28)-PD1	70.50(19)
C(28)-C(27)-C(13A)	107.9(3)
C(28)-C(27)-PD1	71.90(19)
C(13A)-C(27)-PD1	86.0(2)
C(26)-C(13A)-C(17A)	120.8(4)
C(26)-C(13A)-C(27)	132.6(3)

C(17A)-C(13A)-C(27)	106.5(3)
C(26)-C(13A)-PD1	128.1(2)
C(17A)-C(13A)-PD1	75.1(2)
C(27)-C(13A)-PD1	59.01(18)
C(25)-C(26)-C(13A)	118.9(4)
C(24)-C(25)-C(26)	121.8(4)
C(25)-C(24)-C(23)	120.8(4)
C(17A)-C(23)-C(24)	118.7(4)
C(23)-C(17A)-C(13A)	119.0(3)
C(23)-C(17A)-C(21)	132.6(3)
C(13A)-C(17A)-C(21)	108.3(3)
C(23)-C(17A)-PD1	129.2(2)
C(13A)-C(17A)-PD1	72.4(2)
C(21)-C(17A)-PD1	62.22(17)
C(20)-SI1-C(19)	110.3(2)
C(20)-SI1-C(18)	111.1(2)
C(19)-SI1-C(18)	109.68(19)
C(20)-SI1-C(21)	107.55(17)
C(19)-SI1-C(21)	112.50(17)
C(18)-SI1-C(21)	105.55(17)
C(145)-C(140)-C(141)	118.4(3)
C(145)-C(140)-P(1)	123.6(3)
C(141)-C(140)-P(1)	117.8(3)
C(142)-C(141)-C(140)	121.3(3)
C(143)-C(142)-C(141)	119.3(4)
C(144)-C(143)-C(142)	120.4(4)
C(143)-C(144)-C(145)	120.2(4)
C(140)-C(145)-C(144)	120.5(3)
C(151)-C(150)-C(155)	118.9(3)
C(151)-C(150)-P(1)	122.1(3)
C(155)-C(150)-P(1)	119.0(3)
C(152)-C(151)-C(150)	119.9(4)
C(153)-C(152)-C(151)	120.9(4)
C(152)-C(153)-C(154)	119.2(4)
C(153)-C(154)-C(155)	121.1(4)
C(154)-C(155)-C(150)	119.9(4)
C(165)-C(160)-C(161)	119.2(3)
C(165)-C(160)-P(1)	118.2(3)
C(161)-C(160)-P(1)	122.5(3)
C(160)-C(161)-C(162)	120.1(4)
C(163)-C(162)-C(161)	121.0(4)
C(164)-C(163)-C(162)	118.9(4)
C(163)-C(164)-C(165)	120.8(4)
C(160)-C(165)-C(164)	120.1(4)
C(23)-PD2-C(22)	38.03(12)
C(23)-PD2-P(2)	100.54(10)
C(22)-PD2-P(2)	128.95(10)
C(23)-PD2-CL2	161.32(10)
C(22)-PD2-CL2	131.55(10)
P(2)-PD2-CL2	95.97(3)
C(23)-PD2-C(21)	61.80(13)
C(22)-PD2-C(21)	36.50(11)
P(2)-PD2-C(21)	162.34(9)
CL2-PD2-C(21)	101.42(9)
C(23)-PD2-C(23A)	34.64(12)
C(22)-PD2-C(23A)	57.97(12)
P(2)-PD2-C(23A)	108.43(8)
CL2-PD2-C(23A)	130.50(8)
C(21)-PD2-C(23A)	57.23(12)
C(23)-PD2-C(27A)	56.37(12)
C(22)-PD2-C(27A)	56.15(12)
P(2)-PD2-C(27A)	137.12(8)
CL2-PD2-C(27A)	105.26(8)
C(21)-PD2-C(27A)	33.73(11)
C(23A)-PD2-C(27A)	31.62(10)
C(180)-P(2)-C(190)	105.70(16)
C(180)-P(2)-C(170)	102.55(16)
C(190)-P(2)-C(170)	104.99(16)
C(180)-P(2)-PD2	115.67(11)
C(190)-P(2)-PD2	110.34(12)
C(170)-P(2)-PD2	116.47(11)
C(22)-C(21)-C(27A)	105.5(3)
C(22)-C(21)-SI2	124.4(3)
C(27A)-C(21)-SI2	128.5(3)
C(22)-C(21)-PD2	65.67(18)
C(27A)-C(21)-PD2	84.48(19)
SI2-C(21)-PD2	125.15(18)
C(23)-C(22)-C(21)	109.4(3)
C(23)-C(22)-PD2	70.21(19)
C(21)-C(22)-PD2	77.83(19)
C(22)-C(23)-C(23A)	108.0(3)
C(22)-C(23)-PD2	71.75(19)
C(23A)-C(23)-PD2	88.3(2)
C(24)-C(23A)-C(27A)	120.2(4)
C(24)-C(23A)-C(23)	133.5(4)
C(27A)-C(23A)-C(23)	106.2(3)
C(24)-C(23A)-PD2	130.7(2)
C(27A)-C(23A)-PD2	76.9(2)
C(23)-C(23A)-PD2	57.08(17)
C(25)-C(24)-C(23A)	118.9(4)
C(24)-C(25)-C(26)	121.3(4)
C(25)-C(26)-C(27)	121.3(4)
C(26)-C(27)-C(27A)	119.4(4)
C(27)-C(27A)-C(23A)	118.9(4)
C(27)-C(27A)-C(21)	131.9(4)
C(23A)-C(27A)-C(21)	109.2(3)
C(27)-C(27A)-PD2	133.2(3)
C(23A)-C(27A)-PD2	71.5(2)
C(21)-C(27A)-PD2	61.79(17)
C(30)-SI2-C(21)	108.78(19)
C(30)-SI2-C(29)	109.6(2)
C(21)-SI2-C(29)	111.36(18)
C(30)-SI2-C(28)	111.1(3)
C(21)-SI2-C(28)	106.1(2)
C(29)-SI2-C(28)	109.8(2)
C(175)-C(170)-C(171)	118.7(3)
C(175)-C(170)-P(2)	122.5(3)
C(171)-C(170)-P(2)	118.7(3)
C(172)-C(171)-C(170)	119.9(4)
C(173)-C(172)-C(171)	121.5(4)
C(172)-C(173)-C(174)	118.6(4)
C(173)-C(174)-C(175)	120.9(4)
C(170)-C(175)-C(174)	120.3(4)
C(185)-C(180)-C(181)	118.1(3)
C(185)-C(180)-P(2)	123.4(3)
C(181)-C(180)-P(2)	118.5(3)
C(182)-C(181)-C(180)	121.2(4)
C(183)-C(182)-C(181)	120.2(4)
C(182)-C(183)-C(184)	119.5(4)
C(183)-C(184)-C(185)	121.5(4)
C(180)-C(185)-C(184)	119.4(4)
C(195)-C(190)-C(191)	119.2(4)
C(195)-C(190)-P(2)	118.8(3)
C(191)-C(190)-P(2)	122.0(3)

C(192)-C(191)-C(190)	120.3(4)	C(190)-C(195)-C(194)	120.2(4)
C(193)-C(192)-C(191)	120.2(5)		
C(192)-C(193)-C(194)	120.0(4)		
C(193)-C(194)-C(195)	120.1(4)		

Table 6. Torsion angles [°] for C30 H30 Cl P Pd Si.

C(3)-PD-P-C(110)	-110.32(16)	P-PD-C(3A)-C(4)	-26.6(4)
C(2)-PD-P-C(110)	-90.27(19)	C(1)-PD-C(3A)-C(4)	151.8(5)
C(1)-PD-P-C(110)	-148.5(3)	CL-PD-C(3A)-C(4)	87.0(4)
CL-PD-P-C(110)	69.18(12)	C(3)-PD-C(3A)-C(7A)	121.2(3)
C(3A)-PD-P-C(110)	-144.92(15)	C(2)-PD-C(3A)-C(7A)	77.6(2)
C(3)-PD-P-C(120)	13.38(16)	P-PD-C(3A)-C(7A)	-144.4(2)
C(2)-PD-P-C(120)	33.4(2)	C(1)-PD-C(3A)-C(7A)	34.0(2)
C(1)-PD-P-C(120)	-24.8(3)	CL-PD-C(3A)-C(7A)	-30.8(3)
CL-PD-P-C(120)	-167.12(13)	C(2)-PD-C(3A)-C(3)	-43.6(2)
C(3A)-PD-P-C(120)	-21.22(15)	P-PD-C(3A)-C(3)	94.3(2)
C(3)-PD-P-C(130)	129.61(15)	C(1)-PD-C(3A)-C(3)	-87.2(2)
C(2)-PD-P-C(130)	149.66(18)	CL-PD-C(3A)-C(3)	-152.0(2)
C(1)-PD-P-C(130)	91.4(3)	C(7A)-C(3A)-C(4)-C(5)	-0.6(6)
CL-PD-P-C(130)	-50.89(12)	C(3)-C(3A)-C(4)-C(5)	-177.4(4)
C(3A)-PD-P-C(130)	95.01(15)	PD-C(3A)-C(4)-C(5)	-98.2(5)
C(3)-PD-C(1)-C(2)	39.2(2)	C(3A)-C(4)-C(5)-C(6)	0.0(7)
P-PD-C(1)-C(2)	82.5(3)	C(4)-C(5)-C(6)-C(7)	0.7(8)
CL-PD-C(1)-C(2)	-136.1(2)	C(5)-C(6)-C(7)-C(7A)	-0.7(7)
C(3A)-PD-C(1)-C(2)	78.4(2)	C(6)-C(7)-C(7A)-C(3A)	0.0(6)
C(3)-PD-C(1)-C(7A)	-70.9(2)	C(6)-C(7)-C(7A)-C(1)	-179.8(4)
C(2)-PD-C(1)-C(7A)	-110.0(3)	C(4)-C(3A)-C(7A)-C(7)	0.6(5)
P-PD-C(1)-C(7A)	-27.5(4)	C(3)-C(3A)-C(7A)-C(7)	178.2(3)
CL-PD-C(1)-C(7A)	113.9(2)	PD-C(3A)-C(7A)-C(7)	129.9(4)
C(3A)-PD-C(1)-C(7A)	-31.7(2)	C(4)-C(3A)-C(7A)-C(1)	-179.5(3)
C(3)-PD-C(1)-SI	158.3(3)	C(3)-C(3A)-C(7A)-C(1)	-1.9(4)
C(2)-PD-C(1)-SI	119.1(3)	PD-C(3A)-C(7A)-C(1)	-50.2(2)
P-PD-C(1)-SI	-158.34(13)	C(2)-C(1)-C(7A)-C(7)	172.7(4)
CL-PD-C(1)-SI	-17.0(2)	SI-C(1)-C(7A)-C(7)	2.7(6)
C(3A)-PD-C(1)-SI	-162.5(3)	PD-C(1)-C(7A)-C(7)	-123.2(4)
C(7A)-C(1)-C(2)-C(3)	13.7(4)	C(2)-C(1)-C(7A)-C(3A)	-7.1(4)
SI-C(1)-C(2)-C(3)	-176.2(2)	SI-C(1)-C(7A)-C(3A)	-177.1(2)
PD-C(1)-C(2)-C(3)	-63.7(2)	PD-C(1)-C(7A)-C(3A)	56.9(3)
C(7A)-C(1)-C(2)-PD	77.3(2)	C(2)-C(1)-SI-C(9)	143.5(3)
SI-C(1)-C(2)-PD	-112.6(3)	C(7A)-C(1)-SI-C(9)	-48.4(4)
C(3)-PD-C(2)-C(1)	-115.7(3)	PD-C(1)-SI-C(9)	61.1(3)
P-PD-C(2)-C(1)	-148.65(18)	C(2)-C(1)-SI-C(22)	21.6(4)
CL-PD-C(2)-C(1)	57.1(2)	C(7A)-C(1)-SI-C(22)	-170.3(3)
C(3A)-PD-C(2)-C(1)	-77.1(2)	PD-C(1)-SI-C(22)	-60.8(3)
P-PD-C(2)-C(3)	-33.0(3)	C(2)-C(1)-SI-C(8)	-97.4(4)
C(1)-PD-C(2)-C(3)	115.7(3)	C(7A)-C(1)-SI-C(8)	70.7(4)
CL-PD-C(2)-C(3)	172.73(18)	PD-C(1)-SI-C(8)	-179.8(2)
C(3A)-PD-C(2)-C(3)	38.6(2)	C(120)-P-C(110)-C(115)	-156.8(3)
C(1)-C(2)-C(3)-C(3A)	-15.2(4)	C(130)-P-C(110)-C(115)	93.9(3)
PD-C(2)-C(3)-C(3A)	-83.2(2)	PD-P-C(110)-C(115)	-28.8(3)
C(1)-C(2)-C(3)-PD	68.0(2)	C(120)-P-C(110)-C(111)	27.0(3)
P-PD-C(3)-C(2)	157.4(2)	C(130)-P-C(110)-C(111)	-82.3(3)
C(1)-PD-C(3)-C(2)	-37.4(2)	C(110)-P-C(120)-C(121)	-123.8(3)
CL-PD-C(3)-C(2)	-20.9(5)	C(130)-P-C(120)-C(121)	-14.5(3)
C(3A)-PD-C(3)-C(2)	-109.5(3)	PD-P-C(120)-C(121)	104.7(3)
C(2)-PD-C(3)-C(3A)	109.5(3)	C(110)-P-C(120)-C(125)	60.4(3)
P-PD-C(3)-C(3A)	-93.2(2)	C(130)-P-C(120)-C(125)	169.7(3)
C(1)-PD-C(3)-C(3A)	72.1(2)	PD-P-C(120)-C(125)	-71.1(3)
CL-PD-C(3)-C(3A)	88.6(4)	P-C(120)-C(125)-C(124)	174.9(3)
C(2)-C(3)-C(3A)-C(4)	-172.5(4)	C(110)-P-C(130)-C(131)	16.8(3)
PD-C(3)-C(3A)-C(4)	117.0(4)	C(120)-P-C(130)-C(131)	-92.5(3)
C(2)-C(3)-C(3A)-C(7A)	10.4(4)	PD-P-C(130)-C(131)	145.7(3)
PD-C(3)-C(3A)-C(7A)	-60.1(3)	C(110)-P-C(130)-C(135)	-165.2(3)
C(2)-C(3)-C(3A)-PD	70.5(2)	C(120)-P-C(130)-C(135)	85.5(3)
C(3)-PD-C(3A)-C(4)	-120.9(5)	PD-P-C(130)-C(135)	-36.4(3)
C(2)-PD-C(3A)-C(4)	-164.6(5)	C(27)-PD1-P(1)-C(140)	-2.14(16)

C(28)-PD1-P(1)-C(140) 22.33(19)
C(21)-PD1-P(1)-C(140) -21.1(3)
CL1-PD1-P(1)-C(140) -176.98(12)
C(13A)-PD1-P(1)-C(140) -37.90(15)
C(17A)-PD1-P(1)-C(140) -58.04(16)
C(27)-PD1-P(1)-C(150) -121.71(16)
C(28)-PD1-P(1)-C(150) -97.24(18)
C(21)-PD1-P(1)-C(150) -140.6(3)
CL1-PD1-P(1)-C(150) 63.46(13)
C(13A)-PD1-P(1)-C(150) -157.47(15)
C(17A)-PD1-P(1)-C(150) -177.60(15)
C(27)-PD1-P(1)-C(160) 114.73(16)
C(28)-PD1-P(1)-C(160) 139.20(18)
C(21)-PD1-P(1)-C(160) 95.8(3)
CL1-PD1-P(1)-C(160) -60.11(12)
C(13A)-PD1-P(1)-C(160) 78.97(15)
C(17A)-PD1-P(1)-C(160) 58.83(16)
C(27)-PD1-C(21)-C(28) 37.9(2)
P(1)-PD1-C(21)-C(28) 59.0(4)
CL1-PD1-C(21)-C(28) -145.4(2)
C(13A)-PD1-C(21)-C(28) 78.2(2)
C(17A)-PD1-C(21)-C(28) 110.4(3)
C(27)-PD1-C(21)-C(17A) -72.5(2)
C(28)-PD1-C(21)-C(17A) -110.4(3)
P(1)-PD1-C(21)-C(17A) -51.4(4)
CL1-PD1-C(21)-C(17A) 104.24(18)
C(13A)-PD1-C(21)-C(17A) -32.11(18)
C(27)-PD1-C(21)-SI1 155.0(3)
C(28)-PD1-C(21)-SI1 117.1(3)
P(1)-PD1-C(21)-SI1 176.12(12)
CL1-PD1-C(21)-SI1 -28.3(2)
C(13A)-PD1-C(21)-SI1 -164.6(3)
C(17A)-PD1-C(21)-SI1 -132.5(3)
C(17A)-C(21)-C(28)-C(27) 12.8(4)
SI1-C(21)-C(28)-C(27) -179.9(2)
PD1-C(21)-C(28)-C(27) -62.7(2)
C(17A)-C(21)-C(28)-PD1 75.5(2)
SI1-C(21)-C(28)-PD1 -117.2(3)
C(27)-PD1-C(28)-C(21) -117.4(3)
P(1)-PD1-C(28)-C(21) -159.16(16)
CL1-PD1-C(28)-C(21) 45.9(3)
C(13A)-PD1-C(28)-C(21) -78.1(2)
C(17A)-PD1-C(28)-C(21) -39.5(2)
P(1)-PD1-C(28)-C(27) -41.8(3)
C(21)-PD1-C(28)-C(27) 117.4(3)
CL1-PD1-C(28)-C(27) 163.27(18)
C(13A)-PD1-C(28)-C(27) 39.3(2)
C(17A)-PD1-C(28)-C(27) 77.9(2)
C(21)-C(28)-C(27)-C(13A) -13.7(4)
PD1-C(28)-C(27)-C(13A) -79.5(2)
C(21)-C(28)-C(27)-PD1 65.8(2)
P(1)-PD1-C(27)-C(28) 149.8(2)
C(21)-PD1-C(27)-C(28) -36.7(2)
CL1-PD1-C(27)-C(28) -47.4(5)
C(13A)-PD1-C(27)-C(28) -110.3(3)
C(17A)-PD1-C(27)-C(28) -76.9(2)
C(28)-PD1-C(27)-C(13A) 110.3(3)
P(1)-PD1-C(27)-C(13A) -99.98(19)
C(21)-PD1-C(27)-C(13A) 73.5(2)
CL1-PD1-C(27)-C(13A) 62.9(4)
C(17A)-PD1-C(27)-C(13A) 33.37(18)
C(28)-C(27)-C(13A)-C(26) -175.3(4)
PD1-C(27)-C(13A)-C(26) 115.2(4)
C(28)-C(27)-C(13A)-C(17A) 8.8(4)
PD1-C(27)-C(13A)-C(17A) -60.7(2)
C(28)-C(27)-C(13A)-PD1 69.5(2)
C(27)-PD1-C(13A)-C(26) -122.2(4)
C(28)-PD1-C(13A)-C(26) -164.5(4)
P(1)-PD1-C(13A)-C(26) -33.8(4)
C(21)-PD1-C(13A)-C(26) 152.2(4)
CL1-PD1-C(13A)-C(26) 80.1(4)
C(17A)-PD1-C(13A)-C(26) 117.8(4)
C(27)-PD1-C(13A)-C(17A) 120.1(3)
C(28)-PD1-C(13A)-C(17A) 77.7(2)
P(1)-PD1-C(13A)-C(17A) -151.60(18)
C(21)-PD1-C(13A)-C(17A) 34.43(19)
CL1-PD1-C(13A)-C(17A) -37.6(2)
C(28)-PD1-C(13A)-C(27) -42.4(2)
P(1)-PD1-C(13A)-C(27) 88.3(2)
C(21)-PD1-C(13A)-C(27) -85.6(2)
CL1-PD1-C(13A)-C(27) -157.69(17)
C(17A)-PD1-C(13A)-C(27) -120.1(3)
C(17A)-C(13A)-C(26)-C(25) -0.3(5)
C(27)-C(13A)-C(26)-C(25) -175.8(4)
PD1-C(13A)-C(26)-C(25) -95.4(4)
C(13A)-C(26)-C(25)-C(24) 1.4(6)
C(26)-C(25)-C(24)-C(23) -1.9(6)
C(25)-C(24)-C(23)-C(17A) 1.3(6)
C(24)-C(23)-C(17A)-C(13A) -0.3(5)
C(24)-C(23)-C(17A)-C(21) 176.3(3)
C(24)-C(23)-C(17A)-PD1 90.1(4)
C(26)-C(13A)-C(17A)-C(23) -0.2(5)
C(27)-C(13A)-C(17A)-C(23) 176.3(3)
PD1-C(13A)-C(17A)-C(23) 125.7(3)
C(26)-C(13A)-C(17A)-C(11 -177.5(3)
C(27)-C(13A)-C(17A)-C(21) -1.0(4)
PD1-C(13A)-C(17A)-C(21) -51.7(2)
C(26)-C(13A)-C(17A)-PD1 -125.8(3)
C(27)-C(13A)-C(17A)-PD1 50.7(2)
C(28)-C(21)-C(17A)-C(23) 176.1(4)
SI1-C(21)-C(17A)-C(23) 9.6(6)
PD1-C(21)-C(17A)-C(23) -119.1(4)
C(28)-C(21)-C(17A)-C(13A) -7.1(4)
SI1-C(21)-C(17A)-C(13A) -173.6(2)
PD1-C(21)-C(17A)-C(13A) 57.7(2)
C(28)-C(21)-C(17A)-PD1 -64.8(2)
SI1-C(21)-C(17A)-PD1 128.7(3)
C(27)-PD1-C(17A)-C(23) -149.5(4)
C(28)-PD1-C(17A)-C(23) 165.4(4)
P(1)-PD1-C(17A)-C(23) -75.1(3)
C(21)-PD1-C(17A)-C(23) 123.9(4)
CL1-PD1-C(17A)-C(23) 39.5(3)
C(13A)-PD1-C(17A)-C(23) -113.5(4)
C(27)-PD1-C(17A)-C(13A) -36.1(2)
C(28)-PD1-C(17A)-C(13A) -81.1(2)
P(1)-PD1-C(17A)-C(13A) 38.4(2)
C(21)-PD1-C(17A)-C(13A) -122.7(3)
CL1-PD1-C(17A)-C(13A) 152.95(18)
C(27)-PD1-C(17A)-C(21) 86.6(2)
C(28)-PD1-C(17A)-C(21) 41.6(2)
P(1)-PD1-C(17A)-C(21) 161.05(16)
CL1-PD1-C(17A)-C(21) -84.39(19)
C(13A)-PD1-C(17A)-C(21) 122.7(3)
C(28)-C(21)-SI1-C(20) 31.6(4)

C(17A)-C(21)-SI1-C(20) -164.0(3)
PD1-C(21)-SI1-C(20) -53.4(3)
C(28)-C(21)-SI1-C(19) 153.3(3)
C(17A)-C(21)-SI1-C(19) -42.4(4)
PD1-C(21)-SI1-C(19) 68.3(3)
C(28)-C(21)-SI1-C(18) -87.1(3)
C(17A)-C(21)-SI1-C(18) 77.2(3)
PD1-C(21)-SI1-C(18) -172.1(2)
PD1-P(1)-C(160)-C(165) -17.7(3)
C(140)-P(1)-C(160)-C(161)-72.2(3)
C(150)-P(1)-C(160)-C(161) 36.7(4)
PD1-P(1)-C(160)-C(161) 165.3(3)
C(165)-C(160)-C(161)-C(162-0.9(6)
P(1)-C(160)-C(161)-C(162)176.0(3)
C(160)-C(161)-C(162)-C(163-0.1(7)
C(161)-C(162)-C(163)-C(164)0.2(8)
C(162)-C(163)-C(164)-C(165)0.7(7)
C(161)-C(160)-C(165)-C(164)1.7(6)
P(1)-C(160)-C(165)-C(164-175.3(3)
C(163)-C(164)-C(165)-C(160-1.7(6)
C(23)-PD2-P(2)-C(180) -3.05(16)
C(22)-PD2-P(2)-C(180) 25.33(18)
CL2-PD2-P(2)-C(180) -174.27(13)
C(21)-PD2-P(2)-C(180) -4.4(3)
C(23A)-PD2-P(2)-C(180) -37.96(15)
C(27A)-PD2-P(2)-C(180) -54.18(18)
C(23)-PD2-P(2)-C(190) 116.85(16)
C(22)-PD2-P(2)-C(190) 145.23(17)
CL2-PD2-P(2)-C(190) -54.37(12)
C(21)-PD2-P(2)-C(190) 115.5(3)
C(23A)-PD2-P(2)-C(190) 81.94(15)
C(27A)-PD2-P(2)-C(190) 65.72(17)
C(23)-PD2-P(2)-C(170) -123.63(16)
C(22)-PD2-P(2)-C(170) -95.25(18)
CL2-PD2-P(2)-C(170) 65.15(13)
C(21)-PD2-P(2)-C(170) -125.0(3)
C(23A)-PD2-P(2)-C(170)-158.54(15)
C(27A)-PD2-P(2)-C(170)-174.76(17)
C(23)-PD2-C(21)-C(22) 38.9(2)
P(2)-PD2-C(21)-C(22) 40.5(4)
CL2-PD2-C(21)-C(22) -149.8(2)
C(23A)-PD2-C(21)-C(22) 79.0(2)
C(27A)-PD2-C(21)-C(22) 109.7(3)
C(23)-PD2-C(21)-C(27A) -70.8(2)
C(22)-PD2-C(21)-C(27A) -109.7(3)
P(2)-PD2-C(21)-C(27A) -69.2(4)
CL2-PD2-C(21)-C(27A) 100.43(19)
C(23A)-PD2-C(21)-C(27A)-30.71(19)
C(23)-PD2-C(21)-SI2 155.0(3)
C(22)-PD2-C(21)-SI2 116.1(3)
P(2)-PD2-C(21)-SI2 156.60(15)
CL2-PD2-C(21)-SI2 -33.7(2)
C(23A)-PD2-C(21)-SI2 -164.9(3)
C(27A)-PD2-C(21)-SI2 -134.2(3)
C(27A)-C(21)-C(22)-C(23) 12.7(4)
SI2-C(21)-C(22)-C(23) 179.2(2)
PD2-C(21)-C(22)-C(23) -63.7(2)
C(27A)-C(21)-C(22)-PD2 76.4(2)
SI2-C(21)-C(22)-PD2 -117.1(3)
P(2)-PD2-C(22)-C(23) -49.3(2)
CL2-PD2-C(22)-C(23) 157.15(17)
C(21)-PD2-C(22)-C(23) 116.0(3)
C(23A)-PD2-C(22)-C(23) 39.2(2)
C(27A)-PD2-C(22)-C(23) 77.0(2)
C(23)-PD2-C(22)-C(21) -116.0(3)
P(2)-PD2-C(22)-C(21) -165.33(16)
CL2-PD2-C(22)-C(21) 41.2(3)
C(23A)-PD2-C(22)-C(21) -76.8(2)
C(27A)-PD2-C(22)-C(21) -39.00(19)
C(21)-C(22)-C(23)-C(23A) -13.3(4)
PD2-C(22)-C(23)-C(23A) -81.9(2)
C(21)-C(22)-C(23)-PD2 68.7(2)
P(2)-PD2-C(23)-C(22) 143.13(19)
CL2-PD2-C(23)-C(22) -65.2(4)
C(21)-PD2-C(23)-C(22) -37.35(19)
C(23A)-PD2-C(23)-C(22) -109.6(3)
C(27A)-PD2-C(23)-C(22) -76.4(2)
C(22)-PD2-C(23)-C(23A) 109.6(3)
P(2)-PD2-C(23)-C(23A) -107.2(2)
CL2-PD2-C(23)-C(23A) 44.5(4)
C(21)-PD2-C(23)-C(23A) 72.3(2)
C(27A)-PD2-C(23)-C(23A) 33.24(19)
C(22)-C(23)-C(23A)-C(24)-172.6(4)
PD2-C(23)-C(23A)-C(24) 117.2(4)
C(22)-C(23)-C(23A)-C(27A) 8.2(4)
PD2-C(23)-C(23A)-C(27A) -62.0(3)
C(22)-C(23)-C(23A)-PD2 70.2(2)
C(23)-PD2-C(23A)-C(24) -121.7(5)
C(22)-PD2-C(23A)-C(24) -164.9(4)
P(2)-PD2-C(23A)-C(24) -39.9(4)
CL2-PD2-C(23A)-C(24) 75.5(4)
C(21)-PD2-C(23A)-C(24) 151.6(4)
C(27A)-PD2-C(23A)-C(24) 118.8(5)
C(23)-PD2-C(23A)-C(27A) 119.5(3)
C(22)-PD2-C(23A)-C(27A) 76.3(2)
P(2)-PD2-C(23A)-C(27A)-158.74(19)
CL2-PD2-C(23A)-C(27A) -43.4(2)
C(21)-PD2-C(23A)-C(27A) 32.7(2)
C(22)-PD2-C(23A)-C(23) -43.2(2)
P(2)-PD2-C(23A)-C(23) 81.8(2)
CL2-PD2-C(23A)-C(23) -162.84(18)
C(21)-PD2-C(23A)-C(23) -86.7(2)
C(27A)-PD2-C(23A)-C(23) -119.5(3)
C(27A)-C(23A)-C(24)-C(25) -1.3(5)
C(23)-C(23A)-C(24)-C(25) 179.6(4)
PD2-C(23A)-C(24)-C(25) -100.2(4)
C(23A)-C(24)-C(25)-C(26) 1.3(6)
C(24)-C(25)-C(26)-C(27) 0.0(7)
C(25)-C(26)-C(27)-C(27A) -1.3(6)
C(26)-C(27)-C(27A)-C(23A) 1.2(5)
C(26)-C(27)-C(27A)-C(21)-179.2(4)
C(26)-C(27)-C(27A)-PD2 92.4(5)
C(24)-C(23A)-C(27A)-C(27) 0.0(5)
C(23)-C(23A)-C(27A)-C(27)179.4(3)
PD2-C(23A)-C(27A)-C(27) 129.8(3)
C(24)-C(23A)-C(27A)-C(21-179.6(3)
C(23)-C(23A)-C(27A)-C(21) -0.3(4)
PD2-C(23A)-C(27A)-C(21) -49.9(2)
C(24)-C(23A)-C(27A)-PD2 -129.8(3)
C(23)-C(23A)-C(27A)-PD2 49.6(2)
C(22)-C(21)-C(27A)-C(27) 172.9(4)
SI2-C(21)-C(27A)-C(27) 7.2(6)
PD2-C(21)-C(27A)-C(27) -124.3(4)
C(22)-C(21)-C(27A)-C(23A) -7.5(4)

SI2-C(21)-C(27A)-C(23A)	-173.2(3)
PD2-C(21)-C(27A)-C(23A)	55.3(3)
C(22)-C(21)-C(27A)-PD2	-62.9(2)
SI2-C(21)-C(27A)-PD2	131.5(3)
C(23)-PD2-C(27A)-C(27)	-149.1(4)
C(22)-PD2-C(27A)-C(27)	164.8(4)
P(2)-PD2-C(27A)-C(27)	-82.2(4)
CL2-PD2-C(27A)-C(27)	34.6(4)
C(21)-PD2-C(27A)-C(27)	122.4(5)
C(23A)-PD2-C(27A)-C(27)	-112.6(5)
C(23)-PD2-C(27A)-C(23A)	-36.5(2)
C(22)-PD2-C(27A)-C(23A)	-82.6(2)
P(2)-PD2-C(27A)-C(23A)	30.4(3)
CL2-PD2-C(27A)-C(23A)	147.24(19)
C(21)-PD2-C(27A)-C(23A)	-125.0(3)
C(23)-PD2-C(27A)-C(21)	88.5(2)
C(22)-PD2-C(27A)-C(21)	42.4(2)
P(2)-PD2-C(27A)-C(21)	155.36(17)
CL2-PD2-C(27A)-C(21)	-87.8(2)
C(23A)-PD2-C(27A)-C(21)	125.0(3)
C(22)-C(21)-SI2-C(30)	24.7(4)
C(27A)-C(21)-SI2-C(30)	-172.1(3)
PD2-C(21)-SI2-C(30)	-57.9(3)
C(22)-C(21)-SI2-C(29)	145.6(3)
C(27A)-C(21)-SI2-C(29)	-51.2(4)
PD2-C(21)-SI2-C(29)	63.0(3)
C(22)-C(21)-SI2-C(28)	-94.9(4)
C(27A)-C(21)-SI2-C(28)	68.3(4)
PD2-C(21)-SI2-C(28)	-177.5(3)
C(180)-P(2)-C(170)-C(175)	17.7(3)
C(190)-P(2)-C(170)-C(175)	-92.6(3)
PD2-P(2)-C(170)-C(175)	145.0(3)

Calcul des plans:

* -0.0043 (0.0026) C3A
* 0.0022 (0.0029) C4
* 0.0023 (0.0035) C5
* -0.0045 (0.0036) C6
* 0.0022 (0.0032) C7
* 0.0021 (0.0027) C7A

Rms deviation of fitted atoms = 0.0031

9.2440 (0.0522) x + 14.8860 (0.0443) y + 1.5697 (0.0400) z = 5.9003 (0.0289)

Angle to previous plane (with approximate esd) = 13.46 (0.36) (FA)

* 0.0000 (0.0000) C1
* 0.0000 (0.0000) C2
* 0.0000 (0.0000) C3
1.9103 (0.0032) Pd
-0.3606 (0.0090) C3A
-0.3369 (0.0092) C7A

Rms deviation of fitted atoms = 0.0000

6.3826 (0.0313) x + 16.6621 (0.0118) y + 2.3321 (0.0306) z = 4.4306 (0.0170)

Angle to previous plane (with approximate esd) = 14.43 (0.37) (HA)

* -0.0065 (0.0013) C1
* 0.0067 (0.0013) C3
* -0.0107 (0.0021) C3A
* 0.0105 (0.0020) C7A
1.9087 (0.0027) Pd
-0.2052 (0.0050) C2
0.0092 (0.0065) C4
0.0367 (0.0088) C5
0.0445 (0.0091) C6
0.0384 (0.0070) C7

Rms deviation of fitted atoms = 0.0088

6.5098 (0.0238) x + 16.5800 (0.0089) y + 2.0995 (0.0295) z = 4.4505 (0.0123)

* -0.0023 (0.0024) C13A
* -0.0030 (0.0027) C14
* 0.0084 (0.0029) C15

* -0.0081 (0.0028) C16
* 0.0026 (0.0026) C17
* 0.0024 (0.0024) C17A

Rms deviation of fitted atoms = 0.0052

- 6.4252 (0.0621) x - 6.3094 (0.0587) y + 10.6423 (0.0743) z = 1.5862 (0.0166)

Angle to previous plane (with approximate esd) = 10.21 (0.58) (FA)

* 0.0000 (0.0000) C11
* 0.0000 (0.0000) C12
* 0.0000 (0.0000) C13
-1.8904 (0.0036) Pd1
0.3285 (0.0095) C13A
0.3141 (0.0095) C17A

Rms deviation of fitted atoms = 0.0000

- 8.8512 (0.0274) x - 8.4566 (0.0281) y + 7.1078 (0.0381) z = 0.7694 (0.0104)

Angle to previous plane (with approximate esd) = 13.26 (0.59)

* 0.0034 (0.0012) C11
* -0.0034 (0.0012) C13
* 0.0055 (0.0020) C13A
* -0.0055 (0.0020) C17A
-1.9102 (0.0026) Pd1
0.1864 (0.0052) C12
-0.0510 (0.0064) C14
-0.1112 (0.0084) C15
-0.1448 (0.0083) C16
-0.0784 (0.0064) C17

Rms deviation of fitted atoms = 0.0046

- 8.2206 (0.0195) x - 8.1443 (0.0219) y + 7.9984 (0.0231) z = 1.0220 (0.0091)

* -0.0045 (0.0024) C23A
* 0.0089 (0.0027) C24
* -0.0044 (0.0030) C25
* -0.0045 (0.0030) C26
* 0.0088 (0.0027) C27
* -0.0042 (0.0025) C27A

Rms deviation of fitted atoms = 0.0062

2.5559 (0.0685) x + 8.1339 (0.0473) y - 12.5508 (0.0298) z = 1.0862 (0.0523)

Angle to previous plane (with approximate esd) = 13.19 (0.31)

* 0.0000 (0.0000) C21
* 0.0000 (0.0000) C22
* 0.0000 (0.0000) C23
-1.9154 (0.0032) Pd2
0.3200 (0.0094) C23A
0.3138 (0.0093) C27A

Rms deviation of fitted atoms = 0.0000

0.4496 (0.0348) x - 9.6384 (0.0258) y + 12.9319 (0.0211) z = 0.4997 (0.0386)

Angle to previous plane (with approximate esd) = 13.06 (0.32)

* -0.0010 (0.0013) C21
* 0.0010 (0.0012) C23
* -0.0016 (0.0020) C23A
* 0.0017 (0.0020) C27A
1.9150 (0.0028) Pd2
-0.1858 (0.0052) C22
0.0076 (0.0064) C24
-0.0068 (0.0085) C25
-0.0040 (0.0085) C26
0.0133 (0.0065) C27

Rms deviation of fitted atoms = 0.0014

0.4608 (0.0238) x - 9.6786 (0.0218) y + 12.9064 (0.0188) z = 0.4815 (0.0329)

Annexe 3: Informations supplémentaires du chapitre VI

Rapport cristallographique de la structure du composé (COD)Pt(η^1-Ind)Cl (**1**).

Table 1. Crystal data and structure refinement for C17 H19 Cl Pt.

Identification code	suse35
Empirical formula	C17 H19 Cl Pt
Formula weight	453.86
Temperature	200(2)K
Wavelength	1.54178 Å
Crystal system	Monoclinic
Space group	C2/c
Unit cell dimensions	a = 22.6640(5) Å α = 90°
	b = 8.2185(2) Å β = 119.9990(10)°
	c = 17.9396(4) Å γ = 90°
Volume	2893.85(11)Å^3
Z	8
Density (calculated)	2.083 Mg/m^3
Absorption coefficient	19.678 mm^{-1}
F(000)	1728
Crystal size	0.32 x 0.14 x 0.12 mm
Theta range for data collection	4.51 to 71.99°
Index ranges	$-27 \le h \le 27$, $-10 \le k \le 9$, $-21 \le \lambda \le 21$
Reflections collected	17441
Independent reflections	2828 [R_{int} = 0.056]
Absorption correction	Semi-empirical from equivalents
Max. and min. transmission	1.0000 and 0.3500
Refinement method	Full-matrix least-squares on F^2
Data / restraints / parameters	2828 / 0 / 173
Goodness-of-fit on F^2	1.089
Final R indices [I>2sigma(I)]	R_1 = 0.0421, wR_2 = 0.1032
R indices (all data)	R_1 = 0.0436, wR_2 = 0.1051
Extinction coefficient	0.00044(3)
Largest diff. peak and hole	2.862 and -3.175 e/Å^3

Table 2. Atomic coordinates (x 10^4) and equivalent isotropic displacement parameters ($Å^2$ x 10^3) for C17 H19 Cl Pt.

U_{eq} is defined as one third of the trace of the orthogonalized Uij tensor.

	x	y	z	U_{eq}
Pt	1254(1)	4483(1)	-8(1)	15(1)
Cl	530(1)	2344(2)	-158(1)	26(1)
C(1)	1996(2)	3313(6)	1127(3)	20(1)
C(2)	1844(3)	3916(8)	1798(3)	27(1)
C(3)	2391(3)	4670(7)	2445(4)	29(1)
C(3A)	2963(3)	4543(6)	2283(4)	22(1)
C(4)	3646(3)	5007(8)	2781(3)	27(1)
C(5)	4087(3)	4632(7)	2493(4)	29(1)
C(6)	3867(3)	3824(7)	1714(3)	26(1)
C(7)	3185(3)	3355(7)	1219(3)	25(1)
C(7A)	2730(2)	3718(6)	1495(3)	19(1)
C(21)	546(3)	5218(8)	-1390(3)	24(1)
C(22)	387(2)	6168(7)	-889(3)	26(1)
C(23)	613(3)	7919(7)	-653(4)	29(1)
C(24)	1266(3)	8080(7)	214(4)	28(1)
C(25)	1771(2)	6745(6)	406(3)	20(1)
C(26)	1933(2)	6050(7)	-184(3)	19(1)
C(27)	1646(2)	6607(7)	-1112(3)	23(1)
C(28)	983(3)	5718(7)	-1761(3)	25(1)

Table 3. Hydrogen coordinates (x 10^4) and isotropic displacement parameters ($Å^2$ x 10^3) for C17 H19 Cl Pt.

	x	y	z	U_{eq}
H(1)	1931	2107	1064	24
H(2)	1418	3787	1774	33
H(3)	2403	5195	2924	35
H(4)	3801	5570	3310	32
H(5)	4553	4930	2831	35
H(6)	4179	3594	1521	31
H(7)	3034	2787	693	30
H(21)	363	4147	-1514	29
H(22)	118	5701	-675	31
H(23A)	246	8540	-636	35
H(23B)	686	8406	-1106	35
H(24A)	1485	9132	229	33
H(24B)	1146	8105	674	33
H(25)	2002	6333	978	24
H(26)	2244	5165	10	22
H(27A)	1995	6427	-1282	27
H(27B)	1555	7790	-1146	27
H(28A)	715	6441	-2260	30
H(28B)	1105	4735	-1974	30

Table 4. Anisotropic parameters ($Å^2$ x 10^3) for C17 H19 Cl Pt.

The anisotropic displacement factor exponent takes the form:

$$-2\pi^2 [h^2 a^{*2} U_{11} + ... + 2 h k a^* b^* U_{12}]$$

	U11	U22	U33	U23	U13	U12
Pt	16(1)	23(1)	7(1)	-1(1)	5(1)	0(1)
Cl	26(1)	31(1)	23(1)	-3(1)	13(1)	-7(1)
C(1)	20(2)	26(3)	8(2)	5(2)	3(2)	-1(2)
C(2)	31(3)	39(3)	14(2)	5(2)	13(2)	-1(2)
C(3)	35(4)	43(3)	13(3)	-2(2)	15(3)	-3(2)
C(3A)	29(3)	27(3)	10(3)	2(2)	11(2)	1(2)
C(4)	35(3)	31(3)	10(2)	-4(2)	7(2)	-2(3)
C(5)	22(3)	34(3)	17(3)	0(2)	-2(2)	0(2)
C(6)	26(3)	32(3)	22(3)	1(2)	12(2)	3(2)
C(7)	25(2)	33(3)	10(2)	-3(2)	3(2)	5(2)
C(7A)	25(2)	21(2)	8(2)	3(2)	6(2)	2(2)
C(21)	15(2)	41(3)	8(2)	5(2)	-1(2)	0(2)
C(22)	18(2)	39(3)	16(2)	7(2)	5(2)	1(2)
C(23)	31(3)	32(3)	27(3)	7(2)	17(2)	8(2)
C(24)	35(3)	21(3)	26(2)	-1(2)	14(2)	1(2)
C(25)	23(2)	20(3)	8(2)	3(2)	2(2)	0(2)
C(26)	18(2)	22(3)	10(2)	1(2)	3(2)	-2(2)
C(27)	21(2)	37(3)	9(2)	2(2)	5(2)	-4(2)
C(28)	22(3)	39(3)	7(2)	1(2)	2(2)	-3(2)

Table 5. Bond lengths [Å] and angles [°] for C17 H19 Cl Pt

Pt-C(1)	2.115(4)	C(26)-PT-CL	162.15(14)
Pt-C(25)	2.125(5)	C(21)-PT-CL	90.11(15)
Pt-C(26)	2.148(5)	C(22)-PT-CL	93.77(15)
Pt-C(21)	2.260(5)	C(7A)-C(1)-C(2)	103.0(4)
Pt-C(22)	2.274(5)	C(7A)-C(1)-PT	120.1(3)
Pt-Cl	2.3266(12)	C(2)-C(1)-PT	103.4(3)
C(1)-C(7a)	1.487(6)	C(3)-C(2)-C(1)	111.2(5)
C(1)-C(2)	1.494(7)	C(2)-C(3)-C(3A)	108.6(5)
C(2)-C(3)	1.352(9)	C(4)-C(3A)-C(7A)	120.9(5)
C(3)-C(3a)	1.468(9)	C(4)-C(3A)-C(3)	131.2(5)
C(3a)-C(4)	1.398(8)	C(7A)-C(3A)-C(3)	107.8(5)
C(3a)-C(7a)	1.410(7)	C(5)-C(4)-C(3A)	118.7(5)
C(4)-C(5)	1.371(10)	C(4)-C(5)-C(6)	121.5(6)
C(5)-C(6)	1.394(8)	C(5)-C(6)-C(7)	119.7(5)
C(6)-C(7)	1.398(7)	C(7A)-C(7)-C(6)	120.0(5)
C(7)-C(7a)	1.382(7)	C(7)-C(7A)-C(3A)	119.3(5)
C(21)-C(22)	1.367(8)	C(7)-C(7A)-C(1)	131.4(4)
C(21)-C(28)	1.502(8)	C(3A)-C(7A)-C(1)	109.2(5)
C(22)-C(23)	1.515(8)	C(22)-C(21)-C(28)	125.7(6)
C(23)-C(24)	1.525(8)	C(22)-C(21)-PT	73.0(3)
C(24)-C(25)	1.495(7)	C(28)-C(21)-PT	107.2(3)
C(25)-C(26)	1.403(7)	C(21)-C(22)-C(23)	124.3(5)
C(26)-C(27)	1.525(6)	C(21)-C(22)-PT	71.9(3)
C(27)-C(28)	1.548(7)	C(23)-C(22)-PT	109.3(3)
C(1)-PT-C(25)	91.54(18)	C(22)-C(23)-C(24)	112.8(5)
C(1)-PT-C(26)	97.48(18)	C(25)-C(24)-C(23)	114.4(5)
C(25)-PT-C(26)	38.35(19)	C(26)-C(25)-C(24)	125.6(4)
C(1)-PT-C(21)	164.6(2)	C(26)-C(25)-PT	71.7(3)
C(25)-PT-C(21)	96.6(2)	C(24)-C(25)-PT	109.7(3)
C(26)-PT-C(21)	81.16(19)	C(25)-C(26)-C(27)	125.0(5)
C(1)-PT-C(22)	160.2(2)	C(25)-C(26)-PT	69.9(3)
C(25)-PT-C(22)	81.00(19)	C(27)-C(26)-PT	113.3(3)
C(26)-PT-C(22)	88.02(19)	C(26)-C(27)-C(28)	113.7(4)
C(21)-PT-C(22)	35.1(2)	C(21)-C(28)-C(27)	113.8(4)
C(1)-PT-CL	86.79(14)		
C(25)-PT-CL	159.34(14)		

Table 6. Torsion angles [°] for C17 H19 Cl Pt.

C(25)-PT-C(1)-C(7A)	-40.0(4)	C(23)-C(24)-C(25)-C(26)	41.0(8)
C(26)-PT-C(1)-C(7A)	-1.9(4)	C(23)-C(24)-C(25)-PT	-40.1(6)
C(21)-PT-C(1)-C(7A)	82.0(8)	C(1)-PT-C(25)-C(26)	100.1(3)
C(22)-PT-C(1)-C(7A)	-107.1(6)	C(21)-PT-C(25)-C(26)	-66.7(3)
CL-PT-C(1)-C(7A)	160.7(4)	C(22)-PT-C(25)-C(26)	-98.3(3)
C(25)-PT-C(1)-C(2)	73.9(4)	CL-PT-C(25)-C(26)	-174.9(3)
C(26)-PT-C(1)-C(2)	111.9(4)	C(1)-PT-C(25)-C(24)	-137.6(4)
C(21)-PT-C(1)-C(2)	-164.2(6)	C(26)-PT-C(25)-C(24)	122.2(5)
C(22)-PT-C(1)-C(2)	6.8(8)	C(21)-PT-C(25)-C(24)	55.5(4)
CL-PT-C(1)-C(2)	-85.5(3)	C(22)-PT-C(25)-C(24)	24.0(4)
C(7A)-C(1)-C(2)-C(3)	3.7(6)	CL-PT-C(25)-C(24)	-52.6(6)
PT-C(1)-C(2)-C(3)	-122.0(4)	C(24)-C(25)-C(26)-C(27)	3.5(8)
C(1)-C(2)-C(3)-C(3A)	-3.4(7)	PT-C(25)-C(26)-C(27)	105.0(5)
C(2)-C(3)-C(3A)-C(4)	-174.6(6)	C(24)-C(25)-C(26)-PT	-101.5(5)
C(2)-C(3)-C(3A)-C(7A)	1.7(6)	C(1)-PT-C(26)-C(25)	-83.0(3)
C(7A)-C(3A)-C(4)-C(5)	-0.5(8)	C(21)-PT-C(26)-C(25)	112.5(3)
C(3)-C(3A)-C(4)-C(5)	175.4(6)	C(22)-PT-C(26)-C(25)	78.0(3)
C(3A)-C(4)-C(5)-C(6)	0.8(9)	CL-PT-C(26)-C(25)	174.1(3)
C(4)-C(5)-C(6)-C(7)	-1.1(9)	C(1)-PT-C(26)-C(27)	156.6(4)
C(5)-C(6)-C(7)-C(7A)	1.1(8)	C(25)-PT-C(26)-C(27)	-120.5(5)
C(6)-C(7)-C(7A)-C(3A)	-0.8(8)	C(21)-PT-C(26)-C(27)	-7.9(4)
C(6)-C(7)-C(7A)-C(1)	-177.0(5)	C(22)-PT-C(26)-C(27)	-42.5(4)
C(4)-C(3A)-C(7A)-C(7)	0.5(8)	CL-PT-C(26)-C(27)	53.6(7)
C(3)-C(3A)-C(7A)-C(7)	-176.2(5)	C(25)-C(26)-C(27)-C(28)	-90.6(6)
C(4)-C(3A)-C(7A)-C(1)	177.5(5)	PT-C(26)-C(27)-C(28)	-9.4(6)
C(3)-C(3A)-C(7A)-C(1)	0.7(6)	C(22)-C(21)-C(28)-C(27)	45.1(7)
C(2)-C(1)-C(7A)-C(7)	173.9(5)	PT-C(21)-C(28)-C(27)	-36.0(6)
PT-C(1)-C(7A)-C(7)	-72.0(7)	C(26)-C(27)-C(28)-C(21)	31.5(7)
C(2)-C(1)-C(7A)-C(3A)	-2.5(5)	C(28)-C(21)-C(22)-PT	-99.2(5)
PT-C(1)-C(7A)-C(3A)	111.6(4)	C(1)-PT-C(22)-C(21)	-175.8(5)
C(1)-PT-C(21)-C(22)	174.7(6)	C(25)-PT-C(22)-C(21)	115.3(4)
C(25)-PT-C(21)-C(22)	-64.0(4)	C(26)-PT-C(22)-C(21)	77.4(4)
C(26)-PT-C(21)-C(22)	-99.2(4)	C(1)-PT-C(22)-C(23)	63.3(7)
CL-PT-C(21)-C(22)	96.4(3)	C(25)-PT-C(22)-C(23)	-5.6(4)
C(1)-PT-C(21)-C(28)	-62.4(9)	C(26)-PT-C(22)-C(23)	-43.5(4)
C(25)-PT-C(21)-C(28)	59.0(4)	C(21)-PT-C(22)-C(23)	-120.9(5)
C(26)-PT-C(21)-C(28)	23.7(4)	CL-PT-C(22)-C(23)	154.3(4)
C(22)-PT-C(21)-C(28)	123.0(6)	C(21)-C(22)-C(23)-C(24)	-94.6(6)
CL-PT-C(21)-C(28)	-140.6(4)	PT-C(22)-C(23)-C(24)	-13.8(6)
C(28)-C(21)-C(22)-C(23)	2.2(8)	C(22)-C(23)-C(24)-C(25)	36.0(7)
PT-C(21)-C(22)-C(23)	101.4(5)		

Rapport cristallographique de la structure du composé (COD)Pt(η^1-Ind)$_2$ (**2**)

Table 1. Crystal data and structure refinement for C26 H26 Pt.

Identification code	suse31
Empirical formula	C26 H26 Pt
Formula weight	533.56
Temperature	125(2)K
Wavelength	0.71073 Å
Crystal system	Triclinic
Space group	P-1
Unit cell dimensions	a = 8.3210(11) Å α = 71.156(2)°
	b = 10.5075(14) Å β = 75.883(2)°
	c = 12.5313(17) Å γ = 69.848(2)°
Volume	962.5(2)Å^3
Z	2
Density (calculated)	1.841 Mg/m^3
Absorption coefficient	7.296 mm^{-1}
F(000)	520
Crystal size	0.12 x 0.09 x 0.05 mm
Theta range for data collection	1.74 to 29.14°
Index ranges	$-11 \le h \le 10$, $-14 \le k \le 14$, $-16 \le \lambda \le 17$
Reflections collected	9852
Independent reflections	5035 [R_{int} = 0.026]
Absorption correction	Semi-empirical from equivalents
Max. and min. transmission	0.0000 and 0.0000
Refinement method	Full-matrix least-squares on F^2
Data / restraints / parameters	5035 / 0 / 325
Goodness-of-fit on F^2	1.032
Final R indices [I>2sigma(I)]	R_1 = 0.0290, wR_2 = 0.0580
R indices (all data)	R_1 = 0.0389, wR_2 = 0.0611
Largest diff. peak and hole	2.323 and -0.950 e/Å^3

Table 2. Atomic coordinates (x 10^4) and equivalent isotropic displacement parameters ($Å^2$ x 10^3) for C26 H26 Pt.

U_{eq} is defined as one third of the trace of the orthogonalized Uij tensor.

	x	y	z	U_{eq}
Pt	9124(1)	7421(1)	6960(1)	14(1)
C(11)	9128(6)	6234(5)	5882(4)	18(1)
C(12)	7843(6)	6994(5)	5084(4)	20(1)
C(13)	6606(6)	6333(5)	5308(4)	21(1)
C(13A)	7024(5)	5065(4)	6229(4)	18(1)
C(14)	6207(6)	4016(5)	6748(4)	21(1)
C(15)	6951(6)	2866(5)	7590(4)	22(1)
C(16)	8471(6)	2787(5)	7919(4)	22(1)
C(17)	9292(6)	3831(5)	7407(4)	20(1)
C(17A)	8564(5)	4973(4)	6562(3)	17(1)
C(1)	6475(5)	7564(5)	7556(4)	16(1)
C(2)	6311(5)	6500(5)	8683(4)	20(1)
C(3)	5293(6)	7116(5)	9496(4)	21(1)
C(3A)	4654(5)	8621(4)	8991(4)	18(1)
C(4)	3506(6)	9703(5)	9456(4)	21(1)
C(5)	3049(6)	11054(5)	8746(4)	21(1)
C(6)	3719(5)	11318(5)	7587(4)	19(1)
C(7)	4866(5)	10247(5)	7121(4)	19(1)
C(7A)	5333(5)	8889(4)	7827(3)	15(1)
C(21)	11954(5)	6537(5)	6915(4)	24(1)
C(22)	11668(5)	7700(5)	6006(4)	22(1)
C(23)	11799(7)	9114(6)	5961(5)	29(1)
C(24)	10815(7)	9653(6)	6995(5)	31(1)
C(25)	9289(6)	9121(5)	7613(4)	24(1)
C(26)	9356(6)	7930(5)	8486(4)	23(1)
C(27)	10958(7)	6884(7)	8924(5)	34(1)
C(28)	12484(7)	6524(6)	7995(5)	33(1)

Table 3. Hydrogen coordinates (x 10^4) and isotropic displacement parameters ($Å^2$ x 10^3) for C26 H26 Pt.

	x	y	z	U_{eq}
H(1)	10220(80)	6080(60)	5580(50)	45(17)
H(2)	7860(70)	7820(60)	4590(50)	38(16)
H(3)	5570(50)	6690(40)	4930(40)	9(10)
H(4)	5250(60)	4040(50)	6500(40)	25
H(5)	6400(60)	2130(50)	7980(40)	26
H(6)	8960(60)	2050(50)	8490(40)	26
H(7)	10310(60)	3700(50)	7630(40)	24
H(11)	6180(60)	7350(50)	6970(40)	20
H(12)	6960(60)	5490(50)	8770(40)	24
H(13)	5000(60)	6670(50)	10290(40)	25
H(14)	3160(60)	9520(50)	10260(40)	25
H(15)	2140(60)	11870(50)	9060(40)	25
H(16)	3480(60)	12250(50)	7130(40)	23
H(17)	5310(60)	10380(50)	6360(40)	22
H(21)	12200(60)	5630(50)	6810(40)	29
H(22)	11690(60)	7520(50)	5330(40)	26
H(23A)	11420(70)	9770(60)	5220(50)	35
H(23B)	13060(70)	9060(50)	5800(40)	35
H(24A)	11630(70)	9380(60)	7530(50)	37
H(24B)	10430(70)	10570(60)	6790(50)	37
H(25)	8300(70)	9700(50)	7580(40)	28
H(26)	8410(70)	7850(50)	8920(40)	28
H(27A)	10740(70)	5990(60)	9300(50)	41
H(27B)	11200(70)	7190(60)	9430(50)	41
H(28A)	13180(70)	7150(60)	7800(50)	40
H(28B)	13110(70)	5540(60)	8320(50)	40

Table 4. Anisotropic parameters ($Å^2$ x 10^3) for C26 H26 Pt.

The anisotropic displacement factor exponent takes the form:

$$-2\pi^2 [h^2 a^{*2} U_{11} + ... + 2 h k a^* b^* U_{12}]$$

	U11	U22	U33	U23	U13	U12
Pt	10(1)	17(1)	17(1)	-7(1)	0(1)	-3(1)
C(11)	15(2)	22(2)	20(2)	-7(2)	-2(2)	-6(2)
C(12)	22(2)	22(2)	18(2)	-7(2)	-1(2)	-7(2)
C(13)	22(2)	22(2)	19(2)	-8(2)	-5(2)	-3(2)
C(13A)	19(2)	19(2)	18(2)	-9(2)	-2(2)	-3(2)
C(14)	17(2)	24(2)	22(2)	-11(2)	0(2)	-5(2)
C(15)	24(2)	20(2)	23(2)	-11(2)	3(2)	-8(2)
C(16)	27(2)	13(2)	20(2)	-5(2)	-4(2)	1(2)
C(17)	13(2)	25(2)	22(2)	-12(2)	-3(2)	-1(2)
C(17A)	16(2)	18(2)	17(2)	-10(2)	0(2)	-4(2)
C(1)	9(2)	23(2)	19(2)	-9(2)	3(2)	-6(2)
C(2)	14(2)	21(2)	25(2)	-10(2)	-1(2)	-4(2)
C(3)	20(2)	23(2)	19(2)	-5(2)	-1(2)	-7(2)
C(3A)	15(2)	22(2)	18(2)	-9(2)	-5(2)	-1(2)
C(4)	19(2)	24(2)	17(2)	-8(2)	-2(2)	-1(2)
C(5)	21(2)	19(2)	22(2)	-10(2)	-4(2)	-1(2)
C(6)	18(2)	18(2)	20(2)	-3(2)	-4(2)	-6(2)
C(7)	13(2)	24(2)	17(2)	-5(2)	1(2)	-6(2)
C(7A)	9(2)	20(2)	20(2)	-11(2)	-1(2)	-5(2)
C(21)	10(2)	30(3)	33(3)	-14(2)	-1(2)	-3(2)
C(22)	17(2)	29(3)	22(2)	-11(2)	3(2)	-9(2)
C(23)	26(3)	32(3)	36(3)	-15(2)	4(2)	-15(2)
C(24)	25(3)	26(3)	44(3)	-15(2)	5(2)	-11(2)
C(25)	17(2)	28(3)	33(3)	-20(2)	3(2)	-9(2)
C(26)	19(2)	39(3)	19(2)	-15(2)	3(2)	-15(2)
C(27)	33(3)	46(3)	29(3)	-11(3)	-11(2)	-13(3)
C(28)	24(3)	40(3)	35(3)	-6(2)	-11(2)	-8(2)

Table 5. Bond lengths [Å] and angles [°] for C26 H26 Pt

Pt-C(11)	2.113(4)	C(22)-PT-C(25)	79.37(16)
Pt-C(1)	2.116(4)	C(12)-C(11)-C(17A)	103.4(3)
Pt-C(21)	2.207(4)	C(12)-C(11)-PT	112.9(3)
Pt-C(26)	2.212(4)	C(17A)-C(11)-PT	110.3(3)
Pt-C(22)	2.228(4)	C(13)-C(12)-C(11)	110.6(4)
Pt-C(25)	2.248(4)	C(12)-C(13)-C(13A)	108.8(4)
C(11)-C(12)	1.483(6)	C(14)-C(13A)-C(17A)	120.5(4)
C(11)-C(17a)	1.484(6)	C(14)-C(13A)-C(13)	131.3(4)
C(12)-C(13)	1.360(6)	C(17A)-C(13A)-C(13)	108.2(4)
C(13)-C(13a)	1.452(6)	C(15)-C(14)-C(13A)	119.0(4)
C(13a)-C(14)	1.393(6)	C(14)-C(15)-C(16)	120.2(4)
C(13a)-C(17a)	1.406(6)	C(17)-C(16)-C(15)	121.2(4)
C(14)-C(15)	1.391(6)	C(17A)-C(17)-C(16)	118.9(4)
C(15)-C(16)	1.392(6)	C(17)-C(17A)-C(13A)	120.3(4)
C(16)-C(17)	1.388(6)	C(17)-C(17A)-C(11)	130.9(4)
C(17)-C(17a)	1.385(6)	C(13A)-C(17A)-C(11)	108.8(4)
C(1)-C(7a)	1.481(5)	C(7A)-C(1)-C(2)	102.2(3)
C(1)-C(2)	1.501(6)	C(7A)-C(1)-PT	117.5(3)
C(2)-C(3)	1.342(6)	C(2)-C(1)-PT	109.2(3)
C(3)-C(3a)	1.458(6)	C(3)-C(2)-C(1)	111.3(4)
C(3a)-C(4)	1.397(6)	C(2)-C(3)-C(3A)	108.9(4)
C(3a)-C(7a)	1.403(6)	C(4)-C(3A)-C(7A)	120.8(4)
C(4)-C(5)	1.389(6)	C(4)-C(3A)-C(3)	131.3(4)
C(5)-C(6)	1.396(6)	C(7A)-C(3A)-C(3)	107.7(4)
C(6)-C(7)	1.389(6)	C(5)-C(4)-C(3A)	118.8(4)
C(7)-C(7a)	1.393(6)	C(4)-C(5)-C(6)	120.3(4)
C(21)-C(22)	1.371(7)	C(7)-C(6)-C(5)	121.1(4)
C(21)-C(28)	1.518(7)	C(6)-C(7)-C(7A)	119.0(4)
C(22)-C(23)	1.509(6)	C(7)-C(7A)-C(3A)	119.9(4)
C(23)-C(24)	1.518(7)	C(7)-C(7A)-C(1)	130.3(4)
C(24)-C(25)	1.501(6)	C(3A)-C(7A)-C(1)	109.8(4)
C(25)-C(26)	1.365(7)	C(22)-C(21)-C(28)	123.2(5)
C(26)-C(27)	1.498(7)	C(22)-C(21)-PT	72.8(3)
C(27)-C(28)	1.531(8)	C(28)-C(21)-PT	110.8(3)
		C(21)-C(22)-C(23)	124.8(4)
C(11)-PT-C(1)	88.64(16)	C(21)-C(22)-PT	71.2(2)
C(11)-PT-C(21)	91.46(17)	C(23)-C(22)-PT	110.7(3)
C(1)-PT-C(21)	157.37(18)	C(22)-C(23)-C(24)	114.2(4)
C(11)-PT-C(26)	160.23(18)	C(25)-C(24)-C(23)	115.7(4)
C(1)-PT-C(26)	91.03(16)	C(26)-C(25)-C(24)	125.0(5)
C(21)-PT-C(26)	81.36(17)	C(26)-C(25)-PT	70.8(3)
C(11)-PT-C(22)	89.99(16)	C(24)-C(25)-PT	112.2(3)
C(1)-PT-C(22)	166.59(17)	C(25)-C(26)-C(27)	126.1(4)
C(21)-PT-C(22)	36.00(17)	C(25)-C(26)-PT	73.6(3)
C(26)-PT-C(22)	94.72(17)	C(27)-C(26)-PT	106.8(3)
C(11)-PT-C(25)	163.19(17)	C(26)-C(27)-C(28)	114.6(4)
C(1)-PT-C(25)	98.68(16)	C(21)-C(28)-C(27)	113.9(4)
C(21)-PT-C(25)	87.54(17)		
C(26)-PT-C(25)	35.65(18)		

Table 6. Torsion angles [°] for C26 H26 Pt.

C(1)-PT-C(11)-C(12)	58.2(3)
C(21)-PT-C(11)-C(12)	-144.5(3)
C(26)-PT-C(11)-C(12)	147.4(4)
C(22)-PT-C(11)-C(12)	-108.5(3)
C(25)-PT-C(11)-C(12)	-58.1(7)
C(1)-PT-C(11)-C(17A)	-57.0(3)
C(21)-PT-C(11)-C(17A)	100.4(3)
C(26)-PT-C(11)-C(17A)	32.3(6)
C(22)-PT-C(11)-C(17A)	136.4(3)
C(25)-PT-C(11)-C(17A)	-173.3(5)
PT-C(11)-C(12)-C(13)	-115.4(4)
C(11)-C(12)-C(13)-C(13A)	-2.5(5)
C(13)-C(13A)-C(14)-C(15)	177.0(4)
C(13A)-C(14)-C(15)-C(16)	1.3(6)
C(14)-C(15)-C(16)-C(17)	-1.1(6)
C(15)-C(16)-C(17)-C(17A)	0.7(6)
C(16)-C(17)-C(17A)-C(13A)	-0.3(6)
C(16)-C(17)-C(17A)-C(11)	179.4(4)
C(14)-C(13A)-C(17A)-C(17)	0.5(6)
C(13)-C(13A)-C(17A)-C(17)	177.9(4)
C(14)-C(13A)-C(17A)-C(11)	-179.3(4)
C(13)-C(13A)-C(17A)-C(11)	2.4(5)
C(12)-C(11)-C(17A)-C(17)	176.6(4)
PT-C(11)-C(17A)-C(17)	-62.5(5)
C(12)-C(11)-C(17A)-C(13A)	-3.7(4)
PT-C(11)-C(17A)-C(13A)	117.3(3)
C(11)-PT-C(1)-C(7A)	-144.3(3)
C(21)-PT-C(1)-C(7A)	125.1(4)
C(26)-PT-C(1)-C(7A)	55.4(3)
C(22)-PT-C(1)-C(7A)	-60.1(8)
C(25)-PT-C(1)-C(7A)	20.5(4)
C(11)-PT-C(1)-C(2)	100.0(3)
C(21)-PT-C(1)-C(2)	9.4(6)
C(26)-PT-C(1)-C(2)	-60.3(3)
C(22)-PT-C(1)-C(2)	-175.8(6)
C(25)-PT-C(1)-C(2)	-95.2(3)
C(7A)-C(1)-C(2)-C(3)	-2.3(5)
PT-C(1)-C(2)-C(3)	122.8(3)
C(1)-C(2)-C(3)-C(3A)	1.4(5)
C(2)-C(3)-C(3A)-C(4)	176.8(4)
C(2)-C(3)-C(3A)-C(7A)	0.2(5)
C(7A)-C(3A)-C(4)-C(5)	-0.2(6)
C(3)-C(3A)-C(4)-C(5)	-176.4(4)
C(3A)-C(4)-C(5)-C(6)	0.5(7)
C(4)-C(5)-C(6)-C(7)	-0.8(7)
C(5)-C(6)-C(7)-C(7A)	0.8(6)
C(6)-C(7)-C(7A)-C(3A)	-0.5(6)
C(6)-C(7)-C(7A)-C(1)	178.2(4)
C(4)-C(3A)-C(7A)-C(7)	0.2(6)
C(3)-C(3A)-C(7A)-C(7)	177.2(4)
C(4)-C(3A)-C(7A)-C(11)	-178.7(4)
C(3)-C(3A)-C(7A)-C(1)	-1.7(5)
C(2)-C(1)-C(7A)-C(7)	-176.4(4)
PT-C(1)-C(7A)-C(7)	64.2(5)
C(2)-C(1)-C(7A)-C(3A)	2.4(4)
PT-C(1)-C(7A)-C(3A)	-117.1(3)
C(11)-PT-C(21)-C(22)	88.0(3)
C(1)-PT-C(21)-C(22)	177.9(4)
C(26)-PT-C(21)-C(22)	-110.5(3)
C(25)-PT-C(21)-C(22)	-75.2(3)
C(11)-PT-C(21)-C(28)	-152.3(4)
C(1)-PT-C(21)-C(28)	-62.4(6)
C(26)-PT-C(21)-C(28)	9.2(4)
C(22)-PT-C(21)-C(28)	119.7(5)
C(25)-PT-C(21)-C(28)	44.5(4)
C(28)-C(21)-C(22)-C(23)	-1.4(7)
PT-C(21)-C(22)-C(23)	102.5(4)
C(28)-C(21)-C(22)-PT	-104.0(4)
C(11)-PT-C(22)-C(21)	-92.5(3)
C(1)-PT-C(22)-C(21)	-176.6(6)
C(26)-PT-C(22)-C(21)	68.3(3)
C(25)-PT-C(22)-C(21)	100.6(3)
C(11)-PT-C(22)-C(23)	146.4(4)
C(1)-PT-C(22)-C(23)	62.3(8)
C(21)-PT-C(22)-C(23)	-121.1(5)
C(26)-PT-C(22)-C(23)	-52.8(4)
C(25)-PT-C(22)-C(23)	-20.5(3)
C(21)-C(22)-C(23)-C(24)	-49.5(7)
PT-C(22)-C(23)-C(24)	31.4(6)
C(22)-C(23)-C(24)-C(25)	-26.6(7)
C(23)-C(24)-C(25)-C(26)	89.5(6)
C(23)-C(24)-C(25)-PT	8.1(6)
C(11)-PT-C(25)-C(26)	-165.5(5)
C(1)-PT-C(25)-C(26)	79.5(3)
C(21)-PT-C(25)-C(26)	-78.6(3)
C(22)-PT-C(25)-C(26)	-113.9(3)
C(11)-PT-C(25)-C(24)	-44.6(8)
C(1)-PT-C(25)-C(24)	-159.6(4)
C(21)-PT-C(25)-C(24)	42.3(4)
C(26)-PT-C(25)-C(24)	120.9(5)
C(22)-PT-C(25)-C(24)	7.0(4)
C(24)-C(25)-C(26)-C(27)	-5.1(7)
PT-C(25)-C(26)-C(27)	99.0(5)
C(24)-C(25)-C(26)-PT	-104.1(4)
C(11)-PT-C(26)-C(25)	167.6(4)
C(1)-PT-C(26)-C(25)	-103.5(3)
C(21)-PT-C(26)-C(25)	97.9(3)
C(22)-PT-C(26)-C(25)	64.4(3)
C(11)-PT-C(26)-C(27)	44.0(6)
C(1)-PT-C(26)-C(27)	132.9(3)
C(21)-PT-C(26)-C(27)	-25.7(3)
C(22)-PT-C(26)-C(27)	-59.3(4)
C(25)-PT-C(26)-C(27)	-123.6(5)
C(25)-C(26)-C(27)-C(28)	-42.2(7)
PT-C(26)-C(27)-C(28)	39.4(5)
C(22)-C(21)-C(28)-C(27)	92.0(6)
PT-C(21)-C(28)-C(27)	9.4(6)

Rapport cristallographique de la structure du composé [(η-Ind)Pt(COD)][BF_4] (**3**).

Table 1. Crystal data and structure refinement for C17 H19 B F4 Pt.

Identification code	suse32
Empirical formula	C17 H19 B F4 Pt
Formula weight	505.22
Temperature	125(2)K
Wavelength	0.71073 Å
Crystal system	Orthorombic
Space group	Aba2
Unit cell dimensions	a = 12.2596(11) Å α = 90° b = 23.111(2) Å β = 90° c = 11.0481(10) Å γ = 90°
Volume	3130.2(5)Å^3
Z	8
Density (calculated)	2.144 Mg/m^3
Absorption coefficient	9.001 mm^{-1}
F(000)	1920
Crystal size	0.45 x 0.25 x 0.06 mm
Theta range for data collection	1.76 to 29.12°
Index ranges	$-16 \le h \le 16$, $-31 \le k \le 31$, $-15 \le \lambda \le 15$
Reflections collected	19174
Independent reflections	4189 [R_{int} = 0.043]
Absorption correction	Semi-empirical from equivalents
Max. and min. transmission	0.084 and 0.583
Refinement method	Full-matrix least-squares on F^2
Data / restraints / parameters	4189 / 1 / 265
Goodness-of-fit on F^2	0.982
Final R indices [I>2sigma(I)]	R_1 = 0.0141, wR_2 = 0.0324
R indices (all data)	R_1 = 0.0170, wR_2 = 0.0336
Absolute structure parameter	0.015(5)
Largest diff. peak and hole	0.516 and -0.947 e/Å^3

Table 2. Atomic coordinates (x 10^4) and equivalent isotropic displacement parameters ($Å^2$ x 10^3) for C17 H19 B F4 Pt.

U_{eq} is defined as one third of the trace of the orthogonalized Uij tensor.

	x	y	z	U_{eq}
Pt	817(1)	1437(1)	7859(1)	14(1)
C(1)	2560(3)	1551(1)	7387(3)	21(1)
C(2)	1929(2)	1954(1)	6702(2)	21(1)
C(3)	1198(3)	1619(2)	5959(3)	20(1)
C(3A)	1566(2)	1014(1)	5986(2)	16(1)
C(4)	1211(2)	527(1)	5357(3)	20(1)
C(5)	1716(2)	5(1)	5598(2)	22(1)
C(6)	2545(2)	-39(1)	6471(2)	23(1)
C(7)	2895(2)	435(1)	7115(2)	22(1)
C(7A)	2405(2)	971(1)	6870(2)	17(1)
C(21)	666(2)	1044(1)	9645(2)	19(1)
C(22)	887(3)	1638(2)	9763(4)	20(1)
C(23)	42(2)	2093(1)	10045(2)	22(1)
C(24)	-1015(2)	2031(1)	9296(3)	22(1)
C(25)	-834(2)	1774(1)	8043(4)	19(1)
C(26)	-886(2)	1178(1)	7785(6)	19(1)
C(27)	-1098(3)	708(1)	8693(3)	25(1)
C(28)	-452(3)	793(1)	9874(3)	23(1)
B	5919(3)	1416(1)	8349(4)	23(1)
F(1)	6296(2)	1463(1)	9530(2)	40(1)
F(2)	6679(2)	1616(1)	7526(2)	39(1)
F(3)	4962(1)	1742(1)	8241(2)	37(1)
F(4)	5678(2)	842(1)	8108(2)	49(1)

Table 3. Hydrogen coordinates ($\times 10^4$) and isotropic displacement parameters ($Å^2 \times 10^3$) for C17 H19 B F4 Pt.

	x	y	z	U_{eq}
H(1)	3070(20)	1622(12)	7780(40)	25
H(2)	1890(30)	2378(14)	6720(30)	25
H(3)	680(20)	1734(17)	5330(40)	24
H(4)	650(20)	538(15)	4760(30)	24
H(5)	1510(30)	-333(14)	5220(30)	26
H(6)	2910(30)	-389(15)	6550(30)	28
H(7)	3390(20)	387(12)	7660(30)	27
H(21)	1240(30)	750(15)	9650(30)	23
H(22)	1590(30)	1708(16)	9860(30)	24
H(23A)	330(30)	2442(15)	9910(30)	26
H(23B)	-90(30)	2064(14)	10960(30)	26
H(24A)	-1540(30)	1818(15)	9720(30)	26
H(24B)	-1380(30)	2401(15)	9210(30)	26
H(25)	-970(20)	2048(16)	7270(30)	23
H(26)	-1050(30)	1035(17)	6990(30)	23
H(27A)	-940(20)	314(16)	8300(30)	30
H(27B)	-1850(30)	703(15)	8860(30)	30
H(28A)	-760(20)	1019(16)	10370(30)	27
H(28B)	-380(30)	411(15)	10210(30)	27

Table 4. Anisotropic parameters ($Å^2$ x 10^3) for C17 H19 B F4 Pt.

The anisotropic displacement factor exponent takes the form:

$$-2\pi^2 [h^2 a^{*2} U_{11} + ... + 2 h k a^* b^* U_{12}]$$

	U11	U22	U33	U23	U13	U12
Pt	13(1)	15(1)	13(1)	0(1)	0(1)	1(1)
C(1)	16(1)	27(1)	20(1)	-2(1)	1(1)	-4(1)
C(2)	20(1)	18(1)	24(1)	1(1)	7(1)	-2(1)
C(3)	22(2)	21(2)	18(2)	3(1)	5(1)	2(2)
C(3A)	15(1)	22(1)	12(1)	1(1)	5(1)	1(1)
C(4)	19(1)	27(1)	15(1)	-2(1)	2(1)	-1(1)
C(5)	23(1)	20(1)	22(2)	-3(1)	6(1)	0(1)
C(6)	25(1)	20(1)	25(1)	4(1)	10(1)	7(1)
C(7)	18(1)	33(2)	16(1)	6(1)	3(1)	7(1)
C(7A)	17(1)	21(1)	14(1)	2(1)	4(1)	2(1)
C(21)	24(1)	20(1)	14(1)	2(1)	-1(1)	6(1)
C(22)	25(2)	20(2)	15(2)	1(1)	-3(1)	1(1)
C(23)	27(2)	17(1)	22(1)	-3(1)	1(1)	-1(1)
C(24)	21(1)	18(1)	26(1)	-1(1)	4(1)	4(1)
C(25)	12(1)	23(1)	22(3)	3(1)	-2(1)	4(1)
C(26)	13(1)	24(1)	21(2)	1(2)	1(2)	-1(1)
C(27)	23(1)	21(1)	30(2)	-1(1)	5(1)	-8(1)
C(28)	27(2)	18(1)	23(1)	1(1)	6(1)	0(1)
B	21(2)	26(2)	23(2)	2(1)	0(1)	3(1)
F(1)	37(1)	52(1)	30(1)	0(1)	-9(1)	6(1)
F(2)	22(1)	50(1)	46(1)	17(1)	10(1)	0(1)
F(3)	22(1)	53(1)	36(1)	-7(1)	-3(1)	13(1)
F(4)	68(1)	29(1)	49(2)	-6(1)	18(1)	-9(1)

Table 5. Bond lengths [Å] and angles [°] for C17 H19 B F4 Pt

Pt-C(22)	2.155(4)	C(1)-PT-C(3A)	59.36(10)
Pt-C(26)	2.174(2)	C(2)-PT-C(3A)	60.05(10)
Pt-C(25)	2.178(2)	C(22)-PT-C(7A)	119.52(11)
Pt-C(21)	2.180(3)	C(26)-PT-C(7A)	128.14(14)
Pt-C(3)	2.192(4)	C(25)-PT-C(7A)	157.85(12)
Pt-C(1)	2.216(3)	C(21)-PT-C(7A)	106.54(9)
Pt-C(2)	2.218(3)	C(3)-PT-C(7A)	59.57(11)
Pt-C(3a)	2.467(2)	C(1)-PT-C(7A)	35.95(10)
Pt-C(7a)	2.480(2)	C(2)-PT-C(7A)	59.79(10)
C(1)-C(2)	1.427(4)	C(3A)-PT-C(7A)	33.41(9)
C(1)-C(7a)	1.470(4)	C(2)-C(1)-C(7A)	108.6(3)
C(2)-C(3)	1.441(5)	C(2)-C(1)-PT	71.29(17)
C(3)-C(3a)	1.470(5)	C(7A)-C(1)-PT	81.84(16)
C(3a)-C(4)	1.391(4)	C(1)-C(2)-C(3)	106.9(3)
C(3a)-C(7a)	1.422(4)	C(1)-C(2)-PT	71.18(16)
C(4)-C(5)	1.384(4)	C(3)-C(2)-PT	69.96(18)
C(5)-C(6)	1.405(4)	C(2)-C(3)-C(3A)	107.9(3)
C(6)-C(7)	1.375(4)	C(2)-C(3)-PT	71.91(18)
C(7)-C(7a)	1.403(4)	C(3A)-C(3)-PT	82.17(19)
C(21)-C(22)	1.405(5)	C(4)-C(3A)-C(7A)	120.8(3)
C(21)-C(28)	1.510(4)	C(4)-C(3A)-C(3)	131.5(3)
C(22)-C(23)	1.508(5)	C(7A)-C(3A)-C(3)	107.6(2)
C(23)-C(24)	1.544(4)	C(4)-C(3A)-PT	128.52(19)
C(24)-C(25)	1.522(5)	C(7A)-C(3A)-PT	73.78(14)
C(25)-C(26)	1.408(4)	C(3)-C(3A)-PT	61.65(16)
C(26)-C(27)	1.502(6)	C(5)-C(4)-C(3A)	118.0(3)
C(27)-C(28)	1.539(4)	C(4)-C(5)-C(6)	121.3(3)
B-F(2)	1.382(4)	C(7)-C(6)-C(5)	121.6(3)
B-F(4)	1.385(4)	C(6)-C(7)-C(7A)	118.0(3)
B-F(1)	1.389(5)	C(7)-C(7A)-C(3A)	120.3(3)
B-F(3)	1.398(4)	C(7)-C(7A)-C(1)	132.4(3)
C(22)-PT-C(26)	97.7(2)	C(3A)-C(7A)-C(1)	107.3(2)
C(22)-PT-C(25)	82.47(14)	C(7)-C(7A)-PT	129.38(18)
C(26)-PT-C(25)	37.76(10)	C(3A)-C(7A)-PT	72.81(14)
C(22)-PT-C(21)	37.83(14)	C(1)-C(7A)-PT	62.21(15)
C(26)-PT-C(21)	80.66(18)	C(22)-C(21)-C(28)	122.4(3)
C(25)-PT-C(21)	89.17(12)	C(22)-C(21)-PT	70.15(19)
C(22)-PT-C(3)	152.24(11)	C(28)-C(21)-PT	112.93(19)
C(26)-PT-C(3)	102.8(2)	C(21)-C(22)-C(23)	124.6(3)
C(25)-PT-C(3)	102.65(14)	C(21)-C(22)-PT	72.02(19)
C(21)-PT-C(3)	164.81(13)	C(23)-C(22)-PT	109.0(2)
C(22)-PT-C(1)	99.55(12)	C(22)-C(23)-C(24)	113.6(2)
C(26)-PT-C(1)	161.86(18)	C(25)-C(24)-C(23)	113.7(2)
C(25)-PT-C(1)	151.16(11)	C(26)-C(25)-C(24)	124.0(3)
C(21)-PT-C(1)	110.16(11)	C(26)-C(25)-PT	70.97(13)
C(3)-PT-C(1)	62.99(13)	C(24)-C(25)-PT	111.1(2)
C(22)-PT-C(2)	114.97(13)	C(25)-C(26)-C(27)	125.5(4)
C(26)-PT-C(2)	135.83(18)	C(25)-C(26)-PT	71.27(13)
C(25)-PT-C(2)	115.67(11)	C(27)-C(26)-PT	109.9(3)
C(21)-PT-C(2)	142.96(11)	C(26)-C(27)-C(28)	112.6(3)
C(3)-PT-C(2)	38.14(13)	C(21)-C(28)-C(27)	111.9(2)
C(1)-PT-C(2)	37.54(11)	F(2)-B-F(4)	109.7(3)
C(22)-PT-C(3A)	152.80(11)	F(2)-B-F(1)	111.6(3)
C(26)-PT-C(3A)	102.50(18)	F(4)-B-F(1)	109.1(3)
C(25)-PT-C(3A)	124.47(12)	F(2)-B-F(3)	109.3(3)
C(21)-PT-C(3A)	128.74(10)	F(4)-B-F(3)	108.7(3)
C(3)-PT-C(3A)	36.18(12)	F(1)-B-F(3)	108.5(3)

Table 6. Torsion angles [°] for C17 H19 B F4 Pt.

C(22)-PT-C(1)-C(2)	-118.92(19)	C(2)-PT-C(3A)-C(4)	-163.7(3)
C(26)-PT-C(1)-C(2)	79.0(4)	C(7A)-PT-C(3A)-C(4)	116.8(3)
C(25)-PT-C(1)-C(2)	-27.2(3)	C(22)-PT-C(3A)-C(7A)	-7.3(4)
C(21)-PT-C(1)-C(2)	-156.60(16)	C(26)-PT-C(3A)-C(7A)	-144.37(18)
C(3)-PT-C(1)-C(2)	38.22(18)	C(25)-PT-C(3A)-C(7A)	-178.27(15)
C(3A)-PT-C(1)-C(2)	79.53(17)	C(21)-PT-C(3A)-C(7A)	-56.4(2)
C(7A)-PT-C(1)-C(2)	112.8(2)	C(3)-PT-C(3A)-C(7A)	121.0(3)
C(22)-PT-C(1)-C(7A)	128.26(19)	C(1)-PT-C(3A)-C(7A)	35.81(16)
C(26)-PT-C(1)-C(7A)	-33.9(5)	C(2)-PT-C(3A)-C(7A)	79.56(17)
C(25)-PT-C(1)-C(7A)	-140.0(2)	C(22)-PT-C(3A)-C(3)	-128.2(3)
C(21)-PT-C(1)-C(7A)	90.58(17)	C(26)-PT-C(3A)-C(3)	94.6(2)
C(3)-PT-C(1)-C(7A)	-74.60(19)	C(25)-PT-C(3A)-C(3)	60.8(2)
C(2)-PT-C(1)-C(7A)	-112.8(2)	C(21)-PT-C(3A)-C(3)	-177.4(2)
C(3A)-PT-C(1)-C(7A)	-33.29(15)	C(1)-PT-C(3A)-C(3)	-85.2(2)
C(7A)-C(1)-C(2)-C(3)	13.0(3)	C(2)-PT-C(3A)-C(3)	-41.4(2)
PT-C(1)-C(2)-C(3)	-61.2(2)	C(7A)-PT-C(3A)-C(3)	-121.0(3)
C(7A)-C(1)-C(2)-PT	74.2(2)	C(7A)-C(3A)-C(4)-C(5)	-1.5(4)
C(22)-PT-C(2)-C(1)	72.2(2)	C(3)-C(3A)-C(4)-C(5)	-178.9(3)
C(26)-PT-C(2)-C(1)	-154.0(2)	PT-C(3A)-C(4)-C(5)	-94.9(3)
C(25)-PT-C(2)-C(1)	165.84(17)	C(3A)-C(4)-C(5)-C(6)	1.6(4)
C(21)-PT-C(2)-C(1)	38.2(3)	C(4)-C(5)-C(6)-C(7)	-0.5(4)
C(3)-PT-C(2)-C(1)	-116.8(3)	C(5)-C(6)-C(7)-C(7A)	-0.5(4)
C(3A)-PT-C(2)-C(1)	-77.57(17)	C(6)-C(7)-C(7A)-C(3A)	0.6(4)
C(7A)-PT-C(2)-C(1)	-38.76(16)	C(6)-C(7)-C(7A)-C(1)	178.8(3)
C(22)-PT-C(2)-C(3)	-171.00(18)	C(6)-C(7)-C(7A)-PT	92.7(3)
C(26)-PT-C(2)-C(3)	-37.2(3)	C(4)-C(3A)-C(7A)-C(7)	0.5(4)
C(25)-PT-C(2)-C(3)	-77.4(2)	C(3)-C(3A)-C(7A)-C(7)	178.4(3)
C(21)-PT-C(2)-C(3)	155.0(2)	PT-C(3A)-C(7A)-C(7)	126.0(2)
C(1)-PT-C(2)-C(3)	116.8(3)	C(4)-C(3A)-C(7A)-C(1)	-178.2(2)
C(3A)-PT-C(2)-C(3)	39.23(18)	C(3)-C(3A)-C(7A)-C(1)	-0.3(3)
C(7A)-PT-C(2)-C(3)	78.0(2)	PT-C(3A)-C(7A)-C(1)	-52.61(18)
C(1)-C(2)-C(3)-C(3A)	-13.1(3)	C(4)-C(3A)-C(7A)-PT	-125.6(2)
PT-C(2)-C(3)-C(3A)	-75.1(2)	C(3)-C(3A)-C(7A)-PT	52.33(19)
C(1)-C(2)-C(3)-PT	62.0(2)	C(2)-C(1)-C(7A)-C(7)	173.6(3)
C(22)-PT-C(3)-C(2)	17.7(4)	PT-C(1)-C(7A)-C(7)	-119.3(3)
C(26)-PT-C(3)-C(2)	154.40(18)	C(2)-C(1)-C(7A)-C(3A)	-8.0(3)
C(25)-PT-C(3)-C(2)	115.66(19)	PT-C(1)-C(7A)-C(3A)	59.09(19)
C(21)-PT-C(3)-C(2)	-104.0(5)	C(2)-C(1)-C(7A)-PT	-67.0(2)
C(1)-PT-C(3)-C(2)	-37.62(18)	C(22)-PT-C(7A)-C(7)	60.8(3)
C(3A)-PT-C(3)-C(2)	-111.8(3)	C(26)-PT-C(7A)-C(7)	-69.1(3)
C(7A)-PT-C(3)-C(2)	-78.64(19)	C(25)-PT-C(7A)-C(7)	-111.6(3)
C(22)-PT-C(3)-C(3A)	129.6(2)	C(21)-PT-C(7A)-C(7)	21.9(3)
C(26)-PT-C(3)-C(3A)	-93.76(19)	C(3)-PT-C(7A)-C(7)	-151.3(3)
C(25)-PT-C(3)-C(3A)	-132.50(18)	C(1)-PT-C(7A)-C(7)	123.6(3)
C(21)-PT-C(3)-C(3A)	7.8(6)	C(2)-PT-C(7A)-C(7)	164.2(3)
C(1)-PT-C(3)-C(3A)	74.22(18)	C(3A)-PT-C(7A)-C(7)	-115.4(3)
C(2)-PT-C(3)-C(3A)	111.8(3)	C(22)-PT-C(7A)-C(3A)	176.20(19)
C(7A)-PT-C(3)-C(3A)	33.20(16)	C(26)-PT-C(7A)-C(3A)	46.3(3)
C(2)-C(3)-C(3A)-C(4)	-174.1(3)	C(25)-PT-C(7A)-C(3A)	3.8(3)
PT-C(3)-C(3A)-C(4)	117.9(3)	C(21)-PT-C(7A)-C(3A)	137.34(16)
C(2)-C(3)-C(3A)-C(7A)	8.3(3)	C(3)-PT-C(7A)-C(3A)	-35.94(18)
PT-C(3)-C(3A)-C(7A)	-59.7(2)	C(1)-PT-C(7A)-C(3A)	-120.9(2)
C(2)-C(3)-C(3A)-PT	68.0(2)	C(2)-PT-C(7A)-C(3A)	-80.42(17)
C(22)-PT-C(3A)-C(4)	109.5(4)	C(22)-PT-C(7A)-C(1)	-62.9(2)
C(26)-PT-C(3A)-C(4)	-27.6(3)	C(26)-PT-C(7A)-C(1)	167.3(2)
C(25)-PT-C(3A)-C(4)	-61.5(3)	C(25)-PT-C(7A)-C(1)	124.7(3)
C(21)-PT-C(3A)-C(4)	60.4(3)	C(21)-PT-C(7A)-C(1)	-101.72(18)
C(3)-PT-C(3A)-C(4)	-122.2(3)	C(3)-PT-C(7A)-C(1)	85.0(2)
C(1)-PT-C(3A)-C(4)	152.6(3)	C(2)-PT-C(7A)-C(1)	40.53(17)

C(3A)-PT-C(7A)-C(1)	120.9(2)
C(26)-PT-C(21)-C(22)	-115.7(2)
C(25)-PT-C(21)-C(22)	-78.75(19)
C(3)-PT-C(21)-C(22)	139.8(5)
C(1)-PT-C(21)-C(22)	79.35(19)
C(2)-PT-C(21)-C(22)	55.7(3)
C(3A)-PT-C(21)-C(22)	145.69(17)
C(7A)-PT-C(21)-C(22)	117.11(18)
C(22)-PT-C(21)-C(28)	117.7(3)
C(26)-PT-C(21)-C(28)	2.0(2)
C(25)-PT-C(21)-C(28)	39.0(2)
C(3)-PT-C(21)-C(28)	-102.5(5)
C(1)-PT-C(21)-C(28)	-162.93(19)
C(2)-PT-C(21)-C(28)	173.38(18)
C(3A)-PT-C(21)-C(28)	-96.6(2)
C(7A)-PT-C(21)-C(28)	-125.2(2)
C(28)-C(21)-C(22)-C(23)	-4.2(5)
PT-C(21)-C(22)-C(23)	101.0(3)
C(28)-C(21)-C(22)-PT	-105.2(3)
C(26)-PT-C(22)-C(21)	63.78(19)
C(25)-PT-C(22)-C(21)	98.42(18)
C(3)-PT-C(22)-C(21)	-158.7(2)
C(1)-PT-C(22)-C(21)	-110.69(18)
C(2)-PT-C(22)-C(21)	-146.72(17)
C(3A)-PT-C(22)-C(21)	-74.1(3)
C(7A)-PT-C(22)-C(21)	-78.70(19)
C(26)-PT-C(22)-C(23)	-57.5(3)
C(25)-PT-C(22)-C(23)	-22.9(2)
C(21)-PT-C(22)-C(23)	-121.3(3)
C(3)-PT-C(22)-C(23)	80.0(4)
C(1)-PT-C(22)-C(23)	128.0(2)
C(2)-PT-C(22)-C(23)	92.0(2)
C(3A)-PT-C(22)-C(23)	164.60(19)
C(7A)-PT-C(22)-C(23)	160.0(2)
C(21)-C(22)-C(23)-C(24)	-45.4(4)
PT-C(22)-C(23)-C(24)	35.4(3)
C(22)-C(23)-C(24)-C(25)	-30.8(4)
C(23)-C(24)-C(25)-C(26)	91.0(3)
C(23)-C(24)-C(25)-PT	10.3(3)
C(22)-PT-C(25)-C(26)	-113.1(3)
C(21)-PT-C(25)-C(26)	-75.7(3)
C(3)-PT-C(25)-C(26)	94.6(3)
C(1)-PT-C(25)-C(26)	150.8(4)
C(2)-PT-C(25)-C(26)	132.8(3)
C(3A)-PT-C(25)-C(26)	62.8(3)
C(7A)-PT-C(25)-C(26)	60.2(4)
C(22)-PT-C(25)-C(24)	7.0(2)
C(26)-PT-C(25)-C(24)	120.1(3)
C(21)-PT-C(25)-C(24)	44.3(2)
C(3)-PT-C(25)-C(24)	-145.3(2)
C(1)-PT-C(25)-C(24)	-89.2(3)
C(2)-PT-C(25)-C(24)	-107.2(2)
C(3A)-PT-C(25)-C(24)	-177.17(18)
C(7A)-PT-C(25)-C(24)	-179.7(2)
C(24)-C(25)-C(26)-C(27)	-1.6(4)
PT-C(25)-C(26)-C(27)	101.5(3)
C(24)-C(25)-C(26)-PT	-103.1(3)
C(22)-PT-C(26)-C(25)	67.0(2)
C(21)-PT-C(26)-C(25)	100.9(2)
C(3)-PT-C(26)-C(25)	-94.2(2)
C(1)-PT-C(26)-C(25)	-130.8(3)
C(2)-PT-C(26)-C(25)	-71.7(3)
C(3A)-PT-C(26)-C(25)	-131.3(2)
C(7A)-PT-C(26)-C(25)	-155.40(17)
C(22)-PT-C(26)-C(27)	-55.0(3)
C(25)-PT-C(26)-C(27)	-121.9(4)
C(21)-PT-C(26)-C(27)	-21.1(3)
C(3)-PT-C(26)-C(27)	143.8(3)
C(1)-PT-C(26)-C(27)	107.2(6)
C(2)-PT-C(26)-C(27)	166.4(2)
C(3A)-PT-C(26)-C(27)	106.7(3)
C(7A)-PT-C(26)-C(27)	82.7(4)
C(25)-C(26)-C(27)-C(28)	-43.6(4)
PT-C(26)-C(27)-C(28)	37.1(4)
C(22)-C(21)-C(28)-C(27)	97.6(3)
PT-C(21)-C(28)-C(27)	17.3(3)
C(26)-C(27)-C(28)-C(21)	-36.1(4)

Rapport cristallographique de la structure du composé (COD)Pt(η^1-Ind)Me (**4**)

Table 1. Crystal data and structure refinement for C18 H22 Pt.

Identification code	suse27
Empirical formula	C18 H22 Pt
Formula weight	433.45
Temperature	100(2)K
Wavelength	1.54178 Å
Crystal system	Monoclinic
Space group	P21/n
Unit cell dimensions	a = 9.5752(3) Å α = 90° b = 13.3133(4) Å β = 106.562(2)° c = 11.7387(4) Å γ = 90°
Volume	1434.34(8)Å^3
Z	4
Density (calculated)	2.007 Mg/m^3
Absorption coefficient	18.136 mm^{-1}
F(000)	832
Crystal size	0.30 x 0.23 x 0.08 mm
Theta range for data collection	5.15 to 72.91°
Index ranges	$-11 \le h \le 11$, $-16 \le k \le 15$, $-14 \le \lambda \le 13$
Reflections collected	11683
Independent reflections	2822 [R_{int} = 0.052]
Absorption correction	Semi-empirical from equivalents
Max. and min. transmission	0.017 and 0.234
Refinement method	Full-matrix least-squares on F^2
Data / restraints / parameters	2822 / 0 / 238
Goodness-of-fit on F^2	1.108
Final R indices [I>2sigma(I)]	R_1 = 0.0426, wR_2 = 0.1057
R indices (all data)	R_1 = 0.0451, wR_2 = 0.1075
Largest diff. peak and hole	1.869 and -2.296 e/Å^3

Table 2. Atomic coordinates (x 10^4) and equivalent isotropic displacement parameters ($Å^2$ x 10^3) for C18 H22 Pt.

U_{eq} is defined as one third of the trace of the orthogonalized Uij tensor.

	x	y	z	U_{eq}
Pt	948(1)	7253(1)	1107(1)	18(1)
C(1)	21(7)	7389(5)	2537(5)	22(1)
C(2)	1324(7)	7603(5)	3589(5)	22(1)
C(3)	1249(5)	8533(4)	4032(4)	24(1)
C(3A)	-152(5)	8974(4)	3385(4)	21(1)
C(4)	-788(6)	9901(4)	3502(4)	24(1)
C(5)	-2195(6)	10094(4)	2801(5)	31(1)
C(6)	-2952(6)	9392(5)	1982(5)	30(1)
C(7)	-2314(5)	8485(4)	1827(5)	26(1)
C(7A)	-895(6)	8275(4)	2540(5)	23(1)
C(8)	1169(7)	5753(4)	1534(6)	30(1)
C(22)	1188(6)	6892(4)	-646(5)	24(1)
C(21)	2527(8)	7187(3)	52(6)	24(1)
C(28)	3210(6)	8194(4)	-25(5)	25(1)
C(27)	2897(5)	9000(4)	818(4)	23(1)
C(26)	1411(5)	8896(4)	1026(4)	20(1)
C(25)	124(5)	8720(3)	152(4)	19(1)
C(24)	17(5)	8628(4)	-1148(4)	23(1)
C(23)	146(6)	7547(6)	-1563(5)	25(1)

Table 3. Hydrogen coordinates (x 10^4) and isotropic displacement parameters ($Å^2$ x 10^3) for C18 H22 Pt.

	x	y	z	U_{eq}
H(1)	-330(100)	7000(60)	2460(70)	27
H(2)	2030(100)	7210(50)	3910(80)	27
H(3)	1930(70)	8830(50)	4590(60)	28
H(4)	-300(80)	10360(50)	4040(60)	29
H(5)	-2750(80)	10720(60)	2770(60)	37
H(6)	-3990(80)	9550(60)	1570(70)	36
H(7)	-2720(80)	8040(60)	1250(70)	32
H(8A)	1490(90)	5470(60)	2330(70)	45
H(8B)	1580(90)	5320(70)	1090(80)	45
H(8C)	610(90)	5480(80)	1190(80)	45
H(22)	1110(70)	6190(60)	-640(60)	29
H(21)	3190(80)	6560(50)	470(60)	29
H(28A)	2980(80)	8380(50)	-800(60)	30
H(28B)	4380(80)	8010(50)	70(60)	30
H(27A)	3610(70)	8890(50)	1610(60)	27
H(27B)	3060(70)	9650(50)	510(60)	27
H(26)	1460(70)	9190(50)	1900(60)	25
H(25)	-590(70)	8870(50)	500(50)	22
H(24A)	870(70)	9050(50)	-1370(60)	28
H(24B)	-830(70)	8880(50)	-1550(60)	28
H(23A)	-670(100)	7160(50)	-1710(80)	30
H(23B)	440(90)	7490(60)	-2220(70)	30

Table 4. Anisotropic parameters ($Å^2$ x 10^3) for C18 H22 Pt.

The anisotropic displacement factor exponent takes the form:

$$-2\pi^2 [h^2 a^{*2} U_{11} + ... + 2 h k a^* b^* U_{12}]$$

	U11	U22	U33	U23	U13	U12
Pt	19(1)	18(1)	21(1)	-1(1)	12(1)	-1(1)
C(1)	25(3)	25(3)	23(3)	4(2)	18(2)	-1(2)
C(2)	26(3)	25(3)	22(3)	7(2)	16(2)	3(2)
C(3)	22(2)	33(3)	20(2)	0(2)	13(2)	-2(2)
C(3A)	19(2)	29(2)	21(2)	2(2)	15(2)	1(2)
C(4)	28(2)	26(2)	24(2)	-2(2)	17(2)	-2(2)
C(5)	33(3)	33(3)	37(3)	12(2)	26(2)	7(2)
C(6)	18(2)	50(3)	26(2)	10(2)	13(2)	2(2)
C(7)	17(2)	45(3)	23(2)	2(2)	16(2)	-4(2)
C(7A)	20(2)	32(3)	24(2)	-1(2)	18(2)	-3(2)
C(8)	33(3)	23(2)	38(3)	0(2)	18(2)	-1(2)
C(22)	28(2)	22(3)	28(3)	-3(2)	19(2)	0(2)
C(21)	33(3)	22(3)	31(3)	-2(2)	30(3)	3(2)
C(28)	22(2)	30(3)	28(3)	1(2)	17(2)	-3(2)
C(27)	20(2)	27(2)	26(2)	-3(2)	14(2)	-5(2)
C(26)	17(2)	25(2)	27(2)	3(2)	18(2)	0(2)
C(25)	20(2)	20(2)	20(2)	0(2)	13(2)	1(2)
C(24)	20(2)	31(2)	20(2)	0(2)	9(2)	-1(2)
C(23)	24(3)	34(2)	20(3)	-3(2)	12(2)	0(2)

Table 5. Bond lengths [Å] and angles [°] for C18 H22 Pt

Pt-C(8)	2.056(6)	C(22)-C(21)-PT	70.9(3)
Pt-C(1)	2.118(5)	C(28)-C(21)-PT	112.1(3)
Pt-C(22)	2.188(5)	C(21)-C(28)-C(27)	114.4(4)
Pt-C(21)	2.212(5)	C(26)-C(27)-C(28)	113.6(4)
Pt-C(26)	2.238(5)	C(25)-C(26)-C(27)	125.2(4)
Pt-C(25)	2.277(4)	C(25)-C(26)-PT	73.7(3)
C(1)-C(7a)	1.470(8)	C(27)-C(26)-PT	107.6(3)
C(1)-C(2)	1.512(9)	C(26)-C(25)-C(24)	123.7(4)
C(2)-C(3)	1.352(8)	C(26)-C(25)-PT	70.7(3)
C(3)-C(3a)	1.464(7)	C(24)-C(25)-PT	110.1(3)
C(3a)-C(7a)	1.398(7)	C(25)-C(24)-C(23)	114.2(4)
C(3a)-C(4)	1.400(7)	C(22)-C(23)-C(24)	114.2(5)
C(4)-C(5)	1.387(9)		
C(5)-C(6)	1.388(10)		
C(6)-C(7)	1.388(8)		
C(7)-C(7a)	1.405(7)		
C(22)-C(21)	1.368(9)		
C(22)-C(23)	1.517(8)		
C(21)-C(28)	1.505(7)		
C(28)-C(27)	1.547(7)		
C(27)-C(26)	1.517(6)		
C(26)-C(25)	1.380(7)		
C(25)-C(24)	1.505(6)		
C(24)-C(23)	1.536(8)		
C(8)-PT-C(1)	85.8(2)		
C(8)-PT-C(22)	89.1(2)		
C(1)-PT-C(22)	160.7(2)		
C(8)-PT-C(21)	93.4(2)		
C(1)-PT-C(21)	162.6(3)		
C(22)-PT-C(21)	36.2(2)		
C(8)-PT-C(26)	162.1(2)		
C(1)-PT-C(26)	94.7(2)		
C(22)-PT-C(26)	95.74(17)		
C(21)-PT-C(26)	80.80(16)		
C(8)-PT-C(25)	161.8(2)		
C(1)-PT-C(25)	98.73(19)		
C(22)-PT-C(25)	80.82(17)		
C(21)-PT-C(25)	87.43(18)		
C(26)-PT-C(25)	35.59(18)		
C(7A)-C(1)-C(2)	101.6(5)		
C(7A)-C(1)-PT	117.1(4)		
C(2)-C(1)-PT	103.3(4)		
C(3)-C(2)-C(1)	111.4(5)		
C(2)-C(3)-C(3A)	108.0(5)		
C(7A)-C(3A)-C(4)	120.6(5)		
C(7A)-C(3A)-C(3)	107.9(4)		
C(4)-C(3A)-C(3)	131.5(5)		
C(5)-C(4)-C(3A)	118.8(5)		
C(4)-C(5)-C(6)	120.9(5)		
C(5)-C(6)-C(7)	120.9(5)		
C(6)-C(7)-C(7A)	118.8(5)		
C(3A)-C(7A)-C(7)	120.0(5)		
C(3A)-C(7A)-C(1)	110.6(5)		
C(7)-C(7A)-C(1)	129.3(5)		
C(21)-C(22)-C(23)	125.1(5)		
C(21)-C(22)-PT	72.8(3)		
C(23)-C(22)-PT	108.5(3)		
C(22)-C(21)-C(28)	124.7(6)		

Table 6. Torsion angles [°] for C18 H22 Pt.

C(8)-PT-C(1)-C(7A)	-159.6(5)
C(22)-PT-C(1)-C(7A)	-84.4(8)
C(21)-PT-C(1)-C(7A)	112.6(7)
C(26)-PT-C(1)-C(7A)	38.4(5)
C(25)-PT-C(1)-C(7A)	2.8(5)
C(8)-PT-C(1)-C(2)	89.8(4)
C(22)-PT-C(1)-C(2)	165.0(5)
C(21)-PT-C(1)-C(2)	2.0(9)
C(26)-PT-C(1)-C(2)	-72.2(4)
C(25)-PT-C(1)-C(2)	-107.9(4)
C(7A)-C(1)-C(2)-C(3)	-7.0(5)
PT-C(1)-C(2)-C(3)	114.7(4)
C(1)-C(2)-C(3)-C(3A)	4.8(5)
C(2)-C(3)-C(3A)-C(7A)	-0.4(5)
C(2)-C(3)-C(3A)-C(4)	178.5(5)
C(7A)-C(3A)-C(4)-C(5)	2.8(7)
C(3)-C(3A)-C(4)-C(5)	-175.9(5)
C(3A)-C(4)-C(5)-C(6)	-1.2(7)
C(4)-C(5)-C(6)-C(7)	-1.0(8)
C(5)-C(6)-C(7)-C(7A)	1.7(7)
C(4)-C(3A)-C(7A)-C(7)	-2.2(7)
C(3)-C(3A)-C(7A)-C(7)	176.9(4)
C(4)-C(3A)-C(7A)-C(1)	176.7(4)
C(3)-C(3A)-C(7A)-C(1)	-4.3(5)
C(6)-C(7)-C(7A)-C(3A)	-0.1(7)
C(6)-C(7)-C(7A)-C(1)	-178.7(5)
C(2)-C(1)-C(7A)-C(3A)	6.7(5)
PT-C(1)-C(7A)-C(3A)	-104.9(5)
C(2)-C(1)-C(7A)-C(7)	-174.6(5)
PT-C(1)-C(7A)-C(7)	73.8(7)
C(8)-PT-C(22)-C(21)	-96.9(3)
C(1)-PT-C(22)-C(21)	-171.5(6)
C(26)-PT-C(22)-C(21)	65.9(3)
C(25)-PT-C(22)-C(21)	98.3(3)
C(8)-PT-C(22)-C(23)	141.0(4)
C(1)-PT-C(22)-C(23)	66.4(7)
C(21)-PT-C(22)-C(23)	-122.1(5)
C(26)-PT-C(22)-C(23)	-56.2(4)
C(25)-PT-C(22)-C(23)	-23.8(4)
C(23)-C(22)-C(21)-C(28)	-3.3(8)
PT-C(22)-C(21)-C(28)	-104.2(5)
C(23)-C(22)-C(21)-PT	100.9(5)
C(8)-PT-C(21)-C(22)	83.9(3)
C(1)-PT-C(21)-C(22)	170.6(6)
C(26)-PT-C(21)-C(22)	-113.1(3)
C(25)-PT-C(21)-C(22)	-77.9(3)
C(8)-PT-C(21)-C(28)	-155.5(5)
C(1)-PT-C(21)-C(28)	-68.8(8)
C(22)-PT-C(21)-C(28)	120.6(6)
C(26)-PT-C(21)-C(28)	7.5(5)
C(25)-PT-C(21)-C(28)	42.7(5)
C(22)-C(21)-C(28)-C(27)	92.2(6)
PT-C(21)-C(28)-C(27)	10.7(7)
C(21)-C(28)-C(27)-C(26)	-32.9(7)
C(28)-C(27)-C(26)-C(25)	-45.0(7)
C(28)-C(27)-C(26)-PT	37.2(5)

C(8)-PT-C(26)-C(25)	170.6(5)
C(1)-PT-C(26)-C(25)	-98.4(3)
C(22)-PT-C(26)-C(25)	65.4(3)
C(21)-PT-C(26)-C(25)	98.5(3)
C(8)-PT-C(26)-C(27)	48.1(7)
C(1)-PT-C(26)-C(27)	139.2(4)
C(22)-PT-C(26)-C(27)	-57.0(3)
C(21)-PT-C(26)-C(27)	-23.9(4)
C(25)-PT-C(26)-C(27)	-122.5(4)
C(27)-C(26)-C(25)-C(24)	-1.4(7)
PT-C(26)-C(25)-C(24)	-101.7(4)
C(27)-C(26)-C(25)-PT	100.4(5)
C(8)-PT-C(25)-C(26)	-170.7(5)
C(1)-PT-C(25)-C(26)	85.9(3)
C(22)-PT-C(25)-C(26)	-113.6(3)
C(21)-PT-C(25)-C(26)	-77.7(3)
C(8)-PT-C(25)-C(24)	-50.8(7)
C(1)-PT-C(25)-C(24)	-154.2(3)
C(22)-PT-C(25)-C(24)	6.3(3)
C(21)-PT-C(25)-C(24)	42.2(3)
C(26)-PT-C(25)-C(24)	119.9(4)
C(26)-C(25)-C(24)-C(23)	92.4(6)
PT-C(25)-C(24)-C(23)	12.8(5)
C(21)-C(22)-C(23)-C(24)	-42.8(7)
PT-C(22)-C(23)-C(24)	38.9(5)
C(25)-C(24)-C(23)-C(22)	-35.1(6)

Rapport cristallographique de la structure du composé [(η-Ind)Pt(PPh_3)$_2$][BF_4] (**6**).

Table 1. Crystal data and structure refinement for C45 H37 B F4 P2 Pt.

Identification code	suse34
Empirical formula	C45 H37 B F4 P2 Pt
Formula weight	921.59
Temperature	200(2)K
Wavelength	1.54178 Å
Crystal system	Monoclinic
Space group	P21/n
Unit cell dimensions	a = 11.6602(3) Å α = 90° b = 20.6255(5) Å β = 95.8830(10)° c = 15.5748(4) Å γ = 90°
Volume	3725.97(16)Å^3
Z	4
Density (calculated)	1.643 Mg/m^3
Absorption coefficient	8.295 mm^{-1}
F(000)	1824
Crystal size	0.20 x 0.10 x 0.08 mm
Theta range for data collection	3.57 to 68.92°
Index ranges	$-12 \le h \le 13$, $-24 \le k \le 24$, $-18 \le \lambda \le 18$
Reflections collected	50471
Independent reflections	6829 [R_{int} = 0.031]
Absorption correction	Semi-empirical from equivalents
Max. and min. transmission	1.0000 and 0.7800
Refinement method	Full-matrix least-squares on F^2
Data / restraints / parameters	6829 / 0 / 478
Goodness-of-fit on F^2	1.037
Final R indices [I>2sigma(I)]	R_1 = 0.0280, wR_2 = 0.0812
R indices (all data)	R_1 = 0.0289, wR_2 = 0.0819
Largest diff. peak and hole	2.132 and -0.729 e/Å^3

Table 2. Atomic coordinates ($\times 10^4$) and equivalent isotropic displacement parameters ($Å^2 \times 10^3$) for C45 H37 B F4 P2 Pt. U_{eq} is defined as one third of the trace of the orthogonalized Uij tensor.

	x	y	z	U_{eq}
Pt	9425(1)	8708(1)	8185(1)	31(1)
P(1)	9532(1)	7619(1)	8042(1)	30(1)
P(2)	9540(1)	9080(1)	6824(1)	29(1)
C(3)	9394(3)	9695(2)	8802(2)	43(1)
C(2)	8663(4)	9263(2)	9193(2)	50(1)
C(1)	9375(4)	8777(2)	9605(2)	51(1)
C(7A)	10564(4)	9007(2)	9674(2)	48(1)
C(7)	11594(6)	8757(3)	10085(3)	68(2)
C(6)	12596(5)	9093(3)	10015(3)	77(2)
C(5)	12615(4)	9655(3)	9532(3)	71(1)
C(4)	11604(4)	9903(2)	9102(3)	54(1)
C(3A)	10582(3)	9582(2)	9179(2)	43(1)
C(21)	8202(3)	7228(2)	7603(2)	34(1)
C(28)	8117(3)	6556(2)	7586(3)	45(1)
C(27)	7067(4)	6259(2)	7386(3)	54(1)
C(26)	6081(4)	6626(2)	7197(3)	51(1)
C(25)	6155(3)	7290(2)	7207(3)	47(1)
C(24)	7210(3)	7594(2)	7414(2)	39(1)
C(21)	9759(3)	7187(2)	9081(2)	33(1)
C(22)	10774(3)	6873(2)	9379(2)	39(1)
C(23)	10862(4)	6545(2)	10156(2)	45(1)
C(24)	9924(4)	6528(2)	10649(2)	44(1)
C(25)	8918(4)	6835(2)	10357(2)	43(1)
C(26)	8831(3)	7164(2)	9578(2)	39(1)
C(31)	10717(3)	7356(2)	7453(2)	37(1)
C(32)	10605(3)	6927(2)	6761(2)	47(1)
C(33)	11564(5)	6768(2)	6338(3)	63(1)
C(34)	12627(4)	7023(2)	6621(3)	62(1)
C(35)	12750(4)	7451(2)	7308(3)	56(1)
C(36)	11800(3)	7620(2)	7718(3)	45(1)
C(41)	8243(3)	9523(2)	6418(2)	31(1)
C(42)	8142(3)	9801(2)	5595(2)	38(1)
C(43)	7161(3)	10144(2)	5297(2)	44(1)
C(44)	6261(3)	10204(2)	5808(3)	44(1)
C(45)	6338(3)	9918(2)	6612(2)	40(1)
C(46)	7322(3)	9580(2)	6919(2)	35(1)
C(51)	10736(3)	9653(2)	6857(2)	34(1)
C(52)	11840(3)	9421(2)	7132(2)	41(1)
C(53)	12779(3)	9833(2)	7188(3)	49(1)
C(54)	12630(4)	10480(2)	6978(3)	55(1)
C(55)	11544(4)	10717(2)	6721(3)	53(1)
C(56)	10596(3)	10308(2)	6651(2)	42(1)
C(61)	9747(3)	8556(2)	5908(2)	32(1)
C(62)	10635(3)	8643(2)	5400(3)	41(1)
C(63)	10717(4)	8262(2)	4673(3)	51(1)
C(64)	9913(4)	7781(2)	4459(2)	51(1)
C(65)	9017(4)	7691(2)	4956(2)	48(1)
C(66)	8931(3)	8074(2)	5682(2)	39(1)
B	353(6)	6124(4)	3667(5)	78(2)
F(1)	-546(6)	6392(3)	3327(6)	219(5)
F(2)	1337(4)	6491(3)	3812(5)	164(3)
F(3)	156(6)	6074(3)	4530(4)	165(2)

F(4)	462(6)	5471(2)	3485(3)	159(2)

Table 3. Hydrogen coordinates (x 10^4) and isotropic displacement parameters ($Å^2$ x 10^3) for C45 H37 B F4 P2 Pt.

	x	y	z	U_{eq}
H(1)	9162	9999	8379	52
H(2)	7866	9292	9181	60
H(3)	9128	8380	9800	61
H(4)	11598	8373	10398	82
H(5)	13281	8938	10301	93
H(6)	13310	9869	9494	85
H(7)	11617	10277	8770	64
H(12)	8776	6305	7711	55
H(13)	7021	5809	7378	65
H(14)	5371	6425	7064	62
H(15)	5495	7539	7075	56
H(16)	7252	8044	7425	47
H(22)	11399	6883	9053	47
H(23)	11545	6335	10351	54
H(24)	9984	6308	11173	53
H(25)	8292	6822	10682	52
H(26)	8146	7372	9384	46
H(32)	9890	6746	6581	57
H(33)	11486	6490	5866	75
H(34)	13269	6907	6347	75
H(35)	13470	7624	7492	67
H(36)	11880	7913	8174	53
H(42)	8737	9754	5245	46
H(43)	7107	10336	4754	53
H(44)	5604	10436	5608	53
H(45)	5728	9953	6949	49
H(46)	7369	9389	7462	41
H(52)	11942	8986	7277	49
H(53)	13511	9674	7368	59
H(54)	13263	10757	7010	66
H(55)	11447	11156	6593	63
H(56)	9867	10470	6467	50
H(62)	11187	8961	5546	50
H(63)	11313	8331	4330	61
H(64)	9978	7520	3980	61
H(65)	8467	7373	4806	58
H(66)	8327	8009	6019	47

Table 4. Anisotropic parameters ($Å^2$ x 10^3) for C45 H37 B F4 P2 Pt.

The anisotropic displacement factor exponent takes the form:

$$-2\pi^2 [h^2 a^{*2} U_{11} + ... + 2 h k a^* b^* U_{12}]$$

	U11	U22	U33	U23	U13	U12
Pt	38(1)	28(1)	27(1)	1(1)	7(1)	3(1)
P(1)	34(1)	28(1)	29(1)	1(1)	4(1)	3(1)
P(2)	31(1)	28(1)	27(1)	2(1)	4(1)	-1(1)
C(3)	60(2)	32(2)	37(2)	-8(1)	4(2)	8(2)
C(2)	60(2)	51(2)	40(2)	-17(2)	19(2)	6(2)
C(1)	86(3)	42(2)	26(2)	-5(1)	21(2)	-1(2)
C(7A)	73(3)	45(2)	27(2)	-5(2)	7(2)	14(2)
C(7)	91(4)	76(3)	36(2)	0(2)	2(2)	39(3)
C(6)	75(4)	106(5)	49(3)	-15(3)	-3(2)	38(3)
C(5)	56(3)	101(4)	55(3)	-28(3)	8(2)	4(3)
C(4)	66(3)	57(2)	38(2)	-13(2)	8(2)	-4(2)
C(3A)	58(2)	42(2)	30(2)	-9(1)	5(2)	7(2)
C(21)	37(2)	36(2)	29(2)	3(1)	3(1)	2(1)
C(28)	48(2)	34(2)	51(2)	1(2)	-11(2)	3(2)
C(27)	61(3)	37(2)	61(3)	5(2)	-14(2)	-8(2)
C(26)	45(2)	59(3)	48(2)	10(2)	-3(2)	-11(2)
C(25)	32(2)	58(2)	52(2)	14(2)	8(2)	3(2)
C(24)	40(2)	38(2)	42(2)	7(1)	12(2)	4(1)
C(21)	39(2)	29(2)	31(2)	1(1)	2(1)	0(1)
C(22)	38(2)	38(2)	41(2)	0(1)	1(1)	0(1)
C(23)	50(2)	40(2)	43(2)	6(2)	-6(2)	3(2)
C(24)	63(2)	35(2)	34(2)	4(2)	-4(2)	-2(2)
C(25)	57(2)	38(2)	36(2)	0(1)	12(2)	-3(2)
C(26)	42(2)	38(2)	37(2)	6(1)	5(1)	3(1)
C(31)	43(2)	36(2)	32(2)	7(1)	9(1)	9(1)
C(32)	56(3)	47(2)	37(2)	0(2)	2(2)	16(2)
C(33)	87(4)	62(3)	41(2)	1(2)	19(2)	30(2)
C(34)	61(3)	74(3)	56(3)	18(2)	29(2)	28(2)
C(35)	41(2)	70(3)	60(3)	21(2)	17(2)	10(2)
C(36)	43(2)	49(2)	42(2)	8(2)	10(2)	6(2)
C(41)	33(2)	27(2)	33(2)	0(1)	-1(1)	-2(1)
C(42)	40(2)	39(2)	35(2)	3(1)	3(1)	-3(1)
C(43)	47(2)	42(2)	42(2)	10(2)	-7(2)	-2(2)
C(44)	39(2)	38(2)	53(2)	1(2)	-10(2)	5(2)
C(45)	33(2)	38(2)	49(2)	-4(2)	3(2)	0(1)
C(46)	35(2)	31(2)	37(2)	1(1)	3(1)	-1(1)
C(51)	37(2)	35(2)	29(2)	-2(1)	4(1)	-6(1)
C(52)	39(2)	45(2)	39(2)	2(2)	3(1)	-3(2)
C(53)	38(2)	68(3)	42(2)	-3(2)	2(2)	-9(2)
C(54)	52(2)	59(3)	54(2)	-8(2)	5(2)	-27(2)
C(55)	62(3)	40(2)	57(2)	-3(2)	4(2)	-15(2)
C(56)	48(2)	36(2)	41(2)	-2(2)	3(2)	-5(2)
C(61)	37(2)	31(2)	27(2)	2(1)	2(1)	1(1)
C(62)	34(2)	49(2)	41(2)	-5(2)	8(2)	-3(1)
C(63)	43(2)	68(3)	42(2)	-9(2)	10(2)	6(2)
C(64)	63(3)	52(2)	36(2)	-10(2)	1(2)	13(2)
C(65)	63(3)	40(2)	40(2)	-3(2)	-5(2)	-9(2)
C(66)	45(2)	39(2)	33(2)	3(1)	2(1)	-7(2)
B	70(4)	76(4)	96(5)	13(4)	49(4)	19(3)
F(1)	201(8)	95(4)	325(11)	33(4)	-152(8)	2(3)

F(2)	86(3)	169(5)	245(7)	87(5)	53(4)	18(3)
F(3)	187(6)	186(5)	133(4)	-55(4)	67(4)	-60(5)
F(4)	251(7)	111(3)	117(3)	-13(3)	32(4)	85(4)

Table 5. Bond lengths [Å] and angles [°] for C45 H37 B F4 P2 Pt

Pt-C(2)	2.202(3)	B-F(1)	1.253(9)
Pt-C(1)	2.223(4)	B-F(2)	1.374(10)
Pt-C(3)	2.254(3)	B-F(4)	1.385(8)
Pt-P(1)	2.2621(8)	B-F(3)	1.390(9)
Pt-P(2)	2.2714(8)	C(2)-PT-C(1)	37.22(16)
Pt-C(7a)	2.624(4)	C(2)-PT-C(3)	36.97(15)
Pt-C(3a)	2.653(4)	C(1)-PT-C(3)	60.94(14)
P(1)-C(21)	1.818(3)	C(2)-PT-P(1)	128.06(12)
P(1)-C(31)	1.818(3)	C(1)-PT-P(1)	99.73(10)
P(1)-C(21)	1.841(3)	C(3)-PT-P(1)	160.5(1)
P(2)-C(41)	1.824(3)	C(2)-PT-P(2)	123.81(12)
P(2)-C(51)	1.825(3)	C(1)-PT-P(2)	156.47(10)
P(2)-C(61)	1.826(3)	C(3)-PT-P(2)	95.62(10)
C(3)-C(2)	1.414(6)	P(1)-PT-P(2)	103.57(3)
C(3)-C(3a)	1.466(6)	C(2)-PT-C(7A)	56.83(15)
C(2)-C(1)	1.412(6)	C(1)-PT-C(7A)	33.75(16)
C(1)-C(7a)	1.459(7)	C(3)-PT-C(7A)	55.93(13)
C(7a)-C(7)	1.399(7)	P(1)-PT-C(7A)	106.99(9)
C(7a)-C(3a)	1.417(5)	P(2)-PT-C(7A)	132.24(10)
C(7)-C(6)	1.371(9)	C(2)-PT-C(3A)	56.57(14)
C(6)-C(5)	1.384(8)	C(1)-PT-C(3A)	55.91(14)
C(5)-C(4)	1.393(7)	C(3)-PT-C(3A)	33.52(13)
C(4)-C(3a)	1.378(6)	P(1)-PT-C(3A)	134.64(9)
C(21)-C(24)	1.387(5)	P(2)-PT-C(3A)	103.87(9)
C(21)-C(28)	1.389(5)	C(7A)-PT-C(3A)	31.14(12)
C(28)-C(27)	1.376(6)	C(21)-P(1)-C(31)	109.92(16)
C(27)-C(26)	1.384(6)	C(21)-P(1)-C(21)	99.03(15)
C(26)-C(25)	1.372(6)	C(31)-P(1)-C(21)	104.53(15)
C(25)-C(24)	1.388(5)	C(21)-P(1)-PT	115.10(11)
C(21)-C(22)	1.387(5)	C(31)-P(1)-PT	113.43(12)
C(21)-C(26)	1.394(5)	C(21)-P(1)-PT	113.46(11)
C(22)-C(23)	1.381(5)	C(41)-P(2)-C(51)	106.83(15)
C(23)-C(24)	1.400(6)	C(41)-P(2)-C(61)	101.37(15)
C(24)-C(25)	1.369(6)	C(51)-P(2)-C(61)	104.14(15)
C(25)-C(26)	1.385(5)	C(41)-P(2)-PT	111.49(11)
C(31)-C(32)	1.390(5)	C(51)-P(2)-PT	108.08(10)
C(31)-C(36)	1.398(6)	C(61)-P(2)-PT	123.66(11)
C(32)-C(33)	1.394(6)	C(2)-C(3)-C(3A)	108.3(3)
C(33)-C(34)	1.377(8)	C(2)-C(3)-PT	69.5(2)
C(34)-C(35)	1.383(7)	C(3A)-C(3)-PT	88.3(2)
C(35)-C(36)	1.379(6)	C(1)-C(2)-C(3)	106.9(4)
C(41)-C(46)	1.394(5)	C(1)-C(2)-PT	72.2(2)
C(41)-C(42)	1.399(5)	C(3)-C(2)-PT	73.5(2)
C(42)-C(43)	1.384(5)	C(2)-C(1)-C(7A)	108.3(4)
C(43)-C(44)	1.387(6)	C(2)-C(1)-PT	70.6(2)
C(44)-C(45)	1.378(5)	C(7A)-C(1)-PT	88.4(2)
C(45)-C(46)	1.386(5)	C(7)-C(7A)-C(3A)	119.8(5)
C(51)-C(56)	1.393(5)	C(7)-C(7A)-C(1)	132.7(4)
C(51)-C(52)	1.398(5)	C(3A)-C(7A)-C(1)	107.4(4)
C(52)-C(53)	1.381(5)	C(7)-C(7A)-PT	130.6(3)
C(53)-C(54)	1.382(6)	C(3A)-C(7A)-PT	75.5(2)
C(54)-C(55)	1.377(7)	C(1)-C(7A)-PT	57.86(19)
C(55)-C(56)	1.387(5)	C(6)-C(7)-C(7A)	118.4(5)
C(61)-C(62)	1.378(5)	C(7)-C(6)-C(5)	121.8(5)
C(61)-C(66)	1.395(5)	C(6)-C(5)-C(4)	120.6(5)
C(62)-C(63)	1.389(5)	C(3A)-C(4)-C(5)	118.6(5)
C(63)-C(64)	1.382(6)	C(4)-C(3A)-C(7A)	120.7(4)
C(64)-C(65)	1.376(6)	C(4)-C(3A)-C(3)	132.7(4)
C(65)-C(66)	1.392(5)	C(7A)-C(3A)-C(3)	106.6(4)

C(4)-C(3A)-PT	131.9(3)
C(7A)-C(3A)-PT	73.3(2)
C(3)-C(3A)-PT	58.13(18)
C(24)-C(21)-C(28)	118.8(3)
C(24)-C(21)-P(1)	120.0(3)
C(28)-C(21)-P(1)	120.4(3)
C(27)-C(28)-C(21)	120.6(4)
C(28)-C(27)-C(26)	120.3(4)
C(25)-C(26)-C(27)	119.6(4)
C(26)-C(25)-C(24)	120.4(4)
C(21)-C(24)-C(25)	120.3(3)
C(22)-C(21)-C(26)	118.8(3)
C(22)-C(21)-P(1)	124.1(3)
C(26)-C(21)-P(1)	117.0(2)
C(23)-C(22)-C(21)	120.4(4)
C(22)-C(23)-C(24)	120.1(4)
C(25)-C(24)-C(23)	119.8(3)
C(24)-C(25)-C(26)	120.0(4)
C(25)-C(26)-C(21)	120.8(3)
C(32)-C(31)-C(36)	119.2(3)
C(32)-C(31)-P(1)	124.4(3)
C(36)-C(31)-P(1)	116.4(3)
C(31)-C(32)-C(33)	119.9(4)
C(34)-C(33)-C(32)	120.0(4)
C(33)-C(34)-C(35)	120.6(4)
C(36)-C(35)-C(34)	119.7(4)
C(35)-C(36)-C(31)	120.6(4)
C(46)-C(41)-C(42)	118.7(3)
C(46)-C(41)-P(2)	120.5(2)
C(42)-C(41)-P(2)	120.8(3)
C(43)-C(42)-C(41)	120.4(3)
C(42)-C(43)-C(44)	120.1(3)
C(45)-C(44)-C(43)	120.0(3)
C(44)-C(45)-C(46)	120.3(3)
C(45)-C(46)-C(41)	120.5(3)
C(56)-C(51)-C(52)	119.0(3)
C(56)-C(51)-P(2)	123.4(3)
C(52)-C(51)-P(2)	117.6(3)
C(53)-C(52)-C(51)	120.5(4)
C(52)-C(53)-C(54)	119.9(4)
C(55)-C(54)-C(53)	120.1(4)
C(54)-C(55)-C(56)	120.5(4)
C(55)-C(56)-C(51)	119.9(4)
C(62)-C(61)-C(66)	118.8(3)
C(62)-C(61)-P(2)	122.6(3)
C(66)-C(61)-P(2)	118.5(3)
C(61)-C(62)-C(63)	120.8(4)
C(64)-C(63)-C(62)	120.0(4)
C(65)-C(64)-C(63)	119.8(4)
C(64)-C(65)-C(66)	120.1(4)
C(65)-C(66)-C(61)	120.3(3)
F(1)-B-F(2)	118.3(7)
F(1)-B-F(4)	115.6(8)
F(2)-B-F(4)	118.5(6)
F(1)-B-F(3)	103.2(7)
F(2)-B-F(3)	95.7(7)
F(4)-B-F(3)	98.9(6)

Table 6. Torsion angles

C(2)-PT-P(1)-C(21)	77.58(19)
C(1)-PT-P(1)-C(21)	104.48(18)
C(3)-PT-P(1)-C(21)	111.6(3)
P(2)-PT-P(1)-C(21)	-78.75(12)
C(7A)-PT-P(1)-C(21)	138.42(15)
C(3A)-PT-P(1)-C(21)	155.44(16)
C(2)-PT-P(1)-C(31)	-154.61(19)
C(1)-PT-P(1)-C(31)	-127.71(18)
C(3)-PT-P(1)-C(31)	-120.6(3)
P(2)-PT-P(1)-C(31)	49.06(13)
C(7A)-PT-P(1)-C(31)	-93.77(16)
C(3A)-PT-P(1)-C(31)	-76.75(17)
C(2)-PT-P(1)-C(21)	-35.52(19)
C(1)-PT-P(1)-C(21)	-8.61(18)
C(3)-PT-P(1)-C(21)	-1.5(3)
P(2)-PT-P(1)-C(21)	168.15(12)
C(7A)-PT-P(1)-C(21)	25.32(16)
C(3A)-PT-P(1)-C(21)	42.35(17)
C(2)-PT-P(2)-C(41)	-39.31(18)
C(1)-PT-P(2)-C(41)	-69.7(4)
C(3)-PT-P(2)-C(41)	-65.13(15)
P(1)-PT-P(2)-C(41)	118.33(11)
C(7A)-PT-P(2)-C(41)	-112.98(16)
C(3A)-PT-P(2)-C(41)	-98.14(14)
C(2)-PT-P(2)-C(51)	77.81(19)
C(1)-PT-P(2)-C(51)	47.5(4)
C(3)-PT-P(2)-C(51)	52.00(16)
P(1)-PT-P(2)-C(51)	-124.55(12)
C(7A)-PT-P(2)-C(51)	4.15(17)
C(3A)-PT-P(2)-C(51)	18.98(15)
C(2)-PT-P(2)-C(61)	-160.43(19)
C(1)-PT-P(2)-C(61)	169.2(4)
C(3)-PT-P(2)-C(61)	173.75(17)
P(1)-PT-P(2)-C(61)	-2.79(14)
C(7A)-PT-P(2)-C(61)	125.91(18)
C(3A)-PT-P(2)-C(61)	140.74(16)
C(1)-PT-C(3)-C(2)	-39.1(3)
P(1)-PT-C(3)-C(2)	-47.1(4)
P(2)-PT-C(3)-C(2)	143.0(2)
C(7A)-PT-C(3)-C(2)	-78.5(3)
C(3A)-PT-C(3)-C(2)	-110.3(3)
C(2)-PT-C(3)-C(3A)	110.3(3)
C(1)-PT-C(3)-C(3A)	71.2(3)
P(1)-PT-C(3)-C(3A)	63.2(4)
P(2)-PT-C(3)-C(3A)	-106.7(2)
C(7A)-PT-C(3)-C(3A)	31.8(2)
C(3A)-C(3)-C(2)-C(1)	-16.1(4)
PT-C(3)-C(2)-C(1)	65.0(2)
C(3A)-C(3)-C(2)-PT	-81.0(2)
C(3)-PT-C(2)-C(1)	-114.4(4)
P(1)-PT-C(2)-C(1)	47.5(3)
P(2)-PT-C(2)-C(1)	-160.5(2)
C(7A)-PT-C(2)-C(1)	-38.6(3)
C(3A)-PT-C(2)-C(1)	-76.0(3)
C(1)-PT-C(2)-C(3)	114.4(4)
P(1)-PT-C(2)-C(3)	161.92(18)
P(2)-PT-C(2)-C(3)	-46.1(3)
C(7A)-PT-C(2)-C(3)	75.8(3)
C(3A)-PT-C(2)-C(3)	38.4(2)
C(3)-C(2)-C(1)-C(7A)	15.7(4)
PT-C(2)-C(1)-C(7A)	81.5(3)
C(3)-C(2)-C(1)-PT	-65.8(2)
C(3)-PT-C(1)-C(2)	38.8(2)
P(1)-PT-C(1)-C(2)	-143.9(2)
P(2)-PT-C(1)-C(2)	44.0(5)
C(7A)-PT-C(1)-C(2)	110.0(3)
C(3A)-PT-C(1)-C(2)	77.9(3)
C(2)-PT-C(1)-C(7A)	-110.0(3)
C(3)-PT-C(1)-C(7A)	-71.2(2)
P(1)-PT-C(1)-C(7A)	106.1(2)
P(2)-PT-C(1)-C(7A)	-66.0(4)
C(3A)-PT-C(1)-C(7A)	-32.1(2)
C(2)-C(1)-C(7A)-C(7)	173.3(4)
PT-C(1)-C(7A)-C(7)	-117.8(4)
C(2)-C(1)-C(7A)-C(3A)	-9.3(4)
PT-C(1)-C(7A)-C(3A)	59.6(3)
C(2)-C(1)-C(7A)-PT	-68.9(2)
C(2)-PT-C(7A)-C(7)	163.9(5)
C(1)-PT-C(7A)-C(7)	121.1(6)
C(3)-PT-C(7A)-C(7)	-151.3(5)
P(1)-PT-C(7A)-C(7)	39.1(5)
P(2)-PT-C(7A)-C(7)	-88.4(5)
C(3A)-PT-C(7A)-C(7)	-117.1(6)
C(2)-PT-C(7A)-C(3A)	-79.0(3)
C(1)-PT-C(7A)-C(3A)	-121.7(3)
C(3)-PT-C(7A)-C(3A)	-34.2(2)
P(1)-PT-C(7A)-C(3A)	156.2(2)
P(2)-PT-C(7A)-C(3A)	28.7(3)
C(2)-PT-C(7A)-C(1)	42.8(3)
C(3)-PT-C(7A)-C(1)	87.5(3)
P(1)-PT-C(7A)-C(1)	-82.0(2)
P(2)-PT-C(7A)-C(1)	150.5(2)
C(3A)-PT-C(7A)-C(1)	121.7(3)
C(3A)-C(7A)-C(7)-C(6)	1.9(6)
C(1)-C(7A)-C(7)-C(6)	179.0(4)
PT-C(7A)-C(7)-C(6)	98.4(5)
C(7A)-C(7)-C(6)-C(5)	-2.0(7)
C(7)-C(6)-C(5)-C(4)	0.5(7)
C(6)-C(5)-C(4)-C(3A)	1.0(6)
C(5)-C(4)-C(3A)-C(7A)	-1.0(6)
C(5)-C(4)-C(3A)-C(3)	-177.9(4)
C(5)-C(4)-C(3A)-PT	-95.8(4)
C(7)-C(7A)-C(3A)-C(4)	-0.4(5)
C(1)-C(7A)-C(3A)-C(4)	-178.2(3)
PT-C(7A)-C(3A)-C(4)	-129.3(3)
C(7)-C(7A)-C(3A)-C(3)	177.2(3)
C(1)-C(7A)-C(3A)-C(3)	-0.6(4)
PT-C(7A)-C(3A)-C(3)	48.4(2)
C(7)-C(7A)-C(3A)-PT	128.8(4)
C(1)-C(7A)-C(3A)-PT	-49.0(2)
C(2)-C(3)-C(3A)-C(4)	-172.5(4)
PT-C(3)-C(3A)-C(4)	119.7(4)
C(2)-C(3)-C(3A)-C(7A)	10.3(4)
PT-C(3)-C(3A)-C(7A)	-57.5(3)
C(2)-C(3)-C(3A)-PT	67.8(2)
C(2)-PT-C(3A)-C(4)	-163.6(5)
C(1)-PT-C(3A)-C(4)	151.3(5)
C(3)-PT-C(3A)-C(4)	-121.0(5)
P(1)-PT-C(3A)-C(4)	83.7(4)

P(2)-PT-C(3A)-C(4)	-42.0(4)
C(7A)-PT-C(3A)-C(4)	116.5(5)
C(2)-PT-C(3A)-C(7A)	79.9(3)
C(1)-PT-C(3A)-C(7A)	34.8(2)
C(3)-PT-C(3A)-C(7A)	122.5(3)
P(1)-PT-C(3A)-C(7A)	-32.8(3)
P(2)-PT-C(3A)-C(7A)	-158.5(2)
C(2)-PT-C(3A)-C(3)	-42.5(2)
C(1)-PT-C(3A)-C(3)	-87.7(3)
P(1)-PT-C(3A)-C(3)	-155.25(19)
P(2)-PT-C(3A)-C(3)	79.0(2)
C(7A)-PT-C(3A)-C(3)	-122.5(3)
C(31)-P(1)-C(21)-C(24)	-132.0(3)
C(21)-P(1)-C(21)-C(24)	118.8(3)
PT-P(1)-C(21)-C(24)	-2.5(3)
C(31)-P(1)-C(21)-C(28)	58.6(3)
C(21)-P(1)-C(21)-C(28)	-50.5(3)
PT-P(1)-C(21)-C(28)	-171.8(3)
C(24)-C(21)-C(28)-C(27)	-0.1(6)
P(1)-C(21)-C(28)-C(27)	169.4(3)
C(21)-C(28)-C(27)-C(26)	0.1(7)
C(28)-C(27)-C(26)-C(25)	0.2(7)
C(27)-C(26)-C(25)-C(24)	-0.7(6)
C(28)-C(21)-C(24)-C(25)	-0.4(5)
P(1)-C(21)-C(24)-C(25)	-169.9(3)
C(26)-C(25)-C(24)-C(21)	0.7(6)
C(21)-P(1)-C(21)-C(22)	127.3(3)
C(31)-P(1)-C(21)-C(22)	13.9(3)
PT-P(1)-C(21)-C(22)	-110.2(3)
C(21)-P(1)-C(21)-C(26)	-50.7(3)
C(31)-P(1)-C(21)-C(26)	-164.1(3)
PT-P(1)-C(21)-C(26)	71.8(3)
C(26)-C(21)-C(22)-C(23)	-0.2(5)
P(1)-C(21)-C(22)-C(23)	-178.2(3)
C(21)-C(22)-C(23)-C(24)	0.0(6)
C(22)-C(23)-C(24)-C(25)	0.3(6)
C(23)-C(24)-C(25)-C(26)	-0.3(6)
C(24)-C(25)-C(26)-C(21)	0.1(6)
C(22)-C(21)-C(26)-C(25)	0.2(5)
P(1)-C(21)-C(26)-C(25)	178.3(3)
C(21)-P(1)-C(31)-C(32)	0.9(4)
C(21)-P(1)-C(31)-C(32)	106.3(3)
PT-P(1)-C(31)-C(32)	-129.6(3)
C(21)-P(1)-C(31)-C(36)	179.7(3)
C(21)-P(1)-C(31)-C(36)	-74.8(3)
PT-P(1)-C(31)-C(36)	49.3(3)
C(36)-C(31)-C(32)-C(33)	-0.4(6)
P(1)-C(31)-C(32)-C(33)	178.4(3)
C(31)-C(32)-C(33)-C(34)	1.7(6)
C(32)-C(33)-C(34)-C(35)	-1.8(7)
C(33)-C(34)-C(35)-C(36)	0.4(7)
C(34)-C(35)-C(36)-C(31)	0.9(6)
C(32)-C(31)-C(36)-C(35)	-1.0(5)
P(1)-C(31)-C(36)-C(35)	-179.8(3)
C(51)-P(2)-C(41)-C(46)	-120.0(3)
C(61)-P(2)-C(41)-C(46)	131.3(3)
PT-P(2)-C(41)-C(46)	-2.1(3)
C(51)-P(2)-C(41)-C(42)	61.2(3)
C(61)-P(2)-C(41)-C(42)	-47.5(3)
PT-P(2)-C(41)-C(42)	179.1(2)
C(46)-C(41)-C(42)-C(43)	2.2(5)
P(2)-C(41)-C(42)-C(43)	-179.0(3)
C(41)-C(42)-C(43)-C(44)	-1.3(5)
C(42)-C(43)-C(44)-C(45)	-0.3(6)
C(43)-C(44)-C(45)-C(46)	1.0(5)
C(44)-C(45)-C(46)-C(41)	-0.1(5)
C(42)-C(41)-C(46)-C(45)	-1.5(5)
P(2)-C(41)-C(46)-C(45)	179.7(3)
C(41)-P(2)-C(51)-C(56)	3.5(3)
C(61)-P(2)-C(51)-C(56)	110.3(3)
PT-P(2)-C(51)-C(56)	-116.5(3)
C(41)-P(2)-C(51)-C(52)	-178.6(3)
C(61)-P(2)-C(51)-C(52)	-71.8(3)
PT-P(2)-C(51)-C(52)	61.3(3)
C(56)-C(51)-C(52)-C(53)	-0.7(5)
P(2)-C(51)-C(52)-C(53)	-178.7(3)
C(51)-C(52)-C(53)-C(54)	0.4(6)
C(52)-C(53)-C(54)-C(55)	0.7(6)
C(53)-C(54)-C(55)-C(56)	-1.5(7)
C(54)-C(55)-C(56)-C(51)	1.1(6)
C(52)-C(51)-C(56)-C(55)	0.0(5)
P(2)-C(51)-C(56)-C(55)	177.8(3)
C(41)-P(2)-C(61)-C(62)	109.5(3)
C(51)-P(2)-C(61)-C(62)	-1.3(3)
PT-P(2)-C(61)-C(62)	-124.9(3)
C(41)-P(2)-C(61)-C(66)	-66.4(3)
C(51)-P(2)-C(61)-C(66)	-177.2(3)
PT-P(2)-C(61)-C(66)	59.3(3)
C(66)-C(61)-C(62)-C(63)	0.4(6)
P(2)-C(61)-C(62)-C(63)	-175.5(3)
C(61)-C(62)-C(63)-C(64)	-1.1(6)
C(62)-C(63)-C(64)-C(65)	1.6(6)
C(63)-C(64)-C(65)-C(66)	-1.2(6)
C(64)-C(65)-C(66)-C(61)	0.5(6)
C(62)-C(61)-C(66)-C(65)	0.0(5)
P(2)-C(61)-C(66)-C(65)	175.9(3)